Delft University of Technology

Alpha Radionuclide Therapy Using Polymeric Nanocarriers
Solution to the Recoil Problem?

de Kruijff, Robin

DOI
Publication date
2018
Document Version
Publisher's PDF, also known as Version of record

Important note
To cite this publication, please use the final published version (if applicable).
Please check the document version above.

Alpha Radionuclide Therapy Using Polymeric Nanocarriers: Solution to the Recoil Problem?

Robine Maria de Kruijff

Alpha Radionuclide Therapy Using Polymeric Nanocarriers: Solution to the Recoil Problem?

Dissertation

for the purpose of obtaining the degree of doctor

at Delft University of Technology

by the authority of the Rector Magnificus prof.dr.ir. T.H.J.J. van der Hagen

chair of the Board for Doctorates

to be defended publicly on Friday the 2nd of March 2018 at 15:00 hours

by

Robine Maria DE KRUIJFF

Master of Science in Applied Physics, Delft University of Technology, the Netherlands

born in Utrecht, the Netherlands

This dissertation has been approved by the promotor and the copromotor.

Composition of the doctoral committee:

Rector Magnificus	Chairman
Prof. dr. H.T. Wolterbeek	Delft University of Technology, promotor
Dr. ir. A.G. Denkova	Delft University of Technology, copromotor

Independent members:

Prof. dr. ir. J.L. Kloosterman	Delft University of Technology
Prof. dr. O.C. Boerman	Radboud UMC
Prof. dr. J.P. Pignol	Erasmus MC
Prof. dr. T. Ross	Hannover MC
Dr. R. Eelkema	Delft University of Technology
Prof. dr. A. van de Wiel	Delft University of Technology, reserve member

Table of Contents

Summary

In radionuclide therapy, radioisotopes are used to irradiate tumours from within the body. Usually beta-emitters coupled to tumour-targeting molecules are used, which specifically accumulate at the tumour site. Instead of using beta-emitters, it is also possible to use radionuclides which emit an alpha particle upon decay. Alpha particles have a shorter range and are much more effective in destroying tumour cells. Alpha radionuclide therapy is steadily gaining interest, although currently in most studies radionuclides with relatively short half-life are used. Long lived radionuclides like the ^{225}Ac employed in this thesis are ideal for the treatment of tumours which take a longer time to reach. The long half-life of ^{225}Ac combined with four alpha particles in its decay chain ensure long irradiation of the targeted tissue. However, upon alpha-decay the daughter nuclide receives a recoil energy decoupling it from any targeting agent, allowing it to diffuse throughout the body to irradiate healthy tissue. The main goal of this thesis is to develop polymeric nanocarriers, so-called polymersomes, which retain the recoiling daughter atoms of ^{225}Ac in order to limit healthy tissue toxicity in alpha radionuclide therapy.

In Chapter 2, the loading and retention is studied of a number of alpha, beta and gamma-emitters in polymersomes containing a hydrophilic chelator. Loading efficiency has been optimized for the different radionuclides, and their retention in polymersomes has revealed hardly any loss for most of the radionuclides. By allowing the radionuclide-ionophore complexation to take place in $CHCl_3$, loading efficiencies of ^{225}Ac and ^{140}La in polymersomes have been significantly improved. Additionally, simultaneous loading of two different radionuclides, like ^{225}Ac and ^{111}In, has successfully been applied allowing for them to be used as theranostic agents.

To improve the ^{225}Ac daughter retention in polymersomes, the Monte Carlo-based simulation tool NANVES has been used to calculate the recoil retention in various polymersome designs (Chapter 3). Incorporation of ^{225}Ac in nanoparticles composed of gold or indium, lanthanum or calcium phosphate was simulated, as well as different scenarios where the polymersome either contained indium ions in solution, many small $InPO_4$ nanoparticles, or one large one in the centre. Vesicle designs surrounded by a 5 nm thick golden shell or with ^{225}Ac incorporated in a nanoparticle within the carrier were found to be the most promising candidates for increased recoil retention. Subsequently, Chapter 4 deals with the actual creation of different types of nanoparticles within a polymersome. The main metal-phosphate complexes studied were $InPO_4$ and $LaPO_4$, which were formed by precipitating the metal ions with phosphate ions in an acidic polymersome cavity (pH 3). This novel loading method allowed for a much larger amount of metal ions to be encapsulated as compared to the method used in Chapter 2, although the $LaPO_4$ was found to precipitate into nano needles capable of puncturing the polymersome membrane. The actual recoil retentions of ^{221}Fr and ^{213}Bi in polymersomes containing an $InPO_4$ or $LaPO_4$ nanoparticle were determined in Chapter 5. ^{225}Ac was co-precipitated with the indium or lanthanum phosphate in polymersomes of different diameters ranging from 100 to 800 nm. Recoil retentions had improved significantly as compared to polymersomes with ^{225}Ac attached to a hydrophilic chelate, with an average absolute increase in recoil retention of 20% and 18% for ^{221}Fr and ^{213}Bi respectively in $InPO_4$ containing polymersomes. The high retention of the recoiling daughters and the ^{225}Ac itself makes this vesicle design very suitable for future in vivo verification.

Upon having designed vesicles with improved recoil retention, the next step was to test them in vitro. In Chapter 6 we describe how the polymersomes interact with U87 glioblastoma cells. They are taken up in cell monolayers within minutes after which they distribute themselves throughout the cytoplasm. 3D multicellular spheroids have been used to study polymersome uptake and distribution in tumours, as they more closely mimic the tumour microenvironment. It has been found that although only 0.15% of the polymersomes added to the spheroid medium are taken up, they do achieve complete spheroid penetration after about 4 days, allowing for irradiation of all cells. Furthermore, an activity as low as 0.1 kBq ^{225}Ac, corresponding to an average alpha dose of 7.19 Gy, resulted in significant spheroid growth inhibition.

In Chapter 7, the in vivo circulation time and recoil retention have been investigated. Polymersomes have been injected intravenously in both healthy as well as MDA-MB-231 tumour-bearing BALB/c mice. It has been found that the circulation time in tumour-bearing mice is significantly shorter than in healthy mice (7 min vs 139 min respectively). The tumour presence likely activates the immune system, which is then able to remove the carriers from the circulation more rapidly. Furthermore, large ($\geq$ 200 nm) polymersomes have been found to be temporary taken up in the lungs of tumour bearing mice, suggesting smaller vesicles are more suitable for intravenous injection. Finally, in this chapter we have investigated the retention of the daughter nuclide ^{213}Bi in both ^{225}Ac-DTPA containing polymersomes as well as those containing ^{225}Ac-InPO$_4$. The latter formulation has shown a two-fold increase in ^{213}Bi retention in the polymersomes present in the blood. The therapeutic efficacy of 10 kBq ^{225}Ac-containing polymersomes was studied in MDA-MB-231 tumour-bearing mice upon intratumoural injection in Chapter 8. Biodistribution studies at 1 and 7 days p.i. has shown a high degree of retention of the vesicles at the tumour site compared to the ^{225}Ac-DOTA control. While the vesicles have shown to result in increased tumour growth inhibition as compared to the ^{225}Ac-DOTA and PBS groups, even in these control groups a large degree of growth inhibition was observed, making it difficult to properly assess the influence of the ^{225}Ac-polymersomes on the tumour growth. However, immunohistochemical analysis of the tumours has shown an increase in double-stranded breaks in the group treated with ^{225}Ac-polymersomes, indicating their suitability for tumour irradiation.

In this thesis, larges strides have been made towards the clinical implementation of polymersomes in targeted alpha therapy. The incorporation of nanoparticles in polymersomes has allowed for high retention of the ^{225}Ac mother and daughter nuclides, and in vitro as well as in vivo their potential in destroying tumours has been proven. However, despite the many developments presented in this thesis, we are not there yet. The main issue which remains to be solved is the short circulation time, especially when looking at tumour-bearing mice. Increasing the PEG length on the polymersome corona should go a long way to overcome the fast uptake by the MPS and subsequent successful implementation of the vesicles in the treatment of metastatic cancer.

Samenvatting

In radionuclidetherapie worden radionucliden gebruikt om tumoren te bestrijden van binnenuit het lichaam. Meestal gebeurt dit door een beta-straler te koppelen aan een molecuul welke zich gericht hecht aan de receptoren van een tumorcel om deze van dichtbij te bestralen. In plaats van dit met beta-stralers te doen, kunnen hiervoor ook radionucliden gebruikt worden die alfadeeltjes uitzenden. Alfadeeltjes hebben een kleinere dracht en zijn veel effectiever in het doodmaken van tumorcellen. Interesse in alfa-radionuclidetherapie groeit gestaag, waarbij in de meeste studies momenteel echter nog radionucliden met een relatief korte halfwaardetijd worden gebruikt. Dit proefschrift onderzoekt de geschiktheid van ^{225}Ac, een nuclide met een langere halfwaardetijd. Deze langere halfwaardetijd in combinatie met het relatief grote aantal alfadeeltjes dat wordt uitgezonden in de vervalreeks van ^{225}Ac zorgen voor langere gerichte bestraling van het weefsel. Echter, door het uitzenden van een alfadeeltje ontvangt de dochternuclide echter een terugslagenergie die in staat is alle chemische bindingen te breken, waarna de (eveneens radioactieve) dochternucliden vrij door het lichaam kunnen zwerven met mogelijke schade voor gezond weefsel tot gevolg. Het hoofddoel van dit proefschrift is om nanodeeltjes van polymeren, zogeheten polymeersomen, te ontwikkelen die in staat zijn om de dochternucliden van ^{225}Ac (onder anderen ^{221}Fr en ^{213}Bi) vast te houden. Op deze wijze kan alfa-radionuclidetherapie ingezet worden om zo effectief mogelijk het doelgebied te bestralen met minimale schade aan gezond weefsel.

In Hoofdstuk 2 zijn de ladings- en retentiekarakteristieken van een aantal alfa-, beta- en gammastralers bestudeerd in polymeersomen die een hydrofiele chelator bevatten. De ladingsefficiëntie is geoptimaliseerd voor de verschillende radionucliden, waarbij er nauwelijks verlies van radionucliden uit de polymeersomen is waargenomen. Door de binding van het radioactieve ^{140}La en ^{225}Ac met de ionofoor A23187 plaats te laten vinden in chloroform is hun ladingsefficiëntie significant verbeterd. Bovendien is aangetoond dat het simultaan laden van twee verschillende radionucliden in polymeersomen, zoals ^{111}In en ^{225}Ac, goed mogelijk is. Dit biedt de mogelijkheid voor het gebruik van polymeersomen voor zowel diagnostische als therapeutische doeleinden.

Om de retentie van de dochternucliden van ^{225}Ac verder te verbeteren is het op de Monte-Carlomethode gebaseerde programma NANVES ingezet om de terugslagretentie te simuleren in verschillende polymeersoomontwerpen (Hoofdstuk 3). Opname van ^{225}Ac in nanodeeltjes gemaakt van goud, $InPO_4$, $LaPO_4$ of $CaPO_4$ is gesimuleerd, alsmede verschillende scenario's waarin de polymeersomen ofwel indiumionen in oplossing bevatten, ofwel verschillende kleine indiumfosfaatnanodeeltjes, of één groot indiumfosfaatnanodeeltje in het midden. De meest succesvolle ontwerpen voor betere dochterretentie zijn de vesikel-ontwerpen omgeven door een 5 nm dikke gouden laag of die met ^{225}Ac ingevangen in een nanodeeltje in de polymeersoom gebleken. In Hoofdstuk 4 zijn een aantal van de gesimuleerde ontwerpen daadwerkelijk gecreëerd in het lab. De voornaamste metaal-fosfaatcomplexen die zijn bestudeerd zijn $InPO_4$ en $LaPO_4$, welke gevormd zijn door het neerslaan van de metaalionen met fosfaationen in de zure polymeersoomholten (pH 3). Middels dit nieuwe ladingsmechanisme kan een veel hogere concentratie metaalionen geladen worden in de polymeersomen in vergelijking met de methode gepresenteerd in Hoofdstuk 2. Echter, het $LaPO_4$ bleek neer te slaan in de vorm van nanonaaldjes die in staat bleken het membraan van de

polymeersomen te doorbreken. De daadwerkelijke terugslagretenties van ^{221}Fr en ^{213}Bi in polymeersomen met een nanodeeltje zijn bepaald in Hoofdstuk 5. ^{225}Ac is neergeslagen met indium- of lantaanfosfaat in polymeersomen met een diameter tussen de 100 en 800 nm. De terugslagretenties hier zijn aanzienlijk beter dan in polymeersomen waarin ^{225}Ac geladen was door binding met een hydrofiele chelator, met een verbetering van 20 procentpunt voor ^{221}Fr en 18 procentpunt voor ^{213}Bi in de polymeersomen met InPO$_4$-nanodeeltjes. De hoge retentie van de teruggeslagen dochters en ^{225}Ac zelf laten zien dat deze vesikels uitermate geschikt zijn om te testen in vivo.

De interactie van de polymeersomen met cellen is vervolgens getest. In Hoofdstuk 6 beschrijven we de interactie van de polymeersomen met U87-glioblastomacellen. Binnen enkele minuten zijn ze opgenomen in een monolaag cellen en verdeeld over het cytoplasma. 3D-meercellige sferoïden zijn vervolgens gebruikt om de opname en verspreiding van de polymeersomen in tumoren te bepalen, omdat deze vorm de micro-omgeving van een echte tumor beter benadert. Hoewel slechts 0.15% van de aan het medium toevoegde polymeersomen wordt opgenomen door de sferoïden, zijn ze wel in staat om zich volledig door de sferoïde te verspreiden na ongeveer 4 dagen, waardoor alle cellen bestraald kunnen worden. Daarnaast is een vrij lage activiteit zoals 0.1 kBq ^{225}Ac, wat correspondeert met een gemiddelde alfadosis van 7.19 Gy, al genoeg gebleken om de celgroei significant te vertragen. Bij hogere activiteiten neemt de tumorgrootte binnen een paar dagen af.

In Hoofdstuk 7 zijn in vivo de circulatietijd en terugslagretentie onderzocht. Polymeersomen zijn intraveneus geïnjecteerd in zowel gezonde BALB/c muizen, als muizen met een MDA-MB-231 tumor. Er is gebleken dat de circulatietijd in muizen met een tumor aanzienlijk korter is dan in gezonde muizen (respectievelijk 7 en 139 minuten). De aanwezigheid van de tumor activeert waarschijnlijk het immuunsysteem van de muis, wat vervolgens in staat is om de polymeersomen sneller uit de circulatie te halen. Daarnaast is gebleken dat grote ($\geq$ 200 nm) polymeersomen tijdelijk worden opgenomen in de longen van tumordragende muizen, wat suggereert dat kleinere vesikels meer geschikt zijn voor intraveneuze injectie. In dit hoofdstuk hebben we ook gekeken naar de retentie van de dochternuclide ^{213}Bi in polymeersomen welke ^{225}Ac-DTPA of ^{225}Ac-InPO$_4$ bevatten. Deze laatste combinatie heeft een twee keer zo hoge retentie van ^{213}Bi laten zien in het bloed vergeleken met polymeersomen met ^{225}Ac-DTPA. De therapeutische effectiviteit van 10 kBq ^{225}Ac-bevattende nanodragers is getest muizen met een MDA-MB-231-tumor middels intratumorale injectie. In Hoofdstuk 8 hebben biodistributiestudies op 1 en 7 dagen na injectie laten zien dat een groot deel van de vesikels worden vastgehouden in de tumor, terwijl er in de tumor van de controlegroep met ^{225}Ac-DOTA vrij weinig activiteit terug te vinden was. Hoewel dit veelbelovend is, en de tumoren die geïnjecteerd zijn met ^{225}Ac-polymeersomen ook daadwerkelijk kleiner zijn geworden, hebben ook de tumoren van de controlegroep niet hun normale groeicurve gevolgd, waardoor er helaas nog geen conclusies te verbinden zijn aan het effect van ^{225}Ac-polymeersomen op tumorgroei. Echter, immunohistochemische analyse heeft laten zien dat er een vergroot aantal dubbelstrengsbreuken waren in de tumoren van de muizen die geïnjecteerd zijn met ^{225}Ac-polymeersomen, wat betekent dat ze geschikt zijn om tumoren mee te bestralen.

In dit proefschrift zijn grote stappen gemaakt richting de uiteindelijke klinische implementatie van polymeersomen in gerichte alfatherapie. De opname van nanodeeltjes in polymeersomen heeft gezorgd voor een hogere retentie van zowel ^{225}Ac als haar dochternucliden. Daarnaast is de geschiktheid om tumoren te vernietigen zowel in vitro als in vivo getest. Hoewel er veel vooruitgang

is geboekt in dit proefschrift, zijn we er nog niet. Het belangrijkste probleem wat nog moet worden opgelost is de korte circulatietijd van de nanodeeltjes, zoals die is gemeten in de tumordragende muizen. Een langere PEG aan de buitenkant van de polymeersomen zou deze snelle opname door de macrofagen voor een groot deel moeten kunnen voorkomen, waarna de weg vrij is om polymeersomen toe te passen voor de behandeling van metastasen.

1

Introduction

Alpha emitting radionuclides in the clinic

Alpha-emitting radionuclides are very promising radiotherapeutic agents showing great potential in the treatment of a broad range of malignancies [1–11]. Due to the short penetration depth of alpha particles, they are capable of destroying tumours while causing very limited damage to the surrounding healthy tissue. In fact, an emitted alpha particle will not travel much further than about 6 cell diameters (*i.e.* 50–100 μm). On the other hand, their high linear energy transfer (LET) gives them an increased relative biological effectiveness (RBE) [12] as compared to other therapeutic radionuclides. Just a few alpha particles through a cell nucleus are sufficient to destroy a cell, as cell death due to alpha-radiation is largely independent of oxygenation or active cell proliferation [13]. Furthermore, when alpha-emitting radionuclides are targeted to specific tumour cells in the body they can be very effective in destroying metastases, which are difficult to treat by currently employed techniques.

Alpha radionuclide therapy has recently been introduced in the clinic, where it has booked a number of successes. Several clinical trials have been done with ^{213}Bi, ^{211}At and ^{212}Pb [1], and pre-clinical studies have been carried out with ^{149}Tb [14]. Using tumour-specific monoclonal antibodies, ^{213}Bi has shown promise in the treatment of metastatic melanoma [2,3] and produced remissions in patients with acute myeloid leukemia [4–6]. A phase I study has been completed on the use of locally injected ^{213}Bi-DOTA-substance P in the treatment of small gliomas. The patients received 1.07–2.00 GBq in one cycle or a total of 7.36 GBq in four cycles of ^{213}Bi-DOTA-substance P, of which more than 96% was retained at the tumour site. Most benefit has been seen in relatively small tumours, where sufficient intratumoural distribution has been achieved causing the tumours to be completely necrotic demarcated making it possible for non-operable gliomas to be surgically removed [7]. ^{211}At is also proving to be a promising alpha-emitter. A pilot study amongst patients with recurrent malignant brain tumours has shown the feasibility of the administration of ^{211}At-ch81C6 into the surgically created resection cavity of patients, and has demonstrated minimal toxicity [8]. Women with recurrent ovarian carcinomas have been treated with varying therapeutic doses (33.6–119.2 MBq) of ^{211}At bound to antibody fragments without detectable adverse effects, indicating that therapeutic doses can be delivered to micrometastases through intraperitoneal administration of the ^{211}At-MX35 F(ab')$_2$ [9].

Despite of the clear promise of alpha radionuclide therapy, its use is limited to easily accessible tumours due the short half-lives of the applied isotopes: from 45.6 min for ^{213}Bi up to 7.2 h for ^{211}At. Less easily accessible sites, where the targeting agent is taken up slowly, or tumours where a longer penetration time of the radiopharmaceutical is necessary, will need longer-lived alpha emitting radionuclides for optimal treatment [15]. So far, three long-lived alpha-emitters, namely ^{224}Ra, ^{223}Ra, and ^{225}Ac, have made their appearance in the clinic. One of the first therapeutic uses of alpha-emitting radionuclides has been the intravenous injection of ^{224}Ra-chloride in ankylosing spondylitis (AS) patients (a chronic inflammatory rheumatic disease). Between 1948 and 1975, 1588 patients were treated with repeated injections, receiving an activity of approximately 50 MBq. Although at the time positive therapeutic effects were confirmed for the AS patients, many patients, especially those aged below 21 when treated, developed malignant bone tumours. This increase in myeloid leukaemia as compared to the control group could be explained by the deposition of ^{224}Ra into the bone. An increase in kidney and thyroid cancer was also observed, as compared to a control group [16,17]. In Germany, the pure ^{224}Ra-chloride compound was approved again for the intravenous administration in AS patients in 2000, under the

1

name ^{224}Spondyl$AT^®$[18]. The dose was much lower than what was used before, as patients now received total activities of only 10 MBq, with 1 MBq per injection [12]. Though the ^{224}Ra treatment seemed to reduce medical costs and lost productivity [19], they could not deliver the clinical evaluation on time so it was discontinued in 2005 [20,21]. Since then ^{224}Ra has not been used in clinical settings.

^{223}Ra dichloride (Xofigo$^®$, formerly Alpharadin$^®$) is clinically approved by the FDA (food and drug administration) for the treatment of bone metastases following castration-resistant prostate cancer [11]. From 2008 to 2011 a total of 921 patients from 19 countries participated in a double-blind randomized phase 3 trial (ALSYMPCA). The patients in the treatment arm received six injections of 50 kBq/kg ^{223}Ra ($t_{1/2}$ = 11.4 d) , the patients in the placebo arm six injections with saline. A 3.6-month prolonged survival as compared to the placebo group has been observed [22]. Dosimetric considerations following the intravenous injection of ^{223}Ra dichloride report a dose of 16 Gy to the bone endosteum, and 1.5 Gy to the red bone marrow, while other organs received a lower dose [23]. Biodistribution experiments have shown that less than 2% of the daughter nuclides migrate away from the bone surface [24] Phase II trials are currently on-going for the use of ^{223}Ra dichloride to control bone metastases of breast cancer patients [25,26]. A phase IIa study investigating the safety and short-term efficacy of the use of ^{223}Ra in the treatment of bone metastases in breast cancer patients has shown the treatment to be safe and well-tolerated [27].

The third radionuclide with alpha-emitting daughters that made it to the clinic is ^{225}Ac ($t_{1/2}$ = 9.9 d). ^{225}Ac-Labeled Humanized Anti-CD33 Monoclonal Antibody HuM195 (Actimab-A) has been used to treat patients with advanced myeloid malignancies. A Phase I trial has demonstrated that it is safe to use at doses ≤ 0.1 MBq/kg. Although dose-limiting toxicity (DLT) has occurred in one patient receiving 0.1 MBq/kg and two patients receiving 0.15 MBq/kg [28], blast reductions of more than 50% have been observed in 6 out of 12 patients [29]. No acute toxicities have been seen other than transient grade 2/3 liver function abnormalities, and no apparent damage to kidneys has been observed [10]. In a subsequent Phase-I trial, elderly patients have been treated with a total administered activity between 2.5 and 7.4 MBq. Bone marrow blast reductions have been seen in four out of six patients, but unfortunately no complete remissions have been reported. DLT has occurred in one patient with grade-4 thrombocytopenia, and other toxicities included grade 3 febrile neutropenia (n = 5) and pneumonia (n = 1). The FDA has cleared the compound for subsequent Phase I/II trials, where response rate, progression-free survival and overall survival will be assessed [30]. Furthermore, ^{225}Ac-labeled PSMA (prostate-specific membrane antigen) has recently been introduced in the clinic. While the trials are still on-going, preliminary response rates of two prostate cancer patients to the alpha therapy have been published by Kratochwil et al. [31]. The results obtained for these patients, both of whom had undergone extensive pre-treatment, were impressive, with PSA (prostate-specific antigen) levels declining to less than 0.1 ng/mL in both patients. Despite these excellent early results, clinical trials on a large scale are currently not yet feasible due to the limited availability of ^{225}Ac.

There is thus potentially a future for radionuclides with multiple alpha-emitting daughters like ^{225}Ac or ^{223}Ra. However, toxicity is still an issue due to the recoil energy the daughters experience upon alpha decay. This energy is in most cases at least 100 keV, more than 1000 times larger than the binding energy of any chemical compound. This simply means that bond rupture will always occur subsequent to alpha decay, implying that the released daughters, which are often themselves alpha emitters, might

cause considerable harm (as seen in some of the clinical trials with e.g. AS patients [17]) since they will no longer be bound to a targeting moiety (Figure 1). Considering the presence of different proteins in blood and their high binding capacity, the chance that the radionuclide will re-associate back with its original ligand is rather small. Therefore, we will discuss the different alpha-emitting radionuclides and the strategies to limit their toxicity.
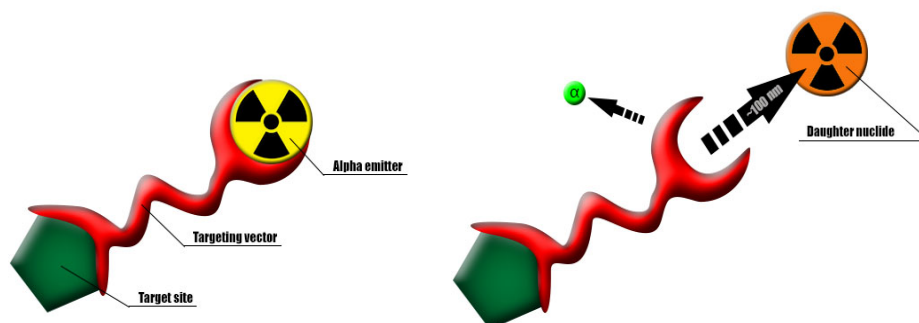
Figure 1. Schematic representation of a recoiling daughter radionuclide detaching from a targeting agent as a consequence of alpha decay.

In vivo alpha generator radionuclides and their decay chains

In Table 1 we have listed the potential alpha-emitting radionuclides having successive alpha-emitting daughters together with their decay characteristics and the recoil energy that the daughter radionuclides receive after decay. In several of the presented decay chains, multiple radionuclides can be used as in vivo generators for alpha-radionuclide therapy. These radionuclides are presented in bold-face in Table 1.

1

Table 1. Alpha emitters that can be used as in vivo generators and their decay characteristics [32].

Radionuclides and Their Decay Chain	Half-Life	Decay	E_α (MeV)*	Calculated E_R (keV)*
^{225}Ac	9.9 d **	α(100%)	5.8	-
^{221}Fr	4.9 min	α(100%)	6.3	105.5
^{217}At	32 ms	α(99.98%) / β⁻(0.01%)	7.1	116.9
^{213}Bi	45.6 min	α(2%) / β⁻(98%)	-	132.8
^{213}Po	4.2 μs	α(100%)	8.4	-
^{209}Pb	3.3 h	β⁻ (100%)	-	160.4
^{209}Bi	stable	-	-	-
^{227}Th	18.7 d	α(100%)	6	-
^{223}Ra	11.4 d	α(100%)	5.7	108.4
^{219}Rn	4.0 s	α(100%)	6.8	104.5
^{215}Po	1.8 ms	α(100%)	7.4	126.9
^{211}Bi	2.2 min	α(99.7%) / β⁻(0.3%)	6.6	140.1
^{207}Tl	4.8 min	β⁻ (100%)	-	128.1
^{207}Pb	stable	-	-	-
^{228}Th	1.9 y	α(100%)	5.4	-
^{224}Ra	3.7 d	α(100%)	5.7	96.9
^{220}Rn	55.6 s	α(100%)	6.3	103.4
^{216}Po	0.15 s	α(100%)	6.8	116.5
^{212}Pb	10.6 h	β⁻ (100%)	-	128
^{212}Bi	60.6 min	α(36%) / β⁻(64%)	6.1/-	-
^{208}Tl / ^{212}Po	3.0 min / 0.3 μs	β⁻ (100%) / α(100%)	- / 8.8	116.5 / -
^{208}Pb	stable	-	-	-
^{230}U	20.8 d	α(100%)	5.9	-
^{226}Th	31 min	α(100%)	6.3	104.3
^{222}Ra	38 s	α(100%)	6.5	114.2
^{218}Rn	35 ms	α(100%)	7.1	120.4
^{214}Po	164 μs	α(100%)	7.7	133.4
^{210}Pb	22.3 y	β⁻ (100%)	-	146.5
^{210}Bi	5.0 d	β⁻ (100%)	-	-
^{210}Po	138.4 d	α(100%)	5.3	-
^{206}Pb	stable	-	-	-

* The alpha and recoil energies have been rounded up; ** is from Pommé et al. [33].

^{225}Ac is typically extracted from ^{229}Th, originating from ^{233}U, produced by neutron capture of ^{232}Th ($^{233}Th \xrightarrow{\beta-} {}^{233}Pa \xrightarrow{\beta-} {}^{233}U \xrightarrow{\alpha} {}^{229}Th$). Due to increasing demand of ^{225}Ac, shortage via this production route is expected and alternative methods are being investigated, from which the proton irradiation of ^{226}Ra targets appears to be the most promising [34]. An alternative to this route is the

bombardment of ^{232}Th targets by protons having an energy of less than 200 MeV, as researched by Weidner et al. [35]. The ^{225}Ac chain has four major alpha particles and recoiling daughters, from which ^{221}Fr, ^{213}Bi and ^{209}Pb are long-lived enough to induce undesired damage to healthy tissue due to subsequent alpha or beta emission.

Distribution of recoil daughters in the body

There are three processes that contribute to the distribution of the recoiling daughters: (1) distance covered due to the recoil energy, (2) diffusion processes and (3) active transport such as convection or blood flow. The importance of each process will depend on the location where the recoil atoms are released. The instantaneous energy that a recoil atom gets will make it cover on average 100 nm and is therefore mostly responsible for the breaking of chemical bonds or the possible escape from carriers [36]. It is the indirect process that allows the recoils to acquire different speciation and distribution than originally intended. Diffusion transport becomes important once the radionuclide reaches certain tissues or organs, such as tumours or kidneys for instance, and will be dependent on the medium as well as the chemical form of the recoil atom. It will differ between diffusion in blood-like media and in the extra/intracellular matrix, as it would be subject to the interaction of the ions with blood or cell components. Most of the time the recoils will be released in the blood stream and their eventual fate will be determined by their affinity for certain organs/tissues provided that they live long enough to reach their biological destination. Table 2 shows a summary of the target organs of several of the elements associated with recoiling daughters.

Table 2. Main targeted organs based on 24 h distribution after intravenous injection (IV).

Element	Main Targeted Organs *
Francium	primarily kidneys [37]
Bismuth	30% urine, 40% kidney, 30% other organs [38]
Radium	25% bone surface, 45% soft tissue, 30% excreted via large intestine [12,24]
Radon	soft tissue to blood: 100 day^{-1}, exhaled 1 min^{-1}, bone to blood: 0.36 d^{-1} [39]
Lead	55% blood, 15% liver, 10%–15% skeleton, kidneys 4% after 1d [39]
Polonium	28% liver, 28% kidneys, 10% red bone marrow, 5% spleen [40]

Several studies have been dedicated to establishing the fate of alpha emitters, including mother and daughter ions. For instance, the radiotoxicity of ^{225}Ac has been evaluated in mice. Biodistribution studies have been done with ^{225}Ac chelated to four different compounds: cyclohexyl diethylenetriamine pentaacetic acid (CHX-DTPA), 1, 4, 7, 10, 13-pentaazacyclopentadecane- N, N', N'', N''', N''''-pentaacetic acid (PEPA), ethylene diamine tetraacetic acid (EDTA) and acetate [41]. In this work, it has been found that ^{225}Ac mainly goes to the liver, but also accumulates in the femur, kidneys and heart. While in time its concentration in the liver and bone increases, it is cleared from the kidney and

the heart. The ^{225}Ac-acetate complex has had a 5.5 times higher %ID/g in the liver than the ^{225}Ac-CHX-DTPA and the ^{225}Ac-PEPA complexes. It must be noted that the biodistribution of ^{225}Ac has been determined immediately after sacrifice using the 218 keV gamma emitted by ^{221}Fr, although with its 4 min half-life ^{221}Fr could have recoiled and diffused away from the location of the mother isotope. A different study by Beyer et al. has also reported a high liver uptake of ^{225}Ac injected as citrate complex in mice and rats [42].

Approaches to deal with the recoil problem

There are generally speaking three strategies proposed in literature to deal with recoil issues: fast uptake of the alpha emitters in tumour cells, local administration such as intratumoural injection, and encapsulation in a nano-carrier. The first approach ensures that the radiopharmaceutical is rapidly taken up by the tumour cells and that the remaining not-adsorbed part is excreted fast from the body. This argument has been used for both peptides and antibodies. Since antibodies take a long time to accumulate at the tumour site, one can imagine that smaller targeting agents like PSMA [31] and octreotide [43] would fit better to this strategy. Nevertheless, this approach is mainly applied with larger targeting agents [15,44–46] The second approach is to insert or inject the alpha-emitting radionuclides directly in the or near the tumour tissue [47–51]. This form of therapy could prove very beneficial for patients with relatively large, accessible tumours, though for smaller metastasis different methods would need to be applied. In this thesis, we have chosen to encapsulate them in nanocarriers, therefore we will describe this method in further detail.

Encapsulation in a nano-carrier

In this approach, some kind of a nano-carrier is chosen which is capable of retaining the recoiling daughters. So far zeolites [52], liposomes [53,54], polymersomes [55], and metal-based particles [56,57] have been investigated. The actual recoil retention is difficult to compare though, as determining the percentage of recoiling daughters is not always straightforward, especially in systems where re-association is possible. For instance, Piotrowska et al. have used zeolites as carriers for ^{224}Ra, showing that the percentage of recoiled daughters (^{212}Bi, ^{212}Pb and ^{208}Tl) escaping from the zeolites is relatively small even under blood serum conditions [52]. However, it needs to be mentioned that in these experiments, most likely equilibrium has been established and the determined values in fact reflect the distribution of the different ions according to their stability constants. Once injected in the blood stream, the ejected radionuclides will not be in thermodynamic equilibrium anymore and their distribution might be of a very different kind.

Sofou et al. have used different types of liposomes (zwitterionic, cationic and anionic) to perform retention studies of ^{225}Ac and its daughters. ^{213}Bi retention has been revealed to have a weak size dependence for liposomes sized between 100 and 800 nm, where a maximum of 12% remained in the carriers [53]. At the same time, Wang et al., have investigated polymeric vesicles for the same decay chain and have reported that nearly 70% of ^{213}Bi is still present in carriers of 800 nm [55]. These discrepancies can be due to the relatively fast decay of ^{225}Ac which creates experimental difficulties prone to measurement errors strongly dependent on the separation method. In the case of ^{225}Ac decay, the separation method should be fast enough otherwise the initial activity of ^{221}Fr and ^{213}Bi might be

wrongly calculated, resulting in underestimation of the recoil retention. Typically, after separation the time is monitored accurately and the activity of ^{221}Fr and ^{213}Bi is determined and plotted against time. The initial activity is then estimated using a simplified version of the secular equilibrium decay equation:

$$A_2(t) = \frac{\lambda_2}{\lambda_2 - \lambda_1} A_1(0)\left(e^{-\lambda_1 t} - e^{-\lambda_2 t}\right) + A_2(0)e^{-\lambda_2 t} \qquad (1)$$

where A_1 and A_2 reflect the activity of the mother and daughter respectively, while λ_1 and λ_2 correspond to the mother and daughter decay constants. A slow separation does not allow for determining the ^{221}Fr escape and leads to uncertainties of the initial ^{213}Bi concentration, *i.e.* the nearer the measured time is to time zero the more accurate the determination of the initial activity and hence the retention.

Liposomes of 80 nm in diameter have also been investigated as carriers of ^{223}Ra, but unfortunately all available recoil data is based on in vivo experiments, which complicates determining the actual retention. Nevertheless, from this study it is clear that that the recoil daughters ^{211}Pb and ^{211}Bi (the third and fourth daughter of ^{223}Ra) are not retained sufficiently in the liposomes, as the activity measured in the kidneys has been found to be much higher than the expected value based on equilibrium assumptions, calculated from the ^{223}Ra activity in the same organ. In addition, ^{223}Ra has also been measured in the bones of the lab-animals. These findings strongly suggest that relatively small sizes of this type of soft nano-carriers will not retain a sufficient percentage of recoils, which can also be anticipated from range calculation of recoiling atoms based on their stopping power [54]. In soft materials like polymers, for instance, the projected range of ^{221}Fr has been reported to be around 90 nm, which can already be larger than the applied nano-carrier [36]. An alpha cascade will result in an even larger distance that the recoils can cover. Therefore in order to achieve sufficient recoil retention materials having higher Z are necessary. This line of reasoning has been followed by Woodward et al. and McLaughlin et al., working on lanthanide-based phosphate nanoparticles doped with ^{225}Ac, where the latter has also applied gold coating to the carriers [56,57]. The retention of ^{221}Fr has been determined in vitro, while the fate of ^{213}Bi has also been assessed in vivo. The gold-layered particles have given the most promising results with nearly 100% initial retention of ^{221}Fr when four layers of gadolinium phosphate are applied, but unfortunately these particles could not be used in vivo due to sedimentation issues. Biodistribution studies based on ^{225}Ac-nanoparticles having less than four gadolinium phosphate layers coupled to mAb 201b have revealed a ^{213}Bi retention of at least 69% and a much-decreased renal uptake of free ^{213}Bi. Although these results are very promising, there is still liver uptake of the ^{225}Ac doped particles due to their size. Considering the nature of the particles it is expected that they will remain in the liver for a considerable time, which might cause adverse effects and should be studied further. Smaller particles may prove to have better bio-distribution and faster clearance but at the expense of recoil retention. Clearly an optimum between recoil retention and uptake of nano-carriers by healthy organs needs to be determined to make this approach applicable in the clinic.

Polymeric nanocarriers

Despite major advances in our understanding of cancer development and treatment, it is now well recognized that early detection, pathological characterization, and personalized treatments are the most important aspects for improving the overall survival rate of cancer patients. Recent developments in

1

polymer chemistry have led to the creation of novel materials that can combine both imaging and therapeutic functionalities to provide comprehensive and personalized treatments. In particular, radiolabelled carriers based on polymeric materials represent a new class of agents that are expected to have a remarkable influence on nuclear medicine due to their enormous potential for a wide range of clinical applications [58].

Polymeric carriers like unimers, dendrimers, and more complex configurations such as micelles, polymersomes, polymeric particles and nanogels, can be used as delivery vehicles to transport a wide variety of payloads for therapeutic or diagnostic purposes. These materials have physicochemical properties that allow fine tuning in size and shape to the desired application and specific attachment of a wide range of functionalities such as radionuclides, targeted moieties (antibodies, peptides) chemotherapeutic drugs and/or other imaging agents. The dimensions of these carriers, ranging from a few nanometers to several hundreds of nanometers, are usually designed to profit from the enhanced permeability and retention (EPR) effect and pass through less tightly bound endothelial cells in regions of inflammation such as the tumour site [59–61].

The combination of these polymeric materials with gamma and positron emitting radionuclides (Figure 2) enables the detection of spatiotemporal processes, permitting to analyse the influence of the polymeric carrier's physicochemical properties on their pharmacokinetics and biodistribution, and to adjust these entities to minimize damage to healthy tissue. The quantitative measurement of the tumour targeting efficacy can then be used to obtain a direct evaluation of the tumour progression and treatment efficacy.

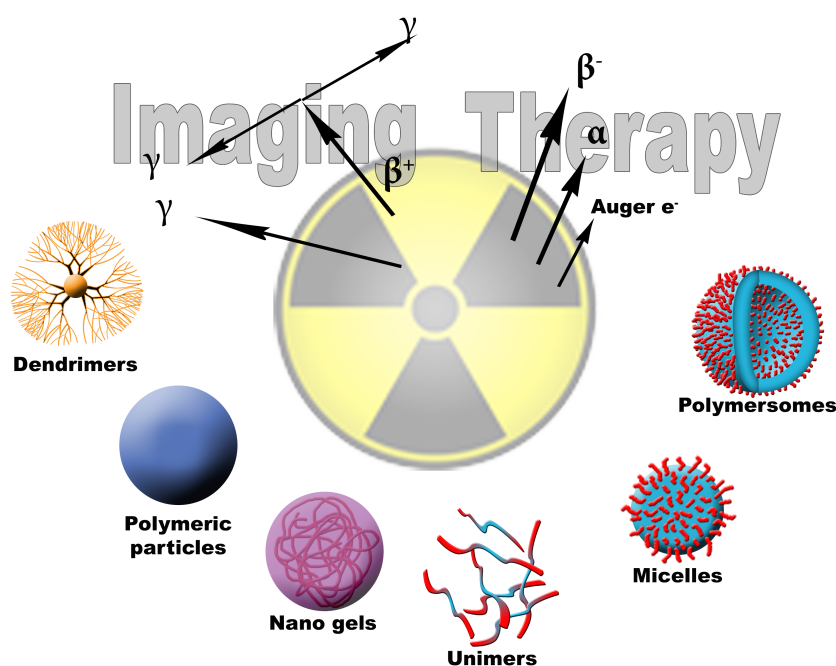

Figure 2: Schematic drawing of different polymeric carriers and the type of radiation used in imaging and therapy.

Typically, radionuclides emitting gamma radiation with an energy in the 60 to 300 keV range are applicable for single photon emission computed tomography (SPECT), while positron-emitters (511 keV) are used for positron emission tomography (PET). Other techniques such as computed

tomography (CT), magnetic resonance imaging (MRI), ultrasound and optical imaging (fluorescence and bioluminescence) are often combined with PET or SPECT (e.g. PET/CT, MRI/SPECT) to increase the strengths of each individual modality. This multimodality imaging approach provides additional information about the biological structure and metabolic processes, and altogether increases the ability for cancer detection and/or screening of tumour progression.

The type of radioactive decay, energy and biological half-life are the major determinants on selecting the potential radionuclides for diagnostic or therapeutic tumour targeting. While gamma and positron emitters are typically used for obtaining imaging data, beta minus and alpha particles, as well as Auger electrons are suitable for therapy. In an ideal scenario, an isotope that emits for example both gamma radiation and beta particles (e.g. ^{166}Ho, ^{177}Lu) would be highly desirable because it enables simultaneous treatment and monitoring of the treatment progression. On the other hand, the selection of the polymeric material for nuclear medicine will mainly depend on its ability to carry an optimal amount of the radioisotopes, its stability and the most favourable pharmacokinetic properties for the intended application (e.g. hydrophilicity, size, charge, surface functionalization). At the moment, radiolabelling of polymeric carriers is primarily carried out to determine their fate in vivo and not to provide tumour regression induced by a radiation dose, mostly due to high liver and spleen uptake and slow clearance which can be harmful in combination with therapeutic radionuclides.

Polymersomes

Polymersomes, vesicles composed of amphiphilic block copolymers, typically consist of an aqueous core surrounded by a hydrophobic bilayer. They are a relatively new class of polymeric carrier [62], and hence the number of studies with polymersomes in nuclear medicine is quite small. Polymersomes are usually prepared by the solvent displacement (nanoprecipitation) method [63–65], where a buffer solution is added dropwise to the block copolymer dissolved in an organic solvent (typically THF (tetrahydrofuran) or DMSO (dimethyl sulfoxide)) which is subsequently removed through dialysis. Otherwise, they are prepared by direct dissolution, where the block copolymer is dissolved in an aqueous buffer and subsequently stirred [55,66]. Using the nanoprecipitation method, drugs like docetaxel can easily be encapsulated in the aqueous polymersome core [65]. When dissolved together with the block copolymer in the organic solvent, during formation high amounts (28 – 49%) of docetaxel can be encapsulated. The addition of ^{3}H-radiolabeled dextran during polymersome formation similarly allowed for a radiolabelled polymersome core. In this study, Lee et al. also labelled the acrylated PEG (polyethylene glycol) chains on the poly(ethylene glycol)-b-poly(D,L-lactide) (PEG-PDLLA) polymersomes surface after formation with ^{14}C-thioglycolic acid [67]. Though unfortunately the stability of the two radiolabels was not specifically determined, they did find very similar circulation kinetics for both the ^{3}H and ^{14}C labels (< 5% difference), implying colloidal polymersome stability.

We can thus distinguish two main polymersome labelling methods: surface labelling and the encapsulation of radionuclides in the aqueous core. While surface labelling always takes place after vesicle formation, core labelling can be done either during or after formation. However, with stable vesicles, surface labelling seems to be less stable than labelling of the core. Brinkhuis et al. added DTPA as chelating end-group to polybutadiene-poly(ethylene glycol) block copolymers (PBd-PEG) and added a small percentage of these functionalized block copolymers during polymersome formation.

1

After polymersome formation, 15 MBq of ^{111}InCl$_3$ was incubated for 30 minutes which generally yielded a labelling efficiency of 95% [64]. However, the radiolabel was found to be relatively instable, where less than 80% of the radiolabel was still associated with the polymersome after 24 h in mouse plasma. The same block copolymer was used in another study by Wang et al., where the core of the vesicles was labelled via active ion transport through the bilayer. Here, DTPA was encapsulated during polymersome formation, and the lipophilic ligand tropolone was employed to transport the ^{111}In through the bilayer, where it formed a complex with the DTPA inside the vesicles. Incubation in serum has shown only a very small loss (< 4%) of ^{111}In radiolabel after 24h, implying greater radiolabel stability for core-labelling as compared to surface-labelling [66,68]. Only one study has been done thus far using polymersomes as therapeutic radionuclide carriers. Here, the polymersome core was labelled after formation with the alpha-emitting radionuclide ^{225}Ac. The nano-carriers were used to retain recoiled (alpha-emitting) daughter atoms, which upon decay decouple from targeting agents due to their high recoil energy. The vesicles have been demonstrated to retain these recoiling daughter nuclides. However, large polymersomes were necessary to retain the daughters to a sufficient degree, and no in vivo studies have been reported yet [55].

Conclusions

During the past few years, some progress has been made in getting a few alpha radionuclide therapy concepts to the clinic, however, by and large we find that in most studies concerning long-lived alpha-emitters, recoiling daughter atoms pose a serious problem. If the distribution of recoiled atoms is not controlled, toxic effects due to the recoiling daughters will be present. At higher injected radionuclide activities, this could induce significant damage to healthy tissue. The question is whether the activity that can be injected without toxic effects will be sufficient to have the expected (much improved) therapeutic effects. The success of each approach depends to a large extent on the type of radionuclide and the type of tumours to be treated. Polymeric nano-carriers that can limit the distribution of the recoiling daughters may offer a solution. They have been known for many years and will continue to develop in the future due to their versatility and multi-functionality allowing applications in many medical disorders. Most of the polymer entities that are developed now-a-days are intended to carry chemotherapeutics to the tumour aiming at lower toxicity and better treatment efficiency. Each of these carriers needs to be evaluated in lab animals first, before it can enter the clinic. Imaging techniques such as microSPECT and microPET offer sub-millimetre resolution and dynamic imaging, and are therefore indispensable in the preclinical phase. Alpha-radionuclide therapy is thus promising, provided that the recoil obstacle can be overcome. Only then will patients have the full benefit of this treatment.

Scope and outline of the thesis

The aim of this thesis is to develop nanocarriers which can retain recoiled ^{225}Ac daughters to a large extend, allowing for their safe application as tumour targeting agents. Polymersomes composed of PBd-PEO were chosen as carriers, as they had shown in previous research to be able to retain daughter atoms to a certain extent [55]. This research is focussed on further developing these vesicles to increase recoil retention, making them suitable for in vivo tumour targeting. The outline of the thesis is given below:

Chapter 2 describes the radiolabelling methods for different radionuclides. We demonstrate optimal encapsulation methods for different alpha, beta and gamma-emitters, as well as the dual-labelling of polymersomes for simultaneous diagnostic and therapeutic studies.

Chapter 3 discusses the application of the Geant4 based simulation platform NANVES to determine optimal vesicle design for recoil retention. We have designed vesicles containing one large nanoparticle, many small ones, ions in solution, or with a golden shell, and the retention of the ^{225}Ac daughter nuclides is determined in polymersomes of different diameters.

Chapter 4 describes the synthesis of polymersomes containing indium, lanthanum and calcium phosphate nanoparticles. We show that this method allows for a much larger amount of metal ions to be encapsulated inside the vesicles.

Chapter 5 examines the co-encapsulation of ^{225}Ac into two of the produced formulations, indium phosphate nanoparticles and lanthanum phosphate nanoneedles. We describe the retention of two of the ^{225}Ac daughter atoms (^{221}Fr and ^{213}Bi) and compare these to the simulated recoil retention to gain a better understanding of the different factors influencing daughter retention.

Chapter 6 assesses the interaction of polymersomes with cells, where cellular uptake is studied in a U87 monolayer as well as in a 3D U87 spheroid model. Furthermore, we determine the effect of ^{225}Ac-labeled polymersomes on spheroidal growth.

Chapter 7 focuses on the intravenous injection of polymersomes containing ^{111}In in both tumour-bearing and healthy mice, assessing their circulation time and biodistribution. Next to that, we study the intravenous injection of ^{225}Ac encapsulated in DTPA or InPO$_4$ containing polymersomes in healthy mice to determine the retention of the daughter nuclide ^{213}Bi.

Chapter 8 evaluates the therapeutic efficacy of 10 kBq ^{225}Ac in polymersomes or coupled to DOTA upon intratumoural injection. We study the biodistribution at 1 and 7 days p.i. as well as any double-stranded breaks in the tumours.

Chapter 9 presents the highlights of the thesis and draws general conclusions.

1

References

1. Meredith, R. F.; Torgue, J.; Azure, M. T.; Shen, S.; Saddekni, S.; Banaga, E.; Carlise, R.; Bunch, P.; Yoder, D.; Alvarez, R. Pharmacokinetics and imaging of 212Pb-TCMC-trastuzumab after intraperitoneal administration in ovarian cancer patients. *Cancer Biother. Radiopharm.* **2014**, *29*, 12–7.

2. Allen, B. J.; Singla, A. A.; Rizvi, S. M. A.; Graham, P.; Bruchertseifer, F.; Apostolidis, C.; Morgenstern, A. Analysis of patient survival in a Phase I trial of systemic targeted α-therapy for metastatic melanoma. *Immunotherapy* **2011**, *3*, 1041–1050.

3. Raja, C.; Graham, P.; Rizvi, S.; Song, E.; Goldsmith, H.; Thompson, J.; Bosserhoff, A.; Morgenstern, A.; Apostolidis, C.; Kearsley, J.; Reisfeld, R.; Allen, B. J. Interim analysis of toxicity and response in phase 1 trial of systemic targeted alpha therapy for metastatic melanoma. *Cancer Biol. Ther.* **2007**, *6*, 846–852.

4. Mcdevitt, M. R.; Finn, R. D.; Ma, D.; Larson, S. M.; Scheinberg, D. A. Preparation of alpha-Emitting 213Bi-Labeled Antibody Constructs for Clinical Use. *J. Nucl. Med.* **1999**, *40*, 1722–1727.

5. Jurcic, J. G.; Larson, S. M.; Sgouros, G.; Mcdevitt, M. R.; Finn, R. D.; Divgi, C. R.; Ballangrud, Å. M.; Hamacher, K. A.; Ma, D.; Humm, J. L.; Brechbiel, M. W.; Molinet, R.; Scheinberg, D. A. Targeted alpha particle immunotherapy for myeloid leukemia. *Blood* **2002**, *100*, 1233–1240.

6. Rosenblat, T. L.; McDevitt, M. R.; Mulford, D. a; Pandit-Taskar, N.; Divgi, C. R.; Panageas, K. S.; Heaney, M. L.; Chanel, S.; Morgenstern, A.; Sgouros, G.; Larson, S. M.; Scheinberg, D. a; Jurcic, J. G. Sequential cytarabine and alpha-particle immunotherapy with bismuth-213-lintuzumab (HuM195) for acute myeloid leukemia. *Clin. Cancer Res.* **2010**, *16*, 5303–11.

7. Cordier, D.; Forrer, F.; Bruchertseifer, F.; Morgenstern, A.; Apostolidis, C.; Good, S.; Müller-Brand, J.; Mäcke, H.; Reubi, J. C.; Merlo, A. Targeted alpha-radionuclide therapy of functionally critically located gliomas with 213Bi-DOTA-[Thi8,Met(O2)11]-substance P: a pilot trial. *Eur. J. Nucl. Med. Mol. Imaging* **2010**, *37*, 1335–44.

8. Zalutsky, M. R.; Reardon, D. A.; Akabani, G.; Coleman, R. E.; Friedman, A. H.; Friedman, H. S.; McLendon, R. E.; Wong, T. Z.; Bigner, D. D. Clinical Experience with α-Particle–Emitting 211At: Treatment of Recurrent Brain Tumor Patients with 211At-Labeled Chimeric Antitenascin Monoclonal Antibody 81C6. *J. Nucl. Med.* **2008**, *49*, 30–38.

9. Andersson, H.; Cederkrantz, E.; Back, T.; Divgi, C.; Elgqvist, J.; Himmelman, J.; Horvath, G.; Jacobsson, L.; Jensen, H.; Lindegren, S.; Palm, S.; Hultborn, R. Intraperitoneal alpha-particle radioimmunotherapy of ovarian cancer patients: pharmacokinetics and dosimetry of (211)At-MX35 F(ab')2--a phase I study. *J. Nucl. Med.* **2009**, *50*, 1153–60.

10. Targeted Atomic Nano-Generators (Actinium-225-Labeled Humanized Anti-CD33 Monoclonal Antibody HuM195) in Patients With Advanced Myeloid Malignancies https://clinicaltrials.gov/ct2/show/NCT00672165 (accessed Jan 1, 2015).

11. Jadvar, H.; Quinn, D. Targeted α-Particle Therapy of Bone Metastases in Prostate Cancer. *Clin. Nucl. Med.* **2013**, *38*.

12. Lassmann, M.; Nosske, D.; Reiners, C. Therapy of ankylosing spondylitis with 224Ra-radium chloride: dosimetry and risk considerations. *Radiat. Environ. Biophys.* **2002**, *41*, 173–8.

13. Morgenstern, A.; Bruchertseifer, F.; Apostolidis, C. Bismuth-213 and Actinium-225 – Generator Performance and Evolving Therapeutic Applications of Two Generator-Derived Alpha-Emitting Radioisotopes. *Curr. Radiopharm.* **2012**, *49*, 221–227.

14. Müller, C.; Reber, J.; Haller, S.; Dorrer, H.; Köster, U.; Johnston, K.; Zhernosekov, K.; Türler, A.; Schibli, R. Folate receptor targeted alpha-therapy using terbium-149. *Pharmaceuticals* **2014**, *7*, 353–65.

15. Song, H.; Hobbs, R. F.; Vajravelu, R.; Huso, D. L.; Esaias, C.; Morgenstern, A.; Sgouros, G. Radioimmunotherapy of breast cancer metastases with {alpha}-particle emitter 225Ac: comparing efficacy with 213Bi and 90Y. *Cancer Res.* **2009**, *69*, 8941–8948.

16. Wick, R. R.; Atkinson, M. J.; Nekolla, E. a Incidence of leukaemia and other malignant diseases following injections of the short-lived alpha-emitter 224Ra into man. *Radiat. Environ. Biophys.* **2009**, *48*, 287–94.

17. Wick, R. R.; Nekolla, E. a; Gaubitz, M.; Schulte, T. L. Increased risk of myeloid leukaemia in patients with ankylosing spondylitis following treatment with radium-224. *Rheumatology (Oxford).* **2008**, *47*, 855–9.

18. Kommission Pharmakotherapie Stellungnahme der Deutschen Gesellschaft für Rheumatologie zur Therapie der ankylosierenden Spondylitis (AS) mit Radiumchlorid (224SpondylAT®). *Z. Rheumatol.* **2001**, *60*, 84–87.

19. Zhang, Z.; Siegert, J.; Maywald, U.; Kirch, W. [Cost-benefit analysis of [224Ra] radium chloride therapy for ankylosing spondylitis (Bekhterev's disease)]. *Med. Klin. (Munich).* **2007**, *102*, 540–9.

20. Schulte, T. L.; Nekolla, E. a; Wick, R. R. [Long-term investigation of the risk of malignant diseases following intravenous radium-224 treatment for ankylosing spondylitis]. *Strahlentherapie und Onkol.* **2009**, *185*, 549–56.

21. Eckert & Ziegler Eckert & Ziegler stoppt klinische Entwicklung von SpondylAT® http://www.ezag.com/de/print/startseite/presse/pressemeldungen/detail/article/eckert-ziegler-stoppt-klinische-entwicklung-von-spondylatR.html.

22. Parker, C.; Nilsson, S.; Heinrich, D.; Helle, S. I.; O'Sullivan, J. M.; Fosså, S. D.; Chodacki, a; Wiechno, P.; Logue, J.; Seke, M.; Widmark, a; Johannessen, D. C.; Hoskin, P.; Bottomley, D.; James, N. D.; Solberg, a; Syndikus, I.; Kliment, J.; Wedel, S.; Boehmer, S.; Dall'Oglio, M.; Franzén, L.; Coleman, R.; Vogelzang, N. J.; O'Bryan-Tear, C. G.; Staudacher, K.; Garcia-Vargas, J.; Shan, M.; Bruland, Ø. S.; Sartor, O. Alpha emitter radium-223 and survival in metastatic prostate cancer. *N. Engl. J. Med.* **2013**, *369*, 213–23.

1

23. Hobbs, R.; Song, H.; Watchman, C.; Bolch, W.; Aksnes, A.-K.; Ramdahl, T.; Flux, G. D.; Sgouros, G. A bone marrow toxicity model for 223Ra alpha-emitter radiopharmaceutical therapy. *Phys. Med. Biol.* **2013**, *57*, 3207–3222.

24. Henriksen, G.; Fisher, D. R.; Roeske, J. C.; Bruland, Ø. S.; Larsen, R. H. Targeting of Osseous Sites with Alpha-Emitting 223Ra: Comparison with the Beta-Emitter 89Sr in Mice. *J. Nucl. Med.* **2003**, *44*, 252–260.

25. Coleman, R.; Fried, G.; Petrenciuc, O.; Sawhney, A.; Li, R.; Rugo, H. Abstract OT1-04-04: A phase 2 randomized, double-blind, placebo-controlled trial of endocrine therapy ± radium-223 dichloride in HER2-negative, hormone receptor–positive breast cancer patients with bone metastases. *Cancer Res.* **2017**, *77*.

26. Rugo, H.; Drumea, K.; Campone, M.; Barnadas, A.; Petrenciuc, O.; Zhang, A.; Li, R.; Coleman, R. Abstract OT1-04-05: A phase 2 randomized, double-blind, placebo-controlled trial of radium-223 dichloride with exemestane and everolimus in patients with HER2-negative, hormone receptor–positive breast cancer and bone metastases. *Cancer Res.* **2017**, *77*.

27. Coleman, R.; Aksnes, A.-K.; Naume, B.; Garcia, C.; Jerusalem, G.; Piccart, M.; Vobecky, N.; Thuresson, M.; Flamen, P. A phase IIa, nonrandomized study of radium-223 dichloride in advanced breast cancer patients with bone-dominant disease. *Breast Cancer Res Treat* **2014**, *145*, 411–418.

28. Jurcic, J. G.; Rosenblat, T. L.; McDevitt, M. R.; Pandit-Taskar, N.; Carrasquillo, J. A.; Chanel, S. M.; Ryan, C.; Frattini, M. G.; Cicic, D.; Larson, S. M.; Scheinberg, D. A. Phase I trial of the targeted alpha-particle nano-generator actinium-225 (225Ac-lintuzumab) (anti-CD33; HuM195) in acute myeloid leukemia (AML). In *2011 ASCO Annual Meeting*; 2011.

29. Jurcic, J. G. What happened to anti-CD33 therapy for acute myeloid leukemia? *Curr. Hematol. Malig. Rep.* **2012**, *7*, 65–73.

30. Jurcic, J. G.; Ravandi, F.; Pagel, J. M.; Park, J. H.; Douer, D.; Estey, E. H.; Kantarjian, H. M.; Cicic, D.; Scheinberg, D. A. Phase I Trial Of The Targeted Alpha-Particle Nano-Generator Actinium-225 (225Ac)-Lintuzumab (Anti-CD33) In Combination With Low-Dose Cytarabine (LDAC) For Older Patients With Untreated Acute Myeloid Leukemia (AML). In *55th ASH Annual Meeting and Exposition*; 2013; p. 1460.

31. Kratochwil, C.; Bruchertseifer, F.; Giesel, F. L.; Weis, M.; Verburg, F. A.; Mottaghy, F.; Kopka, K.; Apostolidis, C.; Haberkorn, U.; Morgenstern, A. 225Ac-PSMA-617 for PSMA-Targeted α-Radiation Therapy of Metastatic Castration-Resistant Prostate Cancer. *J. Nucl. Med.* **2016**, *57*, 1941–1944.

32. Magill, J.; Pfennig, G.; Galy, J. Karlsruher Nuklidkarte 7th edition 2009.

33. Pommé, S.; Marouli, M.; Suliman, G.; Dikmen, H.; Van Ammel, R.; Jobbágy, V.; Dirican, A.; Stroh, H.; Paepen, J.; Bruchertseifer, F.; Apostolidis, C.; Morgenstern, A. Measurement of the 225Ac half-life. *Appl. Radiat. Isot.* **2012**, *70*, 2608–2614.

34. Morgenstern, A.; Abbas, K.; Bruchertseifer, F.; Apostolidis, C. Production of Alpha Emitters for Targeted Alpha Therapy. *Curr. Radiopharm.* **2008**, *1*, 135–143.

35. Weidner, J. W.; Mashnik, S. G.; John, K. D.; Hemez, F.; Ballard, B.; Bach, H.; Birnbaum, E. R.; Bitteker, L. J.; Couture, A.; Dry, D.; Fassbender, M. E.; Gulley, M. S.; Jackman, K. R.; Ullmann, J. L.; Wolfsberg, L. E.; Nortier, F. M. Proton-induced cross sections relevant to production of 225Ac and 223Ra in natural thorium targets below 200 MeV. *Appl. Radiat. Isot.* **2012**, *70*, 2602–7.

36. Thijssen, L.; Schaart, D. R.; de Vries, D.; Morgenstern, A.; Bruchertseifer, F.; Denkova, A. G. Polymersomes as nano-carriers to retain harmful recoil nuclides in alpha radionuclide therapy: a feasibility study. *Radiochim. Acta* **2012**, *100*, 473.

37. Jaggi, J. S.; Kappel, B. J.; Mcdevitt, M. R.; Sgouros, G.; Flombaum, C. D.; Cabassa, C.; Scheinberg, D. A. Efforts to Control the Errant Products of a Targeted In vivo Generator. *Cancer Res.* **2005**, *65*, 4888–4896.

38. Beninson, D. J.; Dunster, H. J.; Jacobi, W.; Jammet, H. P.; Liniecki, J.; Meinhold, C. B.; Moiseev, A. A.; Rowley, K. A.; Sinclair, W. K.; Takahashi, S.; Upton, A. C.; Vennart, J.; Morgan, K. Z.; Pachin, E. E.; Taylor, L. S. Limits for Intakes of Radionuclides by Workers. In *Annals of the ICRP*; Sowby, F. D., Ed.; Pergamon Press, 1980; p. 67.

39. Beninson, D.; Dunster, H. J.; Ilyin, I. A.; Jacobi, W.; Jammet, H. P.; Kaul, A.; Li, D.; Liniecki, J.; Matsudaira, H.; Mettler, F.; Sinclair, W. K.; Lindell, B.; Morgan, K. Z.; Taylor, L. S. Age-dependent Doses to Members of the Public from Intake of Radionuclides: Part 2 Ingestion Dose Coefficients. In *Annals of the ICRP*; Smith, H., Ed.; Pergamon Press, 1993; pp. 75–87.

40. Keverling Buisman, A. S. *Handboek Radionucliden*; BetaText, 1996.

41. Davis, I. A.; Glowienka, K. A.; Boll, R. A.; Deal, K. A.; Brechbiel, M. W.; Stabin, M.; Bochsler, P. N.; Mirzadeh, S.; Kennel, S. J. Comparison of Actinium Chelates: Tissue Distribution and Radiotoxicity. *Nucl. Med. Biol.* **1999**, *26*, 581–589.

42. Beyer, G. J.; Bergmann, R.; Schomäcker, K.; Rösch, F.; Schäfer, G.; Kulikov, E. V.; Novgorodov, a. F. Comparison of the Biodistribution of 225 Ac and Radio-Lanthanides as Citrate Complexes. *Isotopenpraxis* **1990**, *26*, 111–114.

43. Miederer, M.; Henriksen, G.; Alke, A.; Mossbrugger, I.; Quintanilla-Martinez, L.; Senekowitsch-Schmidtke, R.; Essler, M. Preclinical evaluation of the alpha-particle generator nuclide 225Ac for somatostatin receptor radiotherapy of neuroendocrine tumors. *Clin. Cancer Res.* **2008**, *14*, 3555–61.

44. Mcdevitt, M. R.; Ma, D.; Lai, L. T.; Simon, J.; Borchardt, P.; Frank, R. K.; Wu, K.; Pellegrini, V.; Curcio, M. J.; Miederer, M.; Bander, N. H.; Scheinberg, D. A. Tumor Therapy with Targeted Atomic Nanogenerators. *Science (80-.).* **2001**, *294*, 1537–1541.

45. Borchardt, P. E.; Yuan, R. R.; Miederer, M.; Mcdevitt, M. R.; Scheinberg, D. A. Targeted Actinium-225 in Vivo Generators for Therapy of Ovarian Cancer. *Cancer Res.* **2003**, *63*, 5084–5090.

1

46. Staudacher, A. H.; Bezak, E.; Borysenko, A.; Brown, M. P. Targeted α-therapy using 227Th-APOMAB and cross-fire antitumour effects: preliminary in-vivo evaluation. *Nucl. Med. Commun.* **2014**, *35*, 1284–90.

47. Arazi, L.; Cooks, T.; Schmidt, M.; Keisari, Y.; Kelson, I. Treatment of solid tumors by interstitial release of recoiling short-lived alpha emitters. *Phys. Med. Biol.* **2007**, *52*, 5025–42.

48. Cooks, T.; Schmidt, M.; Bittan, H.; Lazarov, E.; Arazi, L.; Kelson, I.; Keisari, Y. Local control of lung derived tumors by diffusing alpha-emitting atoms released from intratumoral wires loaded with radium-224. *Int. J. Radiat. Oncol. Biol. Phys.* **2009**, *74*, 966–73.

49. Cooks, T.; Tal, M.; Raab, S.; Efrati, M.; Reitkopf, S.; Lazarov, E.; Etzyoni, R.; Schmidt, M.; Arazi, L.; Kelson, I.; Keisari, Y. Intratumoral 224 Ra-Loaded Wires Spread Alpha-Emitters Inside Solid Human Tumors in Athymic Mice Achieving Tumor Control. *Anticancer Res.* **2012**, *32*, 5315–5321.

50. Horev-Drori, G.; Cooks, T.; Bittan, H.; Lazarov, E.; Schmidt, M.; Arazi, L.; Efrati, M.; Kelson, I.; Keisari, Y. Local control of experimental malignant pancreatic tumors by treatment with a combination of chemotherapy and intratumoral 224radium-loaded wires releasing alpha-emitting atoms. *Transl. Res.* **2012**, *159*, 32–41.

51. Confino, H.; Hochman, I.; Efrati, M.; Schmidt, M.; Umansky, V.; Kelson, I.; Keisari, Y. Tumor ablation by intratumoral Ra-224-loaded wires induces anti-tumor immunity against experimental metastatic tumors. *Cancer Immunol. Immunother.* **2014**.

52. Piotrowska, A.; Leszczuk, E.; Bruchertseifer, F.; Morgenstern, A.; Bilewicz, A. Functionalized NaA nanozeolites labeled with (224,225)Ra for targeted alpha therapy. *J. Nanoparticle Res.* **2013**, *15*, 2082.

53. Sofou, S.; Thomas, J. L.; Lin, H.; McDevitt, M. R.; Scheinberg, D. a; Sgouros, G. Engineered liposomes for potential alpha-particle therapy of metastatic cancer. *J. Nucl. Med.* **2004**, *45*, 253–60.

54. Jonasdottir, T. J.; Fisher, D. R.; Borrebaek, J.; Bruland, O. S.; Larsen, R. H. First in vivo evaluation of liposome-encapsulated 223Ra as a potential alpha-particle-emitting cancer therapeutic agent. *Anticancer Res.* **2006**, *26*, 2841–8.

55. Wang, G.; de Kruijff, R. M.; Rol, A.; Thijssen, L.; Mendes, E.; Morgenstern, A.; Bruchertseifer, F.; Stuart, M. C. A.; Wolterbeek, H. T.; Denkova, A. G. Retention studies of recoiling daughter nuclides of 225Ac in polymer vesicles. *Appl. Radiat. Isot.* **2014**, *85*, 45–53.

56. Woodward, J.; Kennel, S. J.; Stuckey, A.; Osborne, D.; Wall, J.; Rondinone, A. J.; Standaert, R. F.; Mirzadeh, S. LaPO4 nanoparticles doped with actinium-225 that partially sequester daughter radionuclides. *Bioconjug. Chem.* **2011**, *22*, 766–76.

57. McLaughlin, M. F.; Woodward, J.; Boll, R. a; Wall, J. S.; Rondinone, A. J.; Kennel, S. J.; Mirzadeh, S.; Robertson, J. D. Gold coated lanthanide phosphate nanoparticles for targeted alpha generator radiotherapy. *PLoS One* **2013**, *8*, e54531.

58. Pant, K.; Sedl????ek, O.; Nadar, R. A.; Hrub??, M.; Stephan, H. Radiolabelled Polymeric Materials for Imaging and Treatment of Cancer: Quo Vadis? *Adv. Healthc. Mater.* 2017, *6*.

59. Stockhofe, K.; Postema, J. M.; Schieferstein, H.; Ross, T. L. Radiolabeling of nanoparticles and polymers for PET imaging. *Pharmaceuticals* **2014**, *7*, 392–418.

60. Park, J. H.; Lee, S.; Kim, J. H.; Park, K.; Kim, K.; Kwon, I. C. Polymeric nanomedicine for cancer therapy. *Prog. Polym. Sci.* 2008, *33*, 113–137.

61. Simone, E. A.; Dziubla, T. D.; Muzykantov, V. R. Polymeric carriers: role of geometry in drug delivery. *Expert Opin. Drug Deliv.* **2008**, *5*, 1283–1300.

62. Discher, B. M.; Won, Y.-Y.; Ege, D. S.; Lee, J. C.-M.; Bates, F. S.; Discher, D. E.; Hammer, D. A. Polymersomes: Tough Vesicles Made from Diblock Copolymers. *Science (80-.).* **1999**, *284*, 1143–1146.

63. Sanson, C.; Schatz, C.; Le Meins, J.-F.; Brûlet, A.; Soum, A.; Lecommandoux, S. Biocompatible and Biodegradable Poly(trimethylene carbonate)- *b* -Poly(l -glutamic acid) Polymersomes: Size Control and Stability. *Langmuir* **2010**, *26*, 2751–2760.

64. Brinkhuis, R. P.; Stojanov, K.; Laverman, P.; Eilander, J.; Zuhorn, I. S.; Rutjes, F. P. J. T.; Hest, J. C. M. Van Size Dependent Biodistribution and SPECT Imaging of 111In-Labeled Polymersomes. *Bioconjug. Chem.* **2012**, *23*, 958–965.

65. Upadhyay, K. K.; Bhatt, A. N.; Castro, E.; Mishra, A. K.; Chuttani, K.; Dwarakanath, B. S.; Schatz, C.; Le Meins, J.-F.; Misra, A.; Lecommandoux, S. In vitro and in vivo evaluation of docetaxel loaded biodegradable polymersomes. *Macromol. Biosci.* **2010**, *10*, 503–512.

66. Wang, G.; de Kruijff, R. M.; Stuart, M. C. A.; Mendes, E.; Wolterbeek, H. T.; Denkova, A. G. Polymersomes as radionuclide carriers loaded via active ion transport through the hydrophobic bilayer. *Soft Matter* **2013**, *9*, 727–734.

67. Lee, J. S.; Ankone, M.; Pieters, E.; Schiffelers, R. M.; Hennink, W. E.; Feijen, J. Circulation kinetics and biodistribution of dual-labeled polymersomes with modulated surface charge in tumor-bearing mice: Comparison with stealth liposomes. *J. Control. Release* **2011**, *155*, 282–288.

68. Wang, G.; de Kruijff, R. M.; Abou, D.; Ramos, N.; Mendes, E.; Franken, L. E.; Wolterbeek, H. T.; Denkova, a. G. Pharmacokinetics of Polymersomes Composed of Poly(Butadiene-Ethylene Oxide); Healthy versus Tumor-Bearing Mice. *J. Biomed. Nanotechnol.* **2016**, *12*, 320–328.

2

Tailoring Radiolabelled Polymersomes for Biomedical Applications

Abstract

Polymersomes, vesicles composed of amphiphilic block copolymers, can serve as carriers of radionuclides for diagnostic imaging and therapeutic applications. Recently, Wang et al. have shown that the aqueous cavity of these polymersomes can be radiolabelled with the radionuclide ^{111}In [1]. Being able to select radionuclides based on their half-life or decay mode will allow for personalized treatment with either beta or alpha emitters, while the carriers' biodistribution and pharmacokinetics can be evaluated simultaneously. This paper outlines procedures for the radiolabelling of polymersomes with gamma-, beta- and alpha-emitting radionuclides. The loading conditions and efficiencies of ^{64}Cu, ^{67}Cu, ^{140}La, ^{177}Lu, ^{213}Bi, and ^{225}Ac in polymersomes composed of PBd-PEO have been optimized for each specific radionuclide. A strong dependence on the choice of both lipophilic ligand and hydrophilic chelate was observed. The influence of different parameters such as pH, loading time, polymersome, and chelate concentration was determined. High loading efficiencies have been obtained for all radionuclides. Simultaneous encapsulation of ^{225}Ac and ^{111}In, as well as ^{64}Cu with either ^{213}Bi or ^{111}In was performed achieving loading efficiencies around 70%, which means they could be used for theranostic studies. The range of radionuclides presented enables polymersomes to be used as both diagnostic and therapeutic agents.

Introduction

Vesicles composed of amphiphilic block copolymers, called polymersomes, are an emerging type of nano-carrier suitable for the delivery of drugs to tumour sites [2–4]. Because of the high molecular weight and the large variety of block copolymers that can be engineered to self-assemble into vesicles, they have an increased mechanical stability, reduced permeability, and their relevant physicochemical properties like membrane thickness can more easily be fine-tuned than their lipid counterparts [5–7]. Studies on the in vivo properties of polymersomes have proven their biocompatibility [8]. Their aqueous cavity can be loaded with hydrophilic drugs [9], proteins [10–12], peptides [13], DNA (deoxyribonucleic acid) and RNA (ribonucleic acid) fragments [14,15], whilst the hydrophobic membrane can be used to enclose water-insoluble drugs like paclitaxel or docetaxel [16]. Due to the wide range of molecules that can be transported, there is a growing interest in using polymersomes to treat several types of cancer [9–11,13,17,18]. Targeted delivery by polymersomes could help to attack diseases such as HIV (human immunodeficiency virus) [19–22] and cardiac fibrosis [23]. Furthermore, different ligands can easily be attached to the hydrophilic corona, enabling the attachment of antibodies or peptides for active targeting of tumour cells if necessary.

In order to determine the fate of polymersomes in vivo, it is important to be able to track them in a non-invasive manner. Loading gamma-emitting radionuclides in the aqueous cavity of preformed polymersomes would allow for the evaluation of the nano-carriers' biodistribution and pharmacokinetics using non-invasive nuclear imaging techniques such as SPECT and PET. Encapsulating beta- and alpha-emitters on the other hand, would allow for them to be used therapeutically. However, the number of studies on the radiolabelling of polymersomes, since their discovery 15 years ago [3], is limited [1,24,25]. Options for the radiolabelling of the aqueous cavity of liposomes on the other hand are numerous, and include the entrapping of radiotracers like ^{111}In [26], ^{99m}Tc [27,28], ^{177}Lu [29], and ^{225}Ac [30,31] in the aqueous core, providing options for SPECT or PET tracing of liposomes in in vivo studies, as well as their use in radiotherapeutic studies. However, polymersomes might be more appropriate than their lipid counterparts in certain applications, especially considering their better stability [32] and potentially longer circulation half-life [33].

In this chapter, we present specific radionuclide loading methods for polymersomes with various SPECT, PET and therapeutic isotopes (Table 3). The radiolabelling of the aqueous cavity was chosen rather than surface labelling, as this allows for increased radionuclide retention in the polymersome. The radiolabelling results of ^{111}In in this study are briefly mentioned to complete the overview presented, for details we refer to [1].

2

Table 3: Applied radionuclides (bold-faced), their decay characteristics and (potential) clinical use [34].

Radionuclides and their decay chain	Half-life	Decay modes	Final decay product	Clinical use
^{111}In	2.8 d	ε	^{111}Cd	SPECT
^{64}Cu	12.7 h	β^+, β^-, ε	^{64}Ni	PET,
			^{64}Zn	Radionuclide therapy
^{67}Cu	61.9 h	β^-	^{67}Zn	Radionuclide therapy
^{225}Ac	10.0 d	α		Alpha-radionuclide therapy
^{221}Fr	4.8 m	α		
^{217}At	32.3 ms	α		
^{213}Bi	45.6 m	β^-		
^{213}Po	4.2 μs	α		
^{209}Pb	3.3 h	β^-	^{209}Bi	
^{140}La	40.3 h	β^-	^{140}Ce	Radionuclide therapy
^{177}Lu	6.6 d	β^-	^{177}Hf	SPECT, radionuclide therapy

Materials and methods

Chemicals

The poly(butadiene-b-ethylene oxide) block copolymer used in this study was purchased from Polymer Source (Quebec, Canada), with ratios of the weight average molecular weight to the number average molecular weight (Mw/Mn) of less than 1.10. The radioactive isotope ^{111}In was a kind gift from the Nuclear Medicine section of the Erasmus Medical Center (Rotterdam, the Netherlands) and had a specific activity of 1.72 MBq pmol^{-1}. The ^{177}Lu was a contribution from IDB Holland B.V. (Baarle-Nassau, the Netherlands). Dry ^{225}Ac and a ^{225}Ac/^{213}Bi generator were prepared at the Directorate for Nuclear Safety and Security (Karlsruhe, Germany). All other isotopes were irradiated and prepared at the Reactor Institute Delft (Delft, the Netherlands). DTPA (diethylenetriamine pentaacetic acid) and tropolone (2-Hydroxy-2,4,6-cycloheptatrien-1-one) were aquired from Merck (Darmstadt, Germany). Ammonium acetate, acetic acid, and HCl were from J.T. Baker (Phillipsburg, USA). The experiments were performed using Econo scintillation vials from Perkin Elmer Nederland BV (Groningen, the Netherlands). All other chemicals were purchased from Sigma-Aldrich (Zwijndrecht, the Netherlands).

Radionuclide production

Both ^{64}Cu and ^{67}Cu were produced in the SmallBeBe facility of the 2 MW research reactor at the Reactor Institute Delft. ^{64}Cu was created by irradiating 40 mg of a ^{64}Zn film with neutrons at a thermal flux of 3.7 x 10^{17} m^{-2} s^{-1}, epithermal flux of 1.66 x 10^{16} m^{-2} s^{-1} and fast flux of 3.47 x 10^{17} m^{-2} s^{-1} for 12 hours. After a cooling time of 3 hours, the film was dissolved in an 8 M HCl (hydrochloric acid) solution. This solution was passed through a 2x8 Dowex resin column equilibrated with 8 M HCl, and the ^{64}Cu was extracted by a wash with 7 ml 1 M HCl. After evaporation of the solvent, the vial was rinsed with 600 µl MilliQ water to collect the ^{64}Cu. ^{67}Cu was created according to the same procedure, following the irradiation of 150 mg of ^{67}Zn powder for 100 hours. ^{213}Bi was obtained by eluting the ^{225}Ac/^{213}Bi generator with a 50/50 solution of 0.2 M HCl and 0.2 M NaI at 0.15 ml/min into a vial containing 4 M ammonium acetate at pH 5.5. ^{140}La was produced in the BP4 facility of the Reactor Institute Delft. Here, 1 mg of LaNO$_3$ was irradiated for 6 hours with neutrons at a thermal flux of 3.1 x 10^{16} m^{-2} s^{-1}, epithermal flux of 7.20 x 10^{14} m^{-2} s^{-1} and fast flux of 2.60 x 10^{15} m^{-2} s^{-1} after which it was left to cool for 1 hour. The ^{140}La was subsequently dissolved in 0.01 M HCl.

Polymersome formation

Polymersomes were prepared by dissolving 0.5 – 5 mg/ml block copolymers in a 10 mM HEPES (4-(2- hydroxyethyl)-1-piperazineethanesulfonic acid) buffer solution at pH 7.4, containing a known concentration of hydrophilic chelator. The chelator used depended on the radionuclide loaded, and will be detailed in the paragraphs below. After one week of stirring, the block copolymers had self-assembled into polymersomes. The size of the polymersomes was adjusted by extrusion through polycarbonate filters with a cut-off membrane of 800, 400, 200 or 100 nm, according to the required size. The remaining free hydrophilic chelate was separated from the polymersomes using a Sephadex G-25 medium mesh size exclusion column ($D \times L = 1 \times 30$ cm). The fractions containing the polymersomes were used for the loading experiments.

Loading of ^{111}In, ^{64}Cu, ^{67}Cu and ^{213}Bi

Loading of ^{111}In, ^{64}Cu, ^{67}Cu and ^{213}Bi in polymersomes was performed at room temperature (20 ± 1°C) with tropolone as ionophore and 10 mM HEPES as buffer solution. The radionuclide solution was added to 10 µL of 2 mM tropolone and 200 µL HEPES buffer at pH 7.4. After 10 minutes, 800 µL polymersome solution was added to the vial. For the loading of ^{111}In and ^{213}Bi, the encapsulated chelator was 1 mM DTPA, while ^{64}Cu and ^{67}Cu were loaded into polymersomes containing 1 mM DTPA, EDTA, NTA (nitrilotriacetic acid), DOTA (1,4,7,10-tetraazacyclododecane-1,4,7,10-tetraacetic acid), or 1 or 5 mM cyclam (1,4,8,11-tetraazacyclotetradecane). For the simultaneous loading of ^{64}Cu and ^{111}In or ^{213}Bi, the polymersomes were prepared in a 10 mM HEPES buffer solution with 1 mM DTPA and 1 mM cyclam. After a predetermined loading time, unencapsulated radionuclides were removed by passing the solution through a PD10 desalting column packed with G-25 M Sephadex. The eluate was portioned per mL, and the activity in the fractions was measured using a high-purity germanium (HPGe) detector.

2

Loading of [140]La and [225]Ac

Radiolabelling the aqueous cavity of the polymersomes with [140]La or [225]Ac was performed according to a previously published study by Wang et al. [25]. In short, the radionuclide was added to a thin film of 0.1 mg calcium ionophore (A23187) in 200 µL 10 mM HEPES buffer at pH 7.4. To improve the loading efficiency, the complexation of [140]La to A23187 was performed in 100 µL $CHCl_3$, after which the $CHCl_3$ was evaporated and 200 µL 10 mM HEPES buffer at pH 7.4 was added. The loading was performed using 5 mg/ml polymersomes containing 1 mM DTPA as hydrophilic chelate at room temperature. Unencapsulated radionuclides were separated from the polymersomes by passing the solution through a PD10 column.

Loading of [177]Lu

The ^{177}Lu was supplied in 0.05 M HCl with a specific activity of 2.66×10^3 GBq/g, and upon arrival diluted in 1 mL 0.05 M HNO_3. The loading method was based on the method described by Wang et al. [29] 300 µL of 68 mM oxine (8-hydroxyquinoline), 300 µL 10 mM HEPES buffer at pH 7.4 and a few µL containing about 50 kBq ^{177}Lu were combined in a scintillation vial and incubated at 50°C for 30 minutes. 400 µL polymersome solution (with either 1 mM DOTA or 1 mM DTPA encapsulated) were incubated with the ^{177}Lu-oxine solution for 30 minutes at either 40°C (DOTA) or room temperature (DTPA). Free ^{177}Lu was separated from encapsulated ^{177}Lu by passing the solution through a PD10 column.

Retention studies

To assess the loss of radiolabel, retention studies were performed by adding 1 mL of 1 mM DTPA (or 1 mM cyclam in the case of ^{64}Cu retention) to a 1 mL polymer solution with encapsulated radionuclides. After 24 hours, the unencapsulated radionuclides chelated by DTPA were separated from the polymersome solution using a PD10 column, where the elution was portioned per ml, and the activity in the fractions was determined using a HPGe detector.

Dynamic light scattering (DLS)

To characterize the polymersomes, a DLS apparatus consisting of a JDS Uniphase 633 nm 35 mW laser, an ALV sp 125 s/w 93 goniometer, a fibre detector and a Perkin Elmer photon counter was used, with an ALV-5000/epp correlator and software to complete the set-up. The DLS tubes were immersed in a toluene-containing temperature-regulated bath (at 20 °C). The intensity autocorrelation function was determined at 90°. The data was fitted using the Contin method, and the hydrodynamic radius of the polymersomes was determined with the Stokes–Einstein equation.

Cryogenic transmission electron microscope (Cryo-TEM)

4 µL of the polymersome solution containing 2 mg/mL block copolymers was deposited on a holey carbon film (Quantifoil 1.2/1.3, Cu 200 mesh grids) supported on a TEM grid. The drop was blotted for two seconds with filter paper in order to obtain a thin layer on the grid, and subsequently vitrified by rapidly immersing in liquid ethane (Leica EM GP version 16222032). The sample was inserted into

a cryo-holder (Gatan model 626) and then transferred to a Jeol JEM 1400 TEM. Images were obtained at an acceleration voltage of 120 keV.

Results and Discussion

In this work, the radiolabelling potential of the aqueous cavity of polymersomes has been assessed for a number of diagnostic or therapeutic radionuclides. The vesicles were prepared containing a hydrophilic chelate in their aqueous cavity. Upon formation, radionuclides were transported to the polymersome interior complexed by a lipophilic ligand, and their loading efficiency has been optimized. In Table 3, an overview of the used radionuclides and their decay characteristics is given. The polymersomes are composed of PBd-PEO block copolymers, having a molecular weight of 1800 g/mol and 900 g/mol respectively. In Figure 3 A, a Cryo-TEM image of the formed polymersomes is displayed. Here, the polymersomes have been extruded to 200 nm, as characterized by DLS (Figure 3 B).
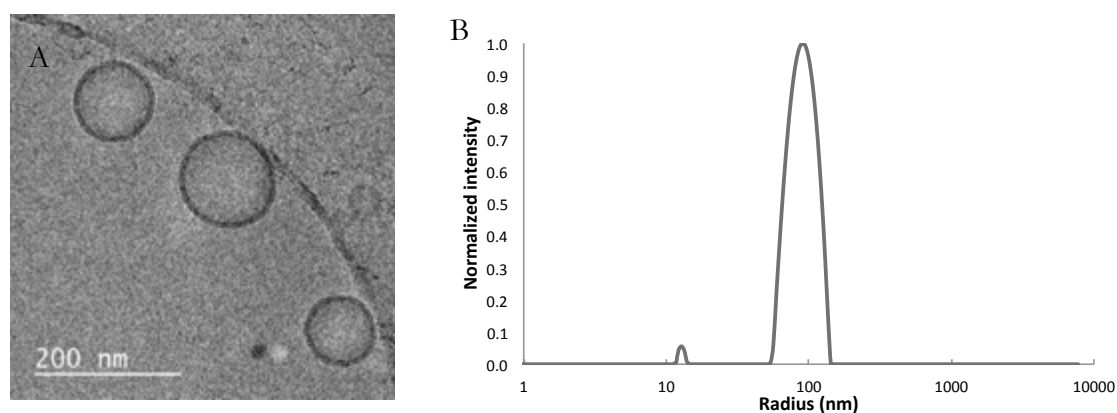
Figure 3: A: Cryo-TEM image of polymersomes composed of PBd-PEO block copolymers extruded to an average diameter of 200 nm through polycarbonate filters, and B: the size distribution of polymersomes extruded through 200 nm polycarbonate filters as characterized by DLS, giving an average hydrodynamic radius of 91 nm

Loading and retention of the copper isotopes ^{64}Cu and ^{67}Cu

We have investigated the encapsulation of two copper isotopes, ^{64}Cu and ^{67}Cu, in polymersomes. For the optimization of the loading process, five different hydrophilic chelators; DOTA, EDTA, NTA, DTPA, and cyclam, have been assessed. The stability constants of copper with the aforementioned hydrophilic chelators can be found in Table 4.

Table 4: Copper-chelator complex stability constants with the relevant chelators and ligand, where $K_{ML}=[ML]/[M][L]$ with [M] the concentration of the metal ion, and [L] the concentration of the chelator.

Complex	Stability constant K_{ML}
DOTA	22.5 [35]
EDTA	19.0 [35]
NTA	12.9 [35]
DTPA	21.4 [35]
Cyclam	27.2 [35]
Tropolone	10.0 [36]/ 8.3 [37,38]

In Figure 4, the loading efficiency of ^{64}Cu in polymersomes containing the different chelators is displayed, with tropolone as lipophilic ligand. Experiments with oxine as ligand yielded loading efficiencies lower than 5 % for all chelators used. A significantly higher loading efficiency can be observed for the polymersomes containing 1 mM EDTA, DTPA and cyclam as compared to those with DOTA or NTA. The near-zero loading efficiency of ^{64}Cu in NTA containing polymersomes corresponds to its much lower stability constant (K_{ML} = 12.9) as compared to the other hydrophilic chelators. Its stability constant is close to that of the copper-tropolone complex (K_{ML} = 10.0 / 8.3), resulting in a low amount of copper ions binding to NTA in the polymersomes. The low loading efficiency of ^{64}Cu in the DOTA polymersomes is most likely explained by either the relatively high pH of the polymersomes (7.4) as compared to the pH at which DOTA-containing liposomes are radiolabelled with [64]Cu (4.0 – 5.9) [39], or the fact that the reaction took place at RT (room temperature), whereas ^{64}Cu-DOTA is usually labelled at higher temperatures [40,41].

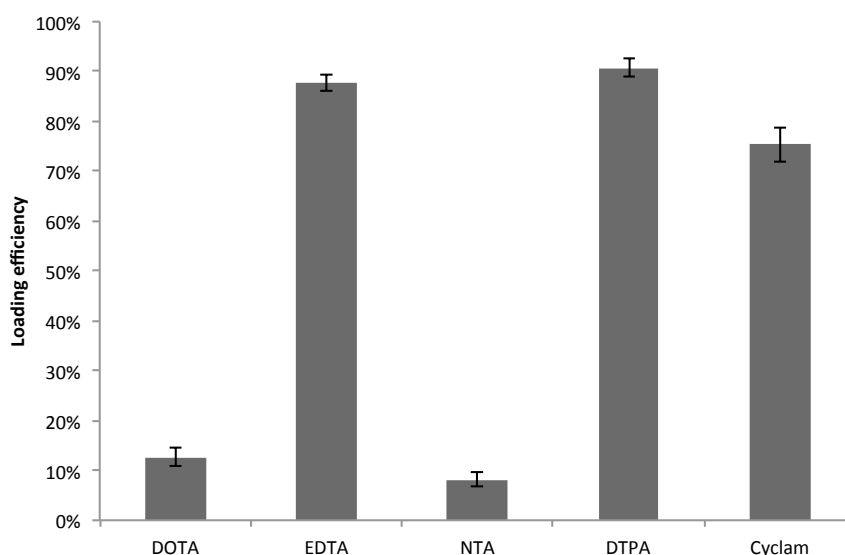Figure 4: Loading efficiency of PBd_{1800}-PEO_{900} polymersomes (0.5 mg/mL) containing 1 mM of different chelators with 20 µM tropolone as ligand, loaded from a 0.15 MBq ^{64}Cu solution at an 1 h incubation time.

The other three chelates, EDTA, DTPA and cyclam, display favourable loading efficiencies. When considering the time-dependence of loading ^{64}Cu in polymersomes containing either of these three chelators, it was found that those with either EDTA or DTPA have very fast loading kinetics, with near-optimal loading within 15 minutes (Table 5) The cyclam polymersomes appear to have slower loading kinetics at the used concentration, where an increase in the loading time from 15 to 30 min results in a corresponding increase in loading efficiency from 42 ± 1% to 78 ± 1%.

Table 5: Loading efficiency of ^{64}Cu in 200 nm diameter polymersomes at different incubation times, for 0.5 mg/mL polymersomes containing either 1 mM EDTA, cyclam, or DTPA.

Loading time (min) (0.15 MBq ^{64}Cu)	Hydrophilic chelate		
	1 mM EDTA	1 mM Cyclam	1 mM DTPA
15	81 ± 3%	42 ± 1%	83 ± 0.2%
30	80 ± 2%	78 ± 1%	85 ± 4%
60	88 ± 2%	75 ± 3%	91 ± 2%

Increasing the polymersome and/or chelator concentration to 5 mg/mL and/or 5 mM respectively, cyclam-containing polymersomes reach a loading efficiency of 93 ± 4% within 15 minutes. Therefore, either a high polymersome or cyclam concentration is required for optimal loading efficiency and speed, whereas at low polymersome concentrations a longer incubation time has to be provided. To determine if larger activities can be loaded, increasing amounts ranging from 0.17 - 13 MBq of ^{64}Cu have been loaded into polymersomes. A consistently high loading efficiency was found at all levels of radioactivity. Assessment of the retention of ^{64}Cu in polymersomes was done by challenging 1 mL of radiolabelled polymersomes with 1 mL 1 mM cyclam. After 24 hours, 87 ± 3% of the ^{64}Cu is still retained in the cyclam-containing polymersomes, whereas only 68 ± 2% was retained in EDTA-containing polymersomes. Considering the difference in stability constant (Table 4), it follows that the more stable ^{64}Cu-cyclam complex is retained better, allowing for its safe in vivo use.

The longer-lived beta-emitter ^{67}Cu, having the same physicochemical properties as ^{64}Cu, has also been encapsulated in polymersomes containing cyclam as hydrophilic chelator. At a polymersome concentration of 0.5 mg/mL containing 5 mM cyclam, high loading efficiencies were already obtained after 15 minutes of loading time (83 ± 3%), which increased slightly after 30 minutes (95 ± 1%). We have thus shown that both ^{64}Cu and ^{67}Cu can efficiently be loaded into polymersomes, and with cyclam as chelator is sufficiently well retained in the aqueous cavity, allowing for the use of copper isotopes in following the in vivo performance of polymersomes containing (radio) therapeutics.

Loading of ^{177}Lu in polymersomes

^{177}Lu is a beta-emitting radionuclide with a longer half-life (6.7 days) and a relatively short penetration depth as compared to the more commonly used beta emitter ^{90}Y. These differences translate in ^{177}Lu being a more suitable radionuclide in the treatment of smaller metastases, likely resulting in a lower bone marrow toxicity [42]. It also emits a gamma ray allowing it to be followed in vivo with SPECT imaging. The loading of ^{177}Lu was based on a procedure described by Wang et al., who loaded DOTA-

2

containing liposomes with [29] ^{177}Lu with high efficiency (>90%) [29]. In polymersomes at a concentration of 0.5 mg/ml, we have obtained an efficiency of 25 ± 4%, which was further optimized to 74 ± 10% by increasing the polymersome concentration to 5 mg/ml. Variations of the pH, loading time and lipophilic ligand did not further improve loading efficiencies. The difference between the results of Wang et al. and the loading efficiency presented in this chapter is likely caused by a lower polymersome concentration as compared to the liposome concentration, although this cannot be substantiated as there is no mention of liposome concentration in their paper. Another explanation can be found in their removal of unlabelled ^{177}Lu prior to adding the ^{177}Lu-oxine to the liposomes. For the labelling of this complex they found an efficiency of around 70%. In the present study, the unlabelled ^{177}Lu was only removed after the loading of the polymersomes, thus contributing to the loading efficiency determination. Further improvements of the loading efficiency to 87 ± 3% were obtained by changing the hydrophilic chelator to DTPA. An explanation for the lower loading efficiency of the polymersomes containing DOTA as compared to DTPA might be due to the time- and temperature dependence of DOTA labelling [43], as the labelling of ^{177}Lu-DOTA complexes usually takes place at higher (>60°C) temperatures [44]. In our studies, labelling of the DOTA-containing vesicles was performed at 40°C. The retention of ^{177}Lu in DOTA polymersomes after 24 h was found to be 77 ± 2%, and in DTPA polymersomes 85 ± 2%, yielding the ^{177}Lu DOTA formulation suitable for further in vivo testing.

Loading efficiency of ^{140}La

Because of the chemical similarity between ^{140}La and ^{225}Ac, a similar radionuclide loading method was adopted as used by Wang et al. [25] for the loading of ^{225}Ac. Here, loading efficiencies of 60 ± 3% were obtained for the loading of ^{140}La in polymersomes. An improvement on this method was implemented by complexing the ^{140}La to the A23187 film in the organic solvent chloroform (CHCl$_3$). When the complexation takes place in an aqueous solvent, only part of the ^{140}La binds to the calcium ionophore film, likely due to the small surface area in which the lanthanum, dissolved in 200 μl HEPES, is in contact with the film. Allowing the complexation to take place in CHCl$_3$ increased the reaction surface of the ^{140}La with the A23187, and increased the loading efficiency to 80 ± 5%.

^{213}Bi and ^{225}Ac

For radiotherapy of smaller metastases, alpha-emitters like ^{213}Bi and ^{225}Ac are ideal candidates. The short-lived ^{213}Bi is optimal for fast-targeting applications, and carries the additional advantage that it has only 1 alpha-particle in its main decay chain, so the recoil effect is not a concern. However, for longer targeting and irradiation times, ^{225}Ac is much more suitable. Therefore, here we have encapsulated both the daughter nuclide ^{213}Bi and its mother ^{225}Ac. Due to its half-life, the loading procedure for ^{213}Bi had to be optimized for short times. In Figure 5 the loading efficiency has been plotted as a function of time. A maximum loading efficiency of 91 ± 3% has been reached after an incubation time of 15 minutes.
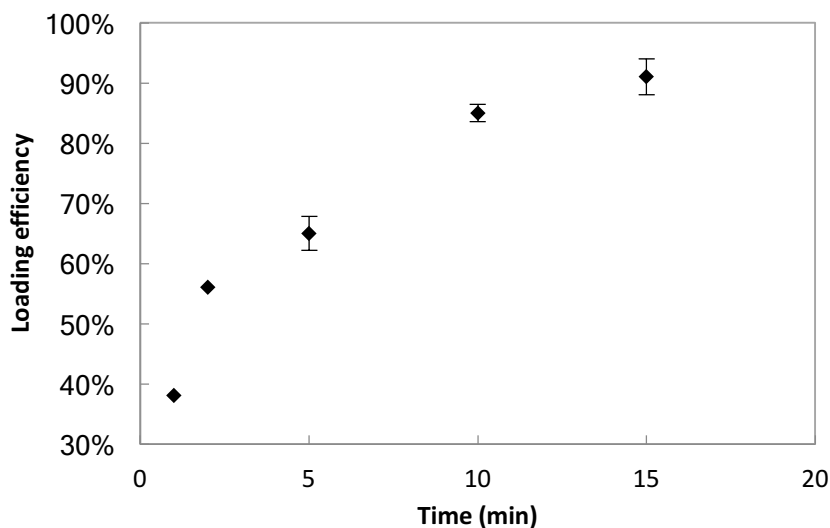
Figure 5: Loading efficiency of [213]Bi in 0.5 mg/mL 1 mM DTPA 200 nm polymersomes at different incubation times.

The encapsulation of [225]Ac in polymersomes has been tested at different incubation times raging between 30 minutes and 8 hours. An average loading efficiency of 66 ± 4% has been obtained, which was already reached after 30 minutes. Due to the long half-life of [225]Ac, there was no need to test shorter incubation times. Similar to [140]La, the low loading efficiency was mainly due to a relatively large amount of [225]Ac which complexed to calcium ionophore on the bottom of the vial instead of remaining in solution. Allowing the complexation to take place in $CHCl_3$ prior to the addition of the polymersomes increased the loading efficiency to 84 ± 5%. The loading efficiency of [225]Ac in different diameter polymersomes was also assessed, with polymersome diameters ranging from 100 nm to 800 nm. The loading efficiency was quite constant (Figure 6), so at all polymersome diameters [225]Ac can reliably be loaded. In an earlier published study by Wang et al. was found that the [225]Ac is retained very well in the polymersomes, with less than 7% loss of radiolabel 30 days after encapsulating the radionuclide [25].
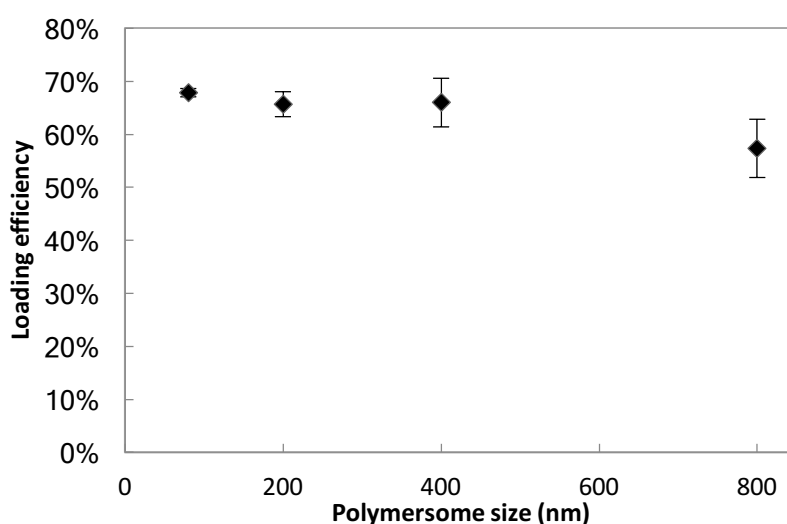

Figure 6: The loading efficiency of [225]Ac in 5 mg/mL polymersomes containing 1 mM DTPA, at different polymersome sizes.

2

Simultaneous loading of radionuclides

The simultaneous encapsulation of two or more radionuclides in polymersomes could be very advantageous for medical applications. Gamma-emitters could be used to track the location of the polymersomes, while the encapsulated beta- or alpha-emitters treat the tumour. Here, as a proof-of-principle, three radionuclide combinations have simultaneously been loaded in polymersomes.

Table 6 shows the loading efficiency for the combined loading of ^{111}In and ^{225}Ac, as well as ^{64}Cu combined with ^{111}In or ^{213}Bi, proving the feasibility of dual-isotope loading. Especially for in vivo studies with ^{225}Ac, the addition of a gamma-emitter allows for following the location of the polymersomes containing very small amounts of the alpha-emitter.

Table 6: Loading efficiencies for different combined loadings: ^{64}Cu and ^{111}In or ^{64}Cu and ^{213}Bi in 0.5 mg/mL 1 mM DTPA 1 mM cyclam polymersomes, or ^{111}In and ^{225}Ac in 5 mg/ml 1 mM DTPA polymersomes.

Loading efficiency ^{111}In / ^{225}Ac		Loading efficiency ^{64}Cu / ^{111}In		Loading efficiency ^{64}Cu / ^{213}Bi	
^{111}In	^{225}Ac	^{64}Cu	^{111}In	^{64}Cu	^{213}Bi
80 ± 8%	62 ± 5%	71 ± 7%	82 ± 2%	69 ± 20%	66 ± 12%

Conclusions

Concluding, in this study we have optimized the loading efficiency for a range of radionuclides in polymersomes. We have shown that high loading efficiencies can be obtained for alpha-, beta- and gamma-emitting radionuclides, where in many cases radiolabelling efficiencies around 90% have been obtained. The binding strength of a radionuclide with the encapsulated hydrophilic chelator has been found to influence both the radiolabelling efficiency, as well as the radionuclide retention. Variations in loading time, polymersome concentration, or choice of lipophilic ligand can likewise largely influence the radiolabelling efficiency. A proof-of-principle study with the dual labelling of polymersomes with two radionuclides allows for the simultaneous tracking of polymersomes with e.g. SPECT or PET, whilst using an encapsulated alpha- or beta-emitter to destroy tumour tissue. With the presented data, depending on the specific application, polymersomes can thus easily be radiolabelled for both diagnostic and therapeutic applications.

References

1. Wang, G.; de Kruijff, R. M.; Stuart, M. C. A.; Mendes, E.; Wolterbeek, H. T.; Denkova, A. G. Polymersomes as radionuclide carriers loaded via active ion transport through the hydrophobic bilayer. *Soft Matter* **2013**, *9*, 727–734.

2. Du, J.; O'Reilly, R. K. Advances and challenges in smart and functional polymer vesicles. *Soft Matter* **2009**, *5*, 3544.

3. Discher, B. M.; Won, Y.-Y.; Ege, D. S.; Lee, J. C.-M.; Bates, F. S.; Discher, D. E.; Hammer, D. A. Polymersomes: Tough Vesicles Made from Diblock Copolymers. *Science (80-.).* **1999**, *284*, 1143–1146.

4. Levine, D. H.; Ghoroghchian, P. P.; Freudenberg, J.; Zhang, G.; Therien, M. J.; Greene, M. I.; Hammer, D. a; Murali, R. Polymersomes: a new multi-functional tool for cancer diagnosis and therapy. *Methods* **2008**, *46*, 25–32.

5. Li, M.-H.; Keller, P. Stimuli-responsive polymer vesicles. *Soft Matter* **2009**, *5*, 927.

6. Rodríguez-García, R.; Mell, M.; López-Montero, I.; Netzel, J.; Hellweg, T.; Monroy, F. Polymersomes: smart vesicles of tunable rigidity and permeability. *Soft Matter* **2011**, *7*, 1532.

7. Qi, W. NIR-Emissive Polymersomal Markers for Molecular-Level Detection of Metastasis, University of Pennsylvania, 2011.

8. Photos, P. J.; Bacakova, L.; Discher, B.; Bates, F. S.; Discher, D. E. Polymer vesicles in vivo: correlations with PEG molecular weight. *J. Control. Release* **2003**, *90*, 323–34.

9. Du, Y.; Chen, W.; Zheng, M.; Meng, F.; Zhong, Z. PH-sensitive degradable chimaeric polymersomes for the intracellular release of doxorubicin hydrochloride. *Biomaterials* **2012**, *33*, 7291–7299.

10. Sun, H.; Meng, F.; Cheng, R.; Deng, C.; Zhong, Z. Reduction and pH dual-bioresponsive crosslinked polymersomes for efficient intracellular delivery of proteins and potent induction of cancer cell apoptosis. *Acta Biomater.* **2014**, *10*, 2159–68.

11. Li, S.; Meng, F.; Wang, Z.; Zhong, Y.; Zheng, M.; Liu, H.; Zhong, Z. Biodegradable polymersomes with an ionizable membrane: Facile preparation, superior protein loading, and endosomal pH-responsive protein release. *Eur. J. Pharm. Biopharm.* **2012**, *82*, 103–111.

12. Liu, G.; Ma, S.; Li, S.; Cheng, R.; Meng, F.; Liu, H.; Zhong, Z. The highly efficient delivery of exogenous proteins into cells mediated by biodegradable chimaeric polymersomes. *Biomaterials* **2010**, *31*, 7575–7585.

13. Lee, J. S.; Groothuis, T.; Cusan, C.; Mink, D.; Feijen, J. Lysosomally cleavable peptide-containing polymersomes modified with anti-EGFR antibody for systemic cancer chemotherapy. *Biomaterials* **2011**, *32*, 9144–53.

2

14. Christian, D. A.; Cai, S.; Bowen, D. M.; Kim, Y.; Pajerowski, J. D.; Discher, D. E. Polymersome carriers: From self-assembly to siRNA and protein therapeutics. *Eur. J. Pharm. Biopharm.* 2009, *71*, 463–474.

15. Lomas, H.; Du, J.; Canton, I.; Madsen, J.; Warren, N.; Armes, S. P.; Lewis, A. L.; Battaglia, G. Efficient encapsulation of plasmid DNA in pH-sensitive PMPC-PDPA polymersomes: Study of the effect of PDPA block length on copolymer-DNA binding affinity. *Macromol. Biosci.* 2010, *10*, 513–530.

16. Upadhyay, K. K.; Bhatt, A. N.; Castro, E.; Mishra, A. K.; Chuttani, K.; Dwarakanath, B. S.; Schatz, C.; Le Meins, J.-F.; Misra, A.; Lecommandoux, S. In vitro and in vivo evaluation of docetaxel loaded biodegradable polymersomes. *Macromol. Biosci.* 2010, *10*, 503–512.

17. Nahire, R.; Haldar, M. K.; Paul, S.; Ambre, A. H.; Meghnani, V.; Layek, B.; Katti, K. S.; Gange, K. N.; Singh, J.; Sarkar, K.; Mallik, S. Multifunctional polymersomes for cytosolic delivery of gemcitabine and doxorubicin to cancer cells. *Biomaterials* 2014, *35*, 6482–6497.

18. Chiang, W. H.; Huang, W. C.; Chang, C. W.; Shen, M. Y.; Shih, Z. F.; Huang, Y. F.; Lin, S. C.; Chiu, H. C. Functionalized polymersomes with outlayered polyelectrolyte gels for potential tumor-targeted delivery of multimodal therapies and MR imaging. *J. Control. Release* 2013, *168*, 280–288.

19. Sakaue, G.; Hiroi, T.; Nakagawa, Y.; Someya, K.; Iwatani, K.; Sawa, Y.; Takahashi, H.; Honda, M.; Kunisawa, J.; Kiyono, H. HIV mucosal vaccine: nasal immunization with gp160-encapsulated hemagglutinating virus of Japan-liposome induces antigen-specific CTLs and neutralizing antibody responses. *J. Immunol.* 2003, *170*, 495–502.

20. Malavia, N. K.; Zurakowski, D.; Schroeder, A.; Princiotto, A. M.; Laury, A. R.; Barash, H. E.; Sodroski, J.; Langer, R.; Madani, N.; Kohane, D. S. Liposomes for HIV prophylaxis. *Biomaterials* 2011, *32*, 8663–8668.

21. Garg, M.; Asthana, A.; Agashe, H. B.; Agrawal, G. P.; Jain, N. K. Stavudine-loaded mannosylated liposomes: in-vitro anti-HIV-I activity, tissue distribution and pharmacokinetics. *J. Pharm. Pharmacol.* 2006, *58*, 605–616.

22. Mamo, T.; Moseman, E. A.; Kolishetti, N.; Salvador-Morales, C.; Shi, J.; Kuritzkes, D. R.; Langer, R.; von Andrian, U.; Farokhzad, O. C. Emerging nanotechnology approaches for HIV/AIDS treatment and prevention. *Nanomedicine* 2010, *5*, 269–285.

23. Yang, J.; Hou, Y.; Ji, G.; Song, Z.; Liu, Y.; Dai, G.; Zhang, Y.; Chen, J. Targeted delivery of the RGD-labeled biodegradable polymersomes loaded with the hydrophilic drug oxymatrine on cultured hepatic stellate cells and liver fibrosis in rats. *Eur. J. Pharm. Sci.* 2014, *52*, 180–190.

24. Brinkhuis, R. P.; Stojanov, K.; Laverman, P.; Eilander, J.; Zuhorn, I. S.; Rutjes, F. P. J. T.; Hest, J. C. M. Van Size Dependent Biodistribution and SPECT Imaging of 111In-Labeled Polymersomes. *Bioconjug. Chem.* 2012, *23*, 958–965.

25. Wang, G.; de Kruijff, R. M.; Rol, A.; Thijssen, L.; Mendes, E.; Morgenstern, A.; Bruchertseifer, F.; Stuart, M. C. A.; Wolterbeek, H. T.; Denkova, A. G. Retention studies of recoiling daughter nuclides of 225Ac in polymer vesicles. *Appl. Radiat. Isot.* **2014**, *85*, 45–53.

26. Harrington, K. J.; Rowlinson-Busza, G.; Syrigos, K. N.; Uster, P. S.; Vile, R. G.; Stewart, J. S. W. Pegylated liposomes have potential as vehicles for intratumoral and subcutaneous drug delivery. *Clin. Cancer Res.* **2000**, *6*, 2528–2537.

27. Bao, A.; Goins, B.; Klipper, R.; Negrete, G.; Phillips, W. T. Direct 99mTc labeling of pegylated liposomal doxorubicin (Doxil) for pharmacokinetic and non-invasive imaging studies. *J. Pharmacol. Exp. Ther.* **2004**, *308*, 419–25.

28. Phillips, W. T.; Rudolph, A. S.; Goins, B.; Timmons, J. H.; Klipper, R.; Blumhardt, R. A simple method for producing a technetium-99m-labeled liposome which is stable in vivo. *Nucl. Med. Biol.* **1992**, *19*, 539–547.

29. Wang, H.-E.; Yu, H.-M.; Lu, Y.-C.; Heish, N.-N.; Tseng, Y.-L.; Huang, K.-L.; Chuang, K.-T.; Chen, C.-H.; Hwang, J.-J.; Lin, W.-J.; Wang, S.-J.; Ting, G.; Whang-Peng, J.; Deng, W.-P. Internal radiotherapy and dosimetric study for 111In/177Lu-pegylated liposomes conjugates in tumor-bearing mice. *Nucl. Instruments Methods Phys. Res.* **2006**, *569*, 533–537.

30. Sofou, S.; Thomas, J. L.; Lin, H.; McDevitt, M. R.; Scheinberg, D. a; Sgouros, G. Engineered liposomes for potential alpha-particle therapy of metastatic cancer. *J. Nucl. Med.* **2004**, *45*, 253–60.

31. Sofou, S.; Kappel, B. J.; Jaggi, J. S.; McDevitt, M. R.; Scheinberg, D. a; Sgouros, G. Enhanced retention of the alpha-particle-emitting daughters of Actinium-225 by liposome carriers. *Bioconjug. Chem.* **2007**, *18*, 2061–7.

32. Discher, D. E.; Eisenberg, A. Polymer vesicles. *Science (80-.).* **2002**, *297*, 967–73.

33. Discher, D. E.; Ortiz, V.; Srinivas, G.; Klein, M. L.; Kim, Y.; Christian, D.; Cai, S.; Photos, P.; Ahmed, F. Emerging Applications of Polymersomes in Delivery: from Molecular Dynamics to Shrinkage of Tumors. *Prog. Polym. Sci.* **2007**, *32*, 838–857.

34. National Nuclear Data Center Interactive Chart of Nuclides http://www.nndc.bnl.gov/chart/.

35. Wadas, T. J.; Wong, E. H.; Weisman, G. R.; Anderson, C. J. Coordinating radiometals of copper, gallium, indium, yttrium, and zirconium for PET and SPECT imaging of disease. *Chem. Rev.* **2010**, *110*, 2858–902.

36. Xue, H.; Sunda, W. G. Comparison of [Cu2+] Measurements in Lake Water Determined by Ligand Exchange and Cathodic Stripping Voltammetry and by Ion-Selective Electrode. *Environ. Sci. Technol.* **1997**, *31*, 1902–1909.

37. Bryant, B. E.; Fernelius, W. C.; Douglas, B. E. Formation Constants of Metal Complexes of Tropolone and Its Derivatives. *J. Am. Chem. Soc.* **1953**, *75*, 3784–3786.

38. Hirai, M.; Oka, Y. Stability of tropolone chelates of the bi- and tervalent metal ions. *Bull. Chem. Soc. Jpn.* **1970**, *43*, 778–782.

39. Petersen, A. L.; Binderup, T.; Rasmussen, P.; Henriksen, J. R.; Elema, D. R.; Kjær, A.; Andresen, T. L. 64Cu loaded liposomes as positron emission tomography imaging agents. *Biomaterials* **2011**, *32*, 2334–2341.

40. Henriksen, J. R.; Petersen, A. L.; Hansen, A. E.; Frankær, C. G.; Harris, P.; Elema, D. R.; Kristensen, A. T.; Kjær, A.; Andresen, T. L. Remote Loading of 64Cu2+ into Liposomes without the Use of Ion Transport Enhancers. *ACS Appl. Mater. Interfaces* **2015**, *7*, 22796–22806.

41. Ghosh, S. C.; Pinkston, K. L.; Robinson, H.; Harvey, B. R.; Wilganowski, N.; Gore, K.; Sevick-muraca, E. M.; Azhdarinia, A. Comparison of DOTA and NODAGA as chelators for Cu-labeled immunoconjugates. *Nucl. Med. Biol.* **2015**, *42*, 177–183.

42. Koppe, M. J.; Bleichrodt, R. P.; Soede, A. C.; Verhofstad, A. A.; Goldenberg, D. M.; Oyen, W. J. G.; Boerman, O. C. Biodistribution and therapeutic efficacy of 125/131I-, 186Re-, 88/90Y-, or 177Lu-labeled monoclonal antibody MN-14 to carcinoembryonic antigen in mice with small peritoneal metastases of colorectal origin. *J. Nucl. Med.* **2004**, *45*, 1224–32.

43. Breeman, W. A. P. Practical Aspects of labeling DTPA-and DOTA- Peptides with Ga for Peptide-Receptor Scintigraphy and Peptide-Receptor Radionuclide Therapy in Preclinical and Clinical Applications; 2012.

44. De León-Rodríguez, L. M.; Kovacs, Z. The Synthesis and Chelation Chemistry of DOTA-Peptide Conjugates. *Bioconjug. Chem.* **2008**, *19*, 391–402.

3

NANVES: Simulating Optimal Vesicle Design for Recoil Retention

Abstract

In this chapter, the recoil retention in different polymersome designs has been simulated. High-z material has been incorporated into the vesicles to improve the daughter nuclide retention when compared to a simple aqueous polymersome design. NANVES, a Monte Carlo simulation package for 3D recoil atom tracking in nanocarriers, was used to calculate the recoil retention in various designs. The NANVES simulation tool was improved and extended to ensure reliable retention output of complex designs. Using NANVES it was determined that vesicle designs where ^{225}Ac is co-precipitated with a nanoparticle within the carrier, or where the vesicle is surrounded by a 5 nm thick golden shell, are promising candidates for increased recoil retention.

Introduction

The main issue arising from targeted alpha therapy with long-lived alpha emitters is that the recoil energy of the daughter nuclides will result in detachment of the targeting agent, as discussed in Chapter 1. One way to deal with this recoil problem is the encapsulation of the radionuclide in nanocarriers, which retain the recoiling daughters and thus prevent the spreading of radionuclides through the body [1]. The Geant4 (GEometry ANd Tracking [3]) based Monte Carlo simulation package NANoVESicle (NANVES) has been developed by Thijssen et al. for 3D recoil atom tracking in nanocarriers [4]. NANVES can be used to investigate to what extend a certain nanovesicle design can retain recoiled atoms and thus determine if it is a good candidate for TAT. The NANVES model is based on the stopping algorithm of Transport and Range of Ions in Matter (TRIM) published in 1987, a simple algorithm for Brownian motion and the Geant4 radioactive decay model [5]. It is used to simulate the recoil distance travelled by the daughter atoms, called the stopping range, which depends on the stopping power of the material that the ion is penetrating. The stopping power is the rate of energy loss by the ion into the target [2], and can be divided into nuclear and electronic stopping. Nuclear stopping represents the energy loss of the ion to the target nuclei, and is dependent on the initial energy of the incident ion, the scattering angle and the atomic mass of the incident ion and target atom. The interaction between the two particles is described by the interatomic potential, which depends on the screening function. The screening function is defined as the ratio of actual atomic potential at a certain radius to the unscreened nucleus (coulombic) potential. Electronic stopping is defined as the energy loss due to interaction with the target electrons. The electronic stopping power calculation requires different approaches based on the atomic number of the elemental or compound target, which for heavy compound targets ($Z > 12$) is based on Bragg's rule. If the simulated stopping range of the daughter nuclide exceeds the nanocarrier dimensions, it is not retained and consequently is free to spread through the body. However, as it is not just the recoil distance accounting for daughter nuclide movement, the Brownian motion experienced by the daughter atom has also been implemented in the NANVES model.

The general trends in the retention data generated by the NANVES model have been shown to be similar to the trends found in the experimental data by Wang et al. [6], although this retention of [225]Ac daughters in polymersomes is not yet satisfactory for potential use in targeted alpha therapy (TAT) [6]. Therefore, new methods have to be developed to further optimize the daughter retention. Simple vesicles containing only PEO, PBd and water do not have enough stopping power to retain a large amount of the recoils, so vesicles containing material with a high atomic number (Z) need to be investigated. In this chapter, four different materials will be simulated: gold, lanthanum, indium and calcium. Gold was chosen as it has been shown through simulations to be very proficient at slowing down recoiling daughters [7]. Gold nanoparticles of a few nanometers are able to form spontaneously, potentially allowing for formation inside polymersomes [8]. Additionally, having gold nanoparticles in a polymer vesicle allows for the combination of therapy and imaging, as gold can be used as CT and X-ray contrast agent as well as for radiation enhancement [9]. As seen in Chapter 2, a large number of radionuclides have been successfully encapsulated in nanocarriers which could also be used to retain recoils at higher concentrations. As has been shown by Sauer et al., it is possible to precipitate metal ions into nanoparticles in a vesicle interior [10]. For the current study, lanthanum, indium and calcium have been chosen as they represent a range of high Z materials. Lanthanum has as additional property

that it is chemically similar to actinium, increasing the likelihood of them precipitating into the same nanoparticle, while calcium is less toxic to the body upon potential release from the nanocarrier. Indium was selected as it is a radionuclide which can be encapsulated very efficiently into a polymersome [11], has an atomic number in between lanthanum and calcium, and the gamma particles emitted during the decay of the radioactive isotope ^{111}In are ideal for imaging purposes.

In this chapter, NANVES was used to determine the nanocarrier design with the highest recoil retention. To investigate new designs, the stopping algorithm was improved so more materials can be integrated into the polymersomes. The current algorithm implemented in the NANVES-DIF class was reviewed for potential diffusion of the daughter atoms trough the PBd-PEO membrane. Subsequently, recoil retention in different nanocarrier designs was simulated, where the influence of vesicle membrane thickness and incorporation of high Z materials was investigated.

Methods

Development and extension of NANVES

The NANVES model is based on the stopping algorithm of TRIM, and the software Stopping and Range of Ions in Matter (SRIM) is used for modeling the stopping and range of low energy heavy ions [12]. The NANVES program control structure is presented in Figure 7, which consists of three classes:

- NANVES-STOP that simulates the STOPping of the recoils, low energy heavy atoms.
- NANVES-DIF which allows the recoils to DIFfuse in fluid compartments of the vesicle.
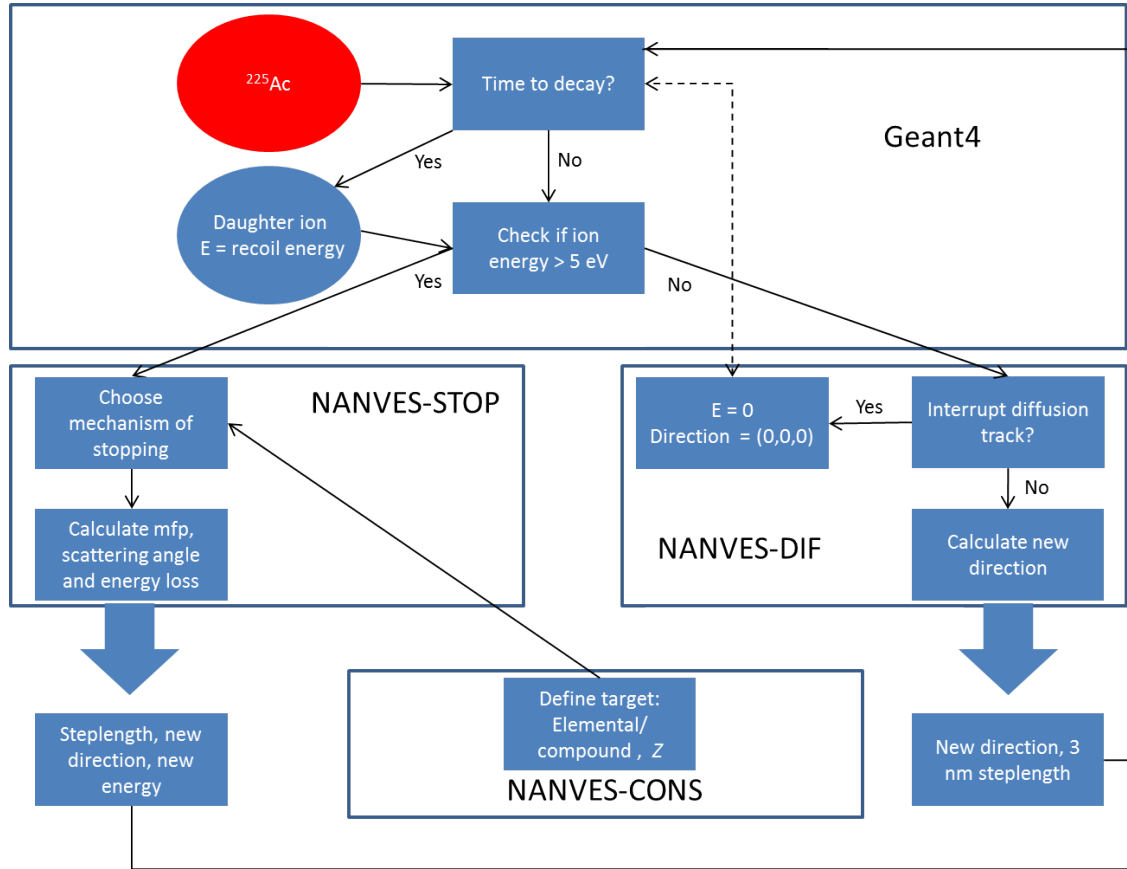- NANVES-CONS enables the user to CONStruct all types of 3D nanovesicles.

Figure 7: NANVES program control structure. The stepping and the radioactive decay are processes that are handled by Geant4. NANVES-STOP determines the steplength, energy loss and direction change in case the energy of the ion is > 5 eV. The mechanism of electronic stopping depends on the target composition and the atomic number. The communication of NANVES-STOP with NANVES-CONS on this matter is not automatic but has to be done manually, as well as the positioning of ^{225}Ac inside the nanocarrier.

The nuclear stopping algorithm of NANVES-STOP did not require any adjustments for the inclusion of heavy targets. The electronic stopping algorithm was however extended to include Bragg's rule, which states that the stopping power of a compound can be estimated by the linear combination of the stopping powers of the individual elements. Braggs rule was implemented in NANVES-STOP so that it calculates the stopping power of a single hit of the recoil with the heavy target material as the average stoichiometry weighted stopping power of the individual atoms according to

$$S_{heavytarget} = \frac{\sum_{i=1}^{n} S_i \cdot v_i}{\sum_{i=1}^{n} v_i} \qquad (2)$$

where S is the stopping power, and v_i the stoichiometric coefficient for n individual elements in the heavy target. Indium, lanthanum and calcium phosphate are heavy targets that were used to test this new line of code of NANVES-STOP. To assess the new NANVES-STOP code, it was compared against the projected range distributions of these heavy targets in SRIM. As SRIM uses the universal screening function based on the Hartree-Fock atomic distributions to simulate ion stopping, this was also the screening function implemented in NANVES-STOP.

3

Diffusion through PBd-PEO membrane

The influence of diffusion on the leakage of daughter nuclides through the polymersome membrane in the NANVES-DIF class was determined. The diffusion coefficient of the ^{225}Ac recoil atoms through PBd-PEO bilayers was estimated based on the diffusion coefficient of hydroxide ions through PBd-PEO bilayers, which is 1 ($\pm$ 0.2) $\cdot 10^{-20}$m^{2}s^{-1} [13]. In water, hydroxide ions diffuse five times faster than heavy ions (5.27 $\cdot 10^{-9}$m^{2}s^{-1} [14] and 0.6 - 2 $\cdot 10^{-9}$m^{2}s^{-1} [15] for the diffusion coefficient of hydroxide ions and heavy ions respectively). Assuming this ratio to be similar in the PBd-PEO bilayer, the diffusion coefficient of ^{225}Ac daughter atoms in PBd-PEO should be 5 times smaller than that of hydroxide ions, and thus amount to approximately 2$\cdot 10^{-21}$m^{2}s^{-1}. The root mean square displacement of the recoiled ions through the polymer membrane was thus calculated.

Nanovesicle design

The vesicles were designed using NANVES-CONS. The PBd-PEO membrane of the vesicles was 7 nm unless mentioned differently, where the ratio of the hydrophilic (PEO) to hydrophobic (PBd) polymer thickness was 0.2. All simulations encompass 2000 events with universal screening, where one event represents the decay chain of one ^{225}Ac atom. The position of ^{225}Ac defines the starting point of the simulation, where the positioning of ^{225}Ac is different for every vesicle design. Vesicles that were compared for their recoil retention and alpha emission from inside the vesicle include (see also Figure 8):

- Polymersomes with a golden shell.
- Polymersomes containing Au, LaPO$_4$, InPO$_4$ or CaPO$_4$ nanoparticles.
- Polymersomes with different concentrations of indium atoms in aqueous vesicle core.
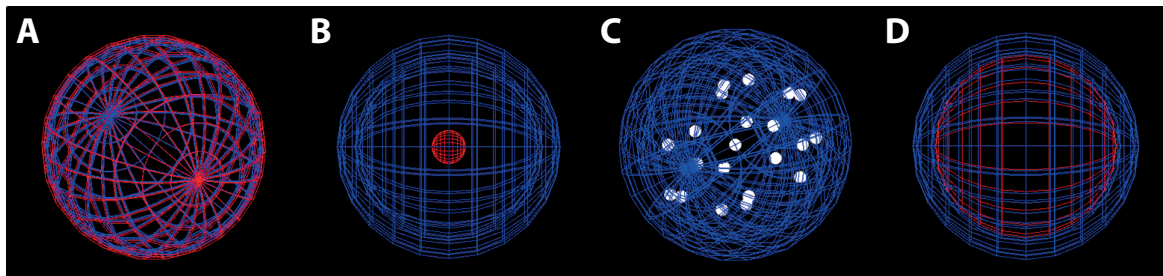
Figure 8: A: polymersome (blue) with a 5 nm thick golden shell (red). B-D: Polymersomes (blue) with three different formations of metal atoms, B: large single nanoparticle (red), C: multiple small nanoparticles (white), and D: indium ions in aqueous solution (red) in NANVES-CONS.

Polymersomes with a golden shell

The influence of a golden shell on the outside of the polymersome bilayer on the recoil retention of ^{225}Ac was determined. A golden shell with a thickness of 5 nm over the polymersome was simulated (Figure 8 D), increasing the total vesicle size with 10 nm. Actinium was given a random position in the aqueous core.

Polymersomes containing nanoparticles

The influence of different high Z materials on the recoil retention in polymersomes was compared using nanoparticles composed of gold, lanthanum phosphate, indium phosphate and calcium phosphate in order of highest stopping power. A solid golden nanoparticle with a 10 nm diameter was simulated in the centre of the polymersome. The phosphate composite nanoparticles ($LaPO_4$, $InPO_4$ and $CaPO_4$) were given diameters corresponding to 0.2 times the diameter of the polymersome [16]. ^{225}Ac was given a random position inside the nanoparticle, which was placed in the centre of the polymersome.

Polymersomes containing indium ions in solution

To determine the influence of a homogeneous distribution of a high-z material, indium ions in solution were simulated dispersed throughout the aqueous core of the polymersome. The maximum realistic concentration of indium ions to be loaded into vesicles was based on a study by Mulas et al., who have loaded different lanthanide(III)-HPDO3A complexes (the lanthanides being gadolinium, dysprosium and europium) into liposomes at a concentration up to 23.4 mM [17]. Polymersomes containing a homogeneous indium concentration of 10 mol% (6.2 mM) and 30 mol% (23.8 mM) were simulated with ^{225}Ac placed randomly in the vesicle core. ^{225}Ac was given a random position in the gold nanoparticle and vesicle core respectively.

Geometry of nanoparticles

The aim of this simulation was to investigate which formation of high Z material (indium as a single large nanoparticle, multiple small nanoparticles or ions in solution) would lead to the highest number of collisions with the recoil atom, resulting in the best recoil retention in a 100 nm polymersome. The amount of collisions of the recoil atom with the indium material was outputted for all simulations. The designs made in NANVES-CONS are shown in Figure 8 A-C. The large nanoparticle was placed in the middle of the vesicle core, the small nanoparticles were equally distributed in the core and a homogeneous solution of indium ions was simulated, where the total volume of indium material inside the polymersomes was kept constant for all options. Daughter atoms were allowed to diffuse in water and ion solution material, but not in the nanoparticles. An overview of the characteristics of the different formations of indium atoms in the polymersomes is given in Table 7. ^{225}Ac was given a random position inside the large gold nanoparticle, in the multiple small nanoparticles simulation it was positioned randomly inside the middle nanoparticle, and in the polymersome containing indium ions in solution it was given a random position within a radius of 10 nm from the polymersome centre. The starting position of actinium was therefore approximately equal for all the simulations, so it would not influence the retention results.

Table 7: Characteristics of the different formations (nanoparticles (NP) or solution (C_{In}) of a certain volume of indium atoms (V_{In}) in the polymersomes.

	Nanoparticles		Solution
Radius (nm)	10	3.42	-
Amount of NP	1	25	-
C_{In} (mol%)	-	-	1.46
V_{In} (nm³)	4188.79	4188.79	4188.79

The influence of the membrane thickness

The thickness of the polymersome membrane depends on the choice of block copolymer length. Thijssen et al. investigated PBD-PEO membranes of 20 nm thickness while experimentally polymersomes with a 7 nm membrane were produced [4,11]. The retention of [221]Fr, [213]Bi and emission of alpha particles were compared between a 7 nm and 20 nm polymersome membrane. [225]Ac was again given a random position inside the aqueous core of the polymersome.

Results and Discussion

Diffusion through PBd-PEO membrane

The estimated diffusion coefficient of the recoiled daughter atoms of [225]Ac was used to calculate the likelihood that the heavy ions would diffuse through PBd-PEO bilayers. Table 8 shows the root mean square displacement (x_{rms}) for heavy ions in PBD-PEO membranes at room temperature and a time corresponding to the half-life of the nuclides. It can be concluded that diffusion of heavy ions through the vesicle membrane (thickness of 7 nm) is unlikely. Although [209]Pb has a x_{rms} value about equal to the thickness of the nanovesicle membrane, it is more likely that [209]Pb will leave the nanovesicle because of the recoil energy than by means of diffusion through the membrane.

Table 8: Root mean square displacement in PBd-PEO membranes after time t= $t_{1/2}$ for the instable daughters of ^{225}Ac based on Brownian motion theory using the estimated diffusion coefficient for heavy ions in PBd-PEO material ($2 \cdot 10^{-21}$m^{2}s^{-1})

Ion	$t_{1/2}$	x_{rms} (nm)
^{221}Fr	4.92 m	1.09
^{217}At	32.3 ms	0.01
^{213}Bi	45.6 m	3.31
^{213}Po	3.7 μs	0.00012
^{209}Pb	3.3 hr	6.89

The stopping range of recoils in heavy targets

The individual tracks of ^{221}Fr recoil atoms in solid $LaPO_4$, $InPO_4$ or $CaPO_4$ spheres are shown in Figure 9. The average projected range was calculated using NANVES (Table 9), where the deviation of the stopping ranges produced by NANVES from SRIM-2008 is similar for all recoil atoms and is an overestimation that ranges from 4.56 to 6.64%.
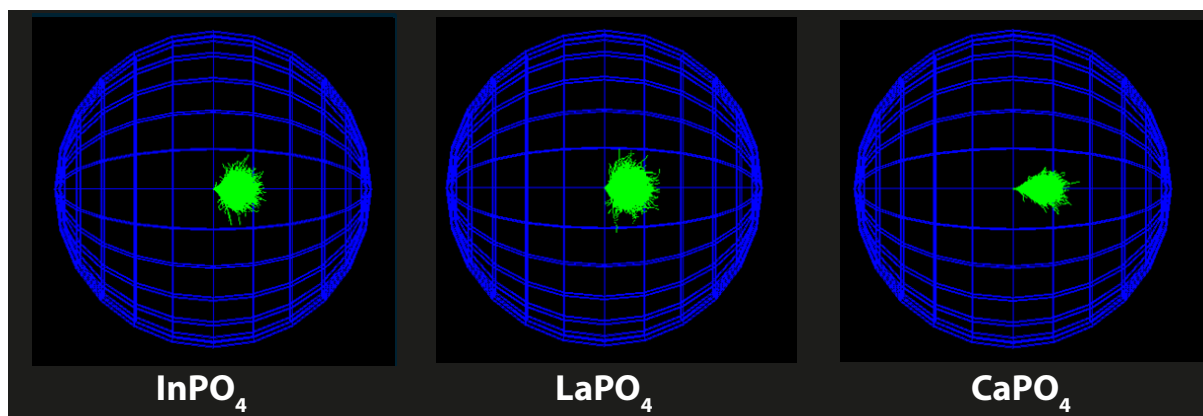

Figure 9: Tracks of ^{221}Fr recoil atoms in a solid $LaPO_4$, $InPO_4$, or $CaPO_4$ sphere.

The approximately 5% deviation of NANVES with SRIM-2008 for all recoil atoms in $InPO_4$, $LaPO_4$ or $CaPO_4$ targets is considered a good agreement. The integration of Bragg's rule in NANVES-STOP can thus be considered successful.

Table 9: Average projected range of the recoils generated by SRIM-2008 and NANVES Range (nm)

		Range (nm)		
Atom	**Medium**	**SRIM-2008**	**NANVES**	**Deviation (%)**
^{221}Fr	InPO$_4$	28.2	29.68	5.25
(105 keV)	LaPO$_4$	27.4	28.96	5.69
	CaPO$_4$	33.7	35.56	5.52
^{217}At	InPO$_4$	30.5	31.89	4.56
(117 keV)	LaPO$_4$	29.6	31.22	5.48
	CaPO$_4$	36.3	38.71	6.64
^{213}Bi	InPO$_4$	33.4	35.28	5.63
(113 keV)	LaPO$_4$	32.4	34.36	6.05
	CaPO$_4$	39.6	42.18	6.52
^{209}Pb	InPO$_4$	38.1	40.02	5.04
(160 keV)	LaPO$_4$	37.1	39.28	5.88
	CaPO$_4$	45.2	48.06	6.33

Comparison of various vesicle designs

The recoil retention and alphas emitted from within the vesicle have been simulated for all vesicle designs. Polymersomes without further modifications have been included as well to quantify the improvement of the complex vesicle designs.

Polymersomes with a golden shell

Since gold has a high Z and is thus very capable of slowing down recoiled daughter atoms, it is ideally suited to keep these daughter atoms from leaving the polymersome. One way to do this, is to coat the outside of the vesicle in a thin gold layer. Rengan et al. have coated liposomes with a thin layer of gold, showing that coating of nanovesicles is possible. However, they did not report the thickness of this Au layer, for our simulations it has been estimated at about 5 nm [18]. NANVES simulations have indicated a rather large increase in recoil retention of gold coated polymersomes as compared to 'normal' polymersomes with a 100 nm diameter (^{221}Fr: 83.1% vs 32.8%, and ^{213}Bi: 27.4% vs 3% respectively). The main cause for this large difference in retention can be found in the high stopping power of Au, which reduces the recoil distance from approximately 100 nm in water to just over 10

nm. A 5 nm thick shell will thus have a rather large impact. An additional positive effect is due to the slightly larger vesicle diameter (110 nm compared to 100 nm). In this design, the [221]Fr recoils are first slowed down by the water and the PBD-PEO membrane, so are expected to have a low energy when they reach the golden shell. The stopping range decreases drastically with the recoil energy, so a golden shell of 5 nm seems to be very effective at stopping the very low energy [221]Fr recoils. From an application point of view, the gold coated liposomes were found to be biocompatible, where at 1 mg/mL concentration the cell viability was still >90%, and they were taken up in the cytosol region of cells [18]. However, since the thickness of the golden shell was not reported, it can result in some uncertainty in our simulation design as a thinner shell would result in a lower recoil retention. Also, due to their changed surface characteristics, this modification of the polymersomes is expected to change the biodistribution and circulation time of the vesicles. Unfortunately, in the liposome study no in vivo experiments were performed so the in vivo impact of this modification cannot be assessed.

Nanoparticle-containing polymersomes

In these simulations, an [225]Ac atom has been placed at a random position in a nanoparticle inside a polymersome. These nanoparticles have been composed of Au, $LaPO_4$, $InPO_4$ or $CaPO_4$, where through these different materials the influence of nanoparticle composition and atomic number could be determined. Gold nanoparticles in a vesicle core were reported to vary in size from 3-15 nm, thus a 10 nm gold particle was used in this simulation [19,20]. CryoTEM image analysis of $InPO_4$ in polymersomes has shown a ratio of 0.2 between nanoparticle and polymersome diameter, so this ratio was simulated for all simulated phosphate based nanoparticles [16]. Retention of two of the alpha-emitting daughters of [225]Ac, namely [221]Fr and [213]Bi, where the [225]Ac was placed randomly in the nanoparticle in the polymersome, can be seen in Figure 10. While all polymersomes containing nanoparticles show a significant improvement in daughter retention as compared to the reference polymersome containing only water, there is no real difference between the different nanoparticle compositions. They show comparable [221]Fr and [213]Bi retention ($\pm$ 8%) despite the different nanoparticle dimensions (10 nm for gold, and 20 or 40 nm $LaPO_4$, $InPO_4$ or $CaPO_4$ nanoparticles in 100 and 200 nm diameter polymersomes respectively).

3

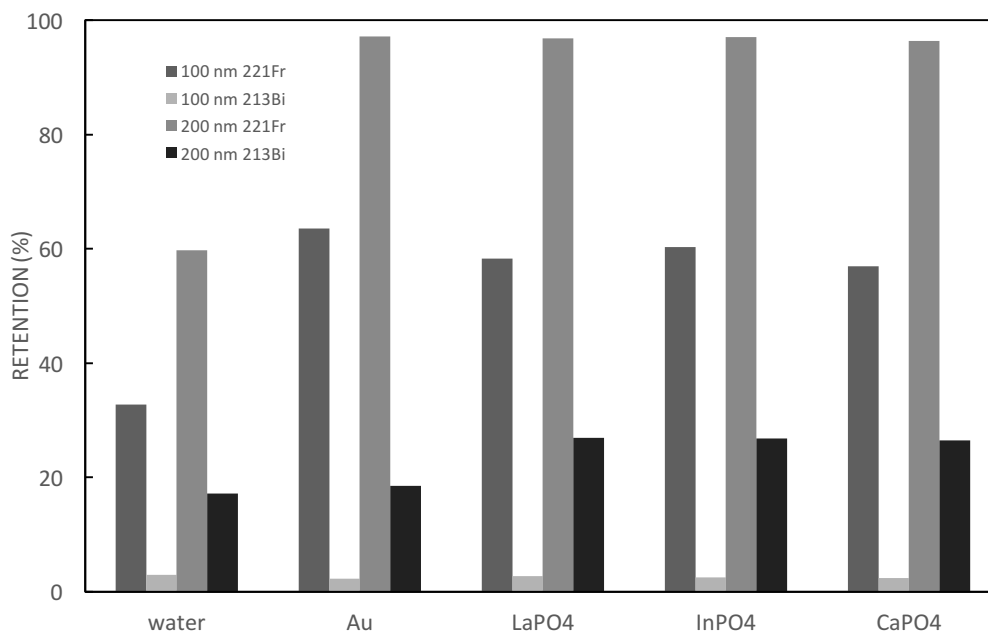Figure 10: Comparison of the recoil retention of [221]Fr and [213]Bi between various nanoparticle formulations, in both 100 and 200 nm diameter polymersomes.

The range of [221]Fr in gold approximately equals the nanoparticle dimensions, while its range in phosphate nanoparticles is larger than the particle, so logically the gold nanoparticle is better able to retain [221]Fr for 100 nm diameter polymersomes. This no longer holds for the 200 nm polymersomes, where the phosphate nanoparticle size is slightly larger than the recoil range while the gold nanoparticles remain the same size. They thus have a similar performance here, as the increase in recoil retention in mainly due to the larger vesicle size. The phosphate nanoparticle designs were expected to have the same simulated [221]Fr recoil retention because the [221]Fr stopping range in these materials is very similar (30 ± 3 nm). Using NANVES it was calculated that a 20 nm and 40 nm $InPO_4$ particle can retain 25.8 % and 43.8 % of the [221]Fr recoils respectively. Despite the difference in atomic number of the lanthanum, indium and calcium, the chance of the recoil hitting the phosphate molecule is much larger (83% chance of hitting the phosphate) explaining the similar range. Introducing nanoparticles in the vesicle core does not improve the [213]Bi retention in small vesicles (100-110 nm) when compared to polymersomes without modifications, because the nanoparticle makes up only 0.16 % (Au) or 1.26 % ($InPO_4$, $LaPO_4$ or $CaPO_4$) of the vesicle core volume in case of a 100 nm polymersome. After the first alpha decay, the daughter atom has likely already left the nanoparticle, and the chance of hitting it again upon alpha decay from elsewhere in the polymersome is very small. Nevertheless, a significantly larger fraction of alpha particles is emitted from within the polymersome (10% more for 100 nm polymersomes, and 20% more for 200 nm polymersomes), making it an interesting option for improved recoil retention, especially considering that there is no surface modification of the polymersomes necessary. However, it should be kept in mind that in these simulations the nanoparticle was always placed in the middle of the polymer vesicle which cannot be achieved experimentally resulting in a decrease in experimental recoil retention.

Distribution of indium in polymersomes (NP, many small NP, solution)

Logically, incorporating high Z material in an aqueous core is expected to increase recoil retention due to the increase in nuclear stopping. In low energy heavy atom stopping, nuclear stopping is the primary mechanism of energy loss, so surrounding the recoiling daughters with atoms with a high atomic number will significantly limit the recoiling range. To determine the optimal distribution of these high Z atoms, three different polymersome formulations were simulated, with either one large $InPO_4$ nanoparticle, multiple small ones, or indium ions in solution. The recoil retention and alpha emission from inside a 100 nm polymersome was determined for the geometries and the results are shown in Table 10. The total volume of the different geometries (1 large particle, 25 small particles and ions in solution) is equal and the starting position of ^{225}Ac is close to the centre for all designs. The best ^{221}Fr retention and alpha emission has been observed for the polymersomes containing 1 large nanoparticle, while the polymersomes containing indium ions in solution has performed the worst. This was to be expected because ^{225}Ac was incorporated inside the nanoparticle, forcing the ^{221}Fr recoil atom to traverse the material of the nanoparticle. ^{213}Bi was retained slightly better in the polymersomes containing indium ions in solution as compared to the vesicles containing nanoparticles. As a number of alpha decays have already occurred prior to the decay to ^{213}Bi, it has a high chance of having recoiled out of the nanoparticle. Because the volume of indium atoms is distributed evenly in the vesicle core, the chance of recoil atom collisions is largest in this scenario, although this effect is not very large. The average number of hits of the recoils with the indium material are the highest in the design with one large nanoparticle and the lowest in the solution, corresponding to the daughter retention.

Table 10: Comparison of ^{221}Fr and ^{213}Bi retention and alpha emission from inside the vesicle for different geometries of indium material (1 large nanoparticle (NP), 25 small nanoparticles and indium atoms in solution).

	Retention / Emission		
Atom	**1 NP**	**25 NP**	**Solution**
^{221}Fr	59.25 %	50.25 %	32.8 %
^{213}Bi	2.75 %	2.60 %	3.00 %
Alpha's	46.83 %	42.84 %	37.55 %
In hits	22	9	7

The volume of the large nanoparticle makes up only 1.26 % of the vesicle core. Distributing the indium material even more (in smaller nanoparticles or solution) thus does not improve the recoil retention when the total volume of indium material is kept constant. While a higher concentration of indium atoms in solution in the vesicle core, like 10 mol% and 30 mol% results in a much more effective recoil stopping (46.35% and 58% for ^{221}Fr, and 4.7% and 9% for ^{213}Bi respectively) it is still not better than one large nanoparticle. The underlying assumption here is that ^{225}Ac can be incorporated inside the

3

nanoparticle, and that polymersomes will still be able to form in such a high indium concentration. Distributing 25 small nanoparticles in the vesicle core is not effective, as this total volume is also too little.

100 nm vs 200 nm diameter polymersomes

In 100 nm diameter polymersomes, vesicles with a golden shell were found to retain the ^{221}Fr daughters best as compared to the other tested formulations. However, when going to larger vesicles (~ 200 nm diameter), ^{221}Fr retention in nanoparticle-containing polymersomes is considerably better than that in polymersomes containing an indium ion solution, and slightly better (about 4% increase in retention) than those with Au shell. This is mainly due to the size of the phosphate nanoparticles, which scale with nanoparticle diameter, and larger nanoparticles slow recoils down more effectively. The ^{213}Bi retention in 200 nm vesicles in shell polymersomes is on the other hand much better than nanoparticle and solution polymersomes, because the nanoparticle volume is only a small fraction of the total vesicle core volume. The chance that a ^{213}Bi atom will hit the nanoparticle is very small while a ^{213}Bi atom is forced to hit the golden shell explaining the better performance of the shell design. Therefore, for optimal recoil retention, polymersomes with either the ^{225}Ac incorporated in a nanoparticle, or covered with golden shell are preferred.

Membrane thickness

The influence of the polymer bilayer thickness on the recoil retention was investigated for two membrane thicknesses (7 nm and 20 nm), the results are shown in Figure 11. A membrane of 20 nm slightly increases the ^{221}Fr and ^{213}Bi retention with respect to the 7 nm membrane, leading to on average over all polymersome sizes 7.7 % and 3.5 % better performance respectively. It was expected that a thicker membrane would improve the recoil retention since the recoil range in PEO and PBd is smaller than for water. The largest effect of the membrane thickness on the ^{221}Fr retention can be seen in polymersomes ranging from 200 – 400 nm in diameter. Since the recoil range of ^{221}Fr in water is around 100 nm, ^{221}Fr will come near the vesicle membrane in those particle sizes. A slight improvement of the ^{213}Bi retention was found for larger polymersome sizes, at 100 nm polymersomes there was no significant difference since nearly all the ^{213}Bi will have recoiled out. However, it has been shown that the loading efficiency of radionuclides like ^{111}In becomes much lower upon increasing the membrane thickness [11], likely causing similar problems for the loading efficiency of radionuclides like ^{225}Ac.
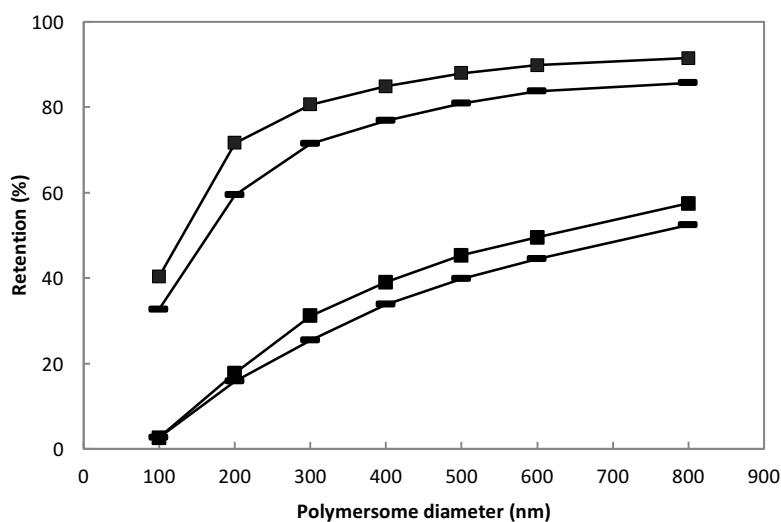
Figure 11: Retention of ^{221}Fr (red) and ^{213}Bi (blue) in a polymersome with 7 nm (–) and a 20 nm (■) membrane.

Conclusions

In this chapter, we have improved on the NANVES Monte Carlo simulation code by including electronic stopping for heavy targets, which was validated by comparison with SRIM-2008 and has shown good agreement for $InPO_4$, $LaPO_4$ and $CaPO_4$ targets. The range uncertainty was found to be similar for all recoil atoms in the simulated target materials ($InPO_4$, $LaPO_4$ and $CaPO_4$). Subsequently, NANVES has been used to simulate polymersomes with these materials. Polymersomes containing either a single nanoparticle in the core where ^{225}Ac is incorporated, or with a golden shell are very promising designs for application in TAT. Recoil retention has also been found in increasing the nanocarrier diameter, although implementing this would cause other problems as larger vesicles are severely limited in tumour uptake and circulation time in vivo. Increasing the membrane thickness likewise has a positive effect on recoil retention, although the loading efficiency might be hampered. The most likely method to improve daughter retention is thus found in the addition of high Z materials to the vesicles. However, even then they are not fully retained in 100 nm vesicles. Therefore, in vivo experiments are required to determine if the percentage of retained daughter nuclides is high enough to avoid side effects from systemically released alpha emitting recoiling daughters in TAT.

3

References

1. Deshpande, P. P.; Biswas, S.; Torchilin, V. P. Current trends in the use of liposomes for tumor targeting. *Nanomedicine (Lond).* **2013**, *8*, 1509–28.

2. Ziegler, J. F.; Ziegler, M. D.; Biersack, J. P. SRIM - The stopping and range of ions in matter (2010). *Nucl. Instruments Methods Phys. Res. Sect. B Beam Interact. with Mater. Atoms* **2010**, *268*, 1818–1823.

3. Agostinelli, S.; Allison, J.; Amako, K.; Apostolakis, J.; Araujo, H.; Arce, P.; Asai, M.; Axen, D.; Banerjee, S.; Barrand, G.; Behner, F.; Bellagamba, L.; Boudreau, J.; Broglia, L.; Brunengo, A.; Burkhardt, H.; Chauvie, S.; Chuma, J.; Chytracek, R.; Cooperman, G.; Cosmo, G.; Degtyarenko, P.; Dell; Depaola, G.; Dietrich, D.; Enami, R.; Feliciello, A.; Ferguson, C.; Fesefeldt, H.; Folger, G.; Foppiano, F.; Forti, A.; Garelli, S.; Giani, S.; Giannitrapani, R.; Gibin, D.; Gomez Cadenas, J. J.; Gonzalez, I.; Gracia Abril, G.; Greeniaus, G.; Greiner, W.; Grichine, V.; Grossheim, A.; Guatelli, S.; Gumplinger, P.; Hamatsu, R.; Hashimoto, K.; Hasui, H.; Heikkinen, A.; Howard, A.; Ivanchenko, V.; Johnson, A.; Jones, F. W.; Kallenbach, J.; Kanaya, N.; Kawabata, M.; Kawabata, Y.; Kawaguti, M. GEANT4—a simulation toolkit. *Nucl. instruments …* **2003**, *506*, 250–303.

4. Thijssen, L.; Schaart, D. R.; de Vries, D.; Morgenstern, A.; Bruchertseifer, F.; Denkova, A. G. Polymersomes as nano-carriers to retain harmful recoil nuclides in alpha radionuclide therapy: a feasibility study. *Radiochim. Acta* **2012**, *100*, 473.

5. Ziegler, J. F.; Biersack, J. P.; Littmark, U. *The Stopping and Range of Ions in Matter*; Pergamon Press: New York, 1985.

6. Wang, G.; de Kruijff, R. M.; Rol, A.; Thijssen, L.; Mendes, E.; Morgenstern, A.; Bruchertseifer, F.; Stuart, M. C. A.; Wolterbeek, H. T.; Denkova, A. G. Retention studies of recoiling daughter nuclides of 225Ac in polymer vesicles. *Appl. Radiat. Isot.* **2014**, *85*, 45–53.

7. Thijssen, L. NANVES: a Monte Carlo Simulation Package for 3D Recoil Atom Tracking in Nanovesicle Carriers for Targeted Alpha Therapy, Delft University of Technology, 2010.

8. Tsuda, T.; Seino, S.; Kuwabata, S. Gold nanoparticles prepared with a room-temperature ionic liquid-radiation irradiation method. *Chem. Commun. (Camb).* **2009**, 6792–6794.

9. Hainfeld, J. F.; Slatkin, D. N.; Smilowitz, H. M. The use of gold nanoparticles to enhance radiotherapy in mice. *Phys. Med. Biol.* **2004**, *49*, 309–315.

10. Sauer, M.; Haefele, T.; Graff, A.; Nardin, C.; Meier, W. Ion-carrier controlled precipitation of calcium phosphate in giant ABA triblock copolymer vesicles. *Chem. Commun.* **2001**, 2452–2453.

11. Wang, G.; de Kruijff, R. M.; Stuart, M. C. A.; Mendes, E.; Wolterbeek, H. T.; Denkova, A. G. Polymersomes as radionuclide carriers loaded via active ion transport through the hydrophobic bilayer. *Soft Matter* **2013**, *9*, 727–734.

12. Ziegler, J. F.; Biersack, J. P.; Ziegler, M. D. *The Stopping and Range of Ions in Matter*; SRIM company, 2008.

13. Paxton, W. F.; Price, D.; Richardson, N. J. Hydroxide ion flux and pH-gradient driven ester hydrolysis in polymer vesicle reactors. *Soft Matter* **2013**, *9*, 11295.

14. Samson, E.; Marchand, J.; Snyder, K. A.; Samsonl, E.; Marchandl, J.; Snyder3, K. A. Calculation of ionic diffusion coefficients on the basis of migration test results. *Mater. Struct. Constr.* **2003**, *36*, 156–165.

15. Kuss, J.; Holzmann, J.; Ludwig, R. An elemental mercury diffusion coefficient for natural waters determined by molecular dynamics simulation. *Environ. Sci. …* **2009**, *43*, 3183–3186.

16. Kruijff, R. M. de; Drost, K.; Thijssen, L.; Morgenstern, A.; Bruchertseifer, F.; Lathouwers, D.; Wolterbeek, H. T.; Denkova, A. G. Improved 225Ac Daughter Retention in InPO4 Containing Polymersomes. *Appl. Radiat. Isot.* **2017**, *128*, 183–189.

17. Mulas, G.; Ferrauto, G.; Dastrù, W.; Anedda, R.; Aime, S.; Terreno, E. Insights on the relaxation of liposomes encapsulating paramagnetic Ln-based complexes. *Magn. Reson. Med.* **2015**, *74*, 468–473.

18. Rengan, A. K.; Jagtap, M.; De, A.; Banerjee, R.; Srivastava, R. Multifunctional gold coated thermo-sensitive liposomes for multimodal imaging and photo-thermal therapy of breast cancer cells. *Nanoscale* **2014**, *6*, 916–923.

19. Popescu, M. T.; Tsitsilianis, C. Controlled delivery of functionalized gold nanoparticles by pH-sensitive polymersomes. *ACS Macro Lett.* **2013**, *2*, 222–225.

20. Hong, K.; Friend, D. S.; Glabe, C. G.; Papahadjopoulos, D. Liposomes containing colloidal gold are a useful probe of liposome-cell interactions. *BBA - Biomembr.* **1983**, *732*, 320–323.

Formation of InPO$_4$, LaPO$_4$ and CaPO$_4$ Nanoparticles in Polymersomes

4

Abstract

The recoil distance of the alpha-emitting daughters of ^{225}Ac is mainly influenced by nuclear stopping, and can subsequently be decreased by creating a high-z environment around the mother nuclide. Different metal-phosphate nanoprecipitates can be used for this purpose through encapsulation in polymer vesicles. In this chapter, polymersomes containing either a $InPO_4$, $LaPO_4$, or $CaPO_4$ nanoparticles in the core have been synthesized. The new loading method relies on polymersome formation in a KH_2PO_4 containing buffer solution at low pH, after which unencapsulated phosphate is removed. Subsequently, the metal ions are loaded and co-precipitated with the phosphate ions in the vesicles. It has been shown that by varying the metal and phosphate concentrations the nanoparticle size can directly be influenced. The three metals investigated in this chapter, indium, lanthanum, and calcium, have all shown to form different structures when co-precipitated with the phosphate ions. Formed $LaPO_4$ nanoneedles were strong enough to rupture the polymer membrane, whereas $InPO_4$ formed spherical structures. The developed loading methodology is not only expected to increase recoil retention, but has also shown to substantially increase the loading capacity of the polymersomes as compared to alternative loading methods employing encapsulated DTPA as hydrophilic chelator.

Introduction

To optimally retain the recoiled daughter atoms of [225]Ac in nanocarriers, it is important to decrease their recoil distance upon decay. As seen in Chapter 3, these heavy daughter ions mainly experience nuclear stopping, with electronic stopping contributing only a little to the total stopping power of the medium. Nuclear stopping of low energy heavy ions predominates in high-z materials [1], where the recoil range of these daughters will be smaller there than in an aqueous environment. Limiting the range of the recoiling daughter atoms can thus be achieved by creating a high-z environment around the mother nuclide. In literature, this approach has been implemented by Woodward et al. and McLaughlin et al. who developed LaPO₄ nanoparticles to retain [225]Ac daughter nuclides. Initially the [225]Ac was encapsulated only in an LaPO₄ nanoparticle with 5 nm diameter [2], the subsequent addition of GdPO₄ and golden shells increased their diameter to 26.8 nm and markedly improved daughter retention to more than 88% for [221]Fr [3]. Later studies by Rojas et al. have shown high retention of alpha-emitting daughters of [223]Ra or [225]Ra encapsulated in the core of LaPO₄ nanoparticles (6.3 nm diameter), e.g. a retention of >99.98% and ~80% for [221]Fr and [213]Bi respectively [4].

In previous work, we have successfully encapsulated [225]Ac in polymersomes to retain the daughter nuclides [5]. However, as the average projected stopping range of the alpha-emitting [225]Ac daughters in water lies around 100 nm [6], they were found not to be retained very well in small (~100 nm) polymersomes [5]. To ensure a long in vivo circulation time of the vesicles, they need to be less than 120 nm in diameter, as found by Brinkhuis et al. [7]. Therefore, the polymersome design needs to be optimized to increase recoil retention in small vesicles. Combining the nanoparticle formulation for enhanced retention with polymeric nanocarriers should yield a significant improvement over daughter retention in polymer vesicles. At the same time, the advantageous chemical and biological properties of polymersomes over inorganic nanoparticles are preserved, such as the possibility to control their physico-chemical properties, easy modification to include a number of targeting agents or other moieties, as well as the possibility to incorporate both hydrophilic and hydrophobic substances simultaneously.

The incorporation of solid metal-phosphate precipitates in vesicles has been demonstrated before by Eanes et al. as well as Sauer et al. [8,9]. In these studies, phosphate was present in the buffer solution during vesicle formation, after which unencapsulated phosphate was removed. Subsequently, calcium ions were loaded and precipitated with the phosphate ions inside the vesicles. Their approaches constitute a reliable and efficient method to precipitate nanoparticles in vesicles after their formation. The reverse method is also possible, as demonstrated by Michel et al., who formed their liposomes in a solution containing calcium, and later precipitated the phosphate in the vesicles with calcium [10]. Similarly, accumulation of anti-cancer drugs like doxorubicin [11] and topotecan [12] in liposomes has also been driven by complexation with metal ions.

It is thus well possible to precipitate high-z metal ions in vesicles and form the basis for increased nuclear stopping. The aim of this chapter is to create a high-z environment inside the polymersome by nanoprecipitation of different metals with phosphate ions. The selected metal ions are indium, lanthanum and calcium. Indium was chosen because we already had experience with the loading of ^{111}In in polymersomes [13], with as additional advantage the availability of radioactive ^{111}In to determine

loading efficiency. Lanthanum phosphate has been shown to be a good compound for the retention of [225]Ac daughters by other groups [4], and due to its similar chemistry as [225]Ac was expected to co-precipitate more readily with the [225]Ac mother atoms [14]. Lanthanum can easily be irradiated to its radioactive form [140]La, allowing for assessment of loading efficacy. Last, calcium phosphate has been shown to easily precipitate in liposomes [8,9] and is less toxic in vitro [15,16]. The end-point of the research presented here is to design a suitable carrier which can be used to limit loss of recoiling daughter nuclides upon decay of an alpha-emitting mother.

Materials and Methods

Chemicals

The poly(butadiene(1,2 addition)-b-ethylene oxide) block copolymer was obtained from Polymer Source (Quebec, Canada), with a Mn of 1900-b-900 g mol^{-1}, with a weight ratio (Mw/Mn) of 1.05. The [111]In ($t_{1/2}$ = 2.81 d) was kindly provided by the section Nuclear Medicine of the Erasmus Medical Center (the Netherlands) with a specific activity of 1.72 MBq pmol^{-1}. [140]La was produced at the Reactor Institute Delft (the Netherlands), where 1 mg $LaNO_3$ was irradiated for 6 hours in the BP4 facility at a thermal flux of 3.1 x 10^{16} n cm^{-2} s^{-1}, epithermal flux of 7.20 x 10^{14} n cm^{-2} s^{-1} and fast flux of 2.60 x 10^{15} n cm^{-2} s^{-1}. Subsequently, it was left to cool for 1 hour, and dissolved in 0.01 M HCl. All other chemicals were purchased from Sigma-Aldrich.

Polymersome preparation

The polymersomes were prepared by adding a ratio of 2 mg block copolymer per 1 mL 0.5 M KH_2PO_4 in 10 mM HEPES buffer at pH 3 to a vial and stirring for a week. Prior to the loading of the radionuclide in the polymersomes, the unencapsulated DTPA or PO_4^{3-} was removed using a 30 cm Sephadex G-25 M column, equilibrated with a 10 mM pH 7.4 HEPES buffer. All experiments were carried out at room temperature T = 20 ± 2 °C. In all experiments, the polymersome concentration mentioned (in mg/ml) refers to the initial concentration (before dilution by passing through size exclusion columns).

Indium-tropolone dissociation

To determine the interior pH of KH_2PO_4 required for successful loading of indium, the pH at which indium would dissociate from tropolone was determined. Indium was incubated with 10 mM tropolone at different pH for 30 minutes, the association was subsequently checked by liquid-liquid extraction in chloroform.

Loading of indium, lanthanum and calcium

Approximately 60 kBq of ^{111}In was added to a vial containing tropolone (10 μL 2 mM – 40 μL 20 mM, depending on the amount of $InCl_3$ added) and 200 μL 10 mM HEPES buffer at pH 7.4 followed by different amounts of cold $InCl_3$ pH 2 solution (0 μL – 2 μL, 0.25 M, used ratios as per Table 11). The solution was incubated for 10 minutes, after which 0.8 mL of the polymersome solution was added and the mixture was left at rest for 1 hour, except for the experiments where the effect of loading time was determined. The unencapsulated ^{111}In was separated from the polymersome solution using a PD10

size exclusion column, where the polymersomes were contained in the 3rd – 5th 1 mL fraction. The loading of lanthanum was performed in a similar fashion, but with calcium ionophore as lipophilic chelator. About 60 kBq of [140]La was added together with cold $LaNO_3$ (0 μL – 2 μL, 0.25 M) to a thin film of 0.1 mg A23187 in 200 μL 10 mM HEPES buffer at pH 7.4. To improve the loading efficiency, complexation of lanthanum to A23187 was later performed in $CHCl_3$, where upon the evaporation of $CHCl_3$ 200 μL 10 mM HEPES buffer at pH 7.4 was added. Subsequently, 0.8 mL KH_2PO_4-containing polymersomes were added, and the loading proceeded as above. Calcium was loaded by adding 5 μL 25 mM $CaCl_2$ together with 200 μL 10 mM HEPES buffer at pH 7.4 to a vial containing either 10 μL 20 mM tropolone or a 0.1 mg A23187 film. Subsequently, the loading proceeded as described above for the loading of lanthanum and indium, with as only difference there was no active calcium added, so the loading efficiency was not determined.

The retention of indium or lanthanum in polymersomes was determined by measuring the ratio of ^{111}In or [140]La within and outside of the polymersomes, 24h after loading. Here, 500 μL polymersome solution was incubated with 500 μL 1 mM DTPA, 10 mM HEPES solution, after which the unencapsulated ^{111}In or [140]La was removed using a PD10 column. In the serum experiments, the polymersome – serum solution (1 mL PS to 1 mL serum) was incubated at both RT and 37°C for 24 hours before being separated using a 30 x 1 cm Sepharose 4B size exclusion column.

Table 11: $InCl_3$ and tropolone added to pH 3 0.5 M PO_4^{3-} polymersomes

Cold InCl₃ added		Tropolone added	
Volume (μL)	Concentration (mM)	Volume (μL)	Concentration (mM)
0	-	10	2
2	2.5	10	2
10	2.5	20	2
5	25	10	20
2	250	40	20

CHEAQS Next speciation

The software program 'CHEAQS Next' (Chemical Equilibria in Aquatic Systems [17]) was used to determine the equilibrium speciation of $InCl_3$ and $LaNO_3$ at a concentration of 10-500 nmol in an 0.5 M KH_2PO_4 medium, at a pH of either 3 or 7.4.

4

Dynamic light scattering (DLS)

To characterize the polymersomes, a DLS apparatus consisting of a JDS Uniphase 633 nm 35 mW laser, an ALV sp 125 s/w 93 goniometer, a fibre detector and a Perkin Elmer photon counter was used, with an ALV-5000/epp correlator and software. The DLS tubes were immersed in a toluene-containing temperature-regulated bath (at 20 °C). The intensity autocorrelation function was determined at an angle of 90°. The data was fitted using the Contin method, and the hydrodynamic radius of the polymersomes was determined with the Stokes–Einstein equation [13].

Cryo-TEM

3 μl of the polymersome solution containing 1 mg/mL block copolymer was deposited on a holey carbon film (Quantifoil 2/2) supported on a TEM grid. After blotting the drop to obtain a thin film on the grid, the sample was vitrified by rapid immersion in liquid ethane (Leica EM GP version 16222032), and subsequently immersing in liquid nitrogen. The specimen was inserted into a cryo-transfer holder (Gatan model 626) and then transferred to a Jeol JEM 1400 TEM. Images were obtained at an acceleration voltage of 120 keV. For the statistical analysis of the polymersome and nanoparticle diameters, about 30-50 images were made of each of the polymersome samples. The diameter of all polymersomes and nanoparticles within those images were measured with ImageJ [18].

X-ray diffraction (XRD)

X-ray diffraction analysis was conducted to determine the crystallinity of the $InPO_4$ inside the vesicles. Approximately 30 mg polymersome solution, containing either only MilliQ, 0.5 M KH_2PO_4, or $InPO_4$ nanoparticles inside the polymersomes was freeze-dried. A thin frozen layer of the sample was created by immersing it into liquid nitrogen, after which it was placed in the freeze-dryer (Kinetics, type MNL-036-A) at -50 °C and 20 mTorr for 24 h. Subsequently, a small amount of the sticky sample (< 1 mg) was placed on a Si510 wafer in a PMMA sample holder L510. X-ray diffraction was performed on a BrukerD8 Advance diffractometer (Bragg-Brentano geometry and a Lynxeye position sensitive detector) with Cu Kα radiation. The measurement was conducted using the θ -2θ scan mode (10° - 70°), with step size 0.030 ° 2θ and a counting time of 5 s per step. The data was evaluated with DiffracSuite.EVA vs 4.2 (Bruker).

Results and discussion

The recoil distance experienced by the daughter nuclide upon the decay of an alpha emitter is much shorter in high-z particles as compared to an aqueous environment. Incorporation of an alpha-emitting radionuclide in a nanoparticle should thus increase its retention [2]. As additional advantage, radiolabelling through precipitation with nanoparticles should allow for a much larger number of atoms per polymersome when compared with 'conventional' loading through binding with a chelator. The nanoparticle precipitation loading method was initially performed and optimized using a combination of ^{111}In and cold $InCl_3$, as loading indium in vesicles containing DTPA as hydrophilic chelate were already well established, and ^{111}In was readily available. Subsequently, the loading and formation mechanism was extended to also include lanthanum and calcium.

InPO$_4$ nanoparticles in polymersomes

Initial experiments have been performed with ^{111}In to determine the labelling characteristics and find the optimal amount of cold indium to co-precipitate with [225]Ac. It has been found that a pH gradient across the polymersome bilayer, with a lower pH in the aqueous cavity, was crucial for the successful encapsulation of indium in the polymersomes. [111]In has been encapsulated with high efficiency (> 90%) when the aqueous cavity containing 0.5 M KH$_2$PO$_4$ had a pH between 2 and 4 (Figure 12). However, it could not be encapsulated when the polymersome interior is at a pH of 7.4. High loading efficiencies (> 90%) were achieved within 15 minutes, and remained constant in time. In subsequent experiments, the pH of the aqueous cavity of the polymersomes was set to pH 3.
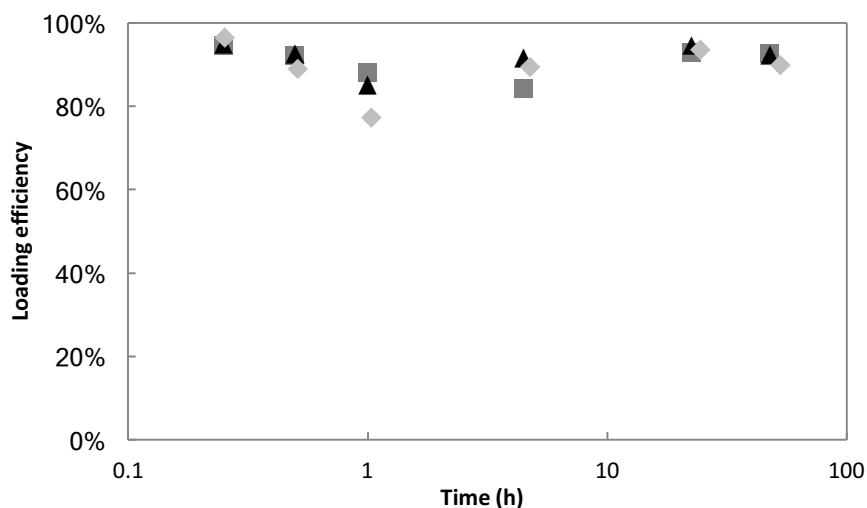

Figure 12: Loading efficiencies of ^{111}In in pH 3 PO₄³⁻ polymersomes at different incubation times. The light grey diamonds signify a pH 2 polymersome interior, the grey squares pH 3 and the black triangles pH 4. Each data point represents one measurement.

The efficient encapsulation at low pH could partially be due to indium ions precipitating more readily with phosphate ions at low pH [19,20]. In fact, pH gradients have already been employed for the labelling of liposomes with [99m]Tc [21] or [186/188]Re [22]. However, in our setup the loading mechanism likely also involves the indium-tropolone complex favouring the hydrophobic bilayer of the polymersomes, and dissociating when nearing the acidic cavity. We have experimentally determined that at pH<5 tropolone does not complex with indium (results not shown), and indeed at a pH of the aqueous polymersome cavity lower than pH 5, loading of indium was successful, whereas at higher pH it was not. The equilibrium speciation inside the polymersomes for this system has been given by the software program CHEAQS Next to be near 100% precipitation of the indium ions with PO$_4^{3-}$, at both an interior pH of 3 and 7.4, where InPO$_4$ was the only precipitated solid. However, these are the results in the absence of tropolone, since this molecule is not incorporated in the software package. This indicates that at higher pH the In-tropolone complex is too strong to allow precipitation with the phosphate.
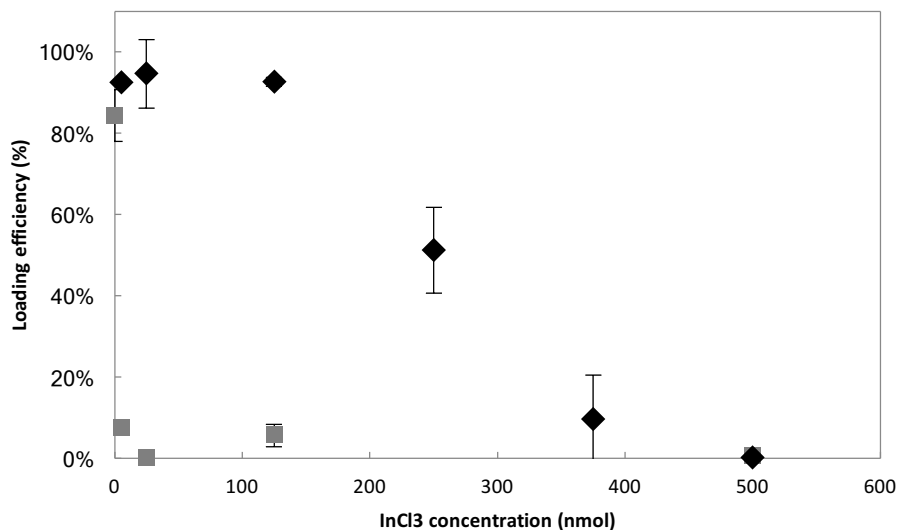
4

Figure 13: Loading efficiencies at different InCl$_3$ concentrations in 1 mL 2 mg/ml PBd$_{1800}$-PEO$_{900}$ polymersomes containing either 1 mM DTPA at pH 7.4 (squares) or 0.5 M KH$_2$PO$_4$ at pH 3 (diamonds) in the aqueous cavity.

Optimal loading efficiency (>95%) for approximately 100 kBq ^{111}In has been achieved within 15 minutes of loading, and remained constant over time. In order to get a measure for the amount of InCl$_3$ that could be loaded with this new method, as compared to the previous encapsulation method with DTPA [13], different amounts of cold InCl$_3$ have been added to a 2 mg/ml polymersome mixture. The loading efficiency of PO$_4^{3-}$ containing polymersomes has been found to be similar to that of DTPA containing polymersomes for small amounts of ^{111}In, with no additional InCl$_3$. However, the amount of indium that can be encapsulated in DTPA containing polymersomes is significantly lower than that for PO$_4^{3-}$ containing polymersomes (Figure 13). Calculations on the total amount of indium that could be encapsulated in the polymersomes, assuming a 1-1 precipitation ratio of indium and phosphate ions, would be 1.48 μmol. As evident from Figure 13, a maximum of 0.13 μmol indium has been successfully encapsulated. Upon adding larger amounts of InCl$_3$ to the loading solution, a white indium-tropolone precipitation has been observed in the vial. This precipitation likely prevents larger amounts of indium to be encapsulated in the polymersomes, as they are no longer free in solution, explaining the difference between the theoretical and actual loading capacity. However, when comparing this to the previously developed method employing a hydrophilic chelator for the loading of radionuclides [13], where only a few nmol of ^{111}In can be encapsulated at low efficiencies (Figure 13), it is clear that a far greater amount of indium can be encapsulated in the polymersomes, extending their possible applications also to carriers of MRI contrast agent like holmium or gadolinium [23].

InPO$_4$ analysis with Cryo-TEM and DLS

To confirm the formation of the InPO$_4$ nanoparticles, the polymersomes have been imaged with Cryo-TEM (Figure 14). It has been observed that InPO$_4$ forms spherical nanoparticles, positioned at seemingly random positions within the vesicles. The nanoparticles appear quite polydisperse, and are also found in the smaller (< 100 nm) polymersomes, required for optimal circulation times. Both the amount of indium added, and the amount of encapsulated phosphate have been varied to study their influence on nanoparticle size. Following from these images, at the lowest concentrations of indium

or phosphate (Figure 14 C and F) the nanoparticles are too small to be imaged (calculated size approximately around 1 nm). Analysis of the images has revealed a dependence of the amount of $InCl_3$ added on the nanoparticle size (Table 12), with the samples with more $InCl_3$ logically containing the larger nanoparticles. When the particles can be made smaller than 10 nm, the liver should, upon degradation of the polymersome, be able to clear the particles relatively quickly, minimalizing liver damage [24]. XRD analysis has revealed these InPO4 nanoparticles to have an amorphous structure.
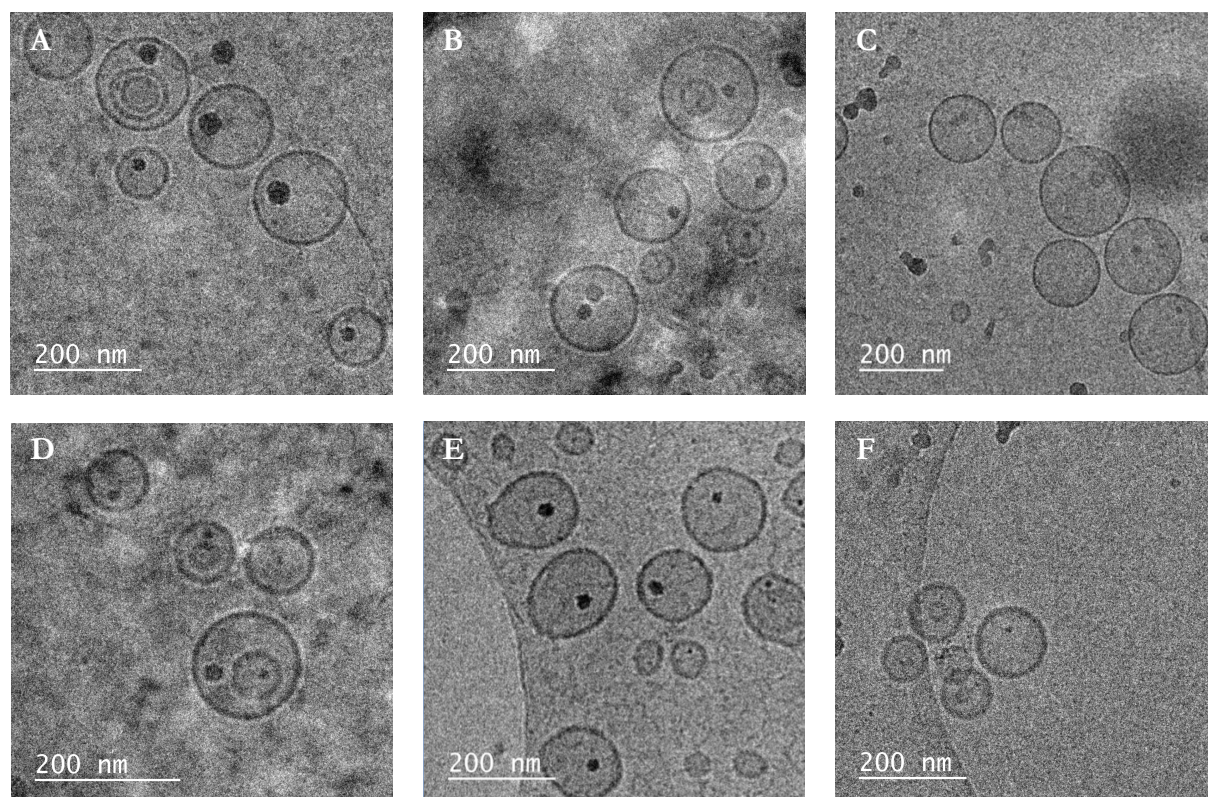
Figure 14: InPO₄ formations at different indium or KH₂PO₄ concentrations. A-C: 0.5 M KH₂PO₄ encapsulated in 100 nm 2 mg/ml polymersomes, to which 0.25 μmol (A), 0.125 μM (B), or 5 nmol (C) InCl₃ was added, and D-E: 5 μL 25 mM InCl₃ added to polymersomes containing 0.5 M (D), 0.1 M (E) or 0.01 M (F) KH₂PO₄.

Table 12: Polymersome (PS) and InPO₄ nanoparticle (NP) sizes for selected indium / phosphate concentrations in 100 nm polymersomes, as measured from Cryo-TEM images using ImageJ

	0.13 nM In 0.1 M PO₄	0.13 nM In 0.5 M PO₄	0.25 nM In 0.5 M PO₄
# PS imaged	122	42	43
PS size:	127 ± 40 nm	97 ± 37 nm	142 ± 60 nm
NP size:	21 ± 7 nm	18 ± 9 nm	31 ± 13 nm
NP/PS:	0.17 ± 0.03	0.18 ± 0.04	0.22 ± 0.05

4

Larger polymersome sizes have also been investigated, to determine the influence of polymersome size on nanoparticle size. They can be used for, for instance, subcutaneous or intratumoural injection, where the larger size should provide enhanced retention at the tumour site, as well as improved daughter retention. However, it was observed that formation of nanoparticles with the current method seems to take place only in smaller vesicles. About 80% of the polymersomes larger than 400 nm do not contain a nanoparticle, based on the Cryo-TEM analysis of nearly 200 polymersomes (containing 0.5 M KH_2PO_4 labelled with 125 nmol $InCl_3$) which had been passed through an 800 nm polycarbonate filter. Although no data on the precipitation of $InPO_4$ in large vesicles is available in literature, similar studies have been performed with the precipitation of $CaPO_4$ nanoparticles inside large lipid vesicles (1 – 2 μm diameter) suggesting that the precipitation of metal-phosphate inside vesicles is possible [9]. The main differences between their study and ours were the concentration of phosphate ions inside the vesicles, which was 10 times less, and the amount of $CaCl_2$ added, which was 400 times more than the amount of $InCl_3$ we added. This large excess of calcium could well explain their nanostructure formation in large vesicles.
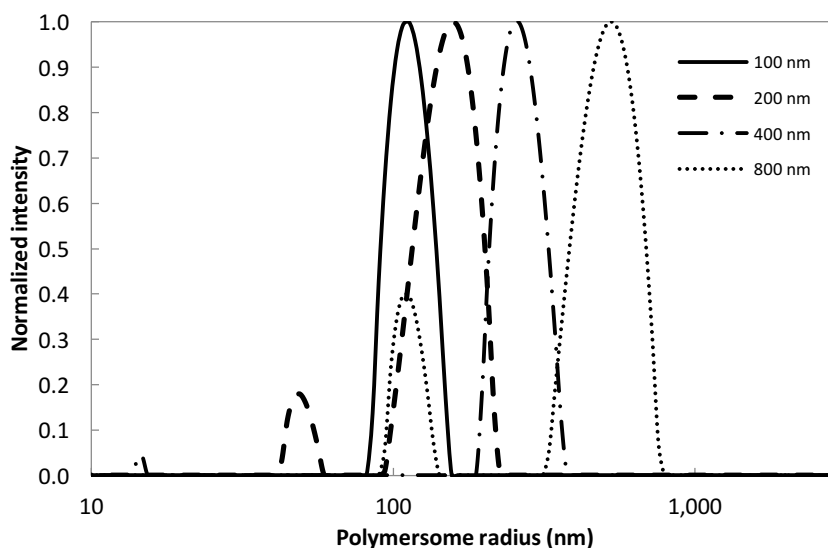
Figure 15: Normalized polymersome sizes measured by DLS of polymersomes extruded to 800 nm, 400 nm, 200 nm or 100 nm. Polymersome radii were, on average, found to be 523 nm, 261 nm, 157 nm, and 113 nm respectively.

In Figure 15, the radii of the different polymersomes as measured by DLS are shown. What immediately becomes apparent is that the average polymersome size is in all cases larger than the pores of the membrane filter they have been extruded through. This is in accordance with what we have observed earlier [5], and is likely due to the fact that DLS tends to overestimate the average particle size for polydisperse particles [25,26]. If we take for instance the polymersomes extruded through a 100 nm polycarbonate filter, DLS measurements yield an average diameter of 226 nm. However, the polymersomes analysed from the Cryo-TEM images (Table 12) had an average diameter of 124 nm, implying only small deviations from the expected polymersome size as based on the extruder pore diameter.

Indium retention

To determine the retention of the indium phosphate particles, a small amount of ^{111}In was co-precipitated with the cold indium. In Figure 16, the retention of ^{111}In in the polymersomes has been displayed for polymersomes with different molecules and pH in the aqueous cavity. About 90% of the indium has been retained in the 100 nm DTPA as well as PO_4^{3-} containing polymersomes, when challenged with DTPA. The latter is irrespective of the amount of InCl₃ added, implying precipitation occurring even at low indium concentrations. About 90% of the radionuclide is retained in PO_4^{3-} containing polymersomes. Serum experiments have been performed for polymersomes containing 0.5 M PO_4^{3-} at pH 3 in the core with 0.125 μmol InCl₃, kept at either RT or 37˙C. They demonstrated 96.1% and 93.5% of the activity to stay in the polymersomes respectively. This proves that the used formulation is suitable for further in vivo testing.
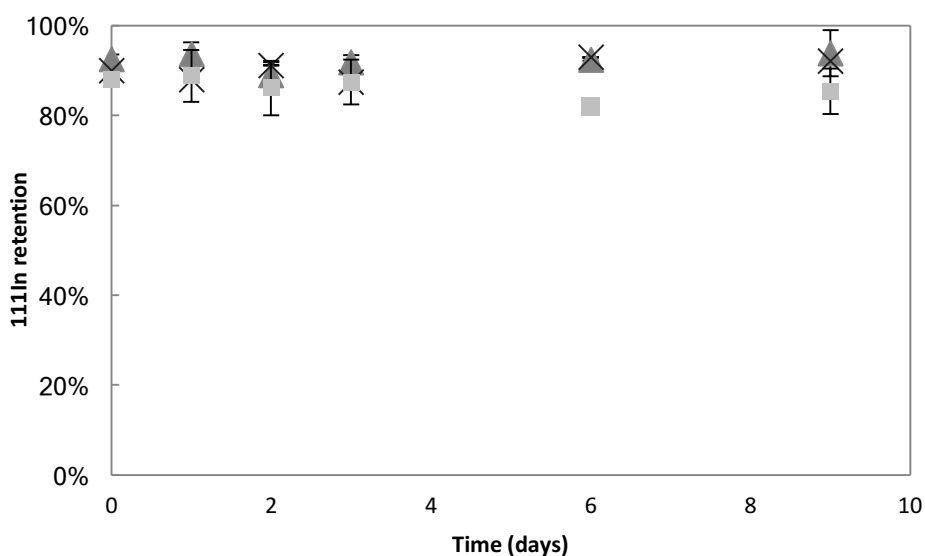
Figure 16: The retention of ^{111}In in polymersomes containing either 1 mM DTPA at pH 7.4 (cross) or 0.5 M KH₂PO₄ at pH 3 (square) with additional 2 μL 2.5 mM InCl₃ encapsulated (triangle) polymersomes.

LaPO₄ nanoneedles in polymersomes

Lanthanum has subsequently been loaded in the phosphate-containing polymersome. Lanthanum has been chosen because the chemistry of lanthanum is quite similar to that of actinium [14]. The co-precipitation [225]Ac was thus expected to be more successful with lanthanum than with indium [2], and the labelling with the active [140]La could be used as indicator for the successful loading of [225]Ac in PO_4^{3-} containing polymersomes. Next to that, the higher atomic number of lanthanum could result in a slightly higher daughter retention, although the simulation experiments in Chapter 3 indicated that no significant difference should be expected. A radiolabelling efficiency of 51 ± 4% for [140]La has been obtained for 0.5 M KH₂PO₄ containing polymersomes at pH 3. As discussed in Chapter 2, complexation of [140]La to the A23187 film in CHCl₃ allowed for more of the lanthanum to bind to the ionophore, increasing loading efficiencies to about 90% (Figure 17). Increasing the amount of encapsulated phosphate to 1 M decreased loading efficiencies, and at 2 M only big flakes were observed but no polymersomes were formed. This is likely caused by the high ionic strength of the medium in

4

which the polymersomes are formed. It has been shown by several groups that that nanoparticles composed of e.g. ethyl cellulose or chitosan tend to aggregate at higher ionic strengths [27–29]. As this effect has not been observed at a KH_2PO_4 concentration of 0.5 M or less, all subsequent experiments were carried out a concentration of 0.5 M.
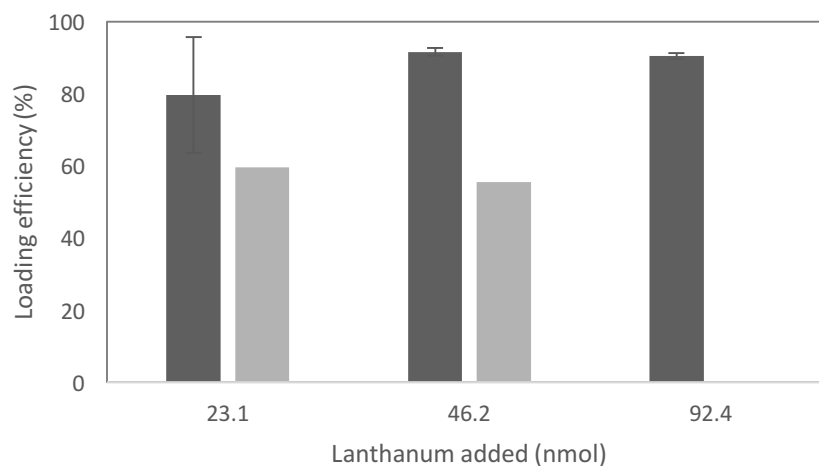
Figure 17: Loading efficiencies of different amounts of lanthanum in either 0.5 M (dark grey) or 1 M KH_2PO_4 (light grey) encapsulated in the polymersomes, obtained using the $CHCl_3$ method.

Cryo-TEM images indicated that, unlike $InPO_4$, the $LaPO_4$ crystals form nanoneedles instead of nanoparticles (Figure 18). When loading the polymersomes with 125 nmol lanthanum, the length of the nanoneedles encompasses on average 77% of the polymersome diameter (Figure 18 A, F). The images indicate that these needles are sharp enough to puncture the polymersome membrane, and subsequently destroy the polymersomes (Figure 18 B-D). When using less lanthanum in the loading solution, the nanoneedles decreased in length to approximately 35% of the polymersome diameter, and likewise they decreased in diameter (Figure 18 E). Thus, while it has been shown that lanthanum can be loaded in phosphate containing polymersomes, the observed polymersome membrane perforation by the formed nanoneedles suggest the formulation to be less suitable for in vivo applications than polymersomes containing $InPO_4$ nanoparticles.

	25 nmol La, 0.5 M PO$_4$	125 nmol La 0.5 M PO$_4$
# PS imaged	107	45
PS size:	170 ± 66	212 ± 148
NL:	58 ± 30	169 ± 129
NW:	6 ± 2	11 ± 5
NL/PS	0.35 ± 0.16	0.77 ± 0.17

Figure 18: LaPO$_4$ crystals formed in 0.5 M KH$_2$PO$_4$ containing 100 nm polymersomes (2 mg/ml) at different lanthanum concentrations. A-D: 0.125 µmol LaNO$_3$ was added, the nanoneedles puncture the polymersome membrane causing the polymersomes to fall apart. E: Smaller nanoneedles are formed upon the encapsulation of 25 nm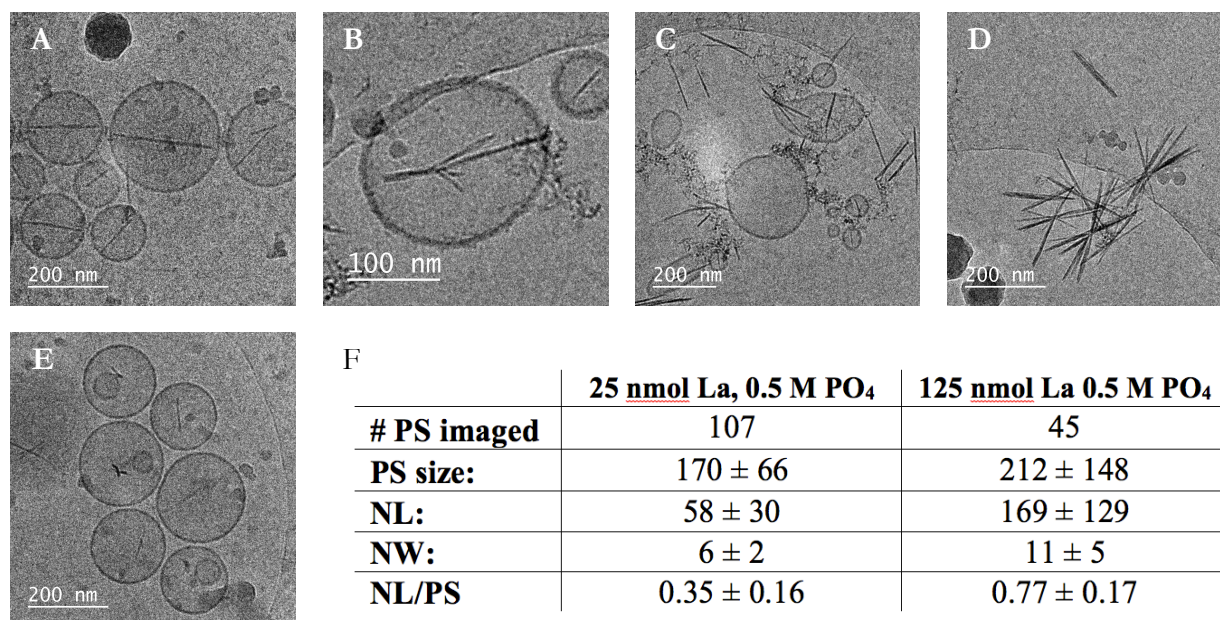ol LaNO$_3$. F: Polymersome (PS) and LaPO$_4$ nanoneedles of certain length (NL) and width (NW) in nm for selected lanthanum / phosphate concentrations in 100 nm polymersomes, as measured from Cryo-TEM images using ImageJ.

CaPO$_4$ nanowires

Because calcium is a less toxic element than lanthanum and indium, possesses a similar capacity for recoiling daughter retention (Chapter 3), and has already been shown to be forming phosphate nanostructures in liposomes [9,8], some initial experiments have been performed to encapsulate calcium in polymersomes. The loading efficiency could unfortunately not be determined, because radioactive calcium was not available. Therefore, the successful loading of calcium was studied with CryoTEM, where calcium was loaded in phosphate-containing polymersomes using either tropolone or calcium ionophore as lipophilic ligand. In Figure 19, representative Cryo-TEM images of polymersomes after loading with these two ligands are shown. It is clear that tropolone does not lead to the successful encapsulation of calcium (Figure 19 A), but with A23187 as ligand calcium nanowires are formed. These are somewhat similar to what was found by Sauer et al., though appear much thinner and more curved [9]. Because the wires were very thin, likely resulting in a lower recoil retention than the lanthanum needles or indium spheres, and quantification of successful loading difficult, the study into the formation of CaPO$_4$ precipitates was discontinued.
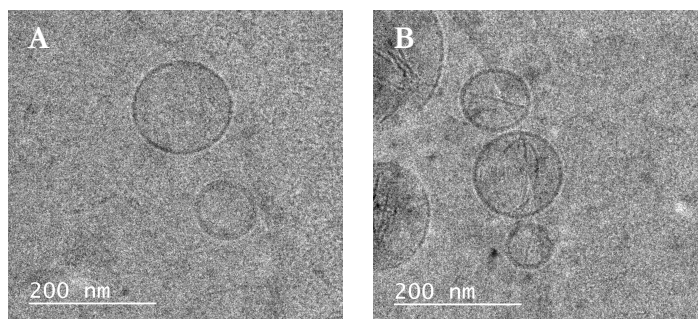
Figure 19: 5 μL 25 mM calcium loaded in polymersomes containing 0.5 M phosphate, using either tropolone (A) or calcium ionophore (B) as lipophilic ligand.

Conclusions

In conclusion, in this research a novel radionuclide loading method has been developed and tested. Polymersomes composed of PBd_{1800}–PEO_{900} block copolymers containing KH_2PO_4 have successfully been loaded with indium, lanthanum and calcium. A direct correlation between the amount of metal encapsulated and the size of the nanoparticles has been observed. Whereas $InPO_4$ forms spherical nanoparticles in polymersomes, $LaPO_4$ produces needles that are capable of puncturing the polymer bilayer, and $CaPO_4$ was found to form nanowires. Of these three options, indium phosphate appears to have the greatest potential for successful daughter radionuclide retention, with additional advantage the large amount of metal that can be encapsulated.

References

1. Virk, H. S.; Randhawa, G. S. Stopping power and range relations for low and high z ions in solids: a critical analysis. *Mater. Sci. Forum Vols.* **1997**, *248–249*, 33–39.

2. Woodward, J.; Kennel, S. J.; Stuckey, A.; Osborne, D.; Wall, J.; Rondinone, A. J.; Standaert, R. F.; Mirzadeh, S. LaPO4 nanoparticles doped with actinium-225 that partially sequester daughter radionuclides. *Bioconjug. Chem.* **2011**, *22*, 766–76.

3. McLaughlin, M. F.; Woodward, J.; Boll, R. a; Wall, J. S.; Rondinone, A. J.; Kennel, S. J.; Mirzadeh, S.; Robertson, J. D. Gold coated lanthanide phosphate nanoparticles for targeted alpha generator radiotherapy. *PLoS One* **2013**, *8*, e54531.

4. Rojas, J. V; Woodward, J. D.; Chen, N.; Rondinone, A. J.; Castano, C. H.; Mirzadeh, S. Synthesis and characterization of lanthanum phosphate nanoparticles as carriers for 223 Ra and 225 Ra for targeted alpha therapy ☆. *Nucl. Med. Biol.* **2015**, *42*, 614–620.

5. Wang, G.; de Kruijff, R. M.; Rol, A.; Thijssen, L.; Mendes, E.; Morgenstern, A.; Bruchertseifer, F.; Stuart, M. C. A.; Wolterbeek, H. T.; Denkova, A. G. Retention studies of recoiling daughter nuclides of 225Ac in polymer vesicles. *Appl. Radiat. Isot.* **2014**, *85*, 45–53.

6. Thijssen, L.; Schaart, D. R.; de Vries, D.; Morgenstern, A.; Bruchertseifer, F.; Denkova, A. G. Polymersomes as nano-carriers to retain harmful recoil nuclides in alpha radionuclide therapy: a feasibility study. *Radiochim. Acta* **2012**, *100*, 473.

7. Brinkhuis, R. P.; Stojanov, K.; Laverman, P.; Eilander, J.; Zuhorn, I. S.; Rutjes, F. P. J. T.; Hest, J. C. M. Van Size Dependent Biodistribution and SPECT Imaging of 111In-Labeled Polymersomes. *Bioconjug. Chem.* **2012**, *23*, 958–965.

8. Eanes, E. D.; Hailer, a W.; Costa, J. L. Calcium phosphate formation in aqueous suspensions of multilamellar liposomes. *Calcif. Tissue Int.* **1984**, *36*, 421–30.

9. Sauer, M.; Haefele, T.; Graff, A.; Nardin, C.; Meier, W. Ion-carrier controlled precipitation of calcium phosphate in giant ABA triblock copolymer vesicles. *Chem. Commun.* **2001**, 2452–2453.

10. Michel, M.; Winterhalter, M.; Darbois, L.; Hemmerle, J.; Voegel, J. C.; Schaaf, P.; Ball, V. Giant Liposome Microreactors for Controlled Production of Calcium Phosphate Crystals.

11. Abraham, S. A.; Edwards, K.; Karlsson, G.; MacIntosh, S.; Mayer, L. D.; McKenzie, C.; Bally, M. B. Formation of transition metal–doxorubicin complexes inside liposomes. *Biochim. Biophys. Acta - Biomembr.* **2002**, *1565*, 41–54.

12. Taggar, A. S.; Alnajim, J.; Anantha, M.; Thomas, A.; Webb, M.; Ramsay, E.; Bally, M. B. Copper–topotecan complexation mediates drug accumulation into liposomes. **2006**.

13. Wang, G.; de Kruijff, R. M.; Stuart, M. C. A.; Mendes, E.; Wolterbeek, H. T.; Denkova, A. G. Polymersomes as radionuclide carriers loaded via active ion transport through the hydrophobic bilayer. *Soft Matter* **2013**, *9*, 727–734.

4

14. Kirby, H. W.; Morss, L. R. Actinium. In; 1994; pp. 18–51.

15. Palmer, R. J.; Butenhoff, J. L.; Stevens, J. B. Cytotoxicity of the Rare Earth Metals Cerium, Lanthanum, and Neodymium in Vitro: Comparisons with Cadmium in a Pulmonary Macrophage Primary Culture System. *Environ. Res.* **1987**, *43*, 142–156.

16. Sciencelab.com Material Safety Data Sheet Calcium phosphate dibasic MSDS http://www.sciencelab.com/msds.php?msdsId=9927123 (accessed Oct 17, 2017).

17. Verweij, W. CHEAQS Next 2016.

18. Rasband, W. . ImageJ. *U.S. Natl. Institutes Heal.* **2016**.

19. Lin, X.-H.; Wang, Y.-C.; Su, Y.-H.; Yang, C.-S. Synthesis, Properties, and Evolution Mechanism of Morphology Tunable InPO4 Crystals. *J. Chinese Chem. Soc.* **2007**, *54*, 1123–1128.

20. Jiang, J.; Liang, D.; Zhong, Q. Precipitation of indium using sodium tripolyphosphate. *Hydrometallurgy* **2011**, *106*, 165–169.

21. Li, S.; Goins, B.; Phillips, W. T.; Bao, A. Remote-loading labeling of liposomes with 99mTc-BMEDA and its stability evaluation: effects of lipid formulation and pH/chemical gradient. *J. Liposome Res.* **2010**, *21*, 17–27.

22. Goins, B.; Bao, A.; Phillips, W. T. Techniques for Loading Technetium-99m and Rhenium-186/188 Radionuclides into Pre-formed Liposomes for Diagnostic Imaging and Radionuclide Therapy. *Methods Mol. Biol.* **2009**, *606*, 469–491.

23. Dumont, M. F.; Baligand, C.; Li, Y.; Knowles, E. S.; Meisel, M. W.; Walter, G. A.; Talham, D. R. DNA Surface Modified Gadolinium Phosphate Nanoparticles as MRI Contrast Agents. *Bioconjug. Chem.* **2012**, *23*, 951–957.

24. Phillips, E.; Penate-Medina, O.; Zanzonico, P. B.; Carvajal, R. D.; Mohan, P.; Ye, Y.; Humm, J.; Gönen, M.; Kalaigian, H.; Schöder, H.; Strauss, H. W.; Larson, S. M.; Wiesner, U.; Bradbury, M. S. Clinical translation of an ultrasmall inorganic optical-PET imaging nanoparticle probe. *Sci. Transl. Med.* **2014**, *6*, 260ra149-260ra149.

25. Panchal, J.; Kotarek, J.; Marszal, E.; Topp, E. M. Analyzing Subvisible Particles in Protein Drug Products: a Comparison of Dynamic Light Scattering (DLS) and Resonant Mass Measurement (RMM). *Am. Assoc. Pharm. Sci.* **2014**, *16*, 440–451.

26. Bain, J.; Ruiz-Pérez, L.; Kennerley, A. J.; Muench, S. P.; Thompson, R.; Battaglia, G.; Staniland, S. S. In situ formation of magnetopolymersomes via electroporation for MRI. *Sci. Rep.* **2015**, *5*, 14311.

27. Harnsilawat, T.; Pongsawatmanit, R.; McClements, D. J. Influence of pH and Ionic Strength on Formation and Stability of Emulsions Containing Oil Droplets Coated by -Lactoglobulin-Alginate Interfaces. *Biomacromolecules* **2006**, *7*, 2052–2058.

28. Jonassen, H.; Kjøniksen, A. L.; Hiorth, M. Effects of ionic strength on the size and compactness of chitosan nanoparticles. *Colloid Polym. Sci.* **2012**, *290*, 919–929.

29. Bizmark, N.; Ioannidis, M. A. Effects of Ionic Strength on the Colloidal Stability and Interfacial Assembly of Hydrophobic Ethyl Cellulose Nanoparticles. *Langmuir2* **2015**, *31*, 9282–9289.

4

5

Improved ^{225}Ac Daughter Retention in Nanoparticles in Polymersomes

Abstract

Alpha-emitting radionuclides like [225]Ac are ideal candidates for the treatment of small metastasised tumours, where the long half-life of [225]Ac enables it to also reach less accessible tumours. The main challenge lies in retaining the recoiled alpha-emitting daughter nuclides, which are decoupled from targeting agents upon emission of an alpha particle and can subsequently cause unwanted toxicity to healthy tissue. Polymersomes are capable of transporting (radio)pharmaceuticals to tumours, and are ideal candidates for the retention of the daughter nuclides. [225]Ac was incorporated in indium or lanthanum phosphate nanoparticles inside polymersomes. The recoil retention of two of the daughter nuclides, [221]Fr and [213]Bi, was determined at different vesicle sizes. Recoil retention was found to have improved significantly as compared to earlier published results by Wang et al. where [225]Ac was encapsulated using a hydrophilic chelate [1]. To better understand the different parameters influencing daughter retention, simulation data was expanded to include vesicle polydispersity and nanoparticle position within the polymersome. The high retention of the recoiling daughters and the [225]Ac itself makes this vesicle design very suitable for future in vivo verification.

Introduction

Alpha radionuclide therapy is steadily gaining importance; due to the short penetration range in tissue (i.e. 50–80 µm) and the high linear energy transfer (up to 200 keV/µm) of alpha particles, they are ideal candidates for the treatment of small malignant tumours. Relatively long-lived radionuclides like ^{225}Ac ($t_{1/2}$ = 10 d) are necessary for the extension of alpha radionuclide therapy to less accessible solid tumours, where a relatively long time is required for the penetration in the malignant tissue or for the optimal distribution of the targeting agent. One of the main challenges in the safe application of ^{225}Ac in alpha radionuclide therapy is minimizing the release of its alpha emitting daughters, which are decoupled from the targeting agent upon the emission of an alpha particle, leaving the daughter atoms free to migrate through the body and damage healthy tissue.

As discussed in Chapter 1, there are three different approaches to deal with this recoil problem: cell internalisation, local administration, or encapsulation in a nano-carrier. Polymersomes are promising nano-carriers, capable of transporting a variety of pharmaceuticals to tumours. By incorporating alpha-emitting radionuclides in these polymersomes, the recoiled daughters can be retained in the vesicle and thus at the tumour site. In a previous study by Wang et al. [1], recoil retentions of respectively 37 ± 4% and 22 ± 1% were obtained for two of the alpha-emitting daughters of ^{225}Ac, ^{221}Fr ($t_{1/2}$ = 4.8 min) and ^{213}Bi ($t_{1/2}$ = 45.6 min), in 100 nm vesicles. A schematic view of this situation can be found in Figure 20 (a). This was already a large step forward from the traditional targeting situation, where the daughter nuclide will always break the chemical bond to a targeting vector upon emission of an alpha particle. However, it is not yet sufficient to significantly limit damage to tissue caused by free daughter nuclides. The goal of this chapter is to further improve upon this system to increase daughter retention. Nuclear stopping of low energy heavy ions predominates in high Z materials, so the range of recoiled daughters will be smaller there than in an aqueous environment. To create a high Z environment around the alpha-emitting radionuclide ^{225}Ac, it was precipitated with indium and phosphate ions to create metal-phosphate nanoparticles inside polymersomes (Figure 20 (b)). Supported by simulation work in the Geant4 based simulation package NANVES, we show that the incorporation of ^{225}Ac in nanoparticles in these polymersomes results in further reduced recoil ranges, allowing for the safe application of ^{225}Ac containing polymersomes as therapeutic agent.

5
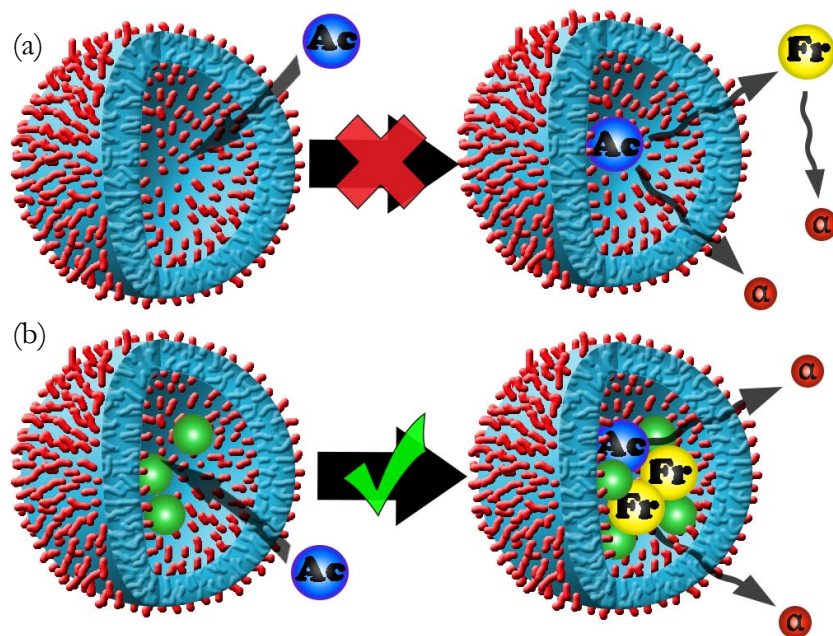
Figure 20: Schematic view of (a) the original situation, where ^{225}Ac is coupled to a chelator inside the polymersome [1], and (b) improved retention of ^{225}Ac daughters like ^{221}Fr by precipitation inside the polymersomes with In^{3+} and PO$_4^{3-}$ ions (green spheres) as presented in this paper.

Materials and Methods

Chemicals

The poly(butadiene(1,2 addition)-b-ethylene oxide) block copolymer was obtained from Polymer Source (Quebec, Canada), with a Mn of 1900-b-900 g/mol, with a weight ratio (Mw/Mn) of 1.05. The ^{111}In ($t_{1/2}$ = 2.81 d) was provided by the section Nuclear Medicine of the Erasmus Medical Center (Rotterdam, the Netherlands) with a specific activity of 1.72 MBq pmol^{-1}. A dry sample containing ^{225}Ac was prepared at the Directorate for Nuclear Safety and Security (Karlsruhe, Germany) [2]. All other chemicals were purchased from Sigma-Aldrich.

Polymersome preparation

The polymersomes were prepared by adding a ratio of 2 mg block copolymer per 1 mL of chelate (1 mM DTPA at pH 7.4 or 0.5 M KH$_2$PO$_4$ at pH 3) in 10 mM HEPES buffer to a vial and stirring for a week. Prior to the loading of the radionuclide in the polymersomes, the unencapsulated DTPA or PO$_4^{3-}$ was removed using a 30 cm Sephadex G-25 M column, equilibrated with a 10 mM pH 7.4 HEPES buffer. All experiments were carried out at room temperature T = 20 ± 2 °C. In all experiments, the polymersome concentration mentioned (in mg/mL) refers to the initial concentration (before dilution by passing through size exclusion columns).

^{225}Ac loading

The actinium solution was prepared by dissolving the dry ^{225}Ac (approximately 111 MBq) in a 1 mL HCl (0.01 M) solution. A thin ionophore (A23187) film was prepared by dissolving 0.1 mg of ionophore solution in 100 μL of chloroform, which was subsequently evaporated. 2 to 5 μL of the actinium solution, depending on the desired ^{225}Ac activity, was added to the film, together with 0.2 mL of 10 mM HEPES buffer. For incorporation in the InPO$_4$ nanoparticles, 0.125 nmol of pH 2 InCl$_3$ solution was subsequently added together with 10 μL 25 mM tropolone. For co-precipitation with LaPO$_4$, 0.125 nmol of pH 2 LaNO$_3$ solution was added to the film together with the ^{225}Ac. The solution was incubated for 10 min, after which 0.8 mL of the polymersome solution was added and the mixture was left at rest for 1 h. The loading efficiency was determined by measuring the gamma emission of ^{221}Fr and ^{213}Bi in the polymersome solution both before and 24 hours after separation, to ensure equilibrium. An HPGe detector was utilized for the activity measurements, and the loading efficiency was calculated using the gamma energy peaks at 218 keV (^{221}Fr) and 440 keV (^{213}Bi).

^{221}Fr and ^{213}Bi retention

For determining the ^{225}Ac daughter retention, the protocol of Wang et al. was followed [1]. In short, the ^{225}Ac-containing polymersome solution was left for 24 hours to attain equilibrium, after which the recoiled ^{221}Fr and ^{213}Bi were filtered out using 0.5 g DOWEX cation resin (50x8, 100/200 mesh, H+ form) through a filter having pore size of 30 μm, with only 1% and 3% breakthrough respectively. Using a stopwatch, the exact time between the separation of the recoiled daughters and the activity measurements of ^{221}Fr and ^{213}Bi was determined. Activity measurements were periodically performed for the 6 hours after separation of the daughter nuclides, and the activity of the daughters at the moment of separation was calculated according to

$$A_2 = A_1\left(1 - e^{-\lambda_2 t}\right) + A_2(0)e^{-\lambda_2 t} \tag{3}$$

where A$_1$ is activity of ^{225}Ac, which is approximately equal to the daughter activity at equilibrium, and λ$_2$ is the decay constant of either ^{213}Bi (0.141 min^{-1}) or ^{221}Fr (0.0151 min^{-1}).

In Figure 21, the measurements of the ingrowth of activity of both ^{221}Fr and ^{213}Bi upon the removal of the free radionuclides are shown. The curves are fitted in OriginPro using equation 2, and are used to extrapolate the activity of the two daughter nuclides at time t = 0. Comparing this to the equilibrium activity allows for determination of the retention of the two daughter nuclides.
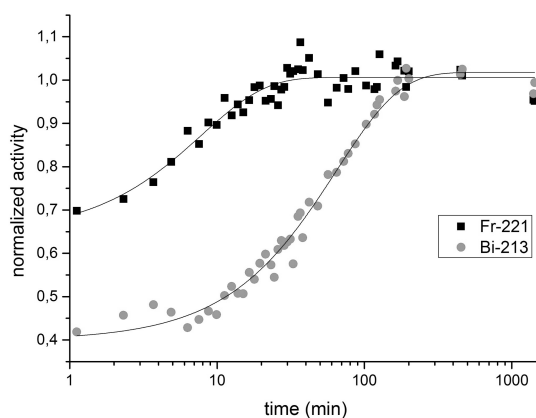
Figure 21: The measured normalized activity of the daughters of [225]Ac as a function of time after separation of the recoiled nuclides.

CHEAQS Next speciation

The software program 'CHEAQS Next' was used to determine the equilibrium speciation of $InCl_3$ and $LaNO_3$ at a concentration of 10-500 nmol in an 0.5 M KH_2PO_4 medium, at a pH of either 3 of 7.4.

NANVES Monte Carlo (MC) simulations of recoil retention in polymersomes

NANVES is a Geant4 based simulation package that can be used for visual 3D tracking of recoil atoms inside nanovesicles and calculates the retention of a specified recoil atom inside the vesicle [3]. NANVES-STOP and NANVES-CONS were expanded to simulate polymersomes containing indium-based nanoparticles, as shown in Chapter 3. In NANVES-CONS a new separate volume was defined for the indium phosphate nanoparticles and lanthanum phosphate nanoneedles. The nanoparticles and needles were positioned in the middle of the polymersome. The size distribution of the polymersomes was modelled according to the size distributions as obtained by dynamic light scattering (Chapter 4). The shape and the size of both the $InPO_4$ and $LaPO_4$ particles inside the polymersome were based on the experimental results of the Cryo-TEM image analysis as presented in Chapter 4, so the deviation of the simulation from the experimental results due to geometrical inconsistencies was minimized. Different nanoparticle sizes were tested within the range of the experimental results. Actinium was assumed to have a random position inside the nanoparticles. DLS data was used as an input for the polydispersity correction of the simulated retention. Simulations of 500 events each were performed for the polymersome designs in question, of varying sizes to create a 'retention database' (containing sizes of 50 - 300 nm with size increments of 25 nm, 300-900 nm with size increments of 50 nm). The uncertainty in the simulated recoil retention from event limitation was approximately ± 2%. The experimental radius determined by DLS was coupled to the corresponding size interval of the retention database. The simulated retention corresponding to the polymersome with the exact radius determined by DLS was then calculated by linear interpolation of the retention data. Subsequently, the retention results for the exact polymersome sizes were weighted according to their measured intensity, which resulted in the corrected retention value. For the simulations of [225]Ac-DTPA in polymersomes, the [225]Ac was placed as a free ion at a random position within the polymersome. The membrane of the

polymersome was assumed to have a thickness of 7 nm and a ratio of Dphil/Dphob of 0.2, where Dphil is the diameter of the PEO, and Dphob the diameter of the hydrophobic PBd part of the bilayer.

Results and Discussion

We have built on our previous results using polymersomes to retain the recoiled daughters of ^{225}Ac. As the average projected stopping range of the alpha-emitting ^{225}Ac daughters lies around 100 nm in either H_2O or the block copolymer used in this study [3], they were found not to be retained very well in small (~100 nm) polymersomes [1]. To ensure long in vivo circulation time of the vesicles, they need to be less than 120 nm in diameter, as found in a recent study by Brinkhuis et al. [4] Therefore, our polymersome design needed to be optimized to increase recoil retention in small vesicles. The recoil ranges of the ^{225}Ac daughters in indium and lanthanum phosphate nanoparticles have been simulated using the NANVES simulation package, showing that decay events in these nanoparticles will result in a reduced recoil range of around 30 nm (Chapter 3). As the recoil range of the daughters is considerably smaller in these nanoparticles, we have developed polymersomes containing 0.5 M KH_2PO_4 at pH 3, to co-precipitate ^{225}Ac with metal ions such as indium or lanthanum to form nanoparticles inside the polymersomes, as discussed in Chapter 4, which should contain the daughters better.

^{225}Ac loading and daughter nuclide retention

To determine the recoil retention of the ^{225}Ac daughters, ^{225}Ac was co-encapsulated in $InPO_4$ nanoparticles or $LaPO_4$ nanoneedles. To ensure PD10 size exclusion columns could be used for the separation of polymersomes from unencapsulated nuclides, the different solutions have been passed through a PD10 column. The elution fractions of Ac-polymersomes and Ac-DTPA were clearly distinguishable, whereas the Ac-ionophore, ^{225}Ac-phosphate and ^{225}Ac did not have any distinguishable peaks, most of the activity here stuck on the column. With less than 5% of the latter three in the polymersome fraction, and less than 1% of the Ac-DTPA, good separation has been achieved.

In Table 13, the loading efficiency and retention are presented for ^{225}Ac co-encapsulated with lanthanum and indium. A sufficiently high loading efficiency has been achieved in both $InPO_4$ and $LaPO_4$ polymersomes. The lower efficiency in the case of the $LaPO_4$ containing vesicles is likely due to competition of the cold lanthanum with the ^{225}Ac, as for these nuclides the same lipophilic ligand (A23187) is used for transportation through the polymer membrane. As indium is transported by tropolone, it forms no direct competition with ^{225}Ac in this regard, allowing for a high loading efficiency of both ions. Retention of ^{225}Ac in the $InPO_4$ containing polymersomes is similar to what has previously been found for the ^{225}Ac-DTPA polymersomes [1]. Retention of ^{225}Ac in the $LaPO_4$ containing polymersomes was lower, which is likely due to the nanoneedles puncturing the polymersome bilayer, allowing ^{225}Ac ions to diffuse through the polymer membrane, or to detach from the unencapsulated nanoneedle.

Table 13: Loading efficiencies of [225]Ac co-encapsulated with indium or lanthanum in 0.5 M PO_4^{3-} containing polymersomes

Nanoparticles	[225]Ac loading efficiency	[225]Ac retention
125 nmol In, 0.5 M PO_4^{3-}	89 ± 0.6%	92 ± 3%
125 nmol La, 0.5 M PO_4^{3-}	65 ± 18 %	70 ± 10%

Daughter Nuclide Retention

With the NANVES simulation package, the theoretical retention of the [225]Ac daughters was determined for a large number of vesicle designs, as shown in Chapter 3. Through simulations, a large variety of designs can quickly be tested for their retention properties, and those with the right properties and high daughter retention can be translated to the lab, and validated by experiments. This greatly reduces the number of (costly) experiments, and helps in a fast optimization of methodologies. In Figure 22, the geometry of the sphere-shaped $InPO_4$, and needle-like $LaPO_4$ nanoparticles in the vesicles as used in the simulations as compared to that obtained from the Cryo-TEM data can be observed. To construct the nanoparticles in the polymersomes for these simulations, their relative size to the polymersome size, as presented in Chapter 4, was used. These ratios have experimentally been found to hold also for larger polymersomes.
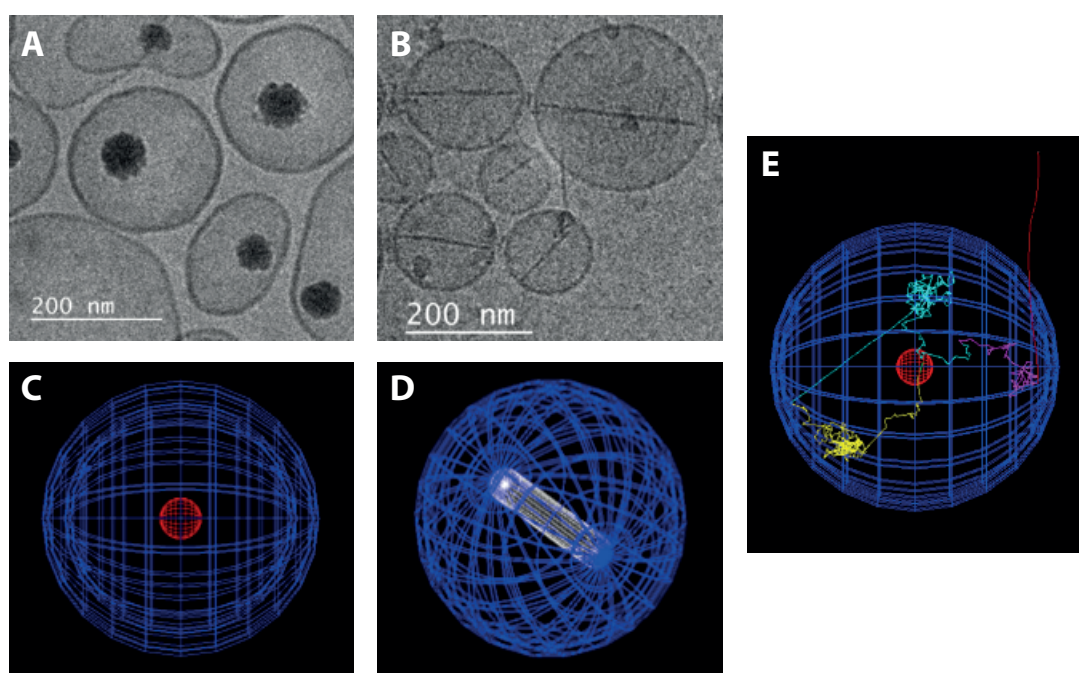

Figure 22: Simulations of the $InPO_4$ (C) and $LaPO_4$ (D) nanoparticles in polymersomes as based on the Cryo-TEM data (A and B respectively), and E: an example of the [225]Ac decay cascade in a 200 nm polymersome, where the [225]Ac decay event originated in the $InPO_4$ nanoparticle in the centre of the polymersome.

InPO$_4$ containing polymersomes

^{225}Ac has been co-encapsulated with indium to precipitate into InPO$_4$ nanoparticles, where the decay from within the nanoparticle is expected to result in a reduced recoil range of the daughter nuclide. Figure 23 displays the recoil retention of ^{225}Ac daughters in polymersomes containing InPO$_4$ nanoparticles, and compares it to our earlier published results without the presence of nanoparticles [1]. Both the ^{221}Fr and ^{213}Bi daughters have increased in recoil retention, which indicates that the ^{225}Ac indeed precipitated with the indium phosphate inside the polymersomes. The retention of the first daughter, ^{221}Fr, has increased on average about 20 percent points for all polymersome sizes. This is to be expected, since it is the first daughter after the initial decay of ^{225}Ac. The recoil thus originates from within the nanoparticle, and will lose most of its energy in its path through the nanoparticle, allowing for a large fraction of the ^{221}Fr to be retained.

The retention of ^{213}Bi has improved about 10 percent points on average as compared to earlier results with DTPA-containing polymersomes [1]. The main improvements here are found for the smaller polymersome sizes, polymersomes greater than 400 nm appear to have a similar recoil retention as those without nanoparticles. ^{213}Bi retention would be expected to improve to a lesser extent, because the average recoil distance of about 30 nm in metal-phosphate nanoparticles will result in either the first or the second daughter of ^{225}Ac to recoil out of the nanoparticle. This leaves ^{213}Bi free in the polymersome, and thus in a situation not so different from the polymersomes where the ^{225}Ac was coupled to DTPA. Furthermore, as observed in the Cryo-TEM images, polymersomes larger than about 400 nm often do not contain an InPO$_4$ nanoparticle. They might contain some small diffuse crystals, which cannot be visualized using Cryo-TEM accounting for the increased ^{221}Fr retention, but no particles large enough to significantly improve ^{213}Bi retention. The smaller polymersomes, 100 nm and 200 nm, do contain nanoparticles, which explains the increase in ^{213}Bi retention observed here. Nevertheless, comparing the current results to the retention of ^{213}Bi in multivesicular liposomes of about 800 nm, which display a retention of about 17-18%, we conclude that a significant improvement to the daughter retention has been made [6]. McLaughlin et al. incorporated ^{225}Ac in gold-coated lanthanide phosphate particles with a diameter of 27 nm [7]. The ^{221}Fr retention of these particles was found to be 70%, which is somewhat similar to what we found for polymersomes containing particles of this size. Their use of Au coating might have a better effect on ^{221}Fr retention than our polymer shell, as the projected range of the recoiled daughters in Au is only 10 nm (results not shown), whereas in water it is about 100 nm. They unfortunately did not study the direct ^{213}Bi retention in the nanoparticles, but in vivo they found 69% of the ^{213}Bi to be retained in the targeted lung tissue, as a combination of retention by the nanoparticle and the cell due to endocytosis. Similar results can be expected for the polymersomes presented in this work as soon as they have been taken up by a cell.

For optimal in vivo circulation times, vesicles of 100 nm in diameter should be preferred, and the ^{221}Fr and ^{213}Bi retention here increased with respectively 20 percent points and 18 percent points on average as compared to polymersomes without nano-particle. It is important to keep in mind that with the much improved ^{221}Fr retention, already two alpha particles have been emitted from within the polymersomes, thus at the targeted site (depending on in vivo targeting efficiency) ensuring optimal irradiation of the tumour and limiting potential harm due to recoiled daughters to, for example, the kidneys.

Figure 23: Recoil retention of ^{221}Fr and ^{213}Bi in polymersomes of different diameters containing 0.5 M PO$_4^{3-}$, where the ^{225}Ac was co-encapsulated with 125 nmol cold indium (black) compared to the previously published retention in DTPA containing polymersomes [1]. The error bars represent the standard deviation based on at least three separate experiments.

LaPO$_4$ containing polymersomes

In Figure 24, the experimentally determined recoil retention of ^{221}Fr and ^{213}Bi in polymersomes containing lanthanum phosphate nanoneedles are plotted together with the retention as simulated using NANVES. In contrast to the spherical LaPO$_4$ model presented in Chapter 3, here the LaPO$_4$ is simulated as nanoneedles based on CryoTEM observations, and should thus more closely resemble the experimental results. Both the simulated and experimental retention show the expected trends, ^{221}Fr and ^{213}Bi retention increases with increasing polymersome diameter, where ^{221}Fr retention is much higher than ^{213}Bi. The difference between experimental and simulation data is partially caused by the uncertainty in nanoneedle size and vesicle polydispersity, but is likely to a large extend the result of the destruction of polymersome bilayer by LaPO$_4$ nanoneedles, as presented in Chapter 4.
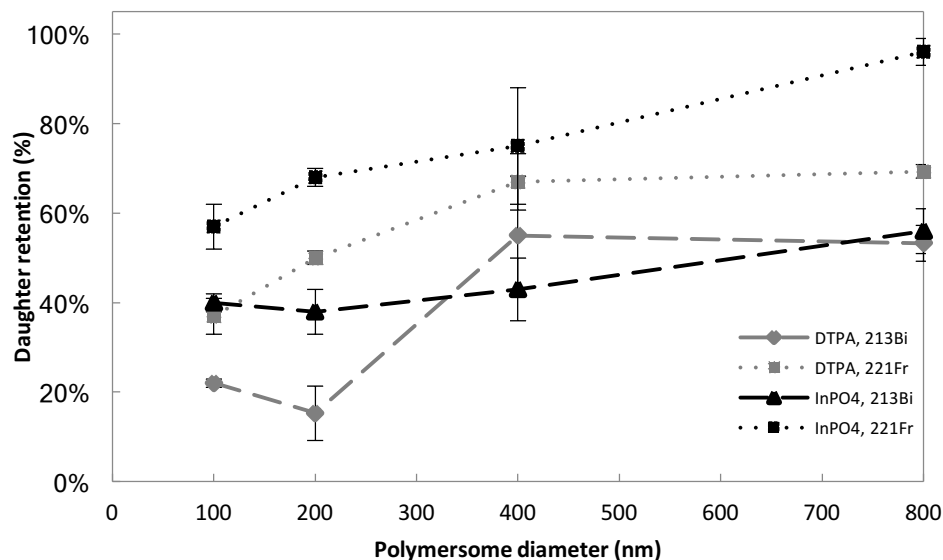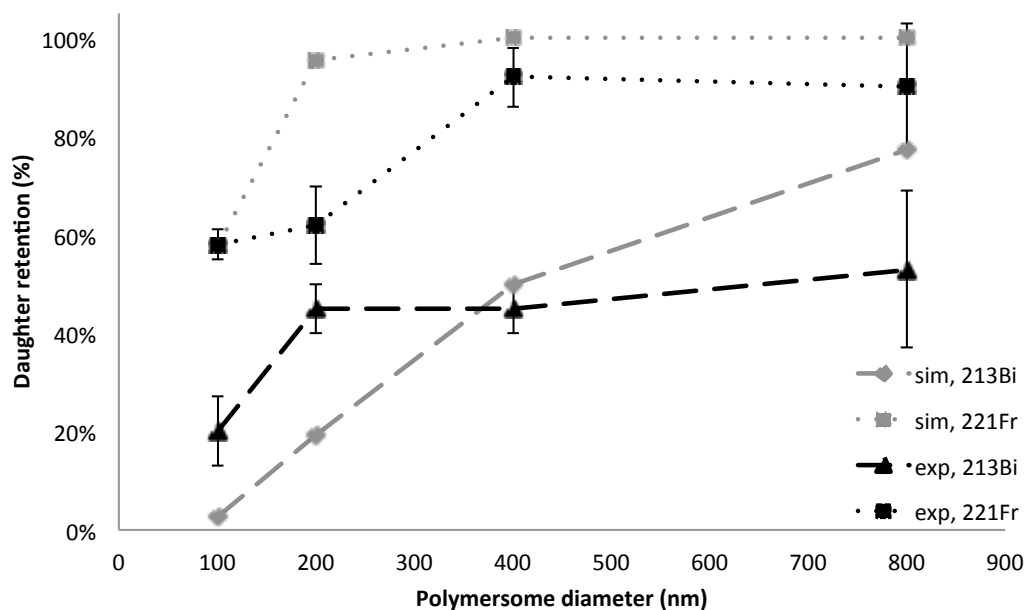
Figure 24: Recoil retention of [221]Fr and [213]Bi in polymersomes of different diameters containing 0.5 M PO_4^{3-}, where the [225]Ac was co-encapsulated with 125 nmol cold lanthanum, as determined by simulations (light grey) and experimentally (black).

In light of the polymer membrane destruction by the needles, experimentally determined recoil retentions (Figure 24) are higher than expected. As the $LaPO_4$ nanoneedles are relatively thin and the recoil distance of any of the [225]Ac daughters in $LaPO_4$ is about 30 nm [8], without a polymersome to contain daughter atoms there should be no retention of the recoiled daughters. Unfortunately, it was not possible to precisely determine which fraction of the polymersomes get ruptured, although an estimation based on Cryo-TEM images of about 150 needles show that approximately half of them are not inside a polymersome, and only 35% reside in intact polymersomes. Therefore, part of the recoil retention can be explained by the nanoneedles inside intact polymersomes. Retention of [225]Ac daughters in relatively small $LaPO_4$ nanoparticles has also been observed by Woodward et al. [9]. They found [221]Fr retention of about 50% within 6 days, with similar [213]Bi retention as what we have observed in nanoparticles with a diameter of 3 – 5 nm. As our 'free' nanoneedles also have a diameter of about 6 nm on average, they are not very different from Woodward's nanoparticles. In a later publication, they report [221]Fr and [213]Bi retention in 6.3 nm diameter $LaPO_4$ nanoparticles containing [225]Ac of 80% after 35 days. However, they offer no explanation for this very high retention, which seems not to correspond very well with an average recoil distance of about 30 nm in $LaPO_4$. A possible reason for this high retention can be found in their measurement method. They determine daughter retention by measuring the dialysate, not taking into account nanoprecipitation in the sample. Part of their high retention has to be due to recoil retention the nanoparticles, suggesting that even without the polymersome surrounding our nanoparticles, we can still be observing daughter retention.

Improvements on the InPO$_4$ model

In the NANVES simulations, the ^{225}Ac atoms are assumed to be encapsulated in the nanoparticles or needles, which are positioned in the centre of the polymersomes with uniform diameter. Both DLS and Cryo-TEM data indicate however, that the polymersomes are polydisperse and the InPO$_4$ nanoparticles are positioned in the vesicles in a seemingly random way. Furthermore, LaPO$_4$ nanoneedles can cause polymersomes to rupture. Here, we have adjusted the Monte Carlo model for InPO$_4$ containing polymersomes taking these points into account. Further development of the NANVES model has been based on the InPO$_4$ polymersomes only which have been considered a better choice of polymersome formulation as the nanoparticles do not damage the vesicles.
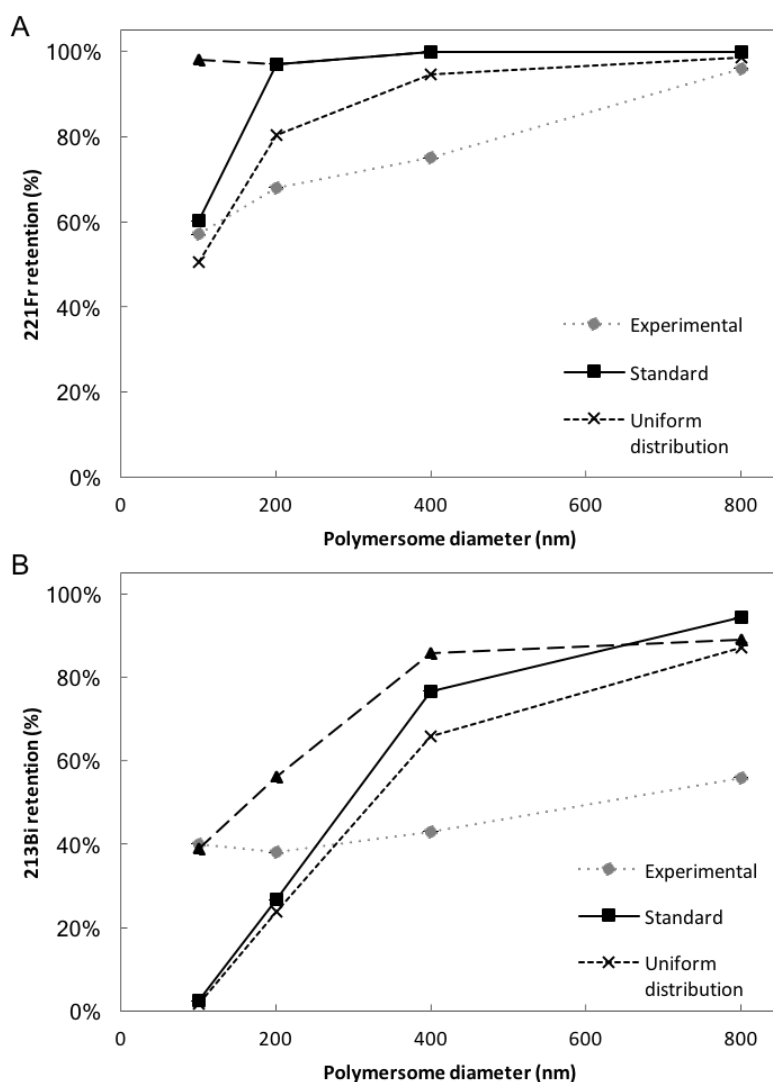
Figure 25: A comparison between experimental (light grey circles) and simulated (black symbols) ^{221}Fr (A) and ^{213}Bi (B) retention in polymersomes containing InPO$_4$ nanoparticles, with diameter ratio of nanoparticle : polymersome of 0.2. In both figures, the simulation data for the uniform vesicle population is displayed, where the InPO$_4$ particle was positioned in the centre of the polymersome ('standard' model - black squares). Variations on this 'standard' model are the 'uniform distribution' model, where the nanoparticle is positioned randomly in the polymersome (black X), and vesicle polydispersity corrected simulation results ('polydisperse' model - black triangles).

In order to obtain a better agreement, this 'standard' model was improved by either allowing for a random position of the nanoparticle within the polymersome ('uniform distribution' model), or by adjusting the polymersome size for the measured polydispersity of the samples, based on DLS analysis ('polydisperse' model). The 'uniform distribution' of the nanoparticle decreases the ^{221}Fr and ^{213}Bi retention, logically providing a calculated retention closer to the experimentally determined one. Sofou et al. theoretically calculated the retention of ^{213}Bi in liposomes, which at all liposome sizes is a bit lower than our simulated retention but follows a similar trend. As the ^{225}Ac daughters are only expected to be stopped by water in their simulations, our higher retention can be explained by the first ^{225}Ac daughters in the decay chain, which experience a much shorter stopping range by the InPO$_4$ nanoparticle and thus cause an overall increase in retention.

The second adjustment of the 'standard' model, correcting for the polydispersity of the polymersomes, mainly resulted in a large increase in retention of both ^{221}Fr and ^{213}Bi in small vesicles. This increase can partly be explained by the fact that the vesicles, on average, are a bit larger than the pore size of the filters through which they are extruded, as also shown by Cryo-TEM measurements. This effect will be especially present in the retention in 100 nm vesicles. However, as discussed before, DLS measurements yield overestimations of the diameter of small vesicles, so for the polymersomes extruded through a 100 nm or 200 nm filter, the simulated retention will be an overestimation. Despite this, DLS measurements were still considered the best method to determine vesicle size, as it is capable of measuring the radii of a large number of vesicles simultaneously. Getting the information on a similar number through the analysis of Cryo-TEM images would be very time-consuming, which is why DLS images were used to build the model upon. The polymersomes extruded through 400 nm or 800 nm filter remain quite polydisperse, with many small vesicles still in the sample. This will result in an overrepresentation of large particles, as in polydisperse samples DLS data tends to be skewed towards large vesicles [10]. Basing the simulation polymersome distribution on DLS data will thus yield a retention which is too high, for both the (relatively monodisperse) small vesicles and polydisperse large vesicles.

To improve the model, a large amount of simulations should be done which incorporate parameters like nanoparticle size and position simultaneously. Unfortunately, this is impossible with the current design of NANVES. Therefore, disparity of the simulation and experimental results would partially still be due to inconsistencies in both of the vesicle populations. In order to make a good comparison, the effects of the 'uniform distribution' model and the 'polydisperse' model should be viewed simultaneously. Then, there will indeed be an agreement between simulations and experimental data, which, especially for the small vesicles, is quite good.

Conclusions

The polymersomes containing either InPO$_4$ or LaPO$_4$ have successfully been loaded with ^{225}Ac. This has resulted in increased recoil retention of both the ^{221}Fr and ^{213}Bi as compared to previous work using DTPA as hydrophilic chelator inside the vesicles. NANVES has been found to be a good tool to predict the general trends in recoil retention inside a polymersome, which can help in assessing nanovesicle designs. However, making a sound comparison between experimental and simulated retention values for complex polymersomes is challenging because NANVES is not flexible enough

to run a large amount of simulations where the influence of multiple factors can be studied simultaneously. Concluding, we can say that we have successfully and significantly managed to increase recoil retention of alpha-emitting ^{225}Ac daughters, thus further reducing potential in vivo toxicities by recoiled daughter nuclides, making these vesicles suitable for further in vivo testing.

5

References

1. Wang, G.; de Kruijff, R. M.; Rol, A.; Thijssen, L.; Mendes, E.; Morgenstern, A.; Bruchertseifer, F.; Stuart, M. C. A.; Wolterbeek, H. T.; Denkova, A. G. Retention studies of recoiling daughter nuclides of 225Ac in polymer vesicles. *Appl. Radiat. Isot.* **2014**, *85*, 45–53.

2. Apostolidis, C.; Molinet, R.; Rasmussen, G.; Morgenstern, A. Production of Ac-225 from Th-229 for targeted alpha therapy. *Anal. Chem.* **2005**, *77*, 6288–6291.

3. Thijssen, L.; Schaart, D. R.; de Vries, D.; Morgenstern, A.; Bruchertseifer, F.; Denkova, A. G. Polymersomes as nano-carriers to retain harmful recoil nuclides in alpha radionuclide therapy: a feasibility study. *Radiochim. Acta* **2012**, *100*, 473.

4. Stojanov, K.; Georgieva, J. V; Brinkhuis, R. P.; Hest, J. C. Van; Rutjes, F. P.; Dierckx, R. A. J. O.; Vries, E. F. J. De; Zuhorn, I. S. In Vivo Biodistribtuion of Prion- and GM1-Targeted Polymersomes following Intravenous Administration in Mice. *Mol. Pharm.* **2012**, *9*, 1620–1627.

5. Kirby, H. W.; Morss, L. R. Actinium. In; 1994; pp. 18–51.

6. Sofou, S.; Kappel, B. J.; Jaggi, J. S.; McDevitt, M. R.; Scheinberg, D. a; Sgouros, G. Enhanced retention of the alpha-particle-emitting daughters of Actinium-225 by liposome carriers. *Bioconjug. Chem.* **2007**, *18*, 2061–7.

7. McLaughlin, M. F.; Woodward, J.; Boll, R. a; Wall, J. S.; Rondinone, A. J.; Kennel, S. J.; Mirzadeh, S.; Robertson, J. D. Gold coated lanthanide phosphate nanoparticles for targeted alpha generator radiotherapy. *PLoS One* **2013**, *8*, e54531.

8. Ziegler, J. F.; Ziegler, M. D.; Biersack, J. P. SRIM - The stopping and range of ions in matter (2010). *Nucl. Instruments Methods Phys. Res. Sect. B Beam Interact. with Mater. Atoms* **2010**, *268*, 1818–1823.

9. Woodward, J.; Kennel, S. J.; Stuckey, A.; Osborne, D.; Wall, J.; Rondinone, A. J.; Standaert, R. F.; Mirzadeh, S. LaPO4 nanoparticles doped with actinium-225 that partially sequester daughter radionuclides. *Bioconjug. Chem.* **2011**, *22*, 766–76.

10. Panchal, J.; Kotarek, J.; Marszal, E.; Topp, E. M. Analyzing Subvisible Particles in Protein Drug Products: a Comparison of Dynamic Light Scattering (DLS) and Resonant Mass Measurement (RMM). *Am. Assoc. Pharm. Sci.* **2014**, *16*, 440–451.

6

Biodistribution and Therapeutic Efficacy of ^{225}Ac Loaded Polymersomes in 2D and 3D in Vitro Glioma Models

Abstract

Due to their high LET, alpha emitters have great potential in targeted tumour therapy, especially in destroying micrometastases. To prevent healthy tissue toxicity caused by recoiled daughter atoms, alpha emitters like ^{225}Ac can be encapsulated in polymeric nanocarriers which are capable of retaining the daughter atoms to a large degree. In the translation to a (pre-)clinical setting, it is essential to understand the interaction of these vesicles with tumour cells. As multicellular tumour spheroids mimic a tumour microenvironment more closely than a two-dimensional cellular monolayer, in this study the uptake and distribution of the polymersomes has been determined in U87 human glioma spheroids. We have found that polymersomes have distributed themselves throughout the spheroid after 4 days, irrespective of polymersome diameter (from 100 to 800 nm). Considering the long half-life of ^{225}Ac (9.9 d) [1], this allows for irradiation and destruction of the entire spheroid within a few days. A decrease in spheroidal growth was observed upon the addition of only 0.1 kBq ^{225}Ac, an effect which was more pronounced for the ^{225}Ac in polymersomes than when only coupled to DTPA. LaPO$_4$ nanoneedle-containing polymersomes proved to be toxic to the cells themselves, while ^{225}Ac co-precipitated with InPO$_4$ nanoparticles in polymersomes has shown equal therapeutic efficacy as ^{225}Ac-DTPA containing polymersomes. We have thus demonstrated that polymersomes loaded with very low ^{225}Ac activities inhibit the growth of spheroids, making them promising candidates for future in vivo testing.

Introduction

Alpha-emitting radionuclides are ideal candidates to destroy tumour metastasis, especially those where it is of great importance to limit damage to surrounding healthy tissue. With their high LET and short penetration ranges (~30 μm), just a few alpha tracks through the nucleus of a cell are sufficient to cause apoptosis. Because of their high energy deposition, they cause mainly double-strand breaks in cellular DNA, which are difficult to repair. Non-repaired DNA double-strand breaks are lethal to the cell. Furthermore, alpha particles have a lower oxygen enhancement ratio (OER) [2], and are thus more capable of inducing damage in hypoxic cells or cancer stem cells. ^{225}Ac is a very promising radionuclide for TAT. With its relatively long half-life it has enough time to target also less-easily accessible tumours, and the 4 emitted alpha's in the decay chain ensure optimal damage once at the targeted site. However, upon the emission of an alpha particle the daughter nuclide experiences a recoil energy. This recoil energy is several orders of magnitude larger than the energy of the chemical bond of the nuclide with a targeting antibody or peptide. The daughter nuclide will thus break free after the first decay, and accumulate in other organs to damage healthy tissue in the subsequent decays [3]. Encapsulation in nano-carriers can be a solution to this problem [4,5], where (partial) retention of the daughter nuclides can be achieved. Polymersomes have shown to be very efficient in encapsulating ^{225}Ac and retaining its recoiling daughters [6,7]. These nanocarriers can be passively targeted to tumour tissue through the EPR effect, where the targeting efficiency can be further improved by attaching targeting moieties [8].

Pre-clinical in vitro studies are an integral part in the development of potential new anti-cancer agents. While cell monolayer experiments are ideal for evaluation of effects at the cellular level, e.g. the localization in the cell where nanoparticles accumulate, they have limited value in predicting the therapeutic effect of anti-cancer compounds for actual tumours [9,10]. Three-dimensional tumour spheroids are a great intermediary between 2D cell cultures and in vivo models [10,11]. The physiological conditions of these spheroids far more closely resemble the microenvironment of actual tumours than their two-dimensional counterparts [12]. Depending on spheroid size, they develop chemical gradients [13], and even a centre containing hypoxic tumour cells [14]. The interaction between cells influences their size and shape, which can directly influence cell functions [15]. The penetration and binding of (radio) pharmaceutics to cells is very different when working with 3D cell cultures, and more closely mimics the in vivo situation [13]. The presence of different mechanisms and the concomitant different phenotype makes spheroids a preferred model over adherent monolayer growing cells for studying effects of irradiation [16]. Recently, Gomez-Roman et al. have shown a differential effect in efficacy of a series of targeted drugs combined with irradiation between monolayer GBM (glioblastoma) cells and in a 3D model, the latter was found to be the most clinically representative and relevant for evaluation of new cancer therapies [17]. Similarly, a differential response to the combination treatment of irradiation with an AKT (protein kinase B) inhibitor between U251 glioma cells growing in monolayer or as multicellular spheroid was reported [18]. Hence, 3D spheroids are a valuable tool to determine their potential in vivo, and are increasingly used to evaluate new drugs [19].

In previous chapters, we have encapsulated the alpha-emitting ^{225}Ac with high efficiency in polymersomes, which retained both the mother nuclide, as well as its alpha-emitting daughters very well [6]. In this chapter, the in vitro characteristics of these vesicles have been evaluated on U87

spheroids, which is a validated and representative model for human glioblastoma tumours. In particular, we investigated the uptake and distribution of the polymersomes throughout the spheroid volume, and determined the therapeutic efficacy of [225]Ac-labelled polymersomes.

Materials and Methods

Chemicals

The poly(butadiene(1,2 addition)-b-ethylene oxide) block copolymer was obtained from Polymer Source (Quebec, Canada), with a Mn of 1900-b-900 g/mol, and a weight ratio (Mw/Mn) of 1.05. A dry [225]Ac sample was prepared at the Directorate for Nuclear Safety and Security (Karlsruhe, Germany) [20]. The PD10 columns were purchased from GE Healthcare, the 96-wells plates, 6-wells plates, the cell culture tubes and the 25 cm^2 cell culture flasks from Corning Inc, and the 30 mm cell culture petri dishes from Greiner Bio-One. The BioWhittaker Dulbecco's Modified Eagle's Medium (DMEM) and Hams F10 were purchased from Lonza (Verviers, Belgium). Sterile phosphate buffered saline (PBS) and 0.25% trypsin-ethylenediaminetetraacetic acid (trypsin-EDTA) were obtained from Gibco (Paisley, UK), and Vectashield-DAPI from Vector Laboratories. All other chemicals were purchased from Sigma Aldrich (Zwijndrecht, The Netherlands).

Polymersome preparation and radionuclide labelling

Polymersomes containing DTPA as hydrophilic chelate were prepared by adding 2 mg block copolymers per 1 mL PBS buffer solution at pH 7.4. The buffer solution contained 1 mM DTPA as hydrophilic chelate at pH 7.4 if it were to be used for radionuclide labelling. Polymersomes were extruded through polycarbonate filters with cut-off of 800, 400, 200 or 100 nm. The solution was stirred for a week, after which the polymersomes had formed. The polymersomes were loaded with ^{111}In or [225]Ac according to earlier published procedures [6,21]. In short, the free chelate was removed using a 30 cm Sephadex G 25 medium mesh column, after which 0.8 mL polymersome solution was added to a 0.2 mL 10 mM HEPES solution containing respectively a few MBq ^{111}In and 10 µL 2 mM tropolone solution or [225]Ac and 0.5 mg Ca-ionophore (A23187). After an incubation time of an hour, the unencapsulated radionuclides were removed using a PD10 purification column. Polymersomes containing InPO$_4$ nanoparticles or LaPO$_4$ nanoneedles were prepared as described in Chapter 4. Here, [225]Ac was added to a vial containing a thin film of 0.1 mg calcium ionophore and 200 µL 10 mM Hepes buffer at pH 7.4, together with 5 µL 25 mM InCl$_3$ and 10 µL 20 mM tropolone, or 5 µL 25 mM LaNO$_3$ solution in pH 2 HCl for the formation of InPO$_4$ or LaPO$_4$ nanoparticles respectively. After an incubation time of 10 minutes, 0.8 mL polymersome solution with 0.5 M KH$_2$PO$_4$ encapsulated at pH 3 was added, and 1 hour later the polymersome solution was purified by passing it through a PD10 column.

Fluorescent labelling of polymersomes

Polymersomes with diameters of 100, 200, 400 and 800 nm were labelled with PKH26 or FITC 'Isomer 1' fluorescent dye. 10 µL PKH26 (1 mM in ethanol diluted) or 2 µL FITC (10 mg/mL FITC in ethanol) was added to 1 mL polymersome solution. After 1 h incubation time the free dye was removed by passing the solution through a PD10 column. Loading efficiency was determined by dissolving the

loaded polymersomes at a 50:50 ratio in THF, and the sample was subsequently measured in a Fluorometer (Agilent). Retention was determined at 24 h after loading by centrifuging the polymersome sample at 2500 rmp for 30 minutes in an Amicon centrifuge tube with 50 KDa filter (polymersomes are too large to pass the filter), and measuring the fluorescence signal of the liquid which had passed the filter.

Monolayer experiments

Polymersomes labelled with FITC were added to a U87 cells growing as monolayer. The U87 cell line was acquired from ATCC (Teddington, UK). Cells were certified mycoplasma free by regular testing. For lysosome labelling experiments, 2 mL of 50 nM Lysotracker Red was added to the cells and incubated for 45 minutes. At different time intervals, the cell medium containing free polymersomes was removed and the cell was directly fixated with 3.7% PFA14. The PFA was allowed to incubate for 15 minutes at room temperature, after which the cells were rinsed with PBS. The cells were mounted with 4 µL Vectashield-DAPI16 and examined using a Leica LS5 confocal microscope.

Uptake of fluorescence labelled polymersomes in spheroids

For the formation of the spheroids, 5000 U87 glioblastoma cells were seeded in 96-well plates coated with 50 µL of 1.5% Agarose in DMEM and Pen/Strep. After one week, spheroids with diameter of 350-400 µm had formed. 50 µL of the labelled polymersome solution was added to each well. After a specified duration (1 d, 2 d, 4 d, or 7 d), spheroids were harvested in a 2 mL Eppendorf vial. The spheroids were frozen using transparent tissue freezing medium (OCT) and glued on a pre-cooled cutting table. In the cryostat, 20 µm thick slices were cut at -25 ℃ [22]. Subsequently, the spheroids were imaged using Confocal Laser Scanning Microscopy with equal microscope settings.

Quantification of polymersome uptake in spheroids

A 50 µL polymersome solution labelled with 0.5 MBq of ^{111}In was added to the wells containing the spheroids. After an incubation time between 1 and 21 days, the spheroid was removed and washed with 1 mL PBS. Subsequently, the ^{111}In activity in the spheroid was determined using an automatic gamma counter (Wallac 2480 Automatic Gamma counter from Perkin Elmer Technologies) and corrected for decay.

Spheroid growth assay

The spheroids were formed according to the same procedure used to determine the uptake of polymersomes. However, in these experiments 4 days after the cells were added to the wells either 50 µL of polymersome solution containing different amounts of ^{225}Ac, or 50 µL PBS solution containing ^{225}Ac-DTPA was added. The growth of the spheroids was followed in time for up to 30 days by taking images through a binocular microscope with 50 x magnification (Olympus Tokyo CK, serial no. 206904) with a normal camera (Olympus SZ-10, serial no. JEQ226246). The spheroid sizes in the images were analysed by ImageJ [23]. In a similar experiment, the effect of nanoparticles in polymersomes has been examined by adding 50 µL polymersome solution containing InPO$_4$ or LaPO$_4$ nanoparticles with or without 5 kBq ^{225}Ac co-encapsulated, with polymersomes containing 5 kBq ^{225}Ac-

DTPA and spheroids which had not been treated as control groups. The spheroidal growth was followed for 10 days post-addition as described before.

Dose calculations

The dose calculations on the spheroids were based on the results of the polymersome uptake, the pictures of the fluorescence labelled polymersomes and data on the energy loss of alpha particles in water obtained from NIST's ASTAR program [24]. The energy deposited by a single decay event was modelled as a rotationally symmetric 'energy' sphere in which the energy deposition density followed from the fluence and the Bragg peak of the respective alpha particle, both as function of distance from the distance of the energy sphere. The sum of the energy deposited in the energy sphere matched the total energy kinetic energy of the alpha particles produced in the [225]Ac decay chain (~28 MeV). This approach was chosen over an individual decay based Monte Carlo method for computational efficiency. For the polymersome-location matrix, uptake pictures were loaded into MATLAB for 200 nm polymersomes during day 1, 2, 4 and 7. The pictures were converted to greyscale and resized to form a near-perfect sphere. The 2D images were mapped onto a 3D matrix which would represent a perfect spheroid with internalized polymersomes. The matrices were scaled for the number of decayed particles during the time frame corresponding to the pictures used and the polymersome uptake during that day. The dose profile was subsequently calculated by the convolution of the four energy matrices with the pictures representing the diffusion of polymersomes into the spheroid (four in total). The sixteen resulting matrices were added up to obtain a total energy distribution.

Results and discussion

Polymersome preparation and radionuclide labelling

Polymersomes were prepared at different average polymersome sizes (100, 200, 400 and 800 nm) as previously described [21]. Labelling efficiencies were 91 ± 14%, with practically no loss of fluorescent label (0.06 ± 0.02%) after 24h. The high stability of the fluorescent label thus allowed for their use in subsequent in vitro studies. Radionuclide labelling efficiencies were consistently high, > 90% for ^{111}In and > 64% for [225]Ac, with < 5% and < 7% loss of radiolabel respectively [6,21].

Internalization and lysosome co-localisation in U87 cells

The internalisation and uptake mechanism of polymersomes were determined in a U87 glioblastoma cell monolayer. Polymersomes were detected in the cell cytoplasm after a few minutes. Uptake has been visualised for all polymersome diameters, but there was no clear difference to be observed between 100 – 800 nm diameter polymersomes. In Figure 26, the uptake and lysosome co-localisation of 100 nm FITC-labelled polymersomes is visualized by confocal microscopy. After an incubation time of 4 hours, polymersomes have been observed throughout the cytoplasm. No uptake in the cell nucleus was observed due to the relatively large vesicle size, consistent with literature data [25]. To determine the uptake pathway, lysosomes were labelled with Lysotracker Red.

| Cell Nuclei | Polymersomes | Lysosomes | Combined image |
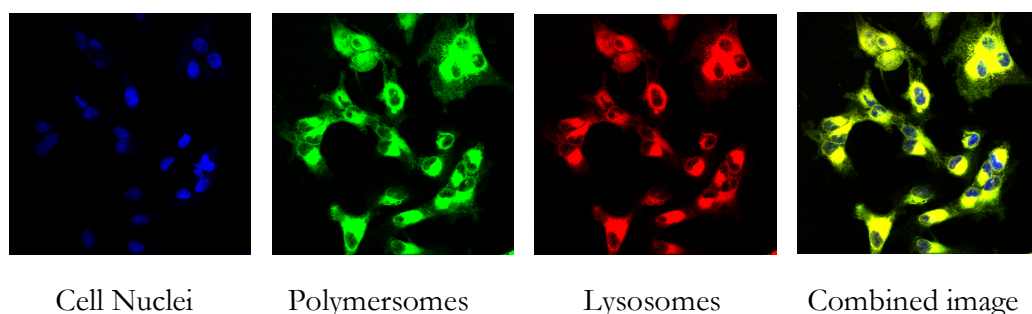
Figure 26: Fluorescent microscopy images of a monolayer of U87 cancer cells, incubated with 100 nm FITC-labelled polymersomes at 4 h after addition of the polymersomes. The nuclei were stained with DAPI, and the lysosomes with Lysotracker Red.

Overlaying the images of the polymersomes and lysosomes shows a complete overlap of the fluorescent signal, indicating that the nanocarriers are, at least in part, taken up through endocytosis and end up in the lysosomes. Literature shows that nanoparticles between 50 and 500 nm are internalized via clathrin-mediated endocytosis, and transported from early endosomes through late endosomes to lysosomes [26]. Although larger (> 750 nm) nanoparticles are generally taken up by phagocytic pathways instead of pinocytotic ones [27–29], we did not observe any difference between small and large vesicles. This can be explained by the polydisperse nature of large polymersomes (i.e. those passed only through a 800 nm extrusion filter, see also [6]), where the presence of the many small vesicles in the sample likely still causes the main uptake mechanism to be clathrin-mediated endocytosis.

Uptake of fluorescence labelled polymersomes in spheroids

Depending on the type of therapy, a uniform distribution can be essential for its success. In targeted alpha radionuclide therapy, it is especially important that the alpha emitters are distributed throughout the tumour to be able to irradiate the entire cell population, whereas this is of lesser importance in beta radionuclide therapy due to the much longer range of beta particles. Therefore, the distribution of polymersomes in U87 tumour spheroids was studied qualitatively in time, by imaging the fluorescent polymersome signal in 20 µm thick spheroid slices with confocal microscopy. In Figure 27 the penetration of polymersomes through the spheroids is visualized at different polymersome diameters. Although no quantitative conclusions can be drawn from this data, the images nicely illustrate the migration of polymersomes through the spheroids. Both the amount of fluorescence and the diffusion through the spheroid increased in time. After an incubation time of 1 day the polymersome concentration was significantly greater at the periphery of the spheroid as compared to the core. While uptake in a 2D cell culture is a relatively rapid process, diffusion throughout a 3D tumour is much slower, taking a few days for the vesicles to distribute themselves completely (Figure 27). The mechanism by which polymersomes diffuse through the spheroid is likely transcellular transport (endocytosis and subsequent exocytosis of the nanovesicles) [30,31].

6
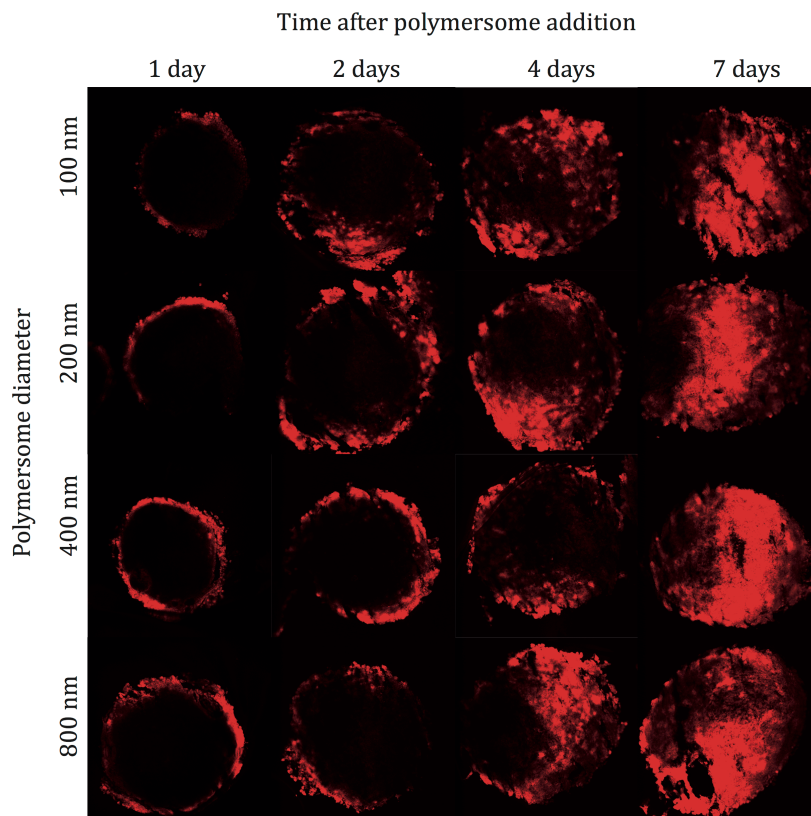
Figure 27: Uptake of polymersome of different diameters, fluorescently labelled with PKH26 in U87 spheroids in time as measured by confocal microscopy, where the spheroid was sliced in 20 um thick slices. Note: due to limitations of the confocal, only the fluorescence of the part of the spheroid that was in focus was imaged, but in fact for e.g. the 7d images the polymersomes were visible throughout the spheroid.

After about 4 days the polymersomes have diffused nearly throughout the spheroid, and after 7 days the distribution was completely homogeneous. Although this might seem a relatively slow distribution of the polymersomes, the speed agrees quite well with literature values. A recent paper by Colley et al. has shown that polymersomes with 200 nm diameter take about five days to be distributed throughout the spheroid [32], which is similar to the distribution uptake rate determined in the present study. In fact, smaller particles (tens of nm in diameter) generally seem to spread faster through spheroids than larger vesicles (~ 100 nm) [33–35], although this naturally depends on, amongst others, shape, surface charge and solubility of the nanocarrier as well as cell type [36]. Studies with 100 nm PEGylated liposomes have also shown that at short incubation times (2 – 6 h), uptake is very limited and only visible in the outer rim of the spheroid [37,38], an effect which has also been reported in vivo [39]. This implies that while a longer time is needed for the diffusion of polymersomes through spheroids than for smaller (< 100 nm) nanoparticles, the polymersomes do manage to diffuse throughout the entire spheroid. However, despite the fact that spheroids are a much better representation of a real tumour than a cell monolayer, they still lack important tumour features such as an extracellular matrix and pressure gradients, which also play an important role in intratumoral nanoparticle distributions.

Quantification of polymersome uptake in spheroids

To quantify polymersome uptake in U87 spheroids, polymersomes labelled with ^{111}In were added to the spheroids, and their uptake in the spheroids was followed for 21 days (Figure 28). Uptake did not increase significantly after 8 days, which is also the point where homogenous distribution of polymersomes was observed (Figure 27). No clear trend can be found between varying polymersome sizes, confirming the observations from the distribution experiments. Control experiments with ^{111}In-DTPA indicated similar spheroid uptake, although we were not able to determine the distribution within the spheroid to see whether it resided mainly in the outer layers or diffused to the centre as well. Medium was not replaced during this experiment to prevent dilution and removal of the polymersomes in the medium resulting in a serum-deprived environment approximately 12 days after seeding, which is 9 days after the addition of polymersomes. This coincides with the growth curve of the spheroids (data not shown), which stabilizes 12 days after seeding, which is also the point (> 8 days) at which polymersome uptake no longer increases. Cells enter the G0 phase upon serum deprivation, and eventually apoptosis will occur, though this takes longer in spheroids as compared to cell monolayers [42]. The rate of cellular uptake of nanoparticles is largely independent of the normal cell cycle [43], though during the G0 resting phase additional uptake will occur at a relatively low rate [44] and decrease further as they move towards apoptosis, thus explaining the stagnation in uptake from 14 days onwards (Figure 28).

6
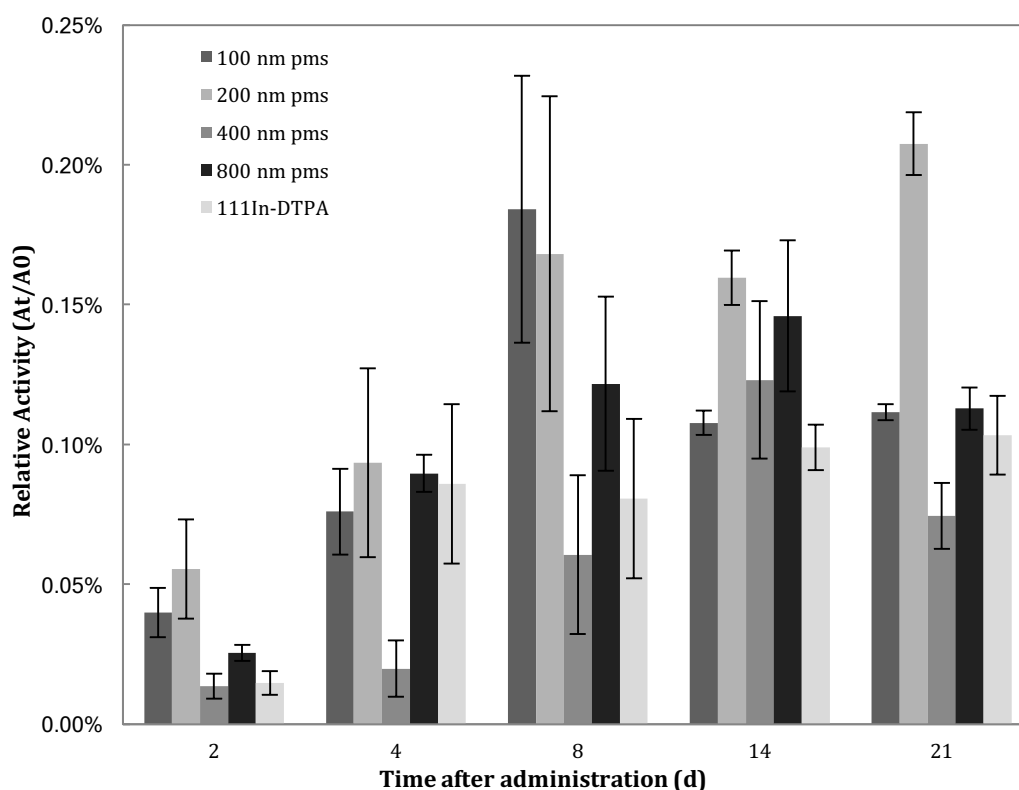
Figure 28: Uptake of both polymersomes labelled with ^{111}In as a trace element, as well as ^{111}In-DTPA in spheroids.

Spheroid growth experiments

The uptake profiles in spheroids indicate that polymersomes are ideally suited for enabling long-lived alpha-emitting radionuclides to accomplish uniform distribution throughout tumour metastasis, allowing for irradiation of all cells with little damage to surrounding healthy tissue. To this end, polymersomes labelled with the alpha-emitter ^{225}Ac were tested in U87 spheroid cultures. In Figure 29 the effect of either 1 kBq or 0.1 kBq of ^{225}Ac loaded in polymersomes on the spheroids is displayed. In all cases, growth of the spheroids was inhibited by the addition of the radioactive vesicles, where as low as 0.1 kBq of ^{225}Ac already had a pronounced effect on spheroidal growth, and an increased activity of 1 kBq led to a significant reduction in spheroid size. Obtaining similar therapeutic efficacies with beta emitters would require much larger amounts of activity [45].
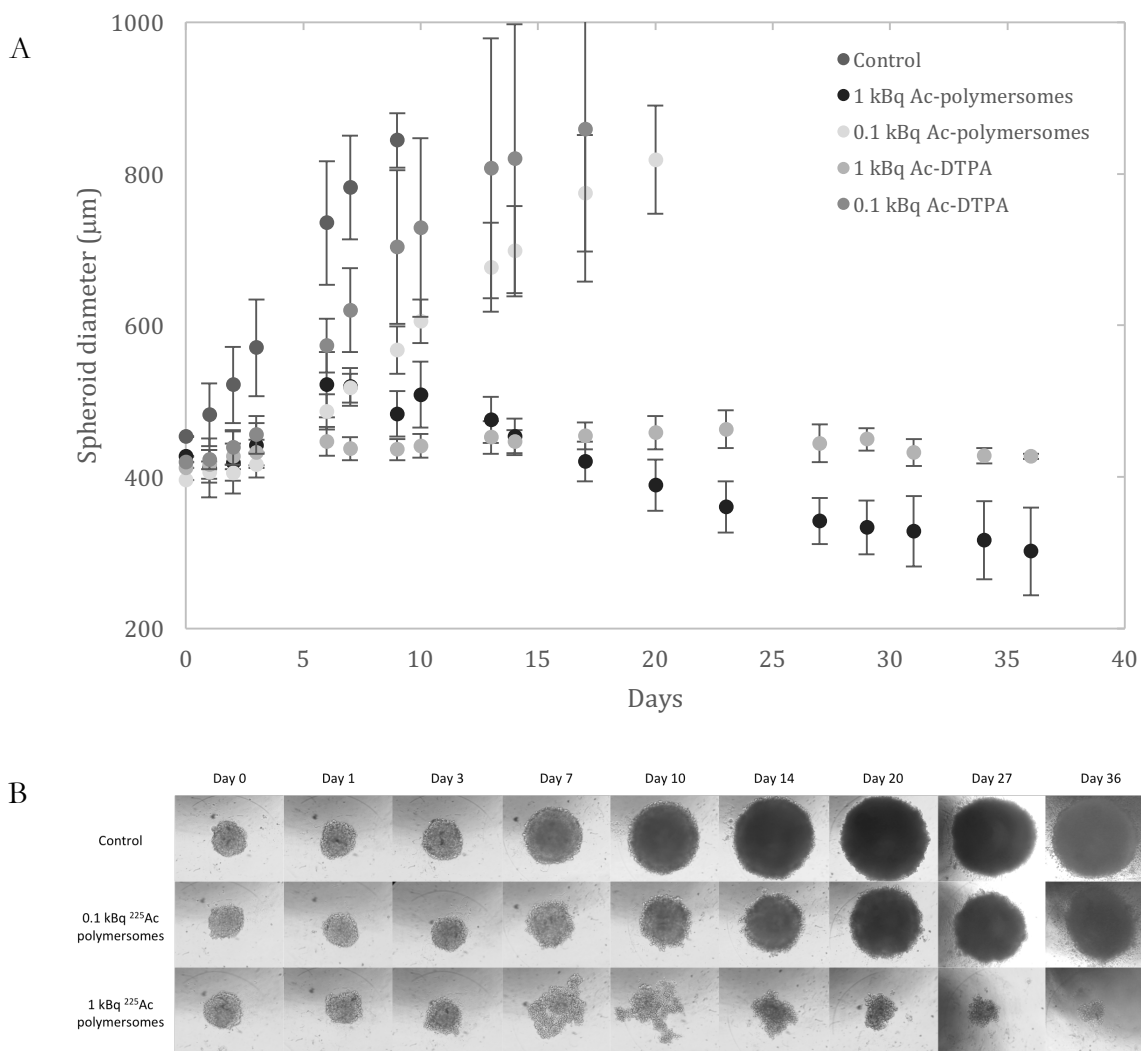
Figure 29: A: U87 tumour spheroid growth followed for more than a month upon the addition of either 1 kBq or 0.1 kBq of ^{225}Ac encapsulated in 80 nm polymersomes or attached to the chelator DTPA, as well as the control group. Time-points where the spheroid growth had exceeded twice its initial diameter have been excluded as they were too large to follow their normal growth pattern. B: Specific instances of U87 tumour spheroidal growth when challenged with ^{225}Ac-containing polymersomes as compared to 'normal' growth of the control group, followed for 36 days.

Control experiments where polymersomes without ^{225}Ac were added to the spheroids have shown that the vesicles themselves are not toxic. When the exact same amount of ^{225}Ac was added to the spheroids, with the radionuclide attached to DTPA instead of encapsulated in polymersomes, growth inhibition of the spheroids was reduced (Figure 29). This implies that the nanocarriers are better capable of irradiating the spheroids than ^{225}Ac-DTPA as they inhibit spheroid growth to a larger degree at the same ^{225}Ac activity. This could be due to a better spheroid penetration combined with internalization in the cells, which allows them to be closer to the nuclei increasing the chance to hit the nuclear DNA. Using ^{111}In as analogue for the ^{225}Ac behaviour, we find that the relative uptake of ^{111}In-DTPA and ^{111}In in polymersomes is not significantly different (Figure 28). The intra-spheroidal and intracellular distribution could explain the difference in tumour growth inhibition. Unfortunately, we were not able to determine intercellular distribution for DTPA-complexes. The effect of vesicle distribution on spheroidal growth has also been shown by Zhu et al. [46]. They compared ^{225}Ac encapsulated in non-targeted liposomes with ^{225}Ac-radiolabeled antibodies. The use of liposomes enhanced tumour killing efficiency due to the better interstitial distribution of the liposome, while the antibodies remained at the edge of the spheroid.

^{225}Ac-InPO$_4$ or LaPO$_4$ nanoparticle-containing polymersomes

As described in Chapter 5, recoil retention of the two daughter nuclides of ^{225}Ac (^{221}Fr and ^{213}Bi) has been improved by co-precipitating the ^{225}Ac with indium or lanthanum and phosphate in a nanoparticle. To determine the toxicity of these two formulations, both InPO$_4$ or LaPO$_4$ containing polymersomes and with co-precipitated 5 kBq ^{225}Ac have been added to 500 µm diameter spheroids. Subsequently the growth profile has been followed for 10 days as can be seen in Figure 30. The vesicles containing ^{225}Ac-DTPA, ^{225}Ac-InPO$_4$ or ^{225}Ac-LaPO$_4$ all have shown a decrease in spheroid size from about 3 days after addition, with no significant difference between the different formulations. It can thus be concluded that cell toxicity of ^{225}Ac-containing polymersomes is not depending on the mode of encapsulation.
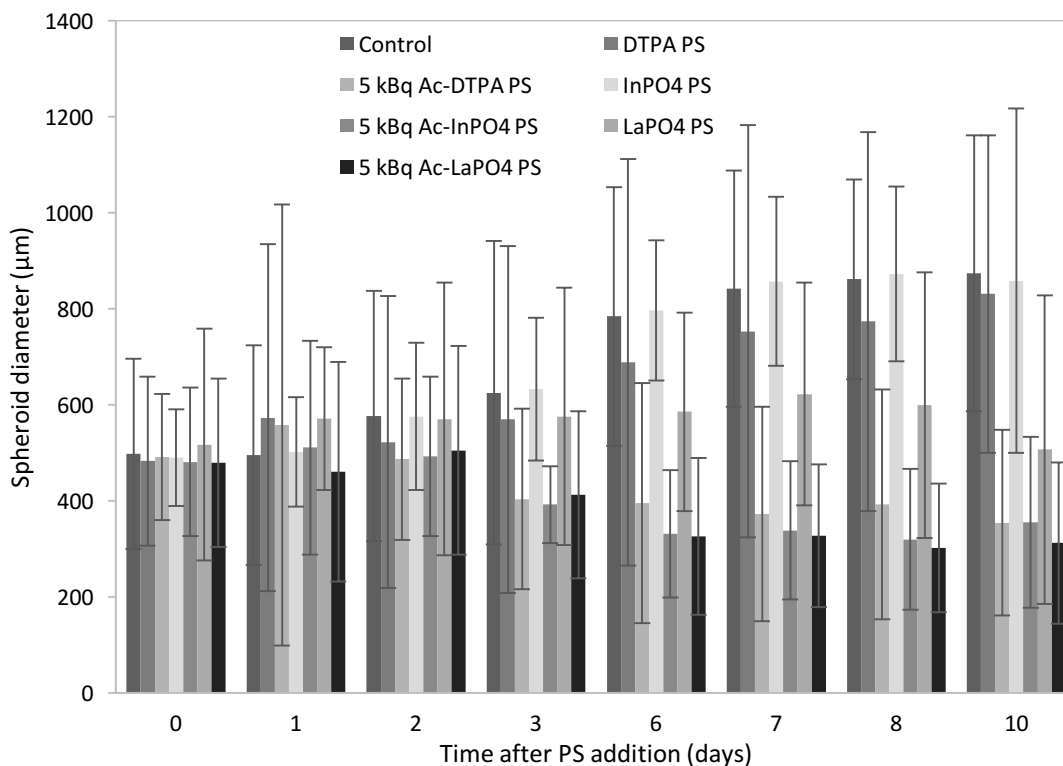
Figure 30: The effect of different polymersome formulations of the growth of U87 multicellular spheroids, until 10 days after the addition of the polymersomes. In the control group, nothing was added to the spheroids. InPO$_4$ or LaPO$_4$ nanoparticles in polymersomes contained 0.125 μmol In or La respectively in 0.5 M KH$_2$PO$_4$. 5 kBq ^{225}Ac was co-encapsulated with DTPA, InPO$_4$ or LaPO$_4$ containing polymersomes.

The vesicles without ^{225}Ac, containing either DTPA or InPO$_4$ have shown to be non-toxic to the cells, with a spheroid growth rate similar to untreated (control) spheroids. However, those containing LaPO$_4$ displayed a significant growth inhibition. As shown in Chapter 4, the LaPO$_4$ nanoneedles are capable of perforating the polymersome membrane, destroying the polymersomes. There are two possible explanations for the observed cellular toxicity. The nanoneedles could have perforated the cell membrane as they did the polymersome membrane, thus causing significant damage to the cells, or the lanthanum phosphate, no longer contained in and protected by the polymersome, in itself is toxic to the cells, irrespective of their form. Nanoneedles have been used extensively for the intracellular delivery of e.g. nanoparticles [49] or nucleic acids [50,51], with minimal impact on cell metabolism and viability. This implies that perforation of the cellular membrane is not the cause of the observed cell death. While the diameters of these nanoneedles were much larger than those of the LaPO$_4$ nanoneedles in the current study, comparison to gold nanorods of similar size which are themselves also non-toxic to cells [52,53] shows that the LaPO$_4$ morphology is likely not the main cause of the observed toxicity. The toxicity is therefore likely due to the toxicity of the lanthanum phosphate compound. Taking into account the loading efficiency of lanthanum in phosphate-containing polymersomes (Chapter 4), the LaPO$_4$ concentration in the cell medium and spheroids will be about 100 μM. Palmer et al. have shown that the LC$_{50}$ value of the soluble lanthanum chloride is at 52 μM whereas for the insoluble lanthanum oxide this lies at 980 μM, which they attribute to the difference in solubility [54]. The dimensions of our LaPO$_4$ nanoparticles are small enough to be dispersed

throughout the solution, thus the LC$_{50}$ value is likely to be closer to that of LaCl$_3$, explaining the observed toxicity in our study. Going forward, we can thus conclude that the InPO$_4$ nanoparticle-containing polymersomes are, unlike LaPO$_4$, themselves not toxic and though when ^{225}Ac has been encapsulated their therapeutic efficacy is similar to other polymersome formulations. Given their performance in vitro combined with better retention characteristics, they are the preferred candidate for future in vivo studies.

Dose calculations

The dose distribution was estimated using experimental data of the polymersome distribution (Figure 27) and uptake (Figure 28). In Figure 5 A the dose at different days after the addition of polymersome can be seen, where the final result of the sum of all convolutions is shown in Figure 5 B. This cumulative dose distribution shows that the minimum dose deposited in the spheroid is found in the rim (around 4 Gy), with a maximum deposited dose of 7.6 Gy after 10 days. The distribution visualized in Figure 31 is equally representative of larger ^{225}Ac activities, the received dose increases linearly with added ^{225}Ac activity at equal polymersome concentration. The lower rim dose is due to the much lower polymersome concentration in the surrounding medium as compared to the spheroid, and the fact that some background values were interpreted as being part of the spheroid, which has caused low-intensity values that correspondingly receive a low dose.
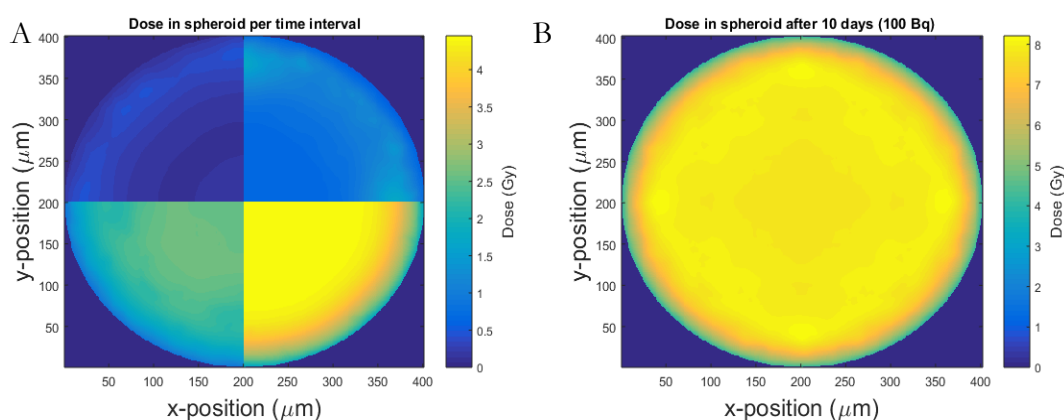
Figure 31: A: the dose in the spheroid at different times after addition of the polymersomes (day 1: top left quarter, day 2: top right quarter, day 4: bottom left quarter and day 7: bottom right quarter) and B: cumulative dose distribution in the cross-section of a spheroid after 10 days, at an added activity of 0.1 kBq ^{225}Ac on day 0.

Comparing the obtained radiation dose with literature values is tricky, as nearly all studies have been performed with external radiation. In our experiments, the internal ^{225}Ac source is continuously decaying and thus irradiates the spheroid over a long period of time, which best be compared with continuous low dose rate irradiation or infinite fractionated irradiation exposures. Ho et al. found that there while there is a large difference in therapeutic effect between a single dose and the same dose in up to 8 fractions (1 log cell kill at 4-4.5 Gy and 7-8 Gy respectively), more than 8 fractions does not make much of a difference. The therapeutic effect we observed for an average alpha dose of 7.19 Gy is very similar to that found in their study for a fractionated 8 Gy X-ray dose over 15 days [47]. As can be seen in Figure 29, spheroids stay approximately their initial size in the first 15 days after the addition

of 1 kBq of ^{225}Ac in polymersomes. Afterwards, they decrease in size, an effect which is similar to that found by Fedrigo et al. where they irradiated spheroid with up to 20 Gy [48]. Our dosimetric model thus corresponds very well to literature data, and can accurately be used to predict spheroid growth inhibition at different ^{225}Ac-levels.

Conclusions

In this chapter, we have determined the uptake of polymersomes in U87 human glioblastoma cells. We have seen on cell-level that initial internalization of the vesicles is a fast process. Immediately upon addition of the vesicles to cells, they are taken up via endocytosis though it takes about a day for equilibrium to be established. In 3D spheroid models, the polymersomes are found mainly in the outer layers within a day after exposure and have distributed evenly throughout the spheroid volume after a few days. There is no discernible difference in uptake characteristics between small (100 nm) and large (800 nm) polymersomes, though quantitative results do indicate a time-dependent increase in uptake. The vesicles with ^{225}Ac encapsulated in the aqueous cavity show enormous therapeutic potential, where spheroid growth inhibition is already observed at just 0.1 kBq of ^{225}Ac added, and the tumours start to shrink significantly at about 1 kBq of activity. A similar but slightly reduced effect is observed for 'free' ^{225}Ac coupled to DTPA, likely due to the lack of internalization as compared to the ^{225}Ac in polymersomes. In terms of cell toxicity, ^{225}Ac loaded in polymersomes containing $InPO_4$ nanoparticles provide an equally efficient therapeutic agent as the DTPA-containing polymersomes, while it has been shown that $LaPO_4$ containing polymersomes, without the addition of an alpha-emitter, are themselves toxic.

References

1. Pommé, S.; Marouli, M.; Suliman, G.; Dikmen, H.; Van Ammel, R.; Jobbágy, V.; Dirican, A.; Stroh, H.; Paepen, J.; Bruchertseifer, F.; Apostolidis, C.; Morgenstern, A. Measurement of the 225Ac half-life. *Appl. Radiat. Isot.* **2012**, *70*, 2608–2614.

2. Vaidyanathan, G.; Zalutsky, M. R. Targeted therapy using alpha emitters. *Phys. Med. Biol.* **1996**, *41*, 1915–1931.

3. de Kruijff, R. M.; Wolterbeek, H. T.; Denkova, A. G. A Critical Review of Alpha Radionuclide Therapy - How to Deal with Recoiling Daughters? *Pharmaceuticals* **2015**, *8*, 321–336.

4. Sofou, S.; Kappel, B. J.; Jaggi, J. S.; McDevitt, M. R.; Scheinberg, D. a; Sgouros, G. Enhanced retention of the alpha-particle-emitting daughters of Actinium-225 by liposome carriers. *Bioconjug. Chem.* **2007**, *18*, 2061–7.

5. Woodward, J.; Kennel, S. J.; Stuckey, A.; Osborne, D.; Wall, J.; Rondinone, A. J.; Standaert, R. F.; Mirzadeh, S. LaPO4 nanoparticles doped with actinium-225 that partially sequester daughter radionuclides. *Bioconjug. Chem.* **2011**, *22*, 766–76.

6. Wang, G.; de Kruijff, R. M.; Rol, A.; Thijssen, L.; Mendes, E.; Morgenstern, A.; Bruchertseifer, F.; Stuart, M. C. A.; Wolterbeek, H. T.; Denkova, A. G. Retention studies of recoiling daughter nuclides of 225Ac in polymer vesicles. *Appl. Radiat. Isot.* **2014**, *85*, 45–53.

7. Kruijff, R. M. de; Drost, K.; Thijssen, L.; Morgenstern, A.; Bruchertseifer, F.; Lathouwers, D.; Wolterbeek, H. T.; Denkova, A. G. Improved 225Ac Daughter Retention in InPO4 Containing Polymersomes. *Appl. Radiat. Isot.* **2017**, *128*, 183–189.

8. Peer, D.; Karp, J. M.; Hong, S.; Farokhzad, O. C.; Margalit, R.; Langer, R. Nanocarriers as an emerging platform for cancer therapy. *Nat. Nanotechnol.* **2007**, *2*, 751–60.

9. Friedrich, J.; Ebner, R.; Kunz-Schughart, L. a Experimental anti-tumor therapy in 3-D: spheroids--old hat or new challenge? *Int. J. Radiat. Biol.* **2007**, *83*, 849–871.

10. Imamura, Y.; Mukohara, T.; Shimono, Y.; Funakoshi, Y.; Chayahara, N.; Toyoda, M.; Kiyota, N.; Takao, S.; Kono, S.; Nakatsura, T.; Minami, H. Comparison of 2D- and 3D-culture models as drug-testing platforms in breast cancer. *Oncol. Rep.* **2015**, *33*, 1837–43.

11. Weiswald, L.-B.; Bellet, D.; Dangles-Marie, V. Spherical Cancer Models in Tumor Biology. *NEO* **2014**, *17*, 1–15.

12. Skov Jensen, S.; Aaberg-Jessen, C.; Pind Jakobsen, I.; Kjaer Hermansen, S.; Kabell Nissen, S.; Winther Kristensen, B. *Three-Dimensional In Vitro Models in Glioma Research – Focus on Spheroids*; Ghosh, D. A., Ed.; InTech, 2011.

13. Hirschhaeuser, F.; Menne, H.; Dittfeld, C.; West, J.; Mueller-Klieser, W.; Kunz-Schughart, L. a Multicellular tumor spheroids: an underestimated tool is catching up again. *J. Biotechnol.* **2010**, *148*, 3–15.

14. Sminia, P.; Acker, H.; Eikesdal, H. P.; Kaaijk, P.; Enger, P. øvind; Slotman, B.; Bjerkvig, R. Oxygenation and response to irradiation of organotypic multicellular spheroids of human glioma. *Anticancer Res.* **2003**, *23*, 1461–6.

15. Baker, B. M.; Chen, C. S. Deconstructing the third dimension – how 3D culture microenvironments alter cellular cues. *J. Cell Sci.* **2012**, *125*.

16. Eke, I.; Cordes, N. Radiobiology goes 3D: How ECM and cell morphology impact on cell survival after irradiation. *Radiother. Oncol.* **2011**, *99*, 271–278.

17. Gomez-Roman, N.; Stevenson, K.; Gilmour, L.; Hamilton, G.; Chalmers, A. J. A novel 3D human glioblastoma cell culture system for modeling drug and radiation responses. *Neuro. Oncol.* **2017**, *19*, 229–241.

18. Narayan, R. S.; Fedrigo, C. A.; Brands, E.; Dik, R.; Stalpers, L. J. A.; Baumert, B. G.; Slotman, B. J.; Westerman, B. A.; Peters, G. J.; Sminia, P. The allosteric AKT inhibitor MK2206 shows a synergistic interaction with chemotherapy and radiotherapy in glioblastoma spheroid cultures. *BMC Cancer* **2017**, *17*, 204.

19. Lee, G. Y.; Kenny, P. A.; Lee, E. H.; Bissell, M. J. Three-dimensional culture models of normal and malignant breast epithelial cells. *Nat. Methods* **2007**, *4*, 359–365.

20. Apostolidis, C.; Molinet, R.; Rasmussen, G.; Morgenstern, A. Production of Ac-225 from Th-229 for targeted alpha therapy. *Anal. Chem.* **2005**, *77*, 6288–6291.

21. Wang, G.; de Kruijff, R. M.; Stuart, M. C. A.; Mendes, E.; Wolterbeek, H. T.; Denkova, A. G. Polymersomes as radionuclide carriers loaded via active ion transport through the hydrophobic bilayer. *Soft Matter* **2013**, *9*, 727–734.

22. Augustin, H. G. *Methods in Endothelial Cell Biology*; Springer Berlin Heidelberg, 2004.

23. Rasband, W. . ImageJ. *U.S. Natl. Institutes Heal.* **2016**.

24. Berger, M. J.; Coursey, J. S.; Zucker, M. A.; Chang, J. ASTAR https://physics.nist.gov/PhysRefData/Star/Text/ASTAR.html.

25. Oh, E.; Delehanty, J. B.; Sapsford, K. E.; Susumu, K.; Goswami, R.; Blanco-Canosa, J. B.; Dawson, P. E.; Granek, J.; Shoff, M.; Zhang, Q.; Goering, P. L.; Huston, A.; Medintz, I. L. Cellular Uptake and Fate of PEGylated Gold Nanoparticles Is Dependent on Both Cell-Penetration Peptides and Particle Size. *ACS Nano* **2011**, *5*, 6434–6448.

26. Bareford, L. M.; Swaan, P. W. Endocytic mechanisms for targeted drug delivery. *Adv. Drug Deliv. Rev.* **2007**, *59*, 748–758.

27. Mao, Z.; Zhou, X.; Gao, C. Influence of structure and properties of colloidal biomaterials on cellular uptake and cell functions. *Biomater. Sci* **2013**, *1*.

28. Zhu, M.; Nie, G.; Meng, H.; Xia, T.; Nel, A.; Zhao, Y. Physicochemical Properties Determine Nanomaterial Cellular Uptake, Transport, and Fate. *Acc. Chem. Res.* **2013**, *622*, 622–631.

29. Parodi, A.; Corbo, C.; Cevenini, A.; Molinaro, R.; Roberto, P.; Pandolfi, L.; Agostini, M.; Salvatore, F.; Tasciotti, E. Enabling cytoplasmic delivery and organelle targeting by surface modification of nanocarriers. *Nanomedicine* **2015**, *10*, 1923–1940.

30. Lu, H.; Utama, R. H.; Kitiyotsawat, U.; Babiuch, K.; Jiang, Y.; Stenzel, M. H. Enhanced transcellular penetration and drug delivery by crosslinked polymeric micelles into pancreatic multicellular tumor spheroids. *Biomater. Sci.* **2015**, *3*, 1085–95.

31. Arranja, A. Development of copolymer-based nanocarriers for imaging and therapy, Université de Strasbourg, 2015.

32. Colley, H. E.; Hearnden, V.; Avila-Olias, M.; Cecchin, D.; Canton, I.; Madsen, J.; MacNeil, S.; Warren, N.; Hu, K.; McKeating, J. A.; Armes, S. P.; Murdoch, C.; Thornhill, M. H.; Battaglia, G. Polymersome-Mediated Delivery of Combination Anticancer Therapy to Head and Neck Cancer Cells: 2D and 3D in Vitro Evaluation. *Mol. Pharm.* **2014**, *11*, 1176–1188.

33. Gao, Y.; Li, M.; Chen, B.; Shen, Z.; Guo, P.; Guillaume Wientjes, M.; L-S Au, J. Predictive Models of Diffusive Nanoparticle Transport in 3-Dimensional Tumor Cell Spheroids. *Am. Assoc. Pharm. Sci.* **2013**, *15*, 816–831.

34. Mikhail, A. S.; Eetezadi, S.; Ekdawi, S. N.; Stewart, J.; Allen, C. Image-based analysis of the size- and time-dependent penetration of polymeric micelles in multicellular tumor spheroids and tumor xenografts. *Int. J. Pharm.* **2014**, *464*, 168–177.

35. Wang, J.; Mao, W.; Lock, L. L.; Tang, J.; Sui, M.; Sun, W.; Cui, H.; Xu, D.; Shen, Y. The Role of Micelle Size in Tumor Accumulation, Penetration, and Treatment. *ACS Nano* **2015**, *9*, 7195–7206.

36. Barua, S.; Mitragotri, S. Challenges associated with Penetration of Nanoparticles across Cell and Tissue Barriers: A Review of Current Status and Future Prospects. *Nano Today* **2014**, *9*, 223–243.

37. Kostarelos, K.; Emfietzoglou, D.; Papakostas, A.; Yang, W.-H.; Ballangrud, Å. M.; Sgouros, G. Engineering Lipid Vesicles of Enhanced Intratumoral Transport Capabilities: Correlating Liposome Characteristics with Penetration into Human Prostate Tumor Spheroids. *J. Liposome Res.* **2005**, *15*, 15–27.

38. Zhu, C.; Sempkowski, M.; Holleran, T.; Linz, T.; Bertalan, T.; Josefsson, A.; Bruchertseifer, F.; Morgenstern, A.; Sofou, S. Alpha-particle radiotherapy: For large solid tumors diffusion trumps targeting. *Biomaterials* **2017**, *130*, 67–75.

39. Cabral, H.; Matsumoto, Y.; Mizuno, K.; Chen, Q.; Murakami, M.; Kimura, M.; Terada, Y.; Kano, M. R.; Miyazono, K.; Uesaka, M.; Nishiyama, N.; Kataoka, K. Accumulation of sub-100 nm polymeric micelles in poorly permeable tumours depends on size. *Nat. Nanotechnol.* **2011**, *6*, 815–823.

40. Horsman, M. R.; Overgaard, J. The impact of hypoxia and its modification of the outcome of radiotherapy. *J. Radiat. Res.* **2016**, *57 Suppl 1*, i90–i98.

41. Hong, B.-J.; Kim, J.; Jeong, H.; Bok, S.; Kim, Y.-E.; Ahn, G.-O. Tumor hypoxia and reoxygenation: the yin and yang for radiotherapy. *Radiat. Oncol. J.* **2016**, *34*, 239–249.

42. Lin, S.-J.; Jee, S.-H.; Hsiao, W.-C.; Yu, H.-S.; Tsai, T.-F.; Chen, J.-S.; Hsu, C.-J.; Young, T.-H. Enhanced cell survival of melanocyte spheroids in serum starvation condition. *Biomaterials* **2006**, *27*, 1462–1469.

43. Kim, J. A.; Åberg, C.; Salvati, A.; Dawson, K. A. Role of cell cycle on the cellular uptake and dilution of nanoparticles in a cell population. *Nat. Nanotechnol.* **2012**, *7*, 62–69.

44. Yan Liu; Chen, W.; Zhang, P.; Jin, X.; Liu, X.; Li, P.; Li, F.; Zhang, H.; Zou, G.; Li, Q. Dynamically-enhanced retention of gold nanoclusters in HeLa cells following X-rays exposure: A cell cycle phase-dependent targeting approach. *Radiother. Oncol.* **2016**, *119*, 544–551.

45. Cunningham, S. H.; Mairs, R. J.; Wheldon, T. E.; Welsh, P. C.; Vaidyanathan, G.; Zalutsky, M. R. Toxicity to neuroblastoma cells and spheroids of benzylguanidine conjugated to radionuclides with short-range emissions. *Br. J. Cancer* **1998**, *77*, 2061–8.

46. Zhu, C.; Holleran, T.; Bruchertseifer, F.; Morgenstern, A.; Sofou, S. Improved spheroid penetration of alpha-particle emitters by diffusing tunable liposomes for potential alpha-radiotherapy of solid tumors. *J. Nucl. Med.* **2015**, *56*, 1197–1197.

47. Ho, J.-T.; Sarkar, A.; Kendall, L. E.; Hoshino, T.; Marton, laurence J.; Deen, D. F. Effects of fractionated radiation therapy on human brain tumor multicellular spheroids. *Int. J. Radiat. Oncol.* **1993**, *25*, 251–258.

48. Fedrigo, C. A.; Grivicich, I.; Schunemann, D. P.; Chemale, I. M.; dos Santos, D.; Jacovas, T.; Boschetti, P. S.; Jotz, G. P.; Braga Filho, A.; da Rocha, A. B. Radioresistance of human glioma spheroids and expression of HSP70, p53 and EGFr. *Radiat. Oncol.* **2011**, *6*, 156.

49. Chiappini, C.; Martinez, J. O.; De Rosa, E.; Almeida, C. S.; Tasciotti, E.; Stevens, M. M. Biodegradable Nanoneedles for Localized Delivery of Nanoparticles in Vivo: Exploring the Biointerface. *ACS Nano* **2015**, *9*, 5500–5509.

50. Chiappini, C.; De Rosa, E.; Martinez, J. O.; Liu, X.; Steele, J.; Stevens, M. M.; Tasciotti, E. Biodegradable silicon nanoneedles delivering nucleic acids intracellularly induce localized in vivo neovascularization Characterization of porous silicon nanoneedles. *Nat. Mater.* **2015**, *14*, 532–539.

51. Han, S.-W.; Nakamura, C.; Kotobuki, N.; Obataya, I.; Ohgushi, H.; Nagamune, T.; Miyake, J. High-efficiency DNA injection into a single human mesenchymal stem cell using a nanoneedle and atomic force microscopy. *Nanomedicine Nanotechnology, Biol. Med.* **2008**, *4*, 215–225.

52. Alkilany, A. M.; Thompson, L. B.; Boulos, S. P.; Sisco, P. N.; Murphy, C. J. Gold nanorods: Their potential for photothermal therapeutics and drug delivery, tempered by the complexity of their biological interactions. *Adv. Drug Deliv. Rev.* **2012**, *64*, 190–199.

53. Rayavarapu, R. G.; Petersen, W.; Hartsuiker, L.; Chin, P.; Janssen, H.; Leeuwen, F. W. B. van; Otto, C.; And, S. M.; Leeuwen, T. G. van In vitro toxicity studies of polymer-coated gold nanorods. *Nanotechnology* **2010**, *21*.

54. Palmer, R. J.; Butenhoff, J. L.; Stevens, J. B. Cytotoxicity of the Rare Earth Metals Cerium, Lanthanum, and Neodymium in Vitro: Comparisons with Cadmium in a Pulmonary Macrophage Primary Culture System. *Environ. Res.* **1987**, *43*, 142–156.

6

7

Intravenously Injected Polymersomes: Biodistribution, Circulation Time and Recoil Retention

Abstract

Research into the use of nanoparticles as tumour targeting agents is steadily increasing. Parameters like nanoparticle size and stealthiness, imparted usually by PEGylation, have shown to significantly influence circulation time as well as tumour uptake mediated by the EPR effect. In this study, the in vivo characteristics of PBD-PEO polymersomes have been investigated. Polymersomes have been loaded with the gamma-emitter ^{111}In for circulation time and biodistribution studies in healthy and tumour-bearing mice. It has been found that the polymersome diameter needs to be smaller than 200 nm, as early lung uptake of larger (200 and 400 nm) vesicles resulted in decreased respiratory functionality. Furthermore, a significant difference in circulation time has been observed between healthy and tumour-bearing mice (139 min and 7 min respectively), likely caused by active macrophages in tumour bearing mice. The retention of the ^{213}Bi daughter of the alpha-emitting ^{225}Ac in polymersomes has been assessed in vivo. Uptake of ^{213}Bi in the blood, spleen and kidneys has been compared to that of ^{225}Ac. Comparing two different encapsulation methods: ^{225}Ac coupled to DTPA or co-precipitated with $InPO_4$ nanoparticles in polymersomes. The latter has shown a two-fold increased retention in the blood. However, it is essential to increase circulation time if PBd-PEO polymersomes are to be used as tumour-targeting agents in TAT.

Introduction

The use of nanoparticles in medicine is increasingly gaining attention, mainly in cancer-related therapies, but also extending to HIV, asthma, and other infections [1]. While only a few nanoparticle-based drugs have made the translation to the clinic [2], they show great promise in e.g. reducing toxicity [3,4]. They provide a versatile platform for a range of theranostic agents, allowing for easy surface modification and/or drug encapsulation. The attachment of imaging probes like gamma-emitting radionuclides or fluorescent dyes allows for the determination of their in vivo fate, and chemo- or radio-therapeutic agents can be incorporated to provide targeted tumour death. One of the main challenges faced in designing nanoparticles in targeted drug delivery is their fast uptake by the mononuclear phagocyte system (MPS). Attaching PEG to the nanoparticle surface has shown to considerably increase circulation time, allowing them to escape notice from the immune system and prevent fast uptake by the macrophages [5]. Another critical factor in circulation time and tumour uptake is the nanoparticle size. 100 nm has been found to be an optimal time for liposome circulation [6], whereas larger diameter result in fast removal from blood circulation [7,8]. A long circulation time is essential for passive tumour targeting via the EPR effect, making use of leaky tumour vasculature combined with poor lymphatic drainage. The accumulation of nanoparticles at the tumour site not only depends on nanoparticle properties, but also physiological properties of the tumour [9], as not all tumour models exhibit the EPR effect [10]. This is important to take into account when selecting a tumour model for passive uptake studies. Tumour models which exhibit the EPR effect include CFPAC-1 [11], MDA-MB-231 [12,13] and 4T1 [14,15].

Polymersomes are versatile nanocarriers composed of amphiphilic block copolymers which can be encapsulated with drugs and/or radionuclides for combined imaging and therapy. They reportedly have a long circulation half-life [16,17], allowing for passive tumour targeting and uptake [18,19]. Radionuclides emitting gamma radiation or positrons are ideal for the non-invasive imaging of nanoparticle distribution in vivo using imaging modalities like SPECT and PET respectively. They can easily be attached to the polymersome corona [17], or be incorporated into the aqueous core [20]. While polymersomes can be used for the delivery of chemotherapeutics, they can also be utilized as radiotherapeutic carriers. Alpha-emitting radionuclides have a high LET and short penetration depth, making them the ideal candidates for targeting small metastases. ^{225}Ac is an attractive radionuclide for cancer treatment, as it has a longer half-life and emits multiple alpha particles. However, to use ^{225}Ac in TAT, it is essential to deal with the recoil problem. If daughter nuclides like ^{221}Fr and ^{213}Bi are not sufficiently retained at the tumour site, they will accumulate in the kidneys and cause renal dysfunction. Incorporating the mother nuclide in a polymersome allows the alpha particles to damage surrounding tumour tissue, while keeping the radioactive daughter nuclides inside. This approach has also been used by Sofou et al. and McLaughlin et al., who incorporated ^{225}Ac in liposomes and lanthanum phosphate particles respectively [21–24]. Polymersomes have shown to be able to retain these recoiled daughters to a large extend (Chapter 5), where the degree of daughter retention depends to a large extend on the polymersome diameter (larger polymersomes retain daughter nuclides better). It is therefore essential to be able to determine the optimal polymersome diameter for tumour targeting (where smaller vesicles have a longer circulation time) and daughter retention.

In this chapter, the in vivo circulation time and distribution of PBd-PEO polymersomes was quantified using the encapsulated SPECT nuclide ^{111}In in the polymersomes. The polymersome diameter was optimized, which is essential to select the polymersomes most suitable as TAT agents with [225]Ac as therapeutic radionuclide. Finally, the in vivo recoil retention of the daughter radionuclide [213]Bi in healthy mice was determined.

Materials and Methods

Chemicals

The block copolymer PBd-PEO with M_w of 1900-900 g/mol was purchased from Polymer Source (Quebec, Canada). The radionuclides used in this study, ^{111}In and [225]Ac, were obtained from Covidien (Petten, the Netherlands) and the Institute for Transuranium Elements (Karlsruhe, Germany) respectively. The PD10 size exclusion columns were obtained from GE Healthcare (Hoevelaken, the Netherlands). All other chemicals were purchased at Sigma Aldrich.

Polymersome preparation

Two types of polymersomes were prepared for these studies, containing either DTPA as hydrophilic chelate or KH_2PO_4 for the formation of nanoparticles. Polymersomes containing DTPA were prepared using either the solvent displacement or the direct dissolution method, depending on the required diameter. Polymersomes with a diameter of 80 nm were prepared by the solvent displacement method. Here, 1 mL PBS buffer solution containing 1 mM DTPA at pH 7.4 was added to a 20 mg/mL block copolymer solution in acetone using a syringe pump under magnetic stirring at 300 rmp. Subsequently, the acetone was evaporated using a rotavapor (Büchi, Switzerland) under reduced pressure (100 mbar) for 15 minutes, and 1 mL PBS was added to bring the final concentration to 10 mg/mL block copolymer. For polymersomes with a diameter of 100, 200 or 400 nm, the direct dissolution method was used as published by Wang et al. [20]. In short, 10 mg/mL block copolymer was added to a 1 mM DTPA PBS solution at pH 7.4, and stirred for a week. Subsequently, the polymersomes were extruded to the required diameter by passing them several times through polycarbonate filters with cut-off membrane of 800, 400, 200 and 100 nm. Polymersomes containing KH_2PO_4 were also prepared according to the direct dissolution method [25], where 10 mg/mL block copolymer was added to a PBS solution containing 0.5 M KH_2PO_4 at pH 3 and stirred for a week, after which the polymersome size was adjusted to an average diameter of 80 nm by extrusion. Before radiolabelling, remaining free DTPA or KH_2PO_4 was removed from the solution by passing it through a 30 x 1 cm (L x D) Sephadex G 25 medium mesh size extrusion column equilibrated in PBS at a pH of 7.4.

Polymersome radiolabelling

Polymersomes were radiolabelled with either ^{111}In or [225]Ac. For radiolabelling with ^{111}In, 20 μL tropolone was added to approximately 200 MBq of [111]InCl₃ in pH 2 HCl and 0.1 M 2-(N-morpholino)ethanesulfonic acid (MES) buffer, where the MES volume added was twice the volume of ^{111}In added. After an incubation time of 10 minutes, 1 mL polymersome solution, from which free DTPA was removed, was added, and incubated for 30 minutes. Subsequently, the unencapsulated [111]In

was removed by passing the solution through a PD10 column, where 0.5 mL fractions were collected and those containing the polymersomes were used for in vivo experiments. For radiolabelling with ^{225}Ac, the required amount of ^{225}Ac in pH 2 HCl was added to a vial containing a thin film of A23187 together with 200 μL 10 mM HEPES buffer. Additionally, for labelling with KH_2PO_4, 5 μL 25 mM $InCl_3$ was added together with 10 μL 20 mM tropolone to the loading solution. After an incubation period of 10 minutes, 800 μL polymersome solution (containing either 1 mM DTPA or 0.5 M KH_2PO_4) was added and incubated for 1 h. The final solution was also purified with a PD10 column.

Radionuclide retention

500 μL of ^{111}In labelled polymersomes were incubated with either 500 μL 1 mM DTPA or 500 μL BALB/c mouse serum for 24 h in 37°C. The polymersomes were separated from any free ^{111}In-DTPA by passing them through a PD10 column, or separated from the serum by passing them through a Sepharose 4B column (h x d = 31 x 1 cm) and collecting 1-mL fractions.

Dynamic light scattering

The polymersome solution was diluted in PBS to a concentration of 0.01 mg/mL, and placed in a toluene filled, temperature regulated bath (20 °C) in a DLS apparatus. The DLS consisted of a JDS Uniphase 633 nm 35 mW laser, a fibre detector, an ALV sp 125 s/w 93 goniometer and a Perkin Elmer photon counter, with an ALV-5000/epp correlator and software. The intensity autocorrelation function was determined at 90°, and the data was fitted using the Contin method [20].

Biodistribution experiments

Three different experiments were performed, with either ^{111}In or ^{225}Ac encapsulated in polymersomes. For each experiment, different groups of 5 female BALB/c nude mice were used which were between 6 and 8 weeks of age. Tumour-bearing mice were injected with 5 x 10^6 MDA-MB-231 breast cancer cells, a model known for its leaky vasculature enabling the EPR effect [13], and tumours were grown for 3 weeks. Just before the experiment, the tumour length, width and height were measured for tumour-bearing mice and tumour volume was calculated. Mice were then sorted based on tumour size and randomly divided (via excel =aselect()) over the groups. Subsequently, 200 μL 3 mg/mL polymersome solution was injected in the tail vain. Biodistribution was assessed for polymersomes of different diameter (80, 100, 200 or 400 nm diameter) in tumour bearing mice, where the injected polymersome solution contained 15 MBq ^{111}In in PBS. In healthy mice, circulation half-life experiments were performed with 80 nm diameter polymersomes containing 15 MBq ^{111}In in PBS, and recoil retention experiments with 80 nm diameter polymersomes containing 5 kBq ^{225}Ac in PBS. At 4 or 24 h p.i. the mice were sacrificed by CO_2 inhalation, and organs of interest were collected and weighted. The radioactivity was counted in an Automated Wizard Gamma Counter (Perkin Elmer). Of each of the injected compounds three standard solutions were measured to allow determination of the injected dose per gram of tissue (%ID/g). When the experiment was performed with ^{225}Ac containing polymersomes, organs collected for biodistribution were counted the following day to allow for the in-growth of ^{221}Fr and ^{213}Bi to equilibrium. All animal experiments were carried out in accordance with national regulations, and approved by the local animal welfare body.

SPECT/CT imaging

SPECT/CT imaging was performed at 1 h, 4 h, and 24 h post injection in the HS 1.0 mm mouse collimator of the U-SPECT-II (MILabs). Just before the 24 h scan the animals were euthanized by CO_2 inhalation, and after the scan ex vivo biodistribution was performed.

Recoil retention in vivo

Recoil retention was determined by first rapidly collecting the organs of interest for ^{213}Bi ingrowth (blood, spleen and kidneys) and measuring both the ^{221}Fr and ^{213}Bi activity continuously on the Wizard gamma counter for approximately 18 h (Figure 32). ^{213}Bi activity at the time of sacrifice was determined by fitting the data with equation 4 and extrapolating back to t=0 [26]:

$$A_2(t) = A_1\left(1 - e^{-\lambda_2 t}\right) + A_2(0)e^{-\lambda_2 t} \qquad (4)$$

where A_1 the activity of ^{225}Ac, and $A_2(t)$ is the ^{213}Bi activity at time t with decay constant λ_2.
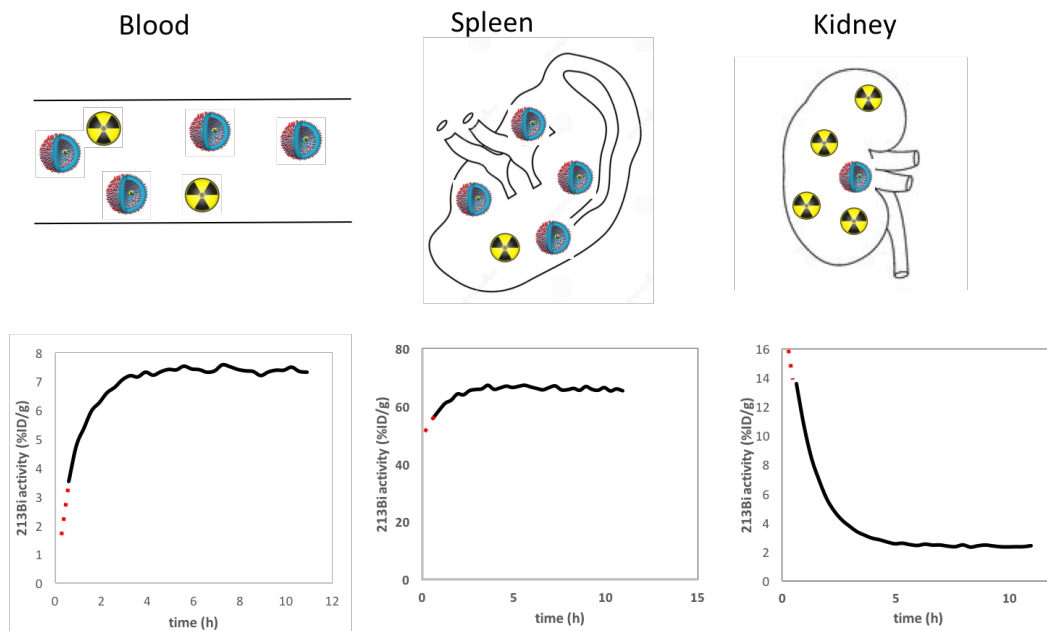
Figure 32: Schematic depictions of the amount of polymersomes (⬤) and free ^{213}Bi (☢) in three organs (blood, spleen and kidney), with underneath per organ the measured %ID/g activity of ^{213}Bi as function of the measurement time. Time t=0 represents the moment of sacrifice, 4 h after the injection of 50 kBq ^{225}Ac in 80 nm polymersomes. The percentage of recoiled ^{213}Bi daughters can be obtained by extrapolation back to t=0, and dividing by the equilibrium activity.

Results and Discussion

Labelling efficiency and retention

Polymersomes have been labelled with either ^{111}In or ^{225}Ac for circulation and recoil retention experiments respectively. Samples containing ^{111}In always contained DTPA in the aqueous cavity, with a labelling efficiency of 94 ± 2% for all polymersome sizes. Polymersomes with ^{225}Ac were labelled containing either DTPA or PO_4^{3-} in the core, and yielded labelling efficiencies of 36 ± 3% and 59 ± 7% respectively. The stability of the encapsulated ^{111}In in polymersomes was determined by challenging them with either 1 mM DTPA at RT or mouse serum for 24 h at 37 °C. The 80 nm and 200 nm diameter polymersomes displayed ^{111}In retention of 98.5 ± 0.9% and 99.0 ± 0.8% respectively when challenged with DTPA. As the other polymersome diameters (100 nm and 400 nm) originated from the same polymersome batch, having been passed through extrusion membranes with different cut-off pores, the retention observed was assumed similar for all polymersome diameters. When incubated with BALB/c mouse serum, only < 1% of the ^{111}In activity was associated with the serum fraction. These polymersome formulations have thus proven stable enough to allow for further in vivo testing.

Circulation and uptake different PS sizes

The effect of the polymersome diameter on circulation time was determined in BALB/c nude mice bearing an MDA-MB-231 tumour on their right back leg. Polymersomes loaded with the gamma-emitting ^{111}In have been injected in the tail vain of tumour-bearing mice. Representative SPECT images taken at 1 h and 24 h p.i. are depicted in Figure 33. For both small (80 nm) and large (400 nm) polymersomes, already after 1 h it is clear that there are (nearly) no polymersomes still circulating. One very clear difference between 80 nm and 400 nm polymersomes is the uptake in the lungs at 1 h p.i. Upon the injection of larger diameter nanovesicles (200 and 400 nm) the animals showed signs of illness due to the injected compound. They sat cramped together, hardly moved and their skin turned a whitish hue. Due to these observations and to minimize animal suffering, the initial division of groups (5 mice which were to be injected with either 80 nm, 200 nm or 400 nm polymersomes) shifted to 3 animals in the 200 nm group, 2 in the 400 nm group, and still 5 in the 80 nm group. Another group of 5 animals which were injected with 100 nm diameter polymersomes was created. The outward signs of extreme discomfort shown by the animals which had been injected with ≥ 200 nm vesicles cleared after approximately 1 – 1.5 h, after which the animals behaved normally for the duration of the experiment. Judging from the SPECT images taken at 1 h p.i. (Figure 33) the discomfort experienced by the animals was most likely a result from decreased respiratory function, caused by uptake of the larger (≥ 200 nm) vesicles in the lungs. This is a phenomenon which, to the best of our knowledge, has not been reported in literature.
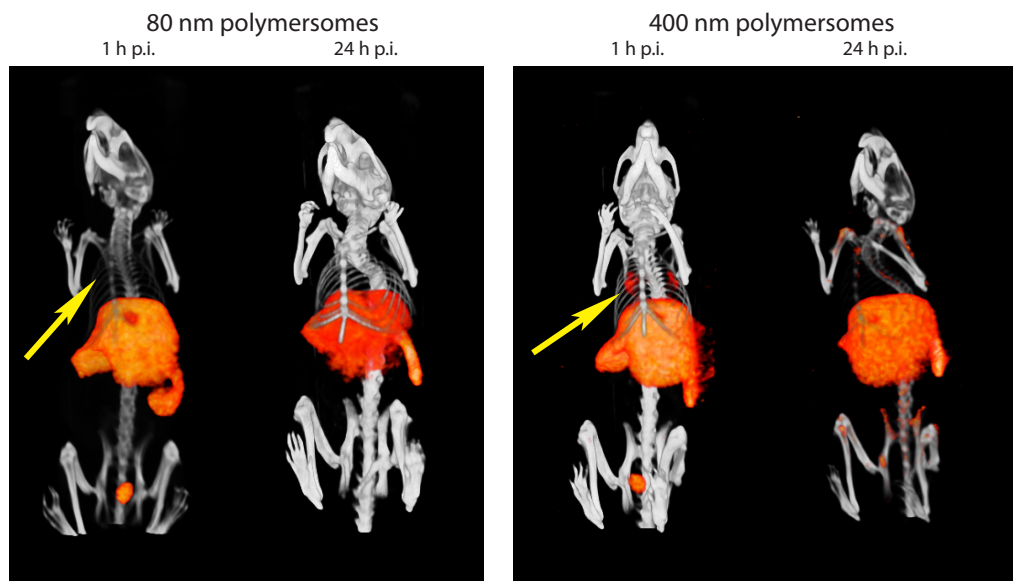
Figure 33: SPECT data of tumour-bearing mice, injected with 15-20 MBq ^{111}In-containing polymersomes with 80 nm or 400 nm diameter, 1 h and 24 h p.i.

In Figure 33, uptake of the polymersomes in the liver, spleen, bone marrow is visible, and at 1 h p.i. also in the lungs. These four organs make up the mononuclear phagocyte system, which is known to phagocytose colloidal particles. Nanoparticles with a hydrophobic surface are known be rapidly opsonized and cleared from circulation by macrophages in the liver and spleen, but also the lungs [27,28]. Although uptake by macrophages can be the cause of lung uptake visible in early SPECT images, it explains neither the signs of distress shown by the animals during the first hour following intravenous injection, nor the rapid clearance from the lungs within a few hours p.i. The most likely cause is blockage of the small pulmonary capillaries by temporarily agglomerated polymersomes with either each other or with e.g. blood cells. Lung capillaries are the smallest capillaries in the body, with diameters down to a few μm [29]. Due to the preparation method of the polymersomes, where the diameter is determined by extrusion through membrane filters with different cut-off pore size the vesicles are rather polydisperse. As can be seen in Figure 34, for e.g. the 400 nm diameter vesicles, there are polymersomes present sizing up to 600 nm diameter.
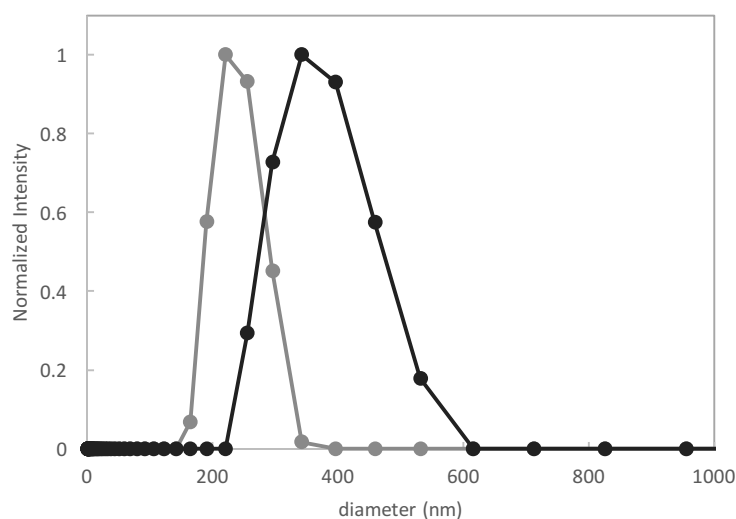
Figure 34: Polymersome diameter of 200 nm (grey) and 400 nm (black) diameter vesicles extruded through the respective polycarbonate filters as measured by DLS.

The injected polymersome diameters are in some cases thus only a factor 2 or 3 smaller than the capillary diameter. Upon the injection of a rather large number of nanovesicles, agglomeration of just a few of the polymersomes is already sufficient to completely block the capillary and cause transient embolism in the lung capillaries. This effect has been observed by Xie and co-workers, who have injected silica nanoparticles in mice. They have found that the nanoparticles aggregate and temporarily accumulate in the lungs, where the particles upon dissociation redistributed to the liver and spleen within a few days [30]. However, at normal conditions (kept at RT in PBS), no aggregation has been observed in the polymersomes used in this study over long (> 1 month) periods of time. Interaction with the serum could be the reason for aggregation, as positively charged particles have been known to form large aggregates in the presence of serum proteins [31] or with blood cells by electrostatic interaction [32], causing temporary embolism in the lung capillaries. Although a similar mechanism might be at work here, given that our polymersomes have a small negative charge (~ -0.7 mV [33]), polymersome agglomeration appears to be unlikely. A last possible explanation could be that the relatively fast injection of a high volume of concentrated polymersomes caused the blocking of capillaries, where time was all that was needed for the blood flow to open up the capillaries again. The smaller 80 and 100 nm diameter polymersomes appear to be too small for this type of agglomerations to grow large enough to be able to block the capillary. Therefore, in future in vivo studies with this type of vesicle, diameters smaller than 200 nm should be used. If large vesicle diameters are deemed essential, a lower polymersome concentration and volume could help solve the problem.
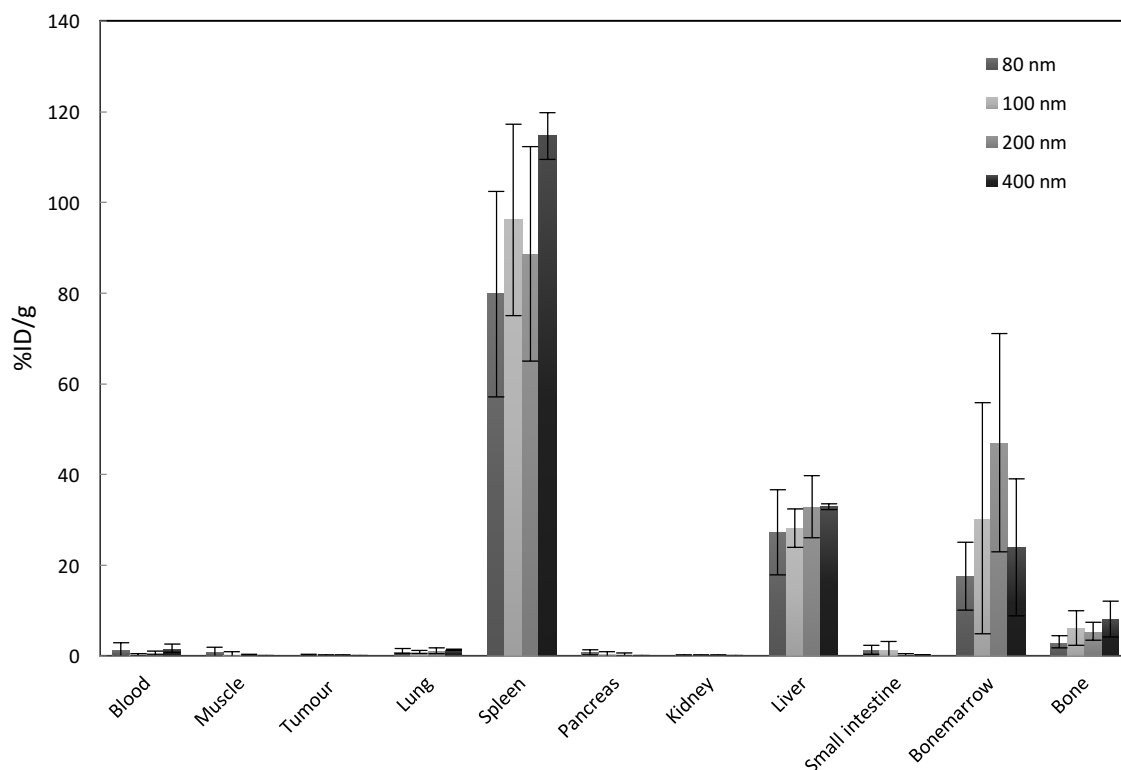
Figure 35: Polymersomes with different diameter (80 nm, 100 nm, 200 nm and 400 nm) have been injected intravenously in BALB/c nude mice bearing an MDA-MB-231 tumour on their back. The biodistribution was performed at 24 h p.i.

Biodistribution data obtained at 24 h p.i. (Figure 35) shows similar organ uptake for all vesicle diameters. There was nearly no activity measured in the lungs for all polymersome sizes, which corresponds well to SPECT images at 4 and 24 h p.i. Tumour uptake was negligible (< 0.20 %ID/g) in all cases, likely due to the very short circulation time, as at least a few hours is required for nanoparticle uptake in the tumour due to the EPR effect [11]. Short circulation times as indicated by the SPECT images are confirmed by the 24 h biodistribution, where nearly no polymersomes have been found in the blood. Uptake in the spleen, liver and bone marrow suggests that the main cause of this short circulation time has been uptake by the MPS, as macrophages are able to remove nanoparticles from the circulation within minutes [34]. Although nanoparticles typically accumulate in the spleen and the liver, depending on the surface characteristics nanoparticles can be taken up by the phagocytic reticuloendothelial cells in the bone marrow [35,36]. While PEGylation of the particles can prevent opsonins from attaching to the surface and thus decrease recognition by phagocytic cells, most research indicates that the typical PEG length necessary to achieve this stealth-like character corresponds to a molecular weight of about 2000, nearly a factor 3 higher than the PEG length of our block copolymers [37,38]. The minimal PEG length requirement is likely because at lower molecular weights the PEG is no longer flexible enough to prevent opsonisation [34].

Circulation time and biodistribution in healthy versus tumour bearing mice

Indications for the short circulation time of these polymersomes in tumour bearing mice have also been found in previous research by Wang et al. [33]. Although the circulation time was not quantitatively determined, SPECT images indicated much faster clearance in tumour bearing mice compared to healthy animals. As our experiments with the different sized polymersomes in tumour-bearing mice similarly indicated very short circulation times, an experiment was designed to determine the circulation half-life of 80 nm diameter polymersomes in both healthy and tumour-bearing mice. As evident from Figure 36, a surprisingly large difference has been observed in circulation time between healthy and tumour-bearing mice. The activity levels have been decay-corrected and subsequently fitted with $A(t) = A_0 e^{\frac{-t \ln 2}{t_{1/2}}}$ to determine the circulation half-life. Here, $t_{1/2}$ is the circulation half-life, t is the time in minutes, $A(t)$ the activity in the blood at time t, and A_0 the initial ^{111}In activity. The circulation half-life has been determined to be 139 min for healthy mice, and 7 min in tumour-bearing mice, which is a surprisingly large difference. This difference likely stems from the tumour presence in the tumour-bearing mice. Tumour presence has been shown to cause a shift in the normal immune system balance from Th1 to Th2 cytokines [39], which induce macrophages to differentiate into M-1 or M2-type macrophages respectively [40]. Jones et al. found that there is a remarkably large difference in nanoparticle clearance rate between the two macrophage types, where M2 macrophages result in much more rapid nanoparticle clearance [41]. This suggested increase in nanoparticle uptake of tumour-bearing mice has also been investigated by Kai et al., who have observed an increase in M2-like macrophages in tumour-bearing mice as compared to healthy ones [40]. They found that tumour presence drastically impacted the circulation time of their hydrogel nanoparticles, while small molecules did not exhibit a difference in circulation time. Unfortunately, there are no studies that directly compare the in vivo circulation time of polymersomes in healthy and tumour-bearing mice. However, for efficient tumour-targeting longer circulation half-lives are required than even the 2.3 h in the present study. This has been found to depend primarily on the ability of nanoparticles to avoid the macrophages, which is largely influenced by the degree of PEGylation. With a longer PEG, PBd-PEO polymersomes have been found to circulate longer (15.8 h and 28.0 h for 1100 g/mol and 2150 g/mol PEG respectively) [16]. Other circulation times in healthy mice are also considerably longer than found in the present study [16–18], and polymersomes with long half-life (19.9 h) have been reported in tumour-bearing mice as well [42]. These long circulating vesicles demonstrate the need of longer PEG chains to increase circulation half-life.

7
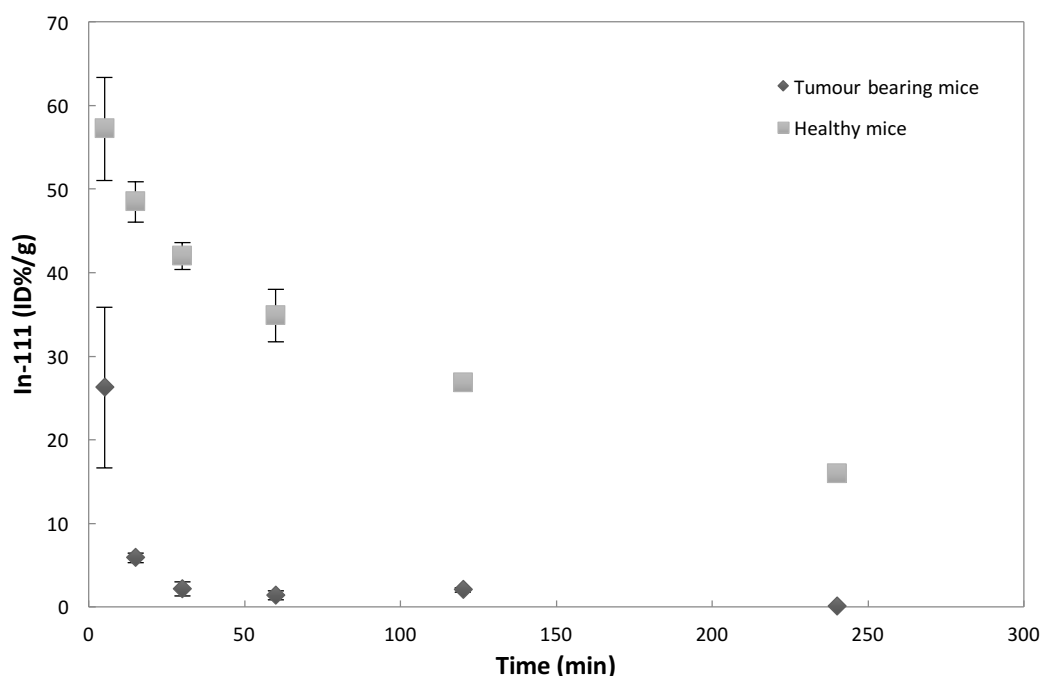
Figure 36: circulation time of 80 nm polymersomes in BALB/c mice, either healthy or bearing an MDA-MB-231 tumour over the course of 4 h.

In Figure 37, the biodistribution data at 4 h p.i. is shown for 80 nm polymersomes in both healthy and tumour-bearing mice. While uptake is quite similar in most organs, large differences in uptake have been observed in the blood and bone marrow, and to a lesser degree in the spleen and liver. Studies have shown an increase in bone-marrow myelopoiesis in the presence of a tumour [40]. Being, to the best of our knowledge, the only study directly comparing nanoparticle kinetics and biodistribution in healthy and tumour-bearing mice, Kai et al. have studied the interaction of their nanoparticle with immune cells in different organs. Liver uptake was significantly higher in tumour-bearing mice though no large differences in uptake were found in the spleen [40]. The difference in liver uptake was found to be associated mainly with a larger proportion of M2 macrophages, again due to the tumour presence. They macrophages are likely also responsible for the increase in liver uptake in the tumour bearing mice in our study.
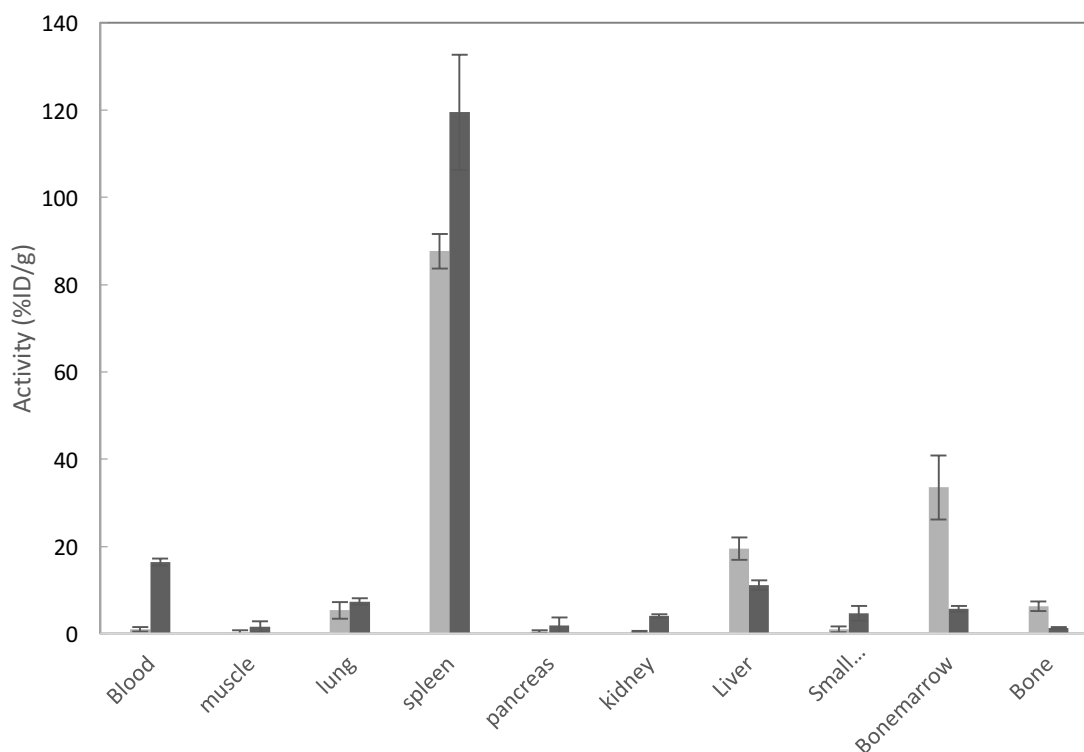
Figure 37: Biodistribution data of polymersomes with 80 nm diameter were injected intravenously in healthy (dark grey) and tumour-bearing (light grey) Balb/c nude mice. Polymersomes containing DTPA were labelled with [111]In. The biodistribution was performed 4 h p.i.

Recoil retention [213]Bi

In order to use the polymersomes as therapeutic agents to target tumour metastases, it is important that they retain as many of the recoiling daughters as possible upon intravenous injection. A novel method was developed to be able to measure the recoil retention in vivo. Due to its short half-life (4.8 min) the retention of [221]Fr unfortunately cannot be determined accurately. However, with a half-life of a little under an hour, the ingrowth of [213]Bi can be determined, which has allowed for extrapolation to the time of sacrifice and a direct comparison of the presence of [213]Bi and [225]Ac at organ level. The levels of radioactivity in the blood, spleen and kidneys have been measured, as those are the organs where accumulation of polymersomes or free [213]Bi would be expected (Figure 32). In Table 14, the fraction of recoiled [213]Bi as compared to the equilibrium [213]Bi activity is given, measured 4 h after the injection of [225]Ac encapsulated in either DTPA-containing polymersomes, or co-precipitated in $InPO_4$ nanoparticles within the polymersomes. In both cases, a clear difference between initial [213]Bi presence and [213]Bi levels at equilibrium with [225]Ac was found. However, twice as much [213]Bi was retained in the blood for the $InPO_4$ containing vesicles as compared to the DTPA ones, and these differences are also reflected in the retention in the spleen and free [213]Bi uptake in the kidneys. It can therefore be concluded that co-precipitation of [225]Ac with $InPO_4$ nanoparticles in polymersomes constitutes a significant improvement over DTPA containing polymersomes, as they are twice as effective in retaining recoiled [213]Bi. Unfortunately, [221]Fr retention was not assessed due to its short half-life, especially since it is mainly this nuclide which is expected to be retained much better by the nanoparticle

containing polymersomes [25]. Biodistribution data of the [225]Ac-loaded vesicles at 4 h p.i. was similar to that reported for ^{111}In-containing polymersomes in Figure 37, for both [225]Ac coupled to DTPA as hydrophilic chelator, or precipitated with $InPO_4$ nanoparticles. As the radionuclides are encapsulated in the aqueous core of the polymersomes, the outer surface remains the same, logically resulting in the similar organ uptake.

Table 14: Fraction of recoiled [213]Bi to [225]Ac in 80 nm polymersomes 4 h p.i. in the blood, spleen and kidneys, calculated as $A_{213_{Bi}}(t = 0)/A_{213_{Bi}}(t = eq)$, with $A_{213_{Bi}}(t)$ the [213]Bi activity at time of death (t=0) or in equilibrium with the mother nuclide [225]Ac (t = eq). [225]Ac was encapsulated in polymersomes containing either the hydrophilic chelate DTPA or $InPO_4$ nanoparticles.

Organ	DTPA	InPO$_4$
Blood	0.06 ± 0.03	0.14 ± 0.07
Spleen	0.67 ± 0.02	0.80 ± 0.06
Kidney	7.75 ± 0.63	7.03 ± 2.04

In Chapter 5, the recoil retention of both [221]Fr and [213]Bi has been determined in polymersomes with different diameters. In this case, [213]Bi retention in [225]Ac-InPO$_4$ containing polymersomes was also about twice as high as in [225]Ac-DTPA-containing polymersomes (40% and 22% respectively), corresponding well to our current findings. The in vivo retention in blood, as displayed in Table 14, should directly reflect the retention of [213]Bi in polymersomes. However, for both DTPA and InPO$_4$ containing polymersomes, the retention in blood is lower than the recoil retentions of [213]Bi as found in Chapter 5. One reason for this difference can be found in the re-association of [213]Bi with the polymersomes when in solution. In an earlier study by Wang et al., re-loading of ^{111}In into polymersomes was found to be 17 ± 8%, which was given as a possible explanation for the high experimentally determined retention of the recoiled [209]Pb (a daughter of [213]Bi) [26]. A similar mechanism could also have been at work for the retention studies as presented in Chapter 5. While this can easily occur within the confines of a scintillation vial, in an animal model there are many molecules present in the blood which take up the recoiled daughter nuclides and transport them to e.g. the kidneys. Re-association is therefore much less likely, resulting in lower daughter retention. Next to that, the measured [213]Bi retention in 100 nm vesicles was probably somewhat overestimating actual retention, as retention in 200 nm vesicles was lower, which is quite unlikely. Therefore, despite the much-improved retention with InPO$_4$ containing polymersomes, also in vivo, it remains worthwhile to investigate 200 nm diameter polymersomes for increased recoil retention. However, it is essential to first deal with the circulation time of the vesicles, preferably using ^{111}In-containing polymersomes, as they can be followed in vivo with SPECT imaging, and have the exact same uptake characteristics.

Conclusion

In this chapter, we have studied the in vivo characteristics upon intravenous injection of polymersomes labelled with either ^{111}In or ^{225}Ac. Despite very short circulation times in tumour bearing mice it has become clear that polymersomes larger than 200 nm in diameter are not feasible, as they are rapidly taken up in the lungs resulting in decreased respiratory functionality. Smaller vesicles (80 nm diameter) have shown a large difference in circulation time between tumour bearing mice and healthy mice. This was likely caused by activated macrophages due to the presence of a tumour, a hypothesis which has also been confirmed by the difference in biodistribution, where a much larger uptake in the bone-marrow was found in the case of tumour-bearing mice. However, the longer circulation time in healthy mice did allow for the determination of ^{213}Bi retention in vivo. Here, a noteworthy difference was found between polymersomes containing DTPA and those with $InPO_4$ nanoparticles. More than twice the amount of ^{213}Bi was retained in the case of the nanoparticles, showing the clear benefit of the shorter recoil distance caused by the presence of the nanoparticle. For the further development of PBd-PEO polymersomes as tumour-targeting agents in targeted alpha therapy, it is essential to increase circulation time. This can probably be realized by increasing the polyethylene glycol length in the polymersome corona and thus decreasing macrophage uptake.

7

References

1. Zhang, L.; Gu, F.; Chan, J.; Wang, A.; Langer, R.; Farokhzad, O. Nanoparticles in Medicine: Therapeutic Applications and Developments. *Clin. Pharmacol. Ther.* **2008**, *83*, 761–769.

2. Anselmo, A. C.; Mitragotri, S. Nanoparticles in the clinic. *Bioeng. Transl. Med.* **2016**, *1*, 10–29.

3. O'Brien, M. E. R.; Wigler, N.; Inbar, M.; Rosso, R.; Grischke, E.; Santoro, A.; Catane, R.; Kieback, D. G.; Tomczak, P.; Ackland, S. P.; Orlandi, F.; Mellars, L.; Alland, L.; Tendler, C. Reduced cardiotoxicity and comparable efficacy in a phase III trial of pegylated liposomal doxorubicin HCl (CAELYXTM/Doxil") versus conventional doxorubicin for first-line treatment of metastatic breast cancer. *Ann. Oncol.* **2004**, *15*, 440–449.

4. Emerich, D. F.; Thanos, C. G. Targeted nanoparticle-based drug delivery and diagnosis. *J. Drug Target.* **2007**, *15*, 163–183.

5. Yoo, J.-W.; Chambers, E.; Mitragotri, S. Factors that control the circulation time of nanoparticles in blood: challenges, solutions and future prospects. *Curr. Pharm. Des.* **2010**, *16*, 2298–307.

6. Nagayasu, A.; Uchiyama, K.; Kiwada, H. The size of liposomes: a factor which affects their targeting efficiency to tumors and therapeutic activity of liposomal antitumor drugs. *Adv. Drug Deliv. Rev.* **1999**, *40*, 75–87.

7. Ishida, O.; Maruyama, K.; Sasaki, K.; Iwatsuru, M. Size-dependent extravasation and interstitial localization of polyethyleneglycol liposomes in solid tumor-bearing mice. *Int. J. Pharm.* **1999**, *190*, 49–56.

8. Litzinger, D. C.; Buiting, A. M. J.; van Rooijen, N.; Huang, L. Effect of liposome size on the circulation time and intraorgan distribution of amphipathic poly(ethylene glycol)-containing liposomes. *Biochim. Biophys. Acta - Biomembr.* **1994**, *1190*, 99–107.

9. Hashizume, H.; Baluk, P.; Morikawa, S.; McLean, J. W.; Thurston, G.; Roberge, S.; Jain, R. K.; McDonald, D. M. Openings between defective endothelial cells explain tumor vessel leakiness. *Am. J. Pathol.* **2000**, *156*, 1363–1380.

10. Cheng, Z.; Al Zaki, A.; Hui, J. Z.; Muzykantov, V. R.; Tsourkas, A. Multifunctional Nanoparticles: Cost Versus Benefit of Adding Targeting and Imaging Capabilities. *Science (80-.).* **2012**, *338*.

11. Bolkestein, M.; de Blois, E.; Koelewijn, S. J.; Eggermont, A. M. M.; Grosveld, F.; de Jong, M.; Koning, G. A. Investigation of Factors Determining the Enhanced Permeability and Retention Effect in Subcutaneous Xenografts. *J. Nucl. Med.* **2016**, *57*, 601–7.

12. Shenoy, D. B.; Amiji, M. M. Poly(ethylene oxide)-modified poly(e-caprolactone) nanoparticles for targeted delivery of tamoxifen in breast cancer. *Int. J. Pharm.* **2005**, *293*, 261–270.

13. Ahmed, F.; Pakunlu, R. I.; Brannan, A.; Bates, F.; Minko, T.; Discher, D. E. Biodegradable polymersomes loaded with both paclitaxel and doxorubicin permeate and shrink tumors, inducing apoptosis in proportion to accumulated drug. *J. Control. Release* **2006**, *116*, 150–158.

14. Charrois, G. J. R.; Allen, T. M. Drug release rate influences the pharmacokinetics, biodistribution, therapeutic activity, and toxicity of pegylated liposomal doxorubicin formulations in murine breast cancer. *Biochim. Biophys. Acta - Biomembr.* **2004**, *1663*, 167–177.

15. Sawant, R. R.; Torchilin, V. P. Enhanced cytotoxicity of TATp-bearing paclitaxel-loaded micelles in vitro and in vivo. *Int. J. Pharm.* **2009**, *374*, 114–118.

16. Photos, P. J.; Bacakova, L.; Discher, B.; Bates, F. S.; Discher, D. E. Polymer vesicles in vivo: correlations with PEG molecular weight. *J. Control. Release* **2003**, *90*, 323–34.

17. Brinkhuis, R. P.; Stojanov, K.; Laverman, P.; Eilander, J.; Zuhorn, I. S.; Rutjes, F. P. J. T.; Hest, J. C. M. Van Size Dependent Biodistribution and SPECT Imaging of 111In-Labeled Polymersomes. *Bioconjug. Chem.* **2012**, *23*, 958–965.

18. Lee, J. S.; Ankone, M.; Pieters, E.; Schiffelers, R. M.; Hennink, W. E.; Feijen, J. Circulation kinetics and biodistribution of dual-labeled polymersomes with modulated surface charge in tumor-bearing mice: Comparison with stealth liposomes. *J. Control. Release* **2011**, *155*, 282–288.

19. Ahmed, F.; Pakunlu, R. I.; Srinivas, G.; Brannan, A.; Bates, F.; Klein, M. L.; Minko, T.; Discher, D. E. Shrinkage of a rapidly growing tumor by drug-loaded polymersomes: pH-triggered release through copolymer degradation. *Mol. Pharm.* **2006**, *3*, 340–350.

20. Wang, G.; de Kruijff, R. M.; Stuart, M. C. A.; Mendes, E.; Wolterbeek, H. T.; Denkova, A. G. Polymersomes as radionuclide carriers loaded via active ion transport through the hydrophobic bilayer. *Soft Matter* **2013**, *9*, 727–734.

21. Zhu, C.; Holleran, T.; Bruchertseifer, F.; Morgenstern, A.; Sofou, S. Improved spheroid penetration of alpha-particle emitters by diffusing tunable liposomes for potential alpha-radiotherapy of solid tumors. *J. Nucl. Med.* **2015**, *56*, 1197–1197.

22. Sofou, S.; Thomas, J. L.; Lin, H.; McDevitt, M. R.; Scheinberg, D. a; Sgouros, G. Engineered liposomes for potential alpha-particle therapy of metastatic cancer. *J. Nucl. Med.* **2004**, *45*, 253–60.

23. Woodward, J.; Kennel, S. J.; Stuckey, A.; Osborne, D.; Wall, J.; Rondinone, A. J.; Standaert, R. F.; Mirzadeh, S. LaPO4 nanoparticles doped with actinium-225 that partially sequester daughter radionuclides. *Bioconjug. Chem.* **2011**, *22*, 766–76.

24. McLaughlin, M. F.; Robertson, D.; Pevsner, P. H.; Wall, J. S.; Mirzadeh, S.; Kennel, S. J. LnPO4 nanoparticles doped with Ac-225 and sequestered daughters for targeted alpha therapy. *Cancer Biother. Radiopharm.* **2014**, *29*, 34–41.

25. Kruijff, R. M. de; Drost, K.; Thijssen, L.; Morgenstern, A.; Bruchertseifer, F.; Lathouwers, D.; Wolterbeek, H. T.; Denkova, A. G. Improved 225Ac Daughter Retention in InPO4 Containing Polymersomes. *Appl. Radiat. Isot.* **2017**, *128*, 183–189.

26. Wang, G.; de Kruijff, R. M.; Rol, A.; Thijssen, L.; Mendes, E.; Morgenstern, A.; Bruchertseifer, F.; Stuart, M. C. A.; Wolterbeek, H. T.; Denkova, A. G. Retention studies of recoiling daughter nuclides of 225Ac in polymer vesicles. *Appl. Radiat. Isot.* **2014**, *85*, 45–53.

27. Brannon-Peppas, L.; Blanchette, J. O. Nanoparticle and targeted systems for cancer therapy. *Adv. Drug Deliv. Rev.* **2004**, *56*, 1649–1659.

28. Brigger, I.; Dubernet, C.; Couvreur, P. Nanoparticles in cancer therapy and diagnosis ☆. *Adv. Drug Deliv. Rev.* **2012**, *64*, 24–36.

29. Mark R Looney; Emily E Thornton; Debasish Sen; Wayne J Lamm; Robb W Glenny; Matthew F Krummel Stabilized imaging of immune surveillance in the mouse lung. *Nat. Methods* **2011**, *8*, 91–98.

30. Xie, G.; Sun, J.; Zhong, G.; Shi, L.; Zhang, D. Biodistribution and toxicity of intravenously administered silica nanoparticles in mice. *Arch. Toxicol.* **2010**, *84*, 183–190.

31. Li, S.-D.; Huang, L. Pharmacokinetics and Biodistribution of Nanoparticles. *Mol. Pharm.* **2008**, *5*, 496–504.

32. He, C.; Hu, Y.; Yin, L.; Tang, C.; Yin, C. Effects of particle size and surface charge on cellular uptake and biodistribution of polymeric nanoparticles. *Biomaterials* **2010**, *31*, 3657–3666.

33. Wang, G.; de Kruijff, R. M.; Abou, D.; Ramos, N.; Mendes, E.; Franken, L. E.; Wolterbeek, H. T.; Denkova, a. G. Pharmacokinetics of Polymersomes Composed of Poly(Butadiene-Ethylene Oxide); Healthy versus Tumor-Bearing Mice. *J. Biomed. Nanotechnol.* **2016**, *12*, 320–328.

34. Owens III, D. E.; Peppas, N. A. Opsonization, biodistribution, and pharmacokinetics of polymeric nanoparticles. *Int. J. Pharm.* **2006**, *307*, 93–102.

35. Avgoustakis, K.; Beletsi, A.; Panagi, Z.; Klepetsanis, P.; Livaniou, E.; Evangelatos, G.; Ithakissios, D. S. Effect of copolymer composition on the physicochemical characteristics, in vitro stability, and biodistribution of PLGA-mPEG nanoparticles. *Int. J. Pharm.* **2003**, *259*, 115–127.

36. Porter, C. J. H.; Moghimi, S. M.; Illum, L.; Davis, S. S. The polyoxyethylene/polyoxypropylene block co-polymer Poloxamer-407 selectively redirects intravenously injected microspheres to sinusoidal endothelial cells of rabbit bone marrow. *FEBS Lett.* **1992**, *305*, 62–66.

37. Gref, R.; Minamitake, Y.; Peracchia, M.; Trubetskoy, V.; Torchilin, V.; Langer, R. Biodegradable long-circulating polymeric nanospheres. *Science (80-.).* **1994**, *263*, 1600–1603.

38. Peracchia, M. T. Stealth nanoparticles for intravenous administration. *STP PHARMA Sci.* **2003**, *13*, 155–161.

39. Kiessling, R.; Wasserman, K.; Horiguchi, S.; Kono, K.; Sjoè Berg, J.; Pisa, P.; Petersson, M. Tumor-induced immune dysfunction. *Cancer Immunol. Immunother.* **1999**, *48*, 353–362.

40. Kai, M. P.; Brighton, H. E.; Fromen, C. A.; Shen, T. W.; Luft, J. C.; Luft, Y. E.; Keeler, A. W.; Robbins, G. R.; Ting, J. P. Y.; Zamboni, W. C.; Bear, J. E.; DeSimone, J. M. Tumor presence induces global immune changes and enhances nanoparticle clearance. *ACS Nano* **2016**, *10*, 861–870.

41. Jones, S. W.; Roberts, R. A.; Robbins, G. R.; Perry, J. L.; Kai, M. P.; Chen, K.; Bo, T.; Napier, M. E.; Ting, J. P. Y.; DeSimone, J. M.; Bear, J. E. Nanoparticle clearance is governed by Th1/Th2 immunity and strain background. *J. Clin. Invest.* **2013**, *123*, 3061–3073.

42. Upadhyay, K. K.; Bhatt, A. N.; Castro, E.; Mishra, A. K.; Chuttani, K.; Dwarakanath, B. S.; Schatz, C.; Le Meins, J.-F.; Misra, A.; Lecommandoux, S. In vitro and in vivo evaluation of docetaxel loaded biodegradable polymersomes. *Macromol. Biosci.* **2010**, *10*, 503–512.

7

8

Intratumoural Administration of ^{225}Ac-Containing Polymersomes

Abstract

While in classic brachytherapy careful placement of the seeds is still essential for optimal irradiation of the tumour, recently a movement towards the use of micro and nano particles for intratumoural administration has begun. These particles are able to distribute themselves to and within the tumour tissue, and can be labelled with either beta or alpha emitters. In this chapter, we evaluate the suitability of ^{225}Ac-containing PBD-PEO polymersomes with a 200 nm diameter as intratumoural therapeutic agents. Vesicles containing 10 kBq ^{225}Ac have been injected intratumourally in MDA-MB-231 tumour-bearing BALB/c nude mice. The tumour size has been followed for 66 days for mice injected with either the polymersomes, or with ^{225}Ac-DOTA or PBS as control, and at 1 and 7 days p.i. their biodistribution has been assessed. Polymersomes have been shown to be very well retained in the tumour tissue, whereas ^{225}Ac-DOTA was rapidly cleared. While a definite tumour growth inhibition has been observed for the tumours injected with ^{225}Ac-polymersomes, a large degree of growth inhibition was observed even in the control group, making it difficult to properly assess the influence of the ^{225}Ac-polymersomes on the tumour growth. However, the observed polymersome retention in the tumour tissue together with an increase in γ-H2AX foci in the tumours treated with ^{225}Ac-polymersomes does indicate that vesicles containing alpha-emitters like ^{225}Ac will be suitable agents for long-term irradiation of tumours.

Introduction

Cancer, still presenting one of the major challenges in modern healthcare, leads to more than 8.8 million deaths annually [1]. While the main treatment options include surgery, chemotherapy, and radiotherapy, increasing attention is given to brachytherapy in e.g. the treatment of prostate cancer. Advantages of brachytherapy, as compared to radical prostatectomy and external beam radiation therapy, lie in the much higher radiation doses which can be given to the tumour tissue whilst spearing healthy tissue. Also, it can be undertaken as a fast outpatient procedure with only one treatment [2]. However, careful treatment planning is essential for an optimal dose distribution, and even then errant seeds can e.g. end up in the bladder and urethra in the case of prostate cancer therapy [3]. Radionuclides used in brachytherapy are typically gamma- or beta-emitting radionuclides like ^{192}Ir and ^{125}I, allowing for the irradiation of a certain area around the seed location. In contrast, alpha-emitting radionuclides emit particles with a much higher LET and short penetration depth in tissue, making them highly cytotoxic and thus ideal radionuclides for tumour therapy. In addition, they kill tumour cells regardless of tumour cell cycle stage and oxygenation level, thereby allowing for treatment in hypoxic areas. Recently, the alpha-emitter ^{224}Ra has been proposed for use in brachytherapy called DaRT (diffusing alpha-emitters radiation therapy) [4], which is currently undergoing clinical trials. This new form of therapy is based on the recoil effect of short-lived alpha-emitting daughter nuclides, which diffuse away from the wires on the surface of which the ^{224}Ra has been loaded, thus covering substantial distances within the tumour while sparing healthy tissue.

Increasing attention is being given to a form of brachytherapy where radionuclides distribute themselves throughout the tumour volume. It is similar to brachytherapy in the sense that radioactivity is still directly inserted into the tumour tissue, but no longer requires the specific placement of seeds. In fact, the brachytherapy market is currently shifting towards the use of microspheres and electronic brachytherapy. These two forms of brachytherapy are commanding 40% of the global brachytherapy market and are mainly responsible for its annual growth [5]. The beta-emitting microspheres (^{90}Y or ^{166}Ho) are used in the treatment of metastatic liver, where upon injection into the hepatic artery they eventually embolise the small blood vessels around the liver tumours, and irradiate surrounding tumours [6,7]. These microspheres are too large to be used in alpha radionuclide therapy, as the range of an alpha particle is only a few cell diameters. Smaller molecules are required for successful local implementation of alpha radionuclide therapy. This has been shown in the very promising clinical trials concerning glioma treatment with ^{213}Bi-DOTA-[Thi^8,Met(O$_2$)^{11}]- substance P [8]. In these trials, the compound is directly injected in the brain tumour, with more than 96% of the compound retained at the tumour site. Rapid intratumoural distribution (required due to the short half-life of ^{213}Bi) and little toxicity to healthy tissue was achieved, increasing median patient survival to 29 months. Currently, replacement of ^{213}Bi with the longer-lived radionuclides like ^{211}At is considered, giving more time for optimal distribution in the tumour tissue [9].

Long-lived alpha emitters provide clear advantages, as the longer half-life enables both better tumour distribution as well as longer irradiation of tumour tissue. However, the recoil energy experienced by the radioactive daughter nuclides upon the emission of an alpha particle causes them to break free from any targeting agent and e.g. cause renal toxicity [10]. Encapsulation in polymersomes can prevent this from happening to a large degree [11], and full tumour penetration is achieved after approximately

4 days as indicated by in vitro studies (Chapter 6). A pilot study was performed with intratumourally injected ^{111}In-containing polymersomes. Here, a good retention at the tumour site was observed at 24 h p.i., whereas ^{111}In-DTPA was cleared rapidly [12]. In this study, we will therefore determine the potential of these carriers loaded with [225]Ac as suitable agents for intratumoural brachytherapy. To this effect, the therapeutic efficacy of intratumourally injected [225]Ac labelled polymersomes will be assessed in BALB/c mice over a period of 66 days. Next to that, the retention of the [225]Ac polymersomes and the daughter [213]Bi in the tumour will be determined, as well as the effect of [225]Ac polymersomes on tumour proliferation, apoptosis, and double strand DNA breaks.

Materials and Methods

Chemicals

The block copolymer PBd-PEO with M_w of 1900-900 g/mol was purchased from Polymer Source (Quebec, Canada). The [225]Ac was obtained from the Directorate for Nuclear Safety and Security (Karlsruhe, Germany). The PD10 size exclusion columns were obtained from GE Healthcare (Hoevelaken, the Netherlands). Instant Thin-Layer Chromatography (ITLC) strips were purchased from Varian (USA). For the immunohistochemical analysis, rabbit-anti-H2AX (Cell Signaling, art.nr. 9718), goat-anti-rabbit (Vector, art.nr. BA-1000), avidin-biotin (Vectastain, art.nr. PK-6100) and Bright DAB (Immunlogic, art.nr. BSO4-500) were used. All other chemicals were purchased at Sigma Aldrich.

[225]Ac-polymersome labelling

Polymersomes were prepared according to the solvent displacement method as described in Chapter 7. In short, 1 mM DTPA in 1 mL PBS buffer solution (pH 7.4) was slowly added to 1 mL acetone containing 20 mg/mL block copolymer under continuous stirring. After evaporation of the acetone, 1 mL PBS was added to bring the final concentration to 10 mg/mL block copolymer. The remaining unencapsulated DTPA was removed by passing it through a Sephadex G 25 size extrusion column (L x D = 30 x 1 cm). 1.6 MBq [225]Ac in pH 2 HCl with 200 μL 10 mM Hepes buffer was added to a vial containing A23187 dissolved in 100 μL $CHCl_3$. Upon the evaporation of the $CHCl_3$, 800 μL polymersome solution was added and incubated for 1 hour. A PD10 column was used for purification, and the 7th 0.5 ml fraction was collected for further in vivo experiments at an [225]Ac concentration of 0.5 kBq/mL.

[225]Ac-DOTA labelling

For the labelling of [225]Ac-DOTA, 0.7 MBq [225]Ac was added to $4 \cdot 10^{-9}$ mol in 40 μL 0.1 M TRIS buffer at pH 9.0. After an incubation time of 1 h at 37°C the labelling efficiency was determined with instant thin layer chromatography (ITLC). A 2 μL droplet of the radiolabelled sample was placed on a 7 cm ITLC strip, with 0.1 M NaOH at pH 12 as mobile phase. The ITLC strip was subsequently imaged with the Phosphor-imager to determine the labelling efficiency. The sample was used without further purification, and diluted in PBS to an [225]Ac concentration of 0.5 kBq/mL for in vivo testing.

In vivo evaluation

The therapeutic potential of intratumourally injected ^{225}Ac-polymersomes and ^{225}Ac-DOTA was evaluated in female BALB/c mice, 6-8 weeks of age. All mice were subcutaneously inoculated with $5 \cdot 10^6$ MDA-MB-231 cells. There were three main treatment groups, each containing one subgroup of 8 mice to determine overall survival, and 2 subgroups of each 3 mice for biodistribution experiments and immunohistochemical analysis of tumour tissue and kidneys. When the tumour volume was approximately 100 mm³, the mice were stratified based on tumour size and randomly divided (via excel =aselect()) over the nine different treatment subgroups. Each mouse was injected intratumourally with a 20 μL solution containing either 10 kBq ^{225}Ac polymersomes, 10 kBq ^{225}Ac-DOTA, or PBS for the three different treatment groups.

Biodistribution of groups having received either ^{225}Ac-polymersomes or the ^{225}Ac-DOTA compound, was analysed at day 1 and at day 7 p.i. by taking 3 mice out of the experiment for these two groups at each time-point. In addition, 3 mice of the PBS group were sacrificed at day 1 and at day 7 day p.i. for immunohistochemical analysis of the tumour and kidneys. In all cases, mice were sacrificed by CO_2 inhalation. A blood sample was drawn from the mice which have been injected with ^{225}Ac, and organs of interest were collected and weighed. Tumours and kidneys of all 18 animals (6 per treatment group) were immediately embedded in paraffin to analyse apoptosis, proliferation and double strand DNA breaks immunohistochemically. Retention of the daughter nuclide ^{213}Bi in the tumour, and accumulation in the kidneys, was assessed as described in Chapter 7. In short, immediately after CO_2 asphyxation vials containing the blood, tumour and kidneys were transferred to a Wizard gamma counter where they were measured continuously for > 9 h. ^{213}Bi activity at the time of sacrifice was determined by extrapolating the in-growth back to time t=0. Unfortunately, initial ^{213}Bi levels could not be determined for all groups, as the ^{225}Ac (and consequently ^{213}Bi) activity was very low.

The remaining 8 mice per group were used to monitor tumour growth and overall survival. Tumour volume was measured twice a week, and mice were taken out of the experiment when they reached one of the humane endpoints. All animal experiments were approved by the local animal welfare committee and performed according to national regulations.

Immunohistochemistry

Tumours were harvested at 1 and 7 days after the intratumoural injection and embedded in paraffin until use. Immunohistochemistry was performed using 4 μm thick tumour sections. For the haematoxylin and eosin (HE) staining, paraffin was removed by incubation with xylene, and subsequently sections were incubated with haematoxylin for 20 minutes and with eosin for 5 minutes.

For the staining with γ-H2AX, first antigen unmasking was performed on the deparaffinated tumour sections by treating the slides with 10 mM citrate buffer (pH 6.0) for 10 minutes at 98°C. After washing the slides with distilled water and PBS, endogeneous peroxidae activity was blocked with 3% H_2O_2 in PBS for 10 minutes at RT. After another PBS wash, aspecific binding was blocked by incubating the sections with $50-150$ μL 20 % normal goat serum (NGS) in PBS for 30 minutes at RT. Subsequently, the tumour sections were incubated overnight with $50-150$ μL rabbit-anti-H2AX diluted 1000 times in a PBS solution containing 1% BSA (bovine serum albumin) at 4°C. After another wash with PBS

the sections were incubated for 30 minutes at RT with 200 times diluted biotinylated goat-anti-rabbit. Finally, an avidin-biotin complex was applied for 30 minutes at RT. To develop the tumour sections, they were incubated with 50-150 μL Bright DAB for 8 minutes at RT. Finally, the sections were washed with consecutively tapwater, 50%, 70%, and twice 100% ethanol, twice with Xylene, after which they were mounted with Permount, dried and imaged.

Results and discussion

Labelling efficiency

Polymersomes have been labelled with ^{225}Ac according to the well-documented labelling procedures as described by Wang et al. [13], with a slight modification. Radiolabelling efficiencies with A23187 as ligand have been increased substantially by incubating the radionuclide with the A23187 in chloroform, as presented in Chapter 2. Thus, a loading efficiency of 61% has been achieved in the DTPA-containing polymersomes. The labelling efficiency of the ^{225}Ac-DOTA compound used for intratumoural injection was 79.1%. This sample was used for the in vivo studies without further purification, as the compound is too small to reliably isolate using size exclusion chromatography or dialysis. Other options, like removing unlabelled radionuclides by passing them through an ion exchange resin would likely influence the buffer composition and were therefore disregarded. While labelling efficiencies are commonly required to be >95% for direct injection without further purification [14], it was decided that the 80% labelling efficiency was sufficient for contrasting the efficacy of polymersomes with ^{225}Ac-DOTA, for this first intratumoural experiment.

Biodistribution

For the therapeutic study, the mice were injected with 10 kBq ^{225}Ac. While two of the daughter nuclides of ^{225}Ac (namely ^{221}Fr and ^{213}Bi) emit gamma particles with energies suitable for SPECT imaging, the activity is much too low for imaging purposes. Next to that, the recoil effect can cause some of the daughter nuclides to have moved to other organs, rendering them unsuitable for accurate determination of the polymersome location. Therefore, biodistribution was performed on 3 mice per group at both 1 and 7 days p.i. In Figure 38, the distribution of both ^{225}Ac-polymersomes and ^{225}Ac-DOTA in selected organs is displayed. When viewing these biodistribution results, it is important to keep in mind that the injected activity as well as volume were very small, due to which the activity measured in various organs was just above background. As expected based on earlier results by Wang et al. [12], the polymersomes are very well retained in the tumour tissue, while the ^{225}Ac-DOTA compound is rapidly cleared. The absolute tumour retention of the polymersomes was found to be $46.0 \pm 21.5\%$ and $37.0 \pm 23.9\%$ at 1 and 7 days p.i. respectively, whereas less than 1% of the ^{225}Ac was retained at the tumour site at both time-points.
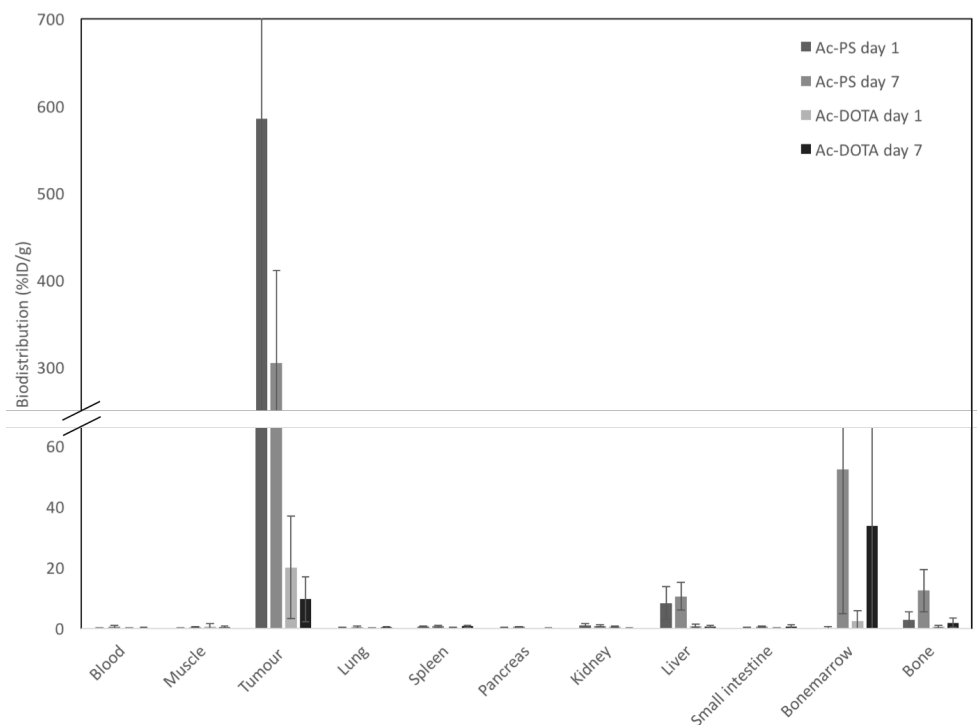
Figure 38: Biodistribution of BALB/c mice bearing an MDA-MB-231 tumour intratumourally injected with 10 kBq [225]Ac either encapsulated in polymersomes, or bound to DOTA, at 1 and 7 days p.i. based on 3 mice per group.

Uptake in most other organs is negligible for both compounds. As has been seen in Chapter 7, intravenously administered polymersomes are largely taken up in the spleen, but no splenic uptake has been observed here. The only organs other than the tumour exhibiting significant uptake of [225]Ac-polymersomes are the liver and bone-marrow, and to a lesser extend also the bone. Free [225]Ac has been shown to distribute mainly to the liver and bones, and is temporarily also retained in the kidneys [15,16], corresponding well to the increase in liver and bone marrow uptake seen in Figure 38. The observed uptake of [225]Ac in the liver and bone marrow thus mainly signify [225]Ac which has been released from the polymersomes, which has been found to be approximately 7% of [225]Ac over a period of 30 days in earlier work [13]. A fraction of the liver uptake could also be caused by the [225]Ac in polymersomes which have diffused out of the tumour tissue and have subsequently been filtered out by Kupffer cells, which are responsible for the phagocytic activity of the liver and represent 80-90% of the total macrophage population [17]. However, as polymersomes are also expected to be taken up in the spleen, this is likely not very significant as no splenic uptake has been observed, and free [225]Ac will thus be the main cause for organ uptake. The only organ taking up [225]Ac-DOTA to a significant extent is the bone marrow. The large standard deviation here is mainly caused by the small amount of bone marrow harvested and low radionuclide activity. Both free [225]Ac as well as chelated [225]Ac have been shown to accumulate in the bones as well as in the liver [16,18,19]. The [225]Ac-DOTA compound had been labelled with only 79% labelling efficiency prior to injection, so 21% of this sample constituted of free [225]Ac. Hence, either free [225]Ac or [225]Ac-DOTA can be responsible for the bone marrow uptake in the present study. These biodistribution results give us no reason to expect problems

concerning [225]Ac-induced dose-limiting toxicity of the polymersomes, though any health issues related to the bone marrow should be carefully studied.

[213]Bi retention in [225]Ac-polymersomes

To determine the potential daughter toxicity to healthy tissue, the distribution of the [213]Bi daughter nuclide immediately upon sacrifice has been quantified. Any [213]Bi recoiling out of the tumour tissue is expected to be transported by the blood to the kidneys. [213]Bi was very well retained in the tumour tissue, with retention determined to be 87 ± 4 % and 91 ± 10% at 1 and 7 days p.i. respectively. Dose limiting toxicity in [225]Ac studies has been observed to be due to [213]Bi accumulation in the kidneys [20,21]. To determine the extent of this effect in the current study, the accumulation of free [213]Bi in the kidneys has been determined. There was a clear difference in [213]Bi uptake in the kidneys (17.42 ± 7.38 %ID/g and 8.90 ± 3.61 %ID/g for 1 and 7 days p.i. respectively) as compared to practically no [225]Ac (Figure 38). However, the resulting tumour : kidney ratio of [213]Bi, 35.57 at 1 day p.i. and 29.49 at 7 days p.i., shows that this is still a very small amount compared to the activity in the tumour. Renal toxicity due to recoiled [225]Ac daughter atoms is thus not expected to become a large problem for the current intratumoural studies. Unfortunately, the radionuclide activity in the blood was too low to be able to determine the amount of [213]Bi.

Tumour growth

The tumour model chosen, MDA-MB-231, is a very well-vascularized tumour model. Upon injection of the compounds (the polymersomes as well as the DOTA and PBS), some blood was observed to flow out of the tumours. In Figure 39, the average tumour growth in 8 mice per group bearing subcutaneous MDA-MB-231 tumours can be observed. At 21 days after inoculation the tumours have been injected with the various compounds. After an initial increase in tumour size, the tumours which have been injected with the [225]Ac-polymersomes can be seen to rapidly decrease in size at 10 days post-injection. Based on the biodistribution study this was to be expected, as the [225]Ac in polymersomes is retained very well at the tumour site, whereas [225]Ac-DOTA is cleared rapidly, and the PBS control should not have any influence on tumour growth. The tumour dose induced by the 10 kBq [225]Ac-polymersomes is equivalent to the dose given by 5 kBq [225]Ac in polymersomes to a 400 µm tumour spheroid as presented in Chapter 6, taking into account the polymersome uptake in the spheroids of only 0.10 − 0.15%. There, a significant reduction in tumour size was observed at 3 − 6 days after addition of the vesicles. The somewhat delayed tumour reduction observed in vivo 10 − 14 days after injection, is likely due to the larger tumour volume as compared to the in vitro case.
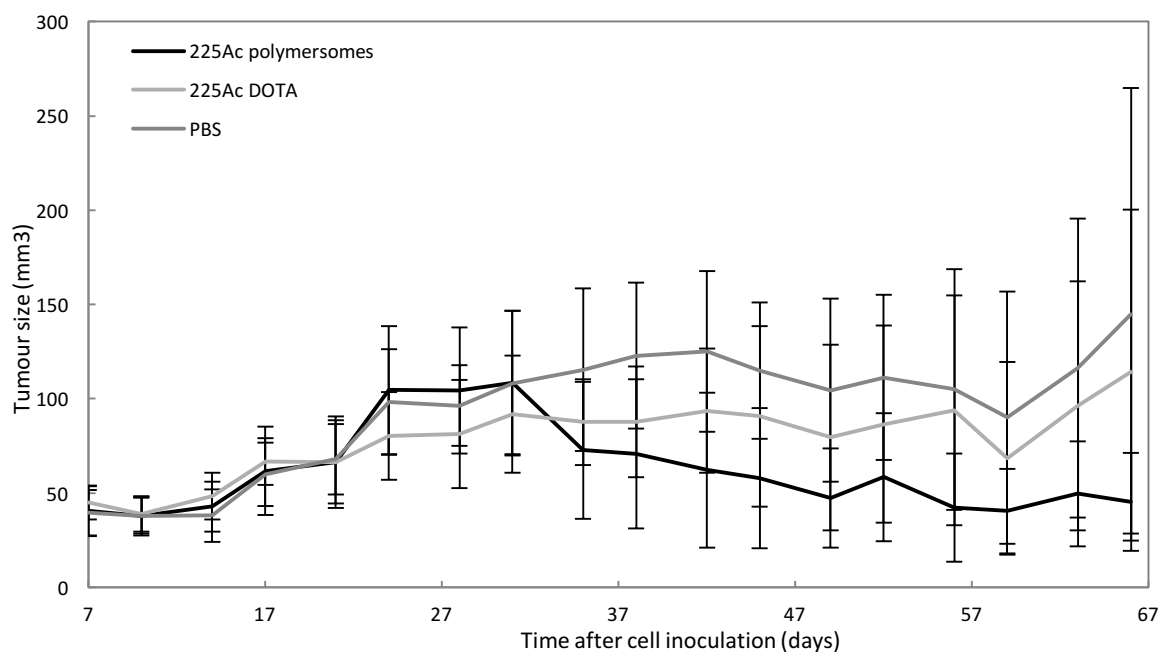
Figure 39: Growth of subcutaneous MDA-MB-231 tumours in female BALB/c mice upon a single intratumoural injection (20 µl) of PBS as control (grey), 10 kBq [225]Ac encapsulated in polymersomes (black), or 10 kBq [225]Ac-DOTA. The compounds were injected at 21 d after the cell inoculation. Error bars correspond to the standard deviation based on 8 animals per time point.

At later time-points the tumour growth of all three treatment groups appears to have stabilized, while at the very least the PBS control group would be expected to exhibit normal tumour growth. Typically, MDA-MB-231 tumours reach a tumour volume exceeding 2000 mm^3 at 36 days after tumour xenografting [22,23]. It is clear that the tumours in Figure 39 do not follow normal growth curves. The reason for this could be found in the intratumoural administration method. Nearly all tumours which were removed and subsequently stained at 1 and 7 days p.i. show a hole at the site of intratumoural injection filled with matrigel. However, there is nothing in the literature to suggest that intratumoural injection in this type of tumour strongly inhibits tumour growth. Bouquet et al. have studied MDA-MB-231 proliferation inhibition through angiogenesis suppression [24]. To this end, they injected 50 µL cytomegalovirus promoter (AdAGT) intratumourally, as well as 50 µL PBS for the control animals, approximately 15 days after tumour xenografting. The tumour volume growth curve of the control animals had grown larger than 2500 mm^3 after 55 days. Clearly, the intratumoural injection itself did not influence the tumour growth in this study, even though the injection volume was higher than in our study. Other groups which have studied the intratumoural administration in subcutaneous MDA-MB-231 tumours did not observe any problems in tumour growth of their control animals either [25,26]. Based on literature, the intratumoural injection itself should thus not cause any irregularities in tumour growth. An alternate explanation for the growth irregularities might be found in the MDA-MB-231 cells themselves. While the cell population was newly cultured to minimize the chance of infections, it is possible that the cells were contaminated by e.g. mycoplasmas. Mycoplasma infections can have very different effects on the cell culture, which can include alteration of proliferation characteristics and cell death [27,28]. As they are the smallest self-replicating organisms known, they

are very difficult to detect, and might very well have infected the cell culture. It is furthermore possible that the PBS with which the tumours were injected was contaminated, as all the injected solutions (including ^{225}Ac-DOTA or ^{225}Ac-polymersomes) were prepared with the same PBS buffer solution. However, as the experiment did not include a control group which was not intratumourally injected, the exact reason for the abnormal tumour growth cannot be determined. To prevent this from happening in follow-up studies, a few control animals which will not be injected should be included to provide a more complete picture on possible causes of spontaneous tumour growth inhibition. Also, the injection method could be changed to subcutaneous injection, after which the polymersomes can diffuse through the tumour tissue themselves to achieve total tumour irradiation.

Immunohistochemistry

To determine the effect of the intratumoural injection of ^{225}Ac-polymersomes, ^{225}Ac-DOTA, as well as PBS on the tumour tissue, they have been stained with HE and γ-H2AX. In these sections, the centre of the tumours has been found not to contain tumour cells, but was instead partially filled with matrigel or dead tumour tissue. The HE histological stain has been used to demonstrate different tissue structures. While hematoxylin stains nuclei blue, eosin stains the cytoplasm as well as tissue fibers and matrigel [29]. Representative tumour sections of each of the treated groups are presented in Figure 40. In these images, it can be seen that there are many small fields of matrigel present in the tumour. Only the border of the tumours contains vital tumour cells, although judging from the images taken at 7 days p.i., these cells were not able to fill the centre of the tumour. The presence of the matrigel combined with the empty centre of the tumours indicates that there was indeed a problem with the tumour growth, which might have been enhanced by the intratumoural injection.

To detect the presence of double-stranded breaks in the DNA the γ-H2AX biomarker has been used. Imaging these γ-H2AX foci in the tumours will give an indication of the distribution and effectiveness of the alpha therapy. While the high LET of alpha radiation causes double strand breaks in DNA [30], the very short range of the alpha particles allows for an indication of the radionuclide distribution within the tumour. The tumours visualised in Figure 40 show a similar uniform distribution of γ-H2AX foci in both the PBS and ^{225}Ac-DOTA groups. The biodistribution data indicated rapid clearance of the ^{225}Ac-DOTA complex from the tumour, thus no significant increase in double stranded breaks as compared to the control (PBS) group would be expected here. In contrast, the images show that the ^{225}Ac-polymersomes treatment groups demonstrate a larger degree of γ-H2AX foci, with an increasing foci gradient towards the centre of the tumour especially at day 1. As the polymersomes have been injected in the centre of the tumour, the largest amount of radiation damage logically occurs in the vicinity of the centre. At 7 days p.i. the vesicles have not yet uniformly distributed themselves throughout the tumour, which is in line with the distribution rate as observed in the 3D tumour spheroids in Chapter 6, and is expected to improve at later time-points. However, it is clear that the treatment with ^{225}Ac-polymersomes did result in an increase in double stranded breaks which generally lead to cell apoptosis.
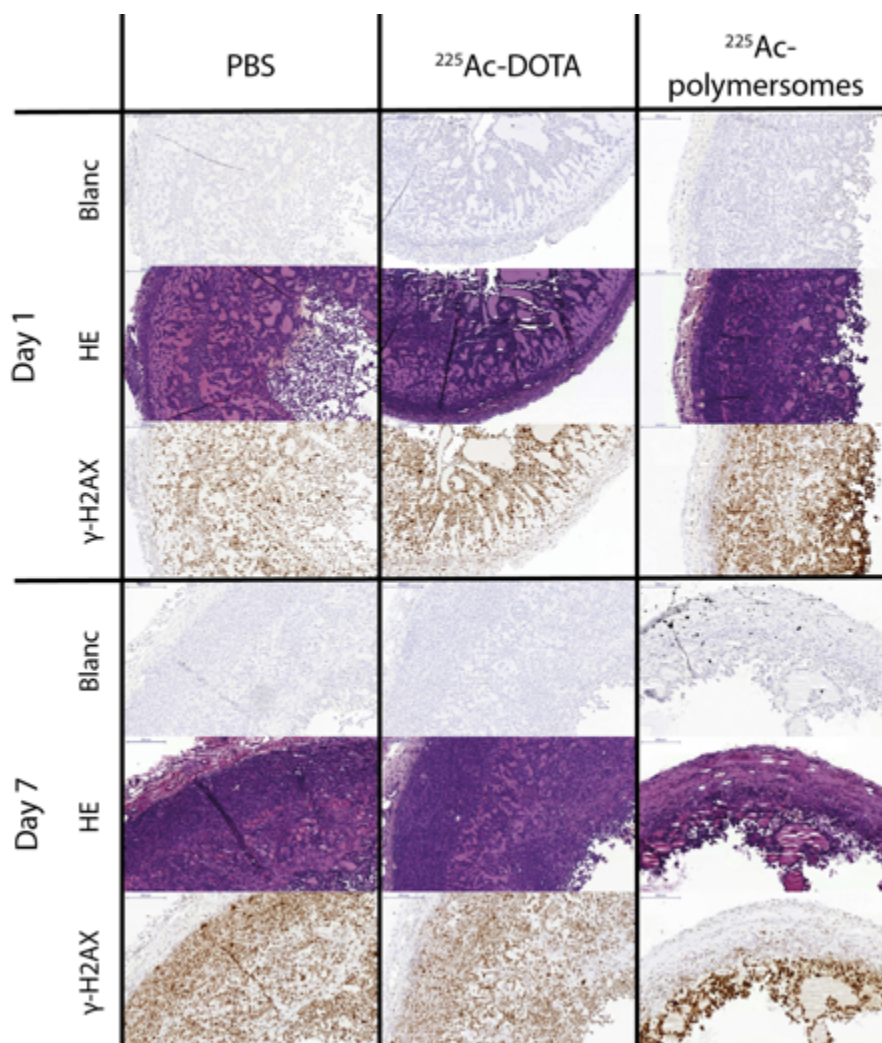
Figure 40: Tumour sections of subcutaneous MDA-MB-231 tumours injected intratumourally with either PBS, ^{225}Ac-DOTA or ^{225}Ac-polymersomes at 1 and 7 days p.i., where the sections have been stained with either HE or γ-H2AX.

Conclusion

In this chapter, the therapeutic potential of ^{225}Ac-containing polymersomes has been assessed. Intratumoural administration had been chosen to deliver 10 kBq ^{225}Ac encapsulated in polymersomes or attached to DOTA, or PBS to the tumour. Biodistribution studies have shown very favourable retention of the polymersomes in the tumour tissue, whereas ^{225}Ac coupled to DOTA was rapidly excreted. In vivo studies using ^{225}Ac as radiotherapeutic agent usually experience renal toxicity due to the recoiled daughter atom ^{213}Bi as dose-limiting toxicity. In the current study, ^{213}Bi has been retained in the tumour tissue to a large extend, with tumour : kidney ratios of ^{213}Bi around 30. Kidney damage due to recoiled daughters is thus unlikely to be dose-limiting in intratumoural ^{225}Ac therapy. Tumour growth was followed for 66 days, and while initially the tumour growth seemed to be inhibited to a larger extend for the mice which had received the ^{225}Ac-polymersomes than for the two control groups, at longer time periods it became clear that none of the tumours were following a normal growth curve. The exact reason for this is unclear, as intratumoural injection has often been performed in this tumour model according to literature, though a contamination in the PBS could be a possible explanation.

Immunohistochemical analysis of the treatment groups at 1d and 7 d p.i. has shown an increase in γ-H2AX foci in the ^{225}Ac-polymersomes group, indicating a larger degree of double-stranded breaks. Concluding, it has been shown that ^{225}Ac-polymersomes are retained very well at the tumour site upon intratumoural administration, and they have no significant side effects or negative impact on the health of the mice. At the current level of radioactivity, they are thus safe to administer. However, other factors have influenced the tumour growth, making a comparison of therapeutic efficacy impossible, and a follow-up study necessary to properly assess ^{225}Ac-polymersomes in vivo.

8

References

1. Wang, H.; Naghavi, M.; Allen, C.; Barber, R.; Bhutta, Z. A.; Carter, C.; Casey, C.; Charlson, F.; Chen, C.; Coates, M.; Dandona, H. Global, regional, and national life expectancy, all-cause mortality, and cause-specific mortality for 249 causes of death, 1980-2015: a systematic analysis for the Global Burden of Disease Study 2015. *Lancet* **2016**, *388*, 1459–1544.

2. Inger Norderhaug; Dahl, O.; Høisæter, P. Å.; Heikkilä, R.; Klepp, O.; Olsen, D. R.; Kristiansen, I. S.; Wæhre, H.; Johansen, T. E. B. Brachytherapy for Prostate Cancer: A Systematic Review of Clinical and Cost Effectiveness. *Eur. Urol.* **2003**, *44*, 40–46.

3. Langley, S. E. M.; Laing, R. Prostate brachytherapy has come of age: a review of the technique and results. *BJU Int.* **2002**, *89*, 241–249.

4. Cooks, T.; Tal, M.; Raab, S.; Efrati, M.; Reitkopf, S.; Lazarov, E.; Etzyoni, R.; Schmidt, M.; Arazi, L.; Kelson, I.; Keisari, Y. Intratumoral 224 Ra-Loaded Wires Spread Alpha-Emitters Inside Solid Human Tumors in Athymic Mice Achieving Tumor Control. *Anticancer Res.* **2012**, *32*, 5315–5321.

5. Goethals, P.-E.; Zimmermann, R. Brachytherapy Market Report & Directory Global; 2016.

6. Vente, M. A. D.; De Wit, T. C.; Van Den Bosch, M. A. A. J.; Bult, W.; Seevinck, P. R.; Zonnenberg, B. A.; De Jong, H. W. A. M.; Krijger, G. C.; Bakker, C. J. G.; Van Het Schip, A. D.; Nijsen, J. F. W. Holmium-166 poly(L-lactic acid) microsphere radioembolisation of the liver: Technical aspects studied in a large animal model. *Eur. Radiol.* **2010**, *20*, 862–869.

7. Hafeli, U. O.; Sweeney, S. M.; Beresford, B. A.; Sim, E. H.; Macklis, R. M. Magnetically directed poly(lactic acid) 90Y-microspheres: Novel agents for targeted intracavitary radiotherapy. *J. Biomed. Mater. Res.* **1994**, *28*, 901–908.

8. Cordier, D.; Forrer, F.; Bruchertseifer, F.; Morgenstern, A.; Apostolidis, C.; Good, S.; Müller-Brand, J.; Mäcke, H.; Reubi, J. C.; Merlo, A. Targeted alpha-radionuclide therapy of functionally critically located gliomas with 213Bi-DOTA-[Thi8,Met(O2)11]-substance P: a pilot trial. *Eur. J. Nucl. Med. Mol. Imaging* **2010**, *37*, 1335–44.

9. Lyczko, M.; Pruszynski, M.; Majkowska-Pilip, A.; Lyczko, K.; Was, B.; Meczynska-Wielgosz, S.; Kruszewski, M.; Szkliniarz, K.; Jastrzebski, J.; Stolarz, A.; Bilewicz, A. 211At labeled substance P (5-11) as potential radiopharmaceutical for glioma treatment. *Nucl. Med. Biol.* **2017**, *53*, 1–8.

10. Song, H.; Hobbs, R. F.; Vajravelu, R.; Huso, D. L.; Esaias, C.; Apostolidis, C.; Morgenstern, A.; Sgouros, G. Radioimmunotherapy of breast cancer metastases with alpha-particle emitter 225Ac: Comparing efficacy with 213Bi and 90Y. *Cancer Res.* **2009**, *69*, 8941–8948.

11. Kruijff, R. M. de; Drost, K.; Thijssen, L.; Morgenstern, A.; Bruchertseifer, F.; Lathouwers, D.; Wolterbeek, H. T.; Denkova, A. G. Improved 225Ac Daughter Retention in InPO4 Containing Polymersomes. *Appl. Radiat. Isot.* **2017**, *128*, 183–189.

8

12. Wang, G.; de Kruijff, R. M.; Abou, D.; Ramos, N.; Mendes, E.; Franken, L. E.; Wolterbeek, H. T.; Denkova, a. G. Pharmacokinetics of Polymersomes Composed of Poly(Butadiene-Ethylene Oxide); Healthy versus Tumor-Bearing Mice. *J. Biomed. Nanotechnol.* **2016**, *12*, 320–328.

13. Wang, G.; de Kruijff, R. M.; Rol, A.; Thijssen, L.; Mendes, E.; Morgenstern, A.; Bruchertseifer, F.; Stuart, M. C. A.; Wolterbeek, H. T.; Denkova, A. G. Retention studies of recoiling daughter nuclides of 225Ac in polymer vesicles. *Appl. Radiat. Isot.* **2014**, *85*, 45–53.

14. Brinkhuis, R. P.; Stojanov, K.; Laverman, P.; Eilander, J.; Zuhorn, I. S.; Rutjes, F. P. J. T.; Hest, J. C. M. Van Size Dependent Biodistribution and SPECT Imaging of 111In-Labeled Polymersomes. *Bioconjug. Chem.* **2012**, *23*, 958–965.

15. Davis, I. A.; Glowienka, K. A.; Boll, R. A.; Deal, K. A.; Brechbiel, M. W.; Stabin, M.; Bochsler, P. N.; Mirzadeh, S.; Kennel, S. J. Comparison of Actinium Chelates: Tissue Distribution and Radiotoxicity. *Nucl. Med. Biol.* **1999**, *26*, 581–589.

16. Beyer, G. J.; Bergmann, R.; Schomäcker, K.; Rösch, F.; Schäfer, G.; Kulikov, E. V.; Novgorodov, a. F. Comparison of the Biodistribution of 225 Ac and Radio-Lanthanides as Citrate Complexes. *Isotopenpraxis* **1990**, *26*, 111–114.

17. Bertrand, N.; Leroux, J.-C. The journey of a drug-carrier in the body: an anatomo-physiological perspective. *J. Control. Release* **2012**, *161*, 152–63.

18. Beyer, G. J.; Offord, R.; Kunzi, G.; Alexandrova, Y.; Ravn, U.; Jahn, S.; Barker, J.; Tengblad, O.; Lindroos, M. The influence of EDTMP-concentration on the biodistribution of radio-lanthanides and 225-Ac in tumor bearing mice. *Nucl. Med. Biol.* **1996**, *24*, 367–372.

19. Deal, K. A.; Davis, I. A.; Mirzadeh, S.; Kennel, S. J.; Brechbiel, M. W. Improved in Vivo Stability of Actinium-225 Macrocyclic Complexes. *J. Med. Chem.* **1999**, *42*, 2988–2992.

20. Jaggi, J. S.; Kappel, B. J.; Mcdevitt, M. R.; Sgouros, G.; Flombaum, C. D.; Cabassa, C.; Scheinberg, D. A. Efforts to Control the Errant Products of a Targeted In vivo Generator. *Cancer Res.* **2005**, *65*, 4888–4896.

21. Song, H.; Hobbs, R. F.; Vajravelu, R.; Huso, D. L.; Esaias, C.; Morgenstern, A.; Sgouros, G. Radioimmunotherapy of breast cancer metastases with {alpha}-particle emitter 225Ac: comparing efficacy with 213Bi and 90Y. *Cancer Res.* **2009**, *69*, 8941–8948.

22. Sun, R.; Liu, Y.; Li, S.-Y.; Shen, S.; Du, X.-J.; Xu, C.-F.; Cao, Z.-T.; Bao, Y.; Zhu, Y.-H.; Li, Y.-P.; Yang, X.-Z.; Wang, J. Co-delivery of all-trans-retinoic acid and doxorubicin for cancer therapy with synergistic inhibition of cancer stem cells. *Biomaterials* **2015**, *37*, 405–414.

23. Yuan, Y.-Y.; Mao, C.-Q.; Du, X.-J.; Du, J.-Z.; Wang, F.; Wang, J. Surface Charge Switchable Nanoparticles Based on Zwitterionic Polymer for Enhanced Drug Delivery to Tumor. *Adv. Mater.* **2012**, *24*, 5476–5480.

24. Bouquet, C.; Lamandé, N.; Brand, M.; Gasc, J.-M.; Jullienne, B.; Faure, G.; Griscelli, F.; Opolon, P.; Connault, E.; Perricaudet, M.; Corvol, P. Suppression of Angiogenesis, Tumor Growth, and Metastasis by Adenovirus-Mediated Gene Transfer of Human Angiotensinogen. *Mol. Ther.* **2006**, *14*, 175–182.

25. Miao, R. Q.; Agata, J.; Chao, L.; Chao, J. Kallistatin is a new inhibitor of angiogenesis and tumor growth. *Blood* **2002**, *100*, 3245–3252.

26. Pillé, J.-Y.; Denoyelle, C.; Varet, J.; Bertrand, J.-R.; Soria, J.; Opolon, P.; Lu, H.; Pritchard, L.-L.; Vannier, J.-P.; Malvy, C.; Soria, C.; Li, H. Anti-RhoA and Anti-RhoC siRNAs Inhibit the Proliferation and Invasiveness of MDA-MB-231 Breast Cancer Cells in Vitro and in Vivo. *Mol. Ther.* **2005**, *11*, 267– 274.

27. Drexler, H. G.; Uphoff, C. C. Mycoplasma contamination of cell cultures: Incidence, sources, effects, detection, elimination, prevention. *Cytotechnology* **2002**, *39*, 75–90.

28. Nikfarjam, L.; Farzaneh, P. Prevention and Detection of Mycoplasma Contamination in Cell Culture. *Cell J.* **2012**, *13*, 203–212.

29. Bancroft, J. D.; Layton, C. (Histologist); Suvarna, S. K. *Bancroft's theory and practice of histological techniques*; Suvarna, S. K.; Layton, C.; Bancroft, J. D., Eds.; illustrate.; Elsevier Health Sciences, 2013.

30. Allen, B. J. Systemic targeted alpha radiotherapy for cancer. *J. Proc. R. Soc. New South Wales* **2012**, *145*, 19–33.

8

9

General Conclusions

General conclusions

The research described in this thesis has been focussed on the development of polymeric nanocarriers for alpha radionuclide therapy. For the effective and efficient application of polymersomes as radiotherapeutic agents, it was found to be essential to extend their radiolabelling capacities. Therefore, the loading conditions and efficiencies of a number of radionuclides have been optimized in Chapters 2 and 4. The encapsulated radionuclides represent a range of opportunities for imaging and therapeutics, with gamma and positron-emitters like ^{111}In and ^{64}Cu for diagnostic, and beta emitters (^{67}Cu, ^{177}Lu and ^{140}La) as well as alpha emitters (^{213}Bi and ^{225}Ac) for therapeutic studies. High loading efficiencies were obtained for all radionuclides when loaded into polymersomes containing a hydrophilic chelator at neutral pH. Allowing the complexation of the radionuclides which utilized A23187 as ligand to take place in $CHCl_3$ increased loading efficiencies due to a larger reactive surface area, e.g. from $66 \pm 4\%$ to $84 \pm 5\%$ for ^{225}Ac. The combined loading of two different radionuclides for theranostic applications has been demonstrated for a number of radionuclides like ^{111}In and ^{225}Ac with loading efficiencies of $80 \pm 8\%$ and $62 \pm 5\%$, respectively. Furthermore, a new loading method has been developed employing phosphate ions encapsulated in the polymersomes in a low-pH environment (pH = 3). Co-precipitation of indium with phosphate ions inside a polymersome allowed for 0.13 μmol of indium to be successfully encapsulated, constituting a significant improvement over the classic loading method. However, careful evaluation of the precipitates is essential, as lanthanum phosphate nano-needles have been shown to be capable of puncturing the polymersome bilayer and thus destroying the nanocarrier. This effect has not been observed in the case of the $InPO_4$ nanoparticles, which has shown a retention of the indium of 96.1% at RT.

In Chapter 3 the efficacy of different vesicle designs to increase recoil retention has been studied using Monte Carlo simulations in line with the general aim to develop carriers which are better able to retain alpha-emitting daughter nuclides of ^{225}Ac. The electronic stopping of heavy targets has further been developed and incorporated into the existing Monte Carlo package NANVES as developed by Thijssen et al. [1] and validated by comparison with SRIM-2008. Recoil retention was determined in a number of different polymersome formulations, including polymersomes with a golden shell, a nanoparticle in the core, various nanoparticles dispersed in the core, and indium ions in solution in the core. Adding high-z materials to the vesicles has been shown to improve recoil retention in all cases. Encapsulation of the mother nuclide in one large nanoparticle has been shown to be much more efficient than to fill the polymersome with multiple smaller nanoparticles or a solution of high-z ions (simulated ^{221}Fr retentions of 59.3%, 50.3% and 32.8% respectively). The thickness of the polymersome membrane has no influence on the recoil retention.

The recoil retention of the ^{225}Ac daughters ^{221}Fr and ^{213}Bi has been assessed in Chapter 4 for polymersomes containing either $InPO_4$ or $LaPO_4$ nanoparticles. An average absolute increase in recoil retention of 20% and 28% for ^{221}Fr and ^{213}Bi respectively in $InPO_4$-containing polymersomes has been observed as compared to vesicles where ^{225}Ac had been attached to DTPA [2]. However, due to the observed polymersome instability in the case of $LaPO_4$ nanoparticles and their inherent cell toxicity, they have been excluded for further in vivo testing. The retention of ^{213}Bi in 80 nm diameter polymersomes containing either ^{225}Ac-DTPA and ^{225}Ac-$InPO_4$ upon intravenous administration in healthy BALB/c mice at 4 hours p.i. has been assessed in Chapter 7. Surprisingly, the retention in vivo

9

was found to be lower than the retention in an aqueous solution as shown in Chapter 5. This difference could partially be due to re-association of ^{213}Bi with the polymersomes, which would not occur in vivo. However, these discrepancies emphasize both the importance of careful evaluation of any experimental setup, as well as the need for in vivo verification of any tumour-targeting drug. Nevertheless, the in vivo experiments have confirmed the enhanced recoil retention through the use of encapsulated InPO$_4$ nanoparticles. Here, ^{213}Bi has been shown to be retained a factor 2 better in InPO$_4$-containing polymersomes compared to DTPA-containing polymersomes (6 ± 3 % and 14 ± 7% respectively). The main difference is expected to occur for the retention of ^{221}Fr, although this could not be evaluated in vivo due to its short half-live.

The therapeutic efficacy of ^{225}Ac-containing polymersomes has been studied in vitro with U87 glioblastoma multicellular spheroids as shown in Chapter 6. They have shown to be able to diffuse throughout the entire spheroid in a little over 4 days, enabling full irradiation of the tumour. Despite the low uptake of the vesicles in the spheroids of approximately 0.15%, 1 kBq ^{225}Ac-polymersomes added to the well did not only inhibit tumour growth but actually reduced the spheroid size in time. In Chapter 8, the therapeutic efficacy upon intratumoural administration of ^{225}Ac-polymersomes has been tested in vivo in BALB/c mice bearing an MDA-MB-231 tumour. While retention of the vesicles upon intratumoural administration has been shown to be very high, 46.0 ± 21.5% and 37.0 ± 23.9% of the injected activity at 1 and 7 days p.i. respectively, the tumours which have been injected with ^{225}Ac-DOTA retained less than 1% at both time-points, demonstrating the advantage of using the vesicles intratumourally. The accumulation of recoiled ^{213}Bi in the kidneys was limited, with a tumour to kidney ratio of 1:30. Tumour volume-reduction was observed for the tumours which had been injected with 10 kBq ^{225}Ac. However, control studies with ^{225}Ac-DOTA or PBS likewise have shown an unexpected tumour growth inhibition. It thus appears that the injection method has interfered with the normal tumour growth, making it difficult to attribute the effect to the presence of ^{225}Ac-polymersomes.

For the use of polymersomes as targeted alpha therapeutic agents, it is essential that they are able to accumulate at the tumour site upon intravenous injection and thus target multiple micrometastases. Intravenous administration of ^{111}In-labeled polymersomes has allowed for the determination of their in vivo characteristics, as discussed in Chapter 7. Surprisingly, a large difference in circulation time has been observed, with a 139 min circulation half-life in healthy mice and 7 min in tumour-bearing mice. This difference can likely be attributed to the presence of activated macrophages in the tumour-bearing mice which are responsible for the fast removal of the nanocarriers from the blood. To our knowledge, the difference in circulation time in healthy and tumour-bearing mice has not been quantified for polymersomes to date, but is essential to take into account when designing such nanocarrier systems. However, it is important to note that even the circulation time in healthy mice is lower than required for optimal tumour accumulation. Increasing the PEG length on the surface of the polymer vesicles is expected to solve this problem to a large degree.

In conclusion, this thesis demonstrates that polymersomes are capable of encapsulating the alpha-emitter ^{225}Ac and in fact retain the daughter atoms to a larger degree when the ^{225}Ac has been co-precipitated in InPO$_4$ nanoparticles. While the vesicles still need additional modifications to increase circulation time in tumour-bearing mice and enable tumour uptake upon intravenous administration, when loaded with ^{225}Ac they do exhibit very favourable characteristics when looking at tumour

penetration and growth inhibition. Thus, although very promising carriers in targeted alpha therapy, essential improvements will need to be made before intravenous administration of the carriers will lead to the destruction of metastasised tumours.

The main challenge will be to design the polymersomes in such a way that they will be able to successfully evade the immune system of, in particular, tumour-bearing mice. Based on the results obtained in preclinical studies using other nanoparticles, increasing the length of their outer PEG layer to a molecular weight of at least 2000 g/mol is expected to yield the required improvement [3]. This can potentially be achieved by using PBd-PEO block copolymers with an inherently longer PEO block to prepare the polymersomes. Alternatively, the stealthiness of the polymersomes composed of the block copolymer used in this research can be increased by combining them with a few wt% of a PBd-PEO block copolymer with longer PEO, or with a PEGylated lipid to form hybrid lipid-polymersomes [4,5]. Once optimal circulation and tumour uptake have been achieved, it could be considered to use larger polymersomes to further enhance recoil retention. However, the current polymersome formulation is already a very suitable candidate for intratumoural administration, especially given that larger vesicle diameters can be selected in these studies resulting in a larger fraction of recoiled daughter nuclides that can be retained [2]. Unfortunately, the tumour growth in the preclinical study as described in Chapter 8 was atypical in all groups, this study would benefit from being repeated - for instance a tumour model which is more suitable for intratumoural studies.

9

Bibliography

1. Thijssen, L.; Schaart, D. R.; de Vries, D.; Morgenstern, A.; Bruchertseifer, F.; Denkova, A. G. Polymersomes as nano-carriers to retain harmful recoil nuclides in alpha radionuclide therapy: a feasibility study. *Radiochim. Acta* **2012**, *100*, 473.

2. Wang, G.; de Kruijff, R. M.; Rol, A.; Thijssen, L.; Mendes, E.; Morgenstern, A.; Bruchertseifer, F.; Stuart, M. C. A.; Wolterbeek, H. T.; Denkova, A. G. Retention studies of recoiling daughter nuclides of 225Ac in polymer vesicles. *Appl. Radiat. Isot.* **2014**, *85*, 45–53.

3. Owens III, D. E.; Peppas, N. A. Opsonization, biodistribution, and pharmacokinetics of polymeric nanoparticles. *Int. J. Pharm.* **2006**, *307*, 93–102.

4. Cheng, Z.; Elias, D. R.; Kamat, N. P.; Johnston, E. D.; Poloukhtine, A.; Popik, V.; Hammer, D. A.; Tsourkas, A. Improved Tumor Targeting of Polymer-Based Nanovesicles Using Polymer - Lipid Blends. *Bioconjug. Chem.* **2011**, *22*, 2021–2029.

5. Nam, J.; Beales, P. A.; Vanderlick, T. K. Giant Phospholipid/Block Copolymer Hybrid Vesicles: Mixing Behavior and Domain Formation. *Langmuir* **2011**, *27*, 1–6.

9

Abbreviations

Acknowledgements

List of Publications

PhD portfolio

Curriculum Vitae

Abbreviations

Abbreviation	Definition
LET	Linear energy transfer
RBE	Relative biological effectiveness
AS	Ankylosing spondylitis
Actimab-A	Humanized Anti-CD33 Monoclonal Antibody HuM195
DLT	Dose-limiting toxicity
FDA	Food and drug administration
PSMA	Prostate-specific membrane antigen
PSA	Prostate-specific antigen
IV	Intravenous injection
CHX-DTPA	Cyclohexyl diethylenetriamine pentaacetic acid
PEPA	1,4,7,10,13-pentaazacyclopentadecane-N, N', N'', N''', N''''-pentaacetic acid
EDTA	Ethylene diamine tetraacetic acid
EPR	Enhanced permeability and retention
SPECT	Single photon emission computed tomography
PET	Positron emission tomography
CT	Computed tomography
MRI	Magnetic resonance imaging
THF	Tetrahydrofuran
DMSO	Dimethyl sulfoxide
PEG	Polyethyleneglycol
PDLLA	Poly(D,L-lactide)
PBd	Polybutadiene
PEO	Polyethyleneoxide
DNA	Deoxyribonucleic acid

RNA	Ribonucleic acid
HIV	Human immunodeficiency virus
DTPA	Diethylenetriamine pentaacetic acid
HCl	Hydrochloric acid
HEPES	4-(2- hydroxyethyl)-1-piperazineethanesulfonic acid
Tropolone	2-Hydroxy-2,4,6-cycloheptatrien-1-one
NTA	Nitrilotriacetic acid
DOTA	1,4,7,10-tetraazacyclododecane-1,4,7,10-tetraacetic acid
Cyclam	1,4,8,11-tetraazacyclotetradecane
HPGe	High-purity germanium
A23187	Calcium ionophore
Oxine	8-hydroxyquinoline
DLS	Dynamic light scattering
Cryo-TEM	Cryogenic transmission electron microscope
RT	Room temperature
Geant4	GEometry ANd Tracking
NANVES	NaNoVESicle
TRIM	Transport and Range of Ions in Matter
SRIM	Stopping and Range of Ions in Matter
TAT	Targeted alpha therapy
CHEAQS	Chemical Equilibria in Aquatic Systems
XRD	X-ray diffraction
MC	Monte Carlo
OER	Oxygen enhancement ratio
GBM	Glioblastoma
AKT	Protein kinase B
PBS	Phosphate buffered saline

DMEM   Dulbecco's modified eagle medium

MPS   Mononuclear phagocyte system

MES   2-(N-morpholino)ethanesulfonic acid

DaRT   Diffusing alpha-emitters radiation therapy

ITLC   Instant thin-layer chromatography

HE   Haematoxylin and eosin

NGS   Normal goat serum

BSA   Bovine serum albumin

DAB   3,3'-diaminobenzidine

Acknowledgements

First and foremost, I want to thank you for everything Antonia. You've not only been an amazing supervisor, but also a very good friend. I have learned a lot from you on so many different aspects, during our lunchtime walks, the conferences we attended together, and all our discussions (whether we agreed or not). You were always there for me, to answer my questions, discuss research options or read my papers and thesis, even if you were very busy, be it a weekend or a holiday. Thank you for your never-ending enthusiasm, support, motivation, and knowledge! I never could have done this without you, and cannot imagine a better supervisor.

I furthermore would like to thank my promotor Bert Wolterbeek for the opportunity to do my PhD thesis at the RIH group. Thank you for our insightful discussions and your continuous support for my PhD work, even after you became the head of the reactor institute! I have learned a lot from your way of approaching each problem from a completely new direction, in a way I had not thought of before.

I also wish to acknowledge the two sponsors of my PhD project, the foundations SK and Zabawas. Needless to say, this project would not have happened without their financial support. I also wish to thank our collaborators from the Joint Research Centre in Karlsruhe for the ^{225}Ac that they send us so many times, and Erik from Erasmus MC for the continuous supply of ^{111}In.

A big thank you to all of my colleagues. Jose and Anouk, thank you for all your help the past four years. Jan-Willem, Pablo, Peter and Dennis, thank you for the great and fruitful working environment. Elisabeth, thank you for all the discussions on the more chemical problems I encountered during my PhD. I wish you all the best at your new job at Aachen, although I will have to miss our shared-birthday cakes! I also would like to acknowledge all the technicians at RIH. Baukje, Astrid, Folkert, Adrie, thank you so much for all you help in and out of the lab, whether it was helping me with irradiations, cell culturing, computer problems, or the Cryo-TEM which just never seems to do what you need it to. Throughout these past four years I have learned a lot from you all, without your invaluable help this thesis would not have been possible.

To all my fellow PhD students and PostDocs in the group, thank you for making my time at RIH unforgettable. I have been so lucky to be part of the group at RIH, both in and out of the office, with you all as colleagues as well as friends. Guanglin, thank you for introducing me into the world of polymersomes back when I was still a master student. Guzman, it has been my honour to share many frustrations in the lab with you, thank you for helping me through. I still think your paella is the best. Jasper, it was great to have you as a colleague. I have learned a lot from you, both scientifically as well as on the upkeep and repair of motorcycles. I am amazed at the speed with which you go through your PhD, even while writing this I'm not sure yet who will finish first. Alexandra, it has been great to get to know you during your secondment in Delft, working together in the lab and organizing the conference in Lisboa. I have learned a lot from you, despite some technical issues. Josette, it's been great to have known you and work with you the past 4 years, in our office as well as during our Spanish classes! Rupali, I have loved being your officemate for the last few months and be able to vent all my research frustrations until you went on your pregnancy leave. Ushma is a wonderful baby and I'm sure you will have a great time with her. Vallin, I will never forget the moment that I picked you up at

Schiphol airport, from that moment onwards you have been a great friend and I have been lucky to have you around in the office! Tiantian, Giacomo, Eelco, Jeremy, Patricia, Boxhue and Stephan, thank you for the great working environment and fun times we had at the office as well as during the coffee breaks!

Furthermore, I would like to thank my bachelor and master students for helping me with the research which has led to this PhD thesis. Thanks for all the great times we had in the lab, you all have made me realize that research should never be a solitary journey, and many hands make light work. Nick, Michal, Louise, Niels, Lennard, Wessel, Thijs, Daniel, Rogier, Jence, Maarten and Mirjam, it was my honour to work with and supervise you during your bachelor thesis. Thijs, it has been great to work with you during your master thesis, which you tackled with as much enthusiasm as all those marathons you ran. Loes and Kirsten, it has been a pleasure to have you around and work on the project together! Laura, you have been a true friend both during and after your master project. We really made a great team, not only while working on the PAC but also during the conference in Portugal, organizing pub quizzes, all our Friday afternoon projects and introducing the fish to our group. And, never forget, polymersomes are awesome!

To all our collaborators, thank you for helping me make this thesis to a success! First and foremost, Sandra, thank you so much for everything! It has been a great pleasure to work with you at Radboud UMC, where I am still amazed at the speed and ease with which all my experiments have been done. You and Janneke were always there to think along, help me with the experiments, and answer all of my questions, I owe you both a lot! I also want to thank all the other colleagues at Radboud UMC for the great working environment you have created, I have always felt very welcome. Also a big thank you to Peter and the team from the VUMC, as well as Stefan, Jeroen and Dik from Erasmus MC for their collaboration and discussions.

I have had so many good times at the RID, it usually did not feel as going to work at all. This would never be possible without the great team and community you have built here. I therefore wish to thank all of the colleagues who have made my working here for the past few years so enjoyable. Everyone from NCSV and INAA, thank you for making the coffee table discussions so lively. I don't know of anyone with whom I would rather read through the 'ditjes en datjes' than with you Klazien! Rene, Ico, Michel, Peter, Jeroen, and Chris, thank you for letting me be part of the 'verzwaard pakketters'. I want to thank you and everyone else in the BHV for the instructive practices and dedication. Of course, a very special heartfelt thank you to Koos and Henk. I have very much enjoyed working in 't Koepeltje with you every Friday, attending the pubquizzes, paintballing, and lately brewing our newest beers!

Ayesha, thank you for bearing with me the last few months of writing my thesis! You have made my evening writing sessions a lot more enjoyable, and you were always there when I needed someone to complain to. Diego, thank you for designing a number of the figures in my thesis which really help to visualize the entire process. Mark, thank you for checking the lay-out of my thesis and finding all those little mistakes in there. Maarten, Freek, Koos, Paul, Rutger, Jermaine, Iris, Valerie, Ory, Marcel, Martine, Max, and Alex, thank you all so much for taking the time to read a part of my thesis and check it for English spelling and grammar! Especially towards the end, I really was not able to find the mistakes anymore.

Lastly, and most importantly, I wish to thank my family for their support throughout my PhD thesis. A special thank you to my sister, Thirza, for her creativity and hard work in designing the cover of my thesis. Thank you all for your encouragement and continued interest in my PhD thesis.

List of Publications

Papers

H. Mahmoud, K. Zhang, **R.M. de Kruijff,** A.G. Denkova and D.A. Koleva. Material properties of cement paste and mortar, modified with N-doped mesoporous carbon spheres (NMCSs), Cement and Concrete Research, *submitted*

R.M. de Kruijff, A. van der Meer, C. Windmeijer, J. Kouwenberg, A. Morgenstern, F. Bruchertseifer, P. Sminia, A.G. Denkova. Biodistribution and therapeutic efficacy of ^{225}Ac loaded polymersomes in 2D and 3D in vitro glioma models, European Journal of Pharmaceutics and Biopharmaceutics, *submitted*

A.G. Denkova, **R.M. de Kruijff,** P. Serra Crespo, Nano-carrier mediated photochemotherapy and photoradiotherapy, Advanced Healthcare Materials, *submitted*

R.M. de Kruijff, A. Arranja, A.G. Denkova, Radiolabeling methods and nuclear imaging techniques in the design of new polymeric carriers for cancer therapy. Current Applied Polymer Science, *submitted*.

R.M. de Kruijff, K. Drost, L. Thijssen, A. Morgenstern, F. Bruchertseifer, D. Lathouwers, H.T. Wolterbeek, A.G. Denkova, Improved ^{225}Ac daughter retention in InPO$_4$ containing polymersomes. Applied Radiation and Isotopes, vol. 128, pp. 183-189, July. 2017

L. Jennings, P. Glazer, A.C. Laan, **R.M. de Kruijff**, G. Waton, F. Schosseler, E. Mendes. The role of confinement and corona crystallinity on the bending modulus of copolymer micelles measured directly by AFM flexural tests. Soft Matter, vol. 12, no. 35, 7324–7329. 2016

R.M. de Kruijff, H.T. Wolterbeek, and A.G. Denkova, "A Critical Review of Alpha Radionuclide Therapy - How to Deal with Recoiling Daughters?" Pharmaceuticals, vol. 8, no. 2, pp. 321–36, June. 2015.

G. Wang, **R.M. de Kruijff**, D. Abou, N. Ramos, J. Lewis, E. Mendes, L.E. Franken, H.T. Wolterbeek, A.G. Denkova, Pharmacokinetics of polymersomes composed of poly(butadiene-ethylene oxide); healthy vs. tumour bearing mice, Journal of Biomedical Nanotechnology, vol. 12, no. pp. 320-328, 2016.

G. Wang, **R.M. de Kruijff**, A. Rol, L. Thijssen, E. Mendes, A. Morgenstern, F. Bruchertseifer, M. C. a Stuart, H. T. Wolterbeek, and a G. Denkova, Retention studies of recoiling daughter nuclides of 225Ac in polymer vesicles., Appl. Radiat. Isot., vol. 85, pp. 45–53, Feb. 2014.

G. Wang, **R.M. de Kruijff**, M.C.A. Stuart, E. Mendes, H.T. Wolterbeek, and A.G. Denkova, Polymersomes as radionuclide carriers loaded via active ion transport through the hydrophobic bilayer, Soft Matter, vol. 9, no. 3, p. 727, 2013.

Conference presentations

R.M. de Kruijff, S. Heskamp, A. van der Meer, J. Kouwenberg, G. Torrelo Villa, A. Morgenstern, F. Bruchertseifer, P. Sminia, A.G. Denkova, Assessing ^{225}Ac-Polymersomes for Targeted Radionuclide Therapy, 10th symposium on Targeted Alpha Therapy in Kanazawa, Japan, July 2017

R.M. de Kruijff. From β to α: Evolution in the radiochemistry of therapeutic radiopharmaceuticals, invited talk at BelNuc, Gent, Belgium, May 2017

A.G. Denkova, **R.M. de Kruijff,** A. van der Meer, K.G.A. Drost, D. Lathouwers, A. Morgenstern, F. Bruchertseifer, H.T. Wolterbeek, P. Sminia. Assessing ^{225}Ac-containing polymersomes for alpha radionuclide therapy in U87 glioblastoma spheroids, conference presentation at ERRS, Amsterdam, the Netherlands, September 2016

R.M. de Kruijff, G. Wang, R. van Oossanen, A. Rol, D. Abou, A. Morgenstern, F. Bruchertseifer, E. Mendes, H.T. Wolterbeek, A.G. Denkova, Polymersomes as alpha-emitting radionuclide carriers, TNT, Lisbon, Portugal, July 2015

R.M. de Kruijff, G. Wang, A. Rol, A. Morgenstern, F. Buchertseifer, H.T. Wolterbeek, A.G. Denkova, Recoil retention of recoiling ^{225}Ac daughters in polymersomes, 9th symposium on Targeted Alpha Therapy in Warsaw, Poland, May 2015

R.M. de Kruijff, G. Wang, D.S. Abou, E. Mendes, H.T. Wolterbeek, A.G. Denkova, In vivo study of 111In-loaded polymersomes, RadChem 2014, Marianske Lazne, Czech Republic, May 2014

R.M. de Kruijff, G. Wang, D. Abou, N. Ramos, J. Lewis, A. Rol, L. Thijssen, A. Morgenstern, F. Bruchertseifer, M.C.A. Stuart, E. Mendes, H.T. Wolterbeek, A.G. Denkova, Radiolabeling of polymersomes and their potential in nuclear medicine, NKRV 2014, Erasmus Medical Center, Rotterdam, The Netherlands, June 2014

Posters

G. Torrelo, **R.M. de Kruijff**, A. van der Meer and A.G. Denkova, Facile and fast preparation of ultra small vesicles in non-toxic organic solvent, 7th International Colloids Conference, Sitges, Spain, June 2017

R.M. de Kruijff, Polymersomes in Alpha Radionuclide Therapy, poster presentation and soundbite at the TU Delft Bioday, Delft, the Netherlands, March 2017

R.M. de Kruijff, A. van der Meer, K.G.A. Dorst, D. Lathouwers, A. Morgenstern, F. Bruchertseifer, H.T. Wolterbeek, P. Sminia, A.G. Denkova, Assessing ^{225}Ac-containing polymersomes for alpha radionuclide therapy in U87 glioblastoma spheroids, ERRS, Amsterdam, the Netherlands, September 2016

A. Gasol Garcia, P. Slangen, **R.M. de Kruijff**, A. Van der Meer, R.S. Narayan, G. Torrelo Villa, B.J. Slotman, B. A. Westerman, A. G. Denkova, P. Sminia, Nanocarrier delivery of the targeted agent MEK162 to brain tumour spheroids, ERRS, Amsterdam, the Netherlands, September 2016

R.M. de Kruijff, K. Drost, P. Sminia, D. Lathouwers, F. Bruchertseifer, A. Morgenstern, T.H. Wolterbeek, A. Denkova, Alpha-Radionuclide Therapy Using Polymeric Nanocarriers, NKRV workshop, Nijmegen, the Netherlands, July 2016

G. Torrelo, **R.M. de Kruijff**, J. Mulder and A.G. Denkova, Biodegradable polymersome formulation and tuning for targeted radionuclides delivery, TNT, Lisbon, Portugal, July 2015

S.L.C. Bogers, **R.M. de Kruijff**, F.D.P. Geurink, M. de Bruin, A.G. Denkova, D.R. Schaart, Determining the state of radionuclides in polymersomes using perturbed angular correlation spectroscopy, TNT, Lisbon, Portugal, July 2015

R.M. de Kruijff, G. Wang, D.S. Abou, E. Mendes, H.T. Wolterbeek, A.G. Denkova, Designing polymersomes for nuclear medical applications, AMBA, Ghent, Belgium, November 2014

R.M. de Kruijff, G. Wang, A. Rol, L. Thijssen, E. Mendes, A. Morgenstern, F. Bruchertseifer, M.C.A. Stuart, H.T. Wolterbeek, A.G. Denkova, Retaining recoiling alpha-emitters in polymersomes, ESCDD, Egmond aan Zee, the Netherlands, April 2014

T.J. Sanders, **R.M. de Kruijff**, N. Stigter, E. Mendes, H.T. Wolterbeek, A.G. Denkova, Active loading of biodegradable PLA-PEO and PCL-PEO polymersome vesicles, Colloid and Interface Science, Delft, the Netherlands, April 2014

PhD portfolio

Name PhD candidate: Robin de Kruijff

Department: Radiation Science and Technology

Research group: Radiation and Isotopes for Health

Research school: TU Delft graduate school

PhD period: January 2014 – January 2018

Promotor: Prof. dr. H.T. Wolterbeek

Co-promotor: Dr. ir. A.G. Denkova

PhD training

General courses, TU Delft graduate school

PhD Start-Up	2014
Coaching individual students	2014
Build a better brain	2014
How to manage research information	2014
The art of presenting science	2014
Spanish for beginners	2015
PROM4 Scientific writing	2015
Professional and Career Development – Personal Branding	2017

Specific courses

AMIE translational imaging workshop: from mouse to man, Rotterdam	2014
IV International GEANT4 School, Belgrade, Servia	2016

Conferences and meetings

International conferences

AMBA, Ghent, Belgium	2014
17th RadChem conference, Marianske Lazne, Czech Republic	2014
13th ESCDD, Egmond aan Zee, the Netherlands	2014

Nuclear Industry Summit, Amsterdam, the Netherlands	2014
9th TAT conference, Warshaw, Poland	2015
TNT conference, Lisbon, Portugal	2015
MTAA14 & NAMLS11 conferences, Delft, the Netherlands	2015
ERR, Amsterdam, the Netherlands	2016
18th BelNuc symposium, Ghent, Belgium	2017
10th TAT conference, Kanazawa, Japan	2017

Scientific meetings

NKRV workshop, Eindhoven, the Netherlands	2013
Colloid and interface science network meeting, Delft, the Netherlands	2014
NKRV workshop, Rotterdam, the Netherlands	2014
Bioday, Delft, the Netherlands	2015
NKRV workshop, Delft, the Netherlands	2016
TUDelft research exhibition, Delft, the Netherlands	2016
NKRV workshop, Nijmegen, the Netherlands	2016
Bioday, Delft, the Netherlands	2017
RST science day, Delft, the Netherlands	2017
TUDelft research exhibition, Delft, the Netherlands	2017

Other

Board member Dutch Young Generation	2015-2017
Vice chair / secretary YoungDelft	2015-2017
MTAA14 & NAMLS11 conference organization	2015
TNT conference organization	2015

Supervising

Master students

Thijs Sanders	master student applied physics	2014
Laura Bogers	master student biomedical engineering	2015
Loes Snell	master student molecular science and technology	2016
Kirsten Drost	master student molecular science and technology	2016

Bachelor students

Nick Stigter	bachelor student applied physics	2013
Michal Galek-Aldridge	bachelor student molecular science and technology	2014
Louise Berghuijs	bachelor student molecular science and technology	2014
Niels Kolen	bachelor student applied physics	2014
Lennard van Gendt	bachelor student molecular science and technology	2015
Wessel van Ekeren	bachelor student molecular science and technology	2015
Thijs Moret	bachelor student applied physics	2015
Daniel Brandenburg	bachelor student molecular science and technology	2015
Rogier van Oossanen	bachelor student applied physics	2015
Jence Mulder	bachelor student molecular science and technology	2016
Maarten Schreuder	bachelor student applied physics	2016
Mirjam de Graaf	bachelor student molecular science and technology	2017

Leren onderzoeken (LO) students

Teunis Louters & Justin van Benten	LO1	2013
Jence Mulder & Daniel Brandenburg	LO2	2013
Annemiek van Leuken	LO1	2015
Kevin Arts & Herman den Beer Poortugael	LO1	2015
Aron Kahn & Guido Hartog	LO1	2016
Zhiwei Cai & Danielle van Dijk	LO1	2016

Curriculum Vitae

Robin de Kruijff was born on the 25th of August, 1989 in Utrecht, the Netherlands. Her childhood was spent in Maarssen-Broek and Amersfoort, as a teenager she moved to Etten-Leur. In 2005, she moved with her family to Shanghai, where she spent the last two years of her high school at the Shanghai American School. She successfully completed the International Baccalaureate program in 2007.

After this international experience, she came back to the Netherlands where she studied Applied Physics at Delft University of Technology, finishing the Bachelor program in 2010. Continuing in Applied Physics for her masters, she worked on her Master research project at the Radiation and Isotopes for Health (RIH) group at the Reactor Institute Delft. Her research topic was on the loading characteristics of polymersomes as radionuclide carriers. Four months doing her internship in the Centro de Energia Nuclear Na Agricultura in Piracicaba, Brazil, completed her Applied Physics Master in 2013.

She subsequently started her research career at RIH, and a few months later she became a PhD candidate at the same group in January 2014 under the supervision of Dr. ir. A.G. Denkova and Prof. dr. H.T. Wolterbeek. During this time, she has supervised a number of Bachelor and Master students. She also enjoyed many extracurricular activities, e.g. giving guided tours in the reactor, joining the emergency response team of the RID, and being a part of the boards of YoungDelft and the Dutch Young Generation.

The thesis you are reading now is the result of the past four years of research as PhD candidate.